

DEVELOPMENT OF SUPERCAPACITORS WITH ONE DIMENSIONAL
NANOMATERIALS

A THESIS SUBMITTED TO
THE GRADUATE SCHOOL OF NATURAL AND APPLIED SCIENCES
OF
MIDDLE EAST TECHNICAL UNIVERSITY

BY

RECEP YÜKSEL

IN PARTIAL FULFILLMENT OF THE REQUIREMENTS
FOR
THE DEGREE OF DOCTOR OF PHILOSOPHY
IN
MICRO AND NANOTECHNOLOGY

JANUARY 2017

Approval of the thesis

**DEVELOPMENT OF SUPERCAPACITORS WITH ONE DIMENSIONAL
NANOMATERIALS**

Submitted by **RECEP YÜKSEL** in partial fulfillment of the requirements for the degree of **Doctor of Philosophy in Micro and Nanotechnology Department, Middle East Technical University** by,

Prof. Dr. Gülbin Dural Ünver _____
Dean, Graduate School of **Natural and Applied Sciences, METU**

Assoc. Prof. Dr. Burcu Akata Kurç _____
Head of Department, **Micro and Nanotechnology Department, METU**

Assoc. Prof. Dr. Hüsnü Emrah Ünal _____
Supervisor, **Metallurgical and Materials Eng. Dept., METU**

Assoc. Prof. Dr. Ali Çırpan _____
Co-Supervisor, **Chemistry Department, METU**

Examining Committee Members:

Prof. Dr. Levent Toppare _____
Chemistry Department, METU

Assoc. Prof. Dr. Hüsnü Emrah Ünal _____
Metallurgical and Materials Engineering Dept., METU

Prof. Dr. Zeki Aktaş _____
Chemical Engineering Dept., Ankara University

Prof. Dr. Kadri Aydınol _____
Metallurgical and Materials Engineering Dept., METU

Assoc. Prof. Dr. Göknur Cambaz Büke _____
Materials Science and Nanotechnology Eng. Dept., TOBB ETU

Date: 16.01.2017

I hereby declare that all information in this document has been obtained and presented in accordance with academic rules and ethical conduct. I also declare that, as required by these rules and conduct, I have fully cited and referenced all material and results that are not original to this work.

Name, Last name: Recep Yüksel

Signature :

ABSTRACT

DEVELOPMENT OF SUPERCAPACITORS WITH ONE DIMENSIONAL NANOMATERIALS

Yüksel, Recep

Ph.D., Department of Micro and Nanotechnology

Supervisor: Assoc. Prof. Dr. Hüsnü Emrah Ünalın

Co- Supervisor: Assoc. Prof. Dr. Ali Çırpan

January 2017, 184 pages

Supercapacitors provide higher power density, longer cycle life than batteries and conventional dielectric capacitors. Energy density of supercapacitors, on the other hand, are less than that of the batteries. Therefore, supercapacitors have an important position between the batteries and capacitors. In supercapacitors, most commonly used electrode active materials are carbon based ones, metal oxides and conducting polymers.

Recent studies showed that one-dimensional nanomaterials such as carbon nanotubes and metal nanowires including their nanocomposites are promising electrode materials for supercapacitors. CNTs are highly promising electrode materials for supercapacitors and their electrochemical properties have been studied by many research groups. Another important one dimensional nanomaterial, silver nanowires (Ag NWs), are recently started to be used in supercapacitor research, where the active surfaces of Ag NWs allow the deposition of capacitive materials to achieve a core-

shell or layered morphology. These nanostructures obtained with Ag NWs advance the charge transport and decrease the overall resistance, which seriously affect the electrochemical performance of the supercapacitor devices.

In this work, high performance supercapacitor electrodes and devices were fabricated and characterized. While doing all these, the main intention was to fabricate supercapacitors with different form factors on unconventional substrates. One dimensional nanomaterials and their nanocomposites that were synthesized via low-cost and solution-based methods were utilized in supercapacitor electrodes to provide distinct advantages, which was the main theme of this thesis. In this regard, independently, CNTs and Ag NWs and their nanocomposites with various metal oxides and conducting polymers in ternary and binary configurations were used in high performance supercapacitor electrodes and supercapacitor devices with added functionality.

Keywords: supercapacitor, energy storage, carbon nanotube, silver nanowire, nanocomposite.

ÖZ

SÜPERKAPASİTÖRLERİN BİR BOYUTLU NANOMALZEMELER İLE GELİŞTİRİLMESİ

Yüksel, Recep

Doktora, Mikro ve Nanoteknoloji Bölümü

Tez Yöneticisi: Doç. Dr. Hüsnü Emrah Ünalın

Ortak Tez Yöneticisi: Doç. Dr. Ali Çırpan

Ocak 2017, 184 sayfa

Süperkapasitörler, piller ve klasik dielektrik kapasitörlerden daha yüksek güç yoğunluğu, daha uzun kullanım ömrü sağlar. Öte yandan, süperkapasitörlerin enerji yoğunluğu pillerin enerji yoğunluğundan daha düşüktür. Bu nedenle, süperkapasitörler piller ve kapasitörler arasında önemli bir yere sahiptirler. Süperkapasitörlerde en çok kullanılan elektrot aktif maddeler karbon esaslı olanlar, metal oksitler ve iletken polimerlerdir.

Son yıllardaki araştırmalar, karbon nanotüpler ve metal nanoteller gibi tek boyutlu nanomalzemelerin ve bunların nanokompozitleri de dahil olmak üzere süperkapasitörler için umut verici elektrot malzemeleri olduğunu gösterdi. KNTler süperkapasitörler için oldukça umut verici elektrot malzemeleri olup, bunların

elektrokimyasal özellikleri birçok araştırma grubu tarafından incelenmiştir. Bir başka önemli tek boyutlu nanomalzeme olan gümüş nanoteller (Ag NTler), süperkapasitör araştırmasında yakın zamanda kullanılmaya başlandı ve Ag NTlerin aktif yüzeyleri çekirdek-kabuk ya da katmanlı morfoloji elde etmek için kapasitif malzemelerin birikimine izin vermektedir. Ag NTler ile elde edilen bu nano yapılar, yük taşınmasını arttırmakta ve toplam direnci düşürmekte ve bu da, süperkapasitör cihazlarının elektrokimyasal performansını ciddi şekilde etkilemektedir.

Bu çalışmada, yüksek performanslı süperkapasitör elektrotları ve cihazları üretilmiş ve karakterize edilmiştir. Tüm bunları yaparken temel amaç, alışılmamış yüzeyler üzerinde farklı form faktörleri olan süperkapasitörler üretmektir. Düşük maliyetli ve çözelti esaslı yöntemlerle sentezlenen tek boyutlu nanomalzemeler ve bunların nanokompozitleri, süperkapasitör elektrotlarında farklı avantajlar sağlamak için kullanılması bu tezin ana temasıdır. Bu bağlamda, KNTler ve Ag NTler ve bunların çeşitli metal oksitler ve iletken polimerlerle nanokompozitleri bağımsız olarak, üçlü ve ikili konfigürasyonlarda, yüksek performanslı süperkapasitör elektrotlarında ve süperkapasitör cihazlarında eklenmiş fonksiyonellik ile kullanılmıştır.

Anahtar Kelimeler: süperkapasitör, enerji depolama, karbon nanotüp, gümüş nanotel, nanokompozit.

To My Family

ACKNOWLEDGEMENTS

This thesis is an interdisciplinary work between the Departments of Metallurgical and Materials Engineering and Chemistry in METU and partially supported by The Scientific and Technological Research Council of Turkey (TÜBİTAK) under grant no 113E596.

Firstly, I would like to express my deepest gratitude to my advisor Assoc. Prof. Dr. H. Emrah Ünalın, for his support, guidance and patience throughout the study. It is a great honor to work under his supervision. I also would like to thank my co-advisor Assoc. Prof. Dr. Ali Çırpan for his support for my studies. I would like to thank Prof. Dr. Levent Toppare and his research group for their help and support. I also would like to thank my thesis progress committee, Prof. Dr. Kadri Aydınol and Assoc. Prof. Dr. Göknur Cambaz Büke and for their valuable suggestions, advices and inputs.

I owe my deepest gratitude to my labmates colleagues and dearest friends, Şahin Coşkun, Selin Özkul, Mete Batuhan Durukan, Sevim Polat, Doğançan Tigan, Alptekin Aydınlı, Can Çuhadar, Doğa Doğanay, Ece Alpugan, Onur Türel, İpek Bayraktar, Serkan Koylan, and Şeyma Koç.

I also appreciate the great moral support from my colleagues Dr. Sara Banu Akkaş, Dr. Eray Şentürk and Semra Tahancalıo and all my friends who helped me throughout this study. They all will be remembered for their intimate friendship. I also acknowledge all the great facilities in Metallurgical and Materials Engineering Department and METU Central Laboratory.

And finally, I would like to thank my family who always gave me hope during my PhD studies. Thank you for everything, thank you for always being there for me.

TABLE OF CONTENT

ABSTRACT.....	v
ÖZ	vii
ACKNOWLEDGEMENTS	x
TABLE OF CONTENT	xi
LIST OF TABLES	xv
LIST OF FIGURES	xvi
ABBREVIATION LIST	xxii
CHAPTERS	
1. INTRODUCTION	1
1.1 Historical Background and Current Status	1
1.2 Principles of Supercapacitors	3
1.2.1 Electrical Double Layer Capacitors	6
1.2.2 Pseudocapacitance.....	7
1.3 Types of Supercapacitors	8
1.3.1 Carbon Based Supercapacitors.....	9
1.3.2 Metal Oxide Based Supercapacitors	11
1.4 Electrolytes	13
1.4.1 Aqueous Electrolytes	14
1.4.2 Organic Electrolytes.....	14
1.4.3 Ionic Liquid Electrolytes.....	15
1.4.4 Gel or Solid State Polymer Electrolytes.....	15
1.5 Electrochemical Testing	15
1.5.1 Electrochemical Cell	15
1.5.1.1 Three-Electrode Configuration.....	16
1.5.1.2 Two-Electrode Configuration.....	16
1.5.2 Cyclic Voltammetry Measurements.....	17
1.5.3 Galvanostatic Charge-Discharge (Chronopotentiometry) Measurements	19
1.5.4 Electrochemical Impedance Spectrometry (EIS)	20

1.6	Carbon Nanotubes	22
1.7	Carbon Nanotube Based Supercapacitors.....	23
1.8	Silver Nanowires	23
1.9	Silver Nanowire Based Supercapacitors.....	24
	DISSERTATION OBJECTIVES.....	26
	2.TRANSPARENT AND FLEXIBLE SUPERCAPACITORS WITH SINGLE WALLED CARBON NANOTUBE THIN FILM ELECTRODES.....	27
2.1	Introduction	27
2.2	Experimental.....	29
2.2.1	Preparation of Samples.....	29
2.2.2	Characterizations	30
2.3	Results and Discussion	30
2.4	Conclusions	37
	3. TERNARY NANOCOMPOSITE SWNT/WO ₃ /PANI THIN FILM ELECTRODES FOR SUPERCAPACITORS.....	39
3.1	Introduction	39
3.2	Experimental.....	40
3.2.1	Preparation of samples	40
3.2.2	Characterization	41
3.3	Results and Discussion	42
3.4	Conclusions	54
	4. TEXTILE SUPERCAPACITORS BASED ON MNO ₂ /SWNT/CONDUCTING POLYMER TERNARY COMPOSITES	55
4.1	Introduction	55
4.2	Experimental Details	58
4.2.1	Materials:.....	58
4.2.2	Manganese (IV) oxide nanoparticles coated textile preparation:	58
4.2.3	SWNT coated textile preparation:.....	58
4.2.4	Conducting polymer coated textile preparation:	59
4.2.5	Preparation of gel electrolyte:	59

4.2.6	Fabrication of supercapacitors:	59
4.3	Characterization.....	59
4.4	Results and Discussions	60
4.5	Conclusions	73
5.	ALL-ORGANIC ELECTROCHROMIC SUPERCAPACITOR ELECTRODES	75
5.1	Introduction	75
5.2	Experimental Details	76
5.2.1	SWNT thin film preparation:	76
5.2.2	Conducting polymer synthesis:.....	77
5.2.3	Characterization	78
5.3	Results and Discussion	78
5.4	Conclusions	86
6.	COAXIAL SILVER NANOWIRE NETWORK CORE MOLYBDENUM OXIDE SHELL SUPERCAPACITOR ELECTRODES.....	87
6.1	Introduction	87
6.2	Experimental Details	89
6.2.1	Preparation of Electrodes	89
6.2.2	Characterization	90
6.3	Results and Discussion	90
6.4	Conclusions	98
7.	FLEXIBLE, SILVER NANOWIRE NETWORK NICKEL HYDROXIDE CORE- SHELL ELECTRODES FOR SUPERCAPACITORS.....	99
7.1	Introduction	99
7.2	Experimental Details	101
7.2.1	Electrode Fabrication	101
7.2.2	Characterization	102
7.3	Results and Discussion	102
7.4	Conclusions	113
8.	AN EFFICIENT ELECTROCHROMIC SUPERCAPACITOR SWITCHING BETWEEN GREEN AND TRANSPARENT.....	115

8.1	Introduction	115
8.2	Experimental Details	118
8.2.1	Preparation of Electrodes	118
8.2.2	Characterization	118
8.3	Results and Discussion	118
8.4	Conclusions	128
9.	CONCLUSIONS AND FUTURE RECOMMENDATIONS	129
	REFERENCES	133
	APPENDIX A: PERMISSION LICENSES	159
	CURRICULUM VITAE	181

LIST OF TABLES

TABLES

Table 1. Battery, Supercapacitor, and Capacitor Comparison.	5
Table 2. Sheet resistance and % transmittance (at 550 nm) change with respect to SWNT weight for the fabricated supercapacitors.	31
Table 3. XPS core-level BEs and FWHMs of the XPS spectrum of the WO ₃	46
Table 4. Textile based SCs from literature in conjunction with obtained results herein (Adapted and modified form ref. [17]).	72
Table 5. MoO ₂ based SC electrode materials (adapted from [205]). (OMC: ordered mesoporous carbon; SWNT: single-walled carbon nanotube; EC: ethylene carbonate; rGO: reduced graphene oxide; DEC: diethyl carbonate; SCE: saturated calomel electrode).	97
Table 6. A comparison of various Ni(OH) ₂ containing SC electrode materials performance.	113

LIST OF FIGURES

FIGURES

Figure 1. Supercapacitor cells and modules with different specifications [8].	2
Figure 2. Mazda6 with layout of components in i-ELOOP [10].	2
Figure 3. Hybrid bus uses supercapacitors and two 67 kW electric motors [11].	3
Figure 4. Ragone plot for different energy storage systems [12].	3
Figure 5. Charge storage mechanisms of conventional capacitors and SCs [15].	5
Figure 6. Basic schematic for an EDLC. Device contains an active material (<i>e.g.</i> , carbon), a current collector, a separating membrane and an electrolyte, (<i>e.g.</i> , sodium sulfate (Na_2SO_4) solutions) [17].	6
Figure 7. (a) Helmholtz and (b) Stern model of the EDLC (IHP: Inner Helmholtz path, OHP: outer Helmholtz path, d : double-layer distance, ϕ_0 :zeta potential) [9].	7
Figure 8. Basic schematic for a pseudocapacitor. Device contains an active material (<i>e.g.</i> , MnO_2), a current collector, a separating membrane and electrolyte, (<i>e.g.</i> , Na_2SO_4 solutions)[17].	8
Figure 9. Taxonomy of supercapacitors.	9
Figure 10. Schematics of carbon based materials (a) graphite, (b) diamond, (c) buckminsterfullerene (C_{60}), (d) nanotube and (e) graphene [34].	10
Figure 11. Doping process of CPs.	12
Figure 12. Structures of electrically conducting polymers [39].	13
Figure 13. Cyclic voltammetry results of identical PANI/MWNT electrodes using three-electrode (top) and two-electrode (bottom) configuration [51].	17
Figure 14. Typical CV curve shapes for supercapacitors [33].	18
Figure 15. (a) Schematic of a typical supercapacitor with, (b) its potential profile at charged state and (c) its equivalent circuit model [9].	21
Figure 16. Typical Nyquist plot and its specific resistive and capacitive regions.	22
Figure 17. (a) A simple schematic and (b) photograph of the fabricated SCs without carbon paste current collectors. c) SEM image of a SWNT electrode with a sheet resistance of 75 ohm/sqr.	31
Figure 18. Optical transmittance characteristics of the full devices with respect to total SWNT weight in both electrodes.	32

Figure 19. (a) CV curves of transparent and flexible SCs with different SWNT mass at 20 mV.s ⁻¹ scan rate. (b) CVs at different rates for a SWNT mass of 0.08 mg.....	33
Figure 20. (a) Percent resistance change in ITO and SWNT thin films on ITO during bending cycles down to a radius of 6 mm [112]. (b) CVs for flexible SCs while bent to different radius of curvatures for the 0.08 mg of SWNT thin film at 20 mV.s ⁻¹ scan rate.....	34
Figure 21. (a) GCD curves for SCs at 1.25 A/g and (b) at different current densities. (c) Dependence of C _{sp} on current densities. (d) Cycleability of fabricated SCs.....	35
Figure 22. (a) Consecutive CVs for the electrodeposition of WO ₃ /PANI on SWNT films and (b) electrodeposited thin film electrodes at 50 mV/s scan rate.	43
Figure 23. SEM images of (a) bare SWNT electrodes, (b) SWNT/WO ₃ films and SWNT/WO ₃ /PANI film in low (c) and high (d) resolution.	44
Figure 24. (a) XPS survey spectrum of the electrodes. XPS spectra of (b) W 4f, (c) O 1s and (d)-(f) C 1s.	46
Figure 25. FTIR spectra of bare SWNT electrodes, SWNT/WO ₃ and SWNT/WO ₃ /PANI nanocomposite electrodes.	47
Figure 26. CV results of the fabricated thin film electrodes in 0.1 M LiClO ₄ in PC at 20 mV/s.	48
Figure 27. CV results of SWNT/WO ₃ /PANI nanocomposite electrodes at scan rates between 20 and 500 mV/s.	49
Figure 28. GCD curves of the fabricated electrodes at 0.13 mA/cm ² current density.	50
Figure 29. GCD curves of SWNT/WO ₃ /PANI nanocomposite electrode in 0.1 M LiClO ₄ in PC at different current densities from 0.13 to 1.5 mA/cm ²	50
Figure 30. (a) Dependence of the specific capacitance of ternary SWNT/WO ₃ /PANI nanocomposite electrodes on current density. Lines are for visual aid. (b) Cycling performance of ternary SWNT/WO ₃ /PANI nanocomposite electrodes measured through GCD current at 0.13 mA/cm ²	52
Figure 31. Impedance spectra of thin films measured within the range of 50 kHz to 50 mHz at a 0 V DCI. Inset shows the magnified high frequency region.....	53
Figure 32. (a) Schematic of the electrode preparation steps, (b) fabricated SCs from ternary composite fabrics. (c) Photographs of the dip-coated textile based electrodes.	61

Figure 33. (a) SEM images of MnO ₂ , (b) MnO ₂ /SWNT, (c) MnO ₂ /SWNT/PANI, and (d) MnO ₂ /SWNT/PEDOT:PSS coated textile electrodes. All scales are the same. Inset shows the EDS spectrum of MnO ₂ coated textile electrodes. (e) XRD pattern of the MnO ₂	63
Figure 34. Surface resistance change with respect to number of dipping cycles into ink solutions of SWNT (black), PEDOT:PSS (red) and PANI (green) solutions. Lines are for visual aid.....	64
Figure 35. CVs of SWNT (black), MnO ₂ /SWNT (red), MnO ₂ /SWNT/PEDOT:PSS (blue) and MnO ₂ /SWNT/PANI (green) coated textile based SCs at 20 mV/s scan rate.	66
Figure 36. CVs of the fabricated (a) MnO ₂ /SWNT/PANI and (b) MnO ₂ /SWNT/PEDOT:PSS ternary nanocomposite electrodes at different rates.....	67
Figure 37. CV results of fabricated SCs with (a) MnO ₂ /SWNT/PANI and (b) MnO ₂ /SWNT/PEDOT:PSS ternary nanocomposite electrodes under different bending angles at 20 mV/s scan rate.	67
Figure 38. GCD profiles of the fabricated SCs at 1 A/g.	68
Figure 39. GCD curves of fabricated SCs with (a) MnO ₂ /SWNT/PANI and (b) MnO ₂ /SWNT/PEDOT:PSS ternary nanocomposite electrodes at current densities from 0.25 to 5 mA/cm ²	69
Figure 40. C _{sp} of the fabricated SC devices (a) with respect to current density (Lines are for visual aid) and (b) with respect to cycle number.	70
Figure 41. Coulombic efficiencies of (a) SWNT, (b) MnO ₂ /SWNT, (c) MnO ₂ /SWNT/PANI and (d) MnO ₂ /SWNT/PEDOT:PSS SC devices.	71
Figure 42. Synthetic pathway for poly(4-(dithieno[3,2-b:2',3'-d]thiophen-2-yl)-2-(2-octyldodecyl)-2H-benzo[d][1,2,3]triazole).	78
Figure 43. SEM images of (a) bare SWNT and (b) SWNT/CP nanocomposite electrodes.....	79
Figure 44. (a) FTIR and (b) Raman spectra of bare SWNT and SWNT/CP nanocomposite electrodes.	80
Figure 45. UV-Vis spectra of (a) CP on ITO thin film and (b) SWNT/CP nanocomposite film electrodes. (c) Photograph of the fabricated SWNT/CP electrodes at different charged states (purple-red: -0.2 V, black: 1.1 V and blue: 1.3 V).....	81
Figure 46. CV results of the SWNT and SWNT/CP nanocomposite electrodes in 0.1 M LiClO ₄ in PC (a) at 20 mV/s and (b) at different scan rates.....	82

Figure 47. GCD curves of SWNT and SWNT/CP nanocomposite electrodes at 1.0 A/g and (b) at various current densities.	83
Figure 48. (a) Current density dependence of the specific capacitance of SWNT/CP nanocomposite electrodes. Lines are for visual aid. (b) Capacity retention and coulombic efficiency of SWNT/CP nanocomposite electrodes measured through a GCD at 1.0 A/g.	84
Figure 49. (a) Impedance spectra of the SWNT and SWNT/CP nanocomposite electrodes measured within the range of 50 kHz to 50 mHz at a 0 V DC potential. Inset shows the magnified high frequency region. (b) Impedance spectra of the SWNT/CP nanocomposite electrodes upon application of different DC potentials. Inset shows the magnified high frequency region.	85
Figure 50. Current-time diagram for MoO ₂ electrodeposition for 800 sec.	89
Figure 51. SEM images of (a) Ag NWs electrodes, Ag NW/MoO ₂ nanocomposite electrodes in low and high (b, c) resolution. (d) TEM image of Ag NW/MoO ₂ nanocomposite electrodes. (e) EDS spectrum of Ag NW/MoO ₂ nanocomposite electrodes. (f) Time-dependent thickness change of MoO ₂ layer during electrodeposition. Lines are for visual-aid.	91
Figure 52. SEM image of the Ag NW/MoO ₂ nanocomposite electrodes electrodeposited for 1600 sec.	92
Figure 53. (a) XRD pattern and (b) Raman spectrum of bare Ag NWs and Ag NW/MoO ₂ nanocomposite electrodes. (c) XPS survey spectrum of the Ag NW/MoO ₂ nanocomposite and (d) deconvoluted core level spectra of Mo 3d of Ag NW/MoO ₂ nanocomposite.	93
Figure 54. CV results of Ag NW (at 20 mV/s) and Ag NW/MoO ₂ nanocomposite electrodes in 1 M LiClO ₄ in PC at different scan rates.	95
Figure 55. (a) GCD curves of Ag NW/MoO ₂ nanocomposite electrode in 1 M LiClO ₄ in PC at currents from 0.25 A/g to 10 A/g. (b) EIS spectra of thin films (Inset: Full spectra). (c) Dependence of the specific capacitance of Ag NW/MoO ₂ nanocomposite electrodes on current density. (d) Cycling performance of Ag NW/MoO ₂ nanocomposite electrodes.	96
Figure 56. SEM images of (a) Ag NW and Ag NW/Ni(OH) ₂ nanocomposite in (b) low and (c) high resolution. (d) Change in the thickness of Ag NW/Ni(OH) ₂ nanocomposite with time during electrodeposition.	103

Figure 57 (a) XRD patterns, (b) Raman spectra and (c) XPS survey spectra of bare Ag NWs and Ag NW/ Ni(OH) ₂ nanocomposite electrodes. (d) Deconvoluted XPS spectrum for Ni 2p of Ag NW/ Ni(OH) ₂ nanocomposite.....	105
Figure 58. BF images of Ni(OH) ₂ shell on Ag NW network core before (a) and after (b) 3000 GCD cycles. The insets represent HAADF, Ni and Ag mapping for conditions (a) and (b). (c) and (d) white arrows show representative nanocrystals in Ni(OH) ₂ shell before and after cycling test.	106
Figure 59. (a) CV results of the electrodeposited Ag NW/Ni(OH) ₂ nanocomposite electrodes in 1 M KOH at 20 mV s ⁻¹ scan rate. (b) CV results of 800 second deposited nanocomposite electrode at various scan rates.....	108
Figure 60. CV results of the Ag NW/Ni(OH) ₂ nanocomposite electrodes following 200, 400, 600, 800 and 1000 bending cycles at 20 mV s ⁻¹ scan rate. Inset show photos of home made bending setup.....	109
Figure 61. GCD curves of 800 second electrodeposited sample at different currents ranging from 3 A g ⁻¹ to 50 A g ⁻¹	110
Figure 62. (a) C _{sp} of the fabricated electrodes as a function of GCD current density. Lines are for visual aid. (b) Capacity retention of Ag NW/Ni(OH) ₂ nanocomposite electrodes measured through a constant GCD at 5 A g ⁻¹	111
Figure 63. EIS spectra of 800 second deposited Ag NW/Ni(OH) ₂ nanocomposite electrodes. Inset shows high frequency part of the EIS analyses.....	112
Figure 64. (a) The molecular structure of the CP used in this work. SEM images of (b) Ag NW networks and (b) Ag NW/CP nanocomposite film on PET substrates.....	119
Figure 65. Cross-sectional SEM image of gold sputtered Ag NW/CP nanocomposite film on PET substrate.....	120
Figure 66. (a) Raman spectra of Ag NW and Ag NW/CP nanocomposite electrodes. (b) Absorbance and (c) transmittance spectra of the fabricated nanocomposite electrodes at different charged states. Inset shows a photo of the electrodes at different charged states.	121
Figure 67. CV curves of bare Ag NW electrodes at a scan rate of 20 mV/s.....	122
Figure 68. (a) CV results of the fabricated electrodes in 1 M LiClO ₄ in PC, at 20 mV s ⁻¹ . (b) at different scan rates. (c) GCD curves of the fabricated electrodes at 0.1 A g ⁻¹ current density and (d) at different current densities.....	123

Figure 69. CV curves of the fabricated electrodes following each bending cycle at 20 mV s⁻¹. (b1)- (b2) shows the photos of bending setup with flat and bended samples and (b3) photo of the fabricated flexible nanocomposite electrode..... 124

Figure 70. EIS spectra of the as-fabricated and 20000 times cycled nanocomposite electrodes. Inset shows the high-frequency region of the impedance spectra. 125

Figure 71. (a) C_{sp} change with respect to current density. (b) Cycling performance of the nanocomposite electrodes measured through GCD at 1 A g⁻¹. 126

Figure 72. (a) CV curve of the Ag NW/CP nanocomposite SC device using a 1 M LiClO₄ in PC electrolyte solution at 20 mV s⁻¹. (b) GCD curve of the fabricated SC at a current density of 0.1 A g⁻¹ 127

ABBREVIATION LIST

ACN	Acetonitrile
CMC	Carboxymethyl cellulose
CP	Conducting polymer
C_{sp}	Specific capacitance
CV	Cyclic voltammetry
EDLC	Electrical double layer capacitor
EDS	Energy dispersive X-Ray spectroscopy
EIS	Electrochemical impedance spectrometry
ESR	Equivalent series resistance
FTIR	Fourier transform infrared spectroscopy
GCD	Galvanostatic charge discharge
IR_{drop}	Internal resistance drop
ITO	Indium tin oxide
MWNT/MWCNT	Multi walled carbon nanotube
PANI	Polyaniline
PC	Propylene carbonate
PDMS	Polydimethylsiloxane
PDOPEQ	Poly(2,3-bis(3,4-bis(decyloxy)phenyl)-5,8-bis(2,3-dihydrothieno[3,4-b][1,4]dioxin-5-yl)quinoxaline)
PEDOT:PSS	Poly(3,4-ethylenedioxythiophene)–poly(styrene sulfonate)
PET	Polyethylene terephthalate
PMMA	Polymethylmethacrylate
PPy	Polypyrrole
PTFE	Polytetrafluoroethylene
PVA	Polyvinyl alcohol
SC	Supercapacitor
SDBS	Sodium dodecyl benzene sulfonate
SEM	Scanning electron microscopy
SWNT/SWCNT	Single walled carbon nanotube

TEM	Transmission electron microscopy
XPS	X-ray photoelectron spectroscopy
XRD	X-Ray diffraction

CHAPTER 1

INTRODUCTION

1.1 Historical Background and Current Status

Supercapacitors (or electrochemical capacitors, electrical double layer capacitors, ultracapacitors, SCs) are important electrochemical energy storage devices. The charge separation (or storage) was first described by Helmholtz in 1853 and he explained concept of the double layer capacitance between electrolyte and electrode at the interface [1]. The first supercapacitor devices were disclosed in a patent by General Electric Corp. in 1957 [2]. In this patent, a supercapacitor device based on high surface area porous carbon material was described. The SOHIO is the first company that attempted to commercialize the supercapacitors with carbon based electrodes and an organic electrolyte [3]. Conway and his coworkers had significant contributions to the development of supercapacitor research in 70's and 80's [4]. They developed ruthenium oxide (RuO_2) based supercapacitors with low internal resistance and high specific capacitance. In the 90's, there was an increasing demand for the supercapacitors due to the hybrid electric motor vehicles [5]. In 1998, U.S. Department of Energy started a 5-year short-term and a long term development program for supercapacitors [6].

There are many granted supercapacitor patents and first commercial supercapacitor products were developed by Pinnacle Research (USA) and Matsushita Electric Industrial (Panasonic, Japan) [7]. The electrodes of these commercial products were based on porous carbon particles with large surface area and also some metal oxides. First commercial products were applied in many systems, such as activators, circuits, power backup for memory devices [7]. Nowadays, commercial supercapacitor devices with different specifications (Figure 1) are used in thousands of different applications. They are utilized [8];

- i. in providing power for portable consumer electronics,
- ii. in capturing energy from brake systems and discharge collected energy to accelerate electrical automobiles, hybrid trains and buses,

- iii. in supplying power in emergency situations such as opening aircraft doors,
- iv. in providing energy storage for wind turbines and solar farms.



Figure 1. Supercapacitor cells and modules with different specifications [8].

There are many automobile companies that use supercapacitors in their models such as Peugeot (308 CC 1.6 e-HDi micro hybrid diesel), Citroen hybrid cars (C5 and C4), and Mazda (Mazda6) [9]. The first automobile to use a supercapacitor for capturing energy from brakes (called i-ELOOP) is Mazda's new Mazda6 (Figure 2) [10]. Maxwell Technologies Inc. declared that it produces BOOSTCAP® ultracapacitors for one of well-known automotive part suppliers (Continental AG), for Continental's "E-booster" power control unit for small cars. E-booster supports low-emission, fuel-efficient, stop-start function for Citroen and Peugeot automobiles. MAN AG produces Lion's City Hybrid Buses, which use supercapacitors and two 67 kW electric motors (Figure 3) [11]. In urban traffic, hybrid buses consume 30 % less fuel than combustion-only buses.



Figure 2. Mazda6 with layout of components in i-ELOOP [10].



Figure 3. Hybrid bus uses supercapacitors and two 67 kW electric motors [11].

1.2 Principles of Supercapacitors

Supercapacitors are controlled by the same basic principles with batteries and capacitors. On the other hand, SCs have higher capacitance and energy than the conventional capacitors. When compared to batteries, SCs have higher power density. Moreover, SCs have additional advantages over batteries such as fast charge-discharge, high cycleability, high coulombic efficiency and long shelf life. Thus, SCs have an important position between the batteries and capacitors as provided in the Ragone plot (Figure 4) [12].

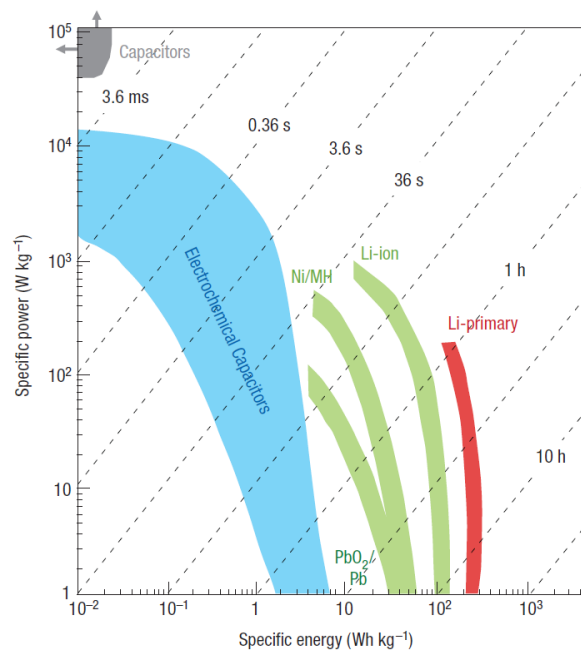


Figure 4. Ragone plot for different energy storage systems [12].

Working principle of SCs is similar to conventional capacitors with slight differences (Figure 5). In conventional capacitors, electrical charge is stored between two parallel metallic plates and an insulating ceramic, or oxide layer is used as a dielectric material. Electrolytic capacitors have electrostatic charge separation similar to ceramic or film capacitors. Anode of the capacitor is produced from metal and its native oxide coating. This oxide layer is utilized as the dielectric layer of the capacitor. An electrolyte (solid or liquid) which coats the oxide layer works as capacitor's cathode. Electrolytic capacitors have higher capacitance values than ceramic capacitors, but less capacitance values than electrochemical capacitors. On the other hand, SCs have high surface area electrodes, which store electrical charges electrostatically or through surface redox reactions.

In a typical SCs device, there are two electrodes (with current collectors) wetted with an electrolyte solution and a separator between them. The electrical charges are separated and collected on electrodes and this resulted in the energy storage as illustrated in Figure 5 [13, 14].

It seems that the collected charges of a SC device heavily depends on the electrode material's specific surface area. It is a fact that the complete electrode surface is not reachable if the electrode is not contacted with the electrolyte, therefore the collected charges of electrode material is not directly proportional with the surface area [12]. The porosity and the pore size distribution of the electrode are the key properties and the mesopores (2-50 nm) of the electrodes are very important for the electrochemical charge storage. For highest double layer capacitance, the pore size of electrode should match with the electrolyte ion size. Large or small pores result in serious capacitance drop. On the other hand, large pore size may also expand the gap between the electrode surface and ion's center, thus, decreases this material's capacitance [13]. Therefore, the capacitance of supercapacitors strongly depends on the electrode's specific surface area which is reachable by the ions.

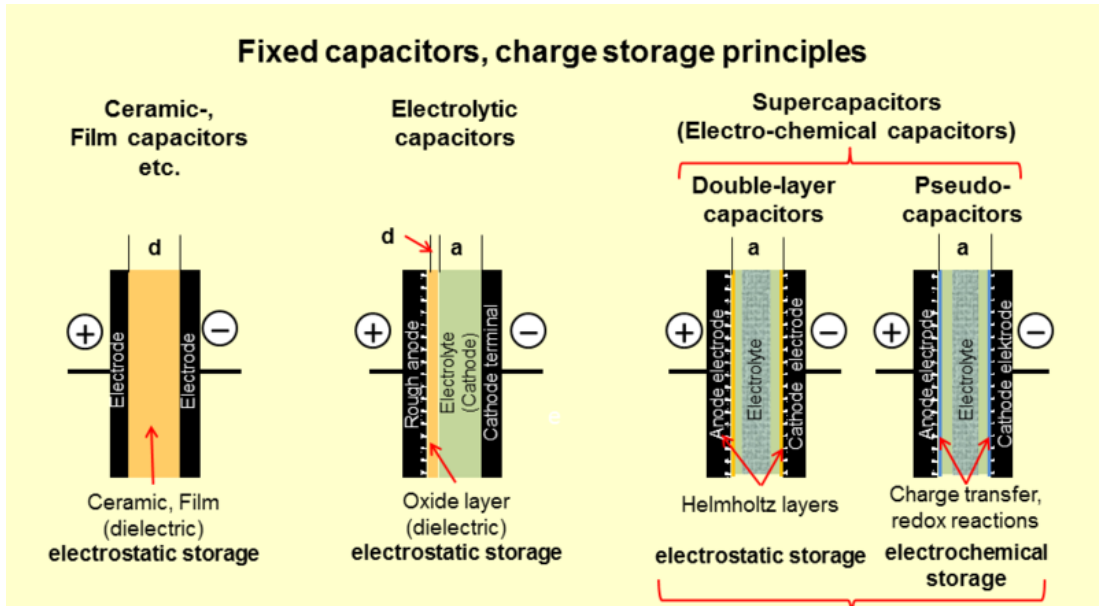


Figure 5. Charge storage mechanisms of conventional capacitors and SCs [15].

SCs differ from the batteries and the capacitors according to their electrochemical properties. The properties and the performance metrics of these devices are compared in the Table 1.

Table 1. Battery, Supercapacitor, and Capacitor Comparison.

Parameter	Battery	Supercapacitor	Capacitor
Charging Time	0.3 ~ 3 h	1 ~ 30 sec	$10^{-6} \sim 10^{-3}$ sec
Discharging Time	1 ~ 5 h	1 ~ 30 sec	$10^{-6} \sim 10^{-3}$ sec
Energy (Wh kg^{-1})	20 ~ 100	1 ~ 10	< 0.1
Power (W kg^{-1})	50 ~ 200	1,000 ~ 2,000	> 10,000
Cycle Life	500 ~ 2,000	> 100,000	> 500,000
Efficiency	0.7 ~ 0.85	0.90 ~ 0.95	~ 1.0

1.2.1 Electrical Double Layer Capacitors

Electrical double layer capacitors (EDLCs) store charges electrostatically. Charges are deposited at the interface between the electrolyte solution and the surface of porous electrodes, as shown in Figure 6. Electrical energy is achieved by the separation of electrostatic charges in a Helmholtz double layer between an electrolyte solution and the surface of a conducting electrode as shown in Figure 7 (a). Stern layer is defined for the presence of diffusive layer because of the charge accumulation on the electrode surface (Figure 7 (b)). There is a few angstrom ($3\text{--}8 \text{ \AA}$) distance between the charges in a double-layer and they are static in origin [9, 12]. EDLC type electrode active materials have lower specific capacitance (F g^{-1}) than pseudocapacitive electrode active materials. Carbon based materials with various morphologies such as powders, fibers, textiles, graphene, fullerenes and nanotubes show EDLC type behavior [16]. Low cost, high surface area, high conductivity and controllable porosity are the main advantages of carbon based materials [9].

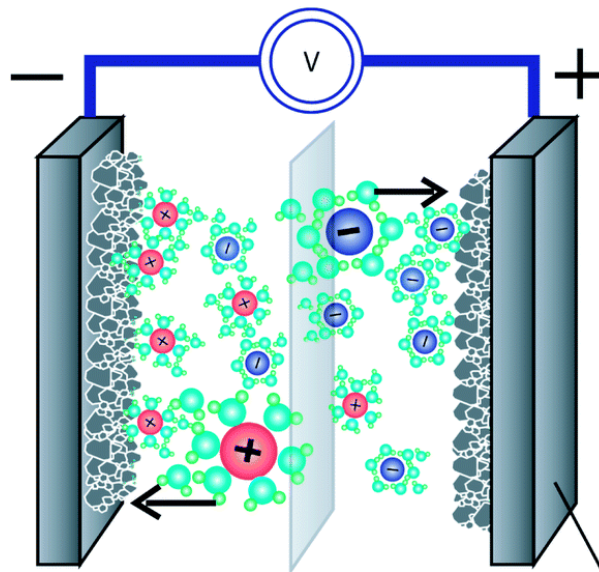


Figure 6. Basic schematic for an EDLC. Device contains an active material (*e.g.*, carbon), a current collector, a separating membrane and an electrolyte, (*e.g.*, sodium sulfate (Na_2SO_4) solutions) [17].

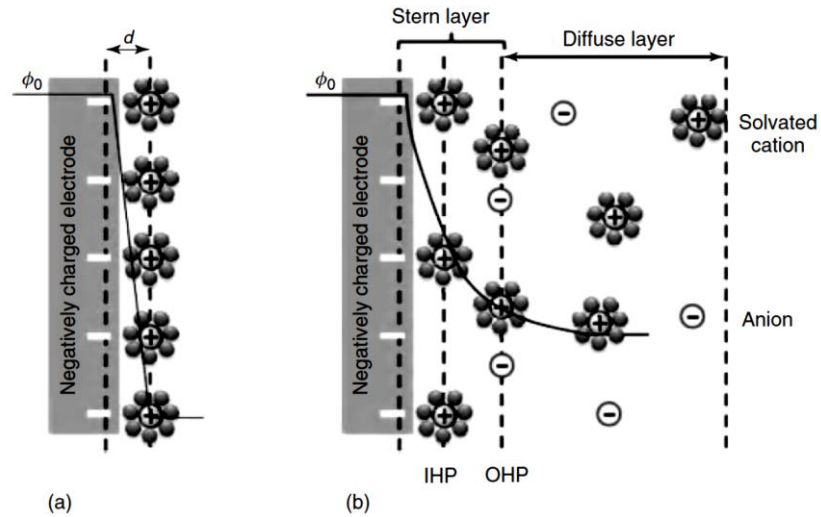


Figure 7. (a) Helmholtz and (b) Stern model of the EDLC (IHP: Inner Helmholtz path, OHP: outer Helmholtz path, d : double-layer distance, ϕ_0 :zeta potential) [9].

1.2.2 Pseudocapacitance

As discussed before, electrodes with double layer charge storage have low capacitance, for instance in the range of $10\text{--}50 \mu\text{F cm}^{-2}$ for porous carbon based electrodes. On the other hand, SC electrodes with pseudocapacitive (redox active) materials have 10–100 times higher capacitance than EDL capacitors. They both deposit electrostatic charges and also have reversible faradaic redox reactions, as shown in Figure 8 [12, 17]. Therefore, the recent research efforts are focused on the development of pseudocapacitive SC electrodes. Pseudocapacitive materials can be listed in two main groups, which are conducting polymers and transition metal oxides.

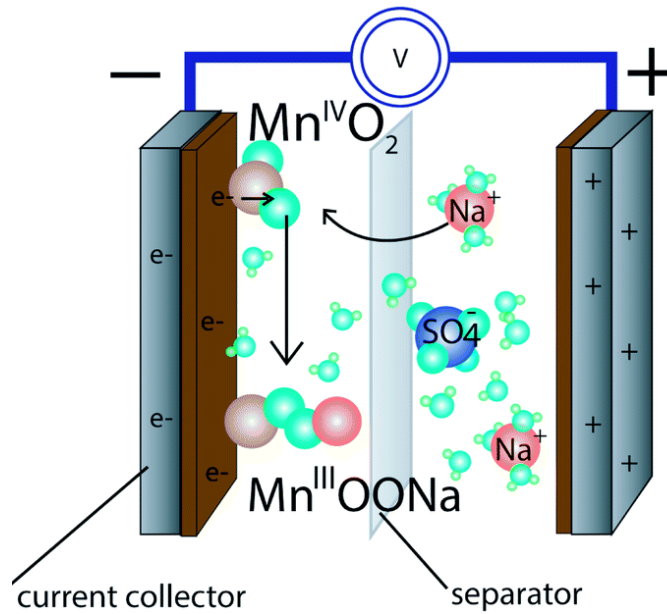


Figure 8. Basic schematic for a pseudocapacitor. Device contains an active material (*e.g.*, MnO_2), a current collector, a separating membrane and electrolyte, (*e.g.*, Na_2SO_4 solutions)[17].

Some prominent pseudocapacitive materials include:

- i. Metal oxides and hydroxides (manganese oxide (MnO_2) [18], nickel oxide (NiO) [19], molybdenum oxide (MoO_x) [20], zinc oxide (ZnO) [21], cobalt oxide (Co_3O_4), tin oxide (SnO_2) [22], iron oxide (Fe_3O_4) [23], vanadium oxide (V_2O_5) [24], titanium oxide (TiO_2) [25], tungsten oxide (WO_3) [26], and iridium oxide (IrO_2) [27]).
- ii. Conducting polymers (polypyrrole [28], polythiophene [29], polyaniline [30] and their derivatives [31]).

1.3 Types of Supercapacitors

SCs are classified according to their electrode active materials. There are three main types of electrode active materials for supercapacitors, which are carbon, metal oxide and conducting polymer based materials. The charge storage mechanism of SCs rely on the active electrode materials (Figure 9).

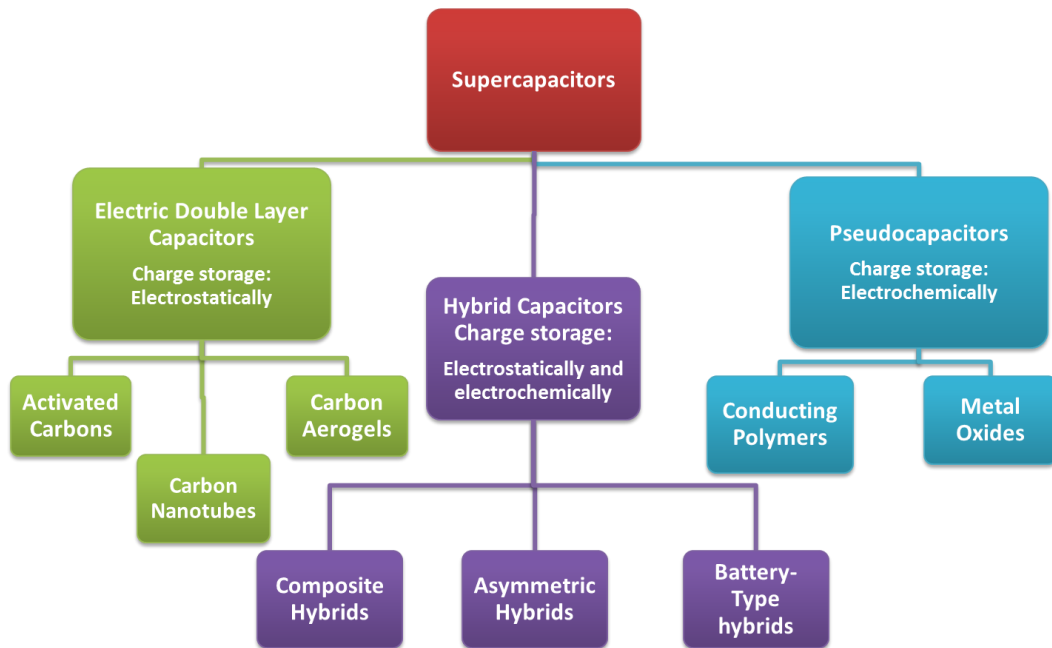


Figure 9. Taxonomy of supercapacitors.

1.3.1 Carbon Based Supercapacitors

Carbon based electrode active materials are promising for commercial SCs. There are many allotropes of carbon as shown in the Figure 10. The main advantages of these materials include light weight, abundance, easy processing, low cost, high conductivity, high surface area, non-toxicity, large operating temperature range and high stability. All these advantages that resulted in the commercialization of carbon based SCs [32]. Typical surface areas of activated carbon, carbon aerogel, carbon cloth and graphene lie in between 1000 ~ 2000 m²/g. Physical and chemical activation processes improve the specific surface area and the porosity of the carbon based electrode materials [33].

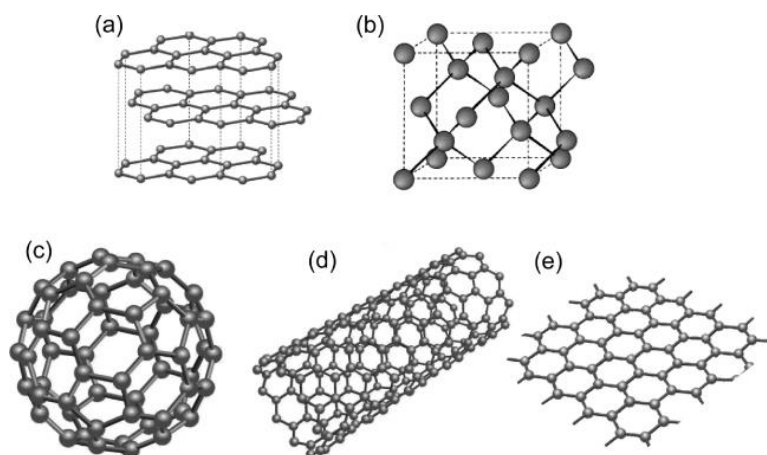


Figure 10. Schematics of carbon based materials (a) graphite, (b) diamond, (c) buckminsterfullerene (C_{60}), (d) nanotube and (e) graphene [34].

The specific capacitance of the carbon based materials are commonly determined by their surface area and the porosity. In addition to this, conductivity and number of accessible pores are also closely related with the capacitance of the electrodes. Surface functionalization can also be used to improve the charge storage properties of the carbon based electrode materials. Functional groups on the surface develop the hydrophilicity of electrodes and this enhances the adsorption of electrolyte ions that lead to rapid and facilitated ion transport and enhanced wettability within the micropores. Functionalized carbon based materials have a specific capacitance increase due to the pseudocapacitance (approximately a 5–10 % capacitance increase) instead of double layer capacitance [35].

The specific surface area, pore structure, pore-size distribution, and shape, surface functionality and electrical conductivity are important properties that affect the electrochemical performance of carbon based electrodes. The specific surface area and the pore-size distribution are the most important factors influencing the SC performance [36]. Conway claimed that the carbon based SCs must have three properties [37]:

- (1) high specific surface area, ($> 1000 \text{ m}^2/\text{g}$),
- (2) good conductivity and
- (3) high accessibility for electrolyte ions.

1.3.2 Metal Oxide Based Supercapacitors

Metal oxides are an important material group for the SCs due to their reversible redox reactions on their surfaces. Ruthenium oxide (RuO_2) is the first metal oxide, which was investigated in the SC studies due to its conductive nature and high charge storage performance [4, 38]. On the other hand, scarcity of ruthenium and its cost restricted the use of RuO_2 in supercapacitor applications. Alternative cheap transition metal oxides such as manganese oxide (MnO_2) [18], nickel oxide (NiO) [19], molybdenum oxide (MoO_x) [20], zinc oxide (ZnO) [21], cobalt oxide (Co_3O_4), tin oxide (SnO_2) [22], iron oxide (Fe_3O_4) [23], vanadium oxide (V_2O_5) [24], titanium oxide (TiO_2) [25], tungsten oxide (WO_3) [26], and iridium oxide (IrO_2) [27] are investigated for supercapacitor electrodes. The main drawbacks of metal oxides are poor cycleability and low conductivities.

The general conditions for metal oxide based supercapacitor electrodes are [32]:

(a) High surface area. Improving the surface area allows the metal centers to provide more multiple redox reactions and it will increase the specific capacitance.

(b) The hydrate in metal oxide. The reversible faradaic reactions need ion exchange.

(c) The crystallinity of metal oxide. The pseudocapacitance of metal oxide depends on the crystallinity. Amorphous metal oxides have less diffusion limitations than the well crystallized counterparts.

(d) The size of $\text{MO}_x \cdot a\text{H}_2\text{O}$. To shorten diffusion path and to facilitate ionic conductivity, small metal oxide particles are important.

(e) Properties of electrolyte solution.

Generally, metal oxide based SC electrodes have higher stability than conducting polymers and greter energy density than carbon based electrode materials. Nanocomposites of metal oxides with conductive additives such as CNTs, carbon black, graphene and metallic nanomaterials enhance the electrochemical properties of metal oxides and improve the specific capacitances.

1.3.3 Conducting Polymer Based Supercapacitors

Conducting polymers (also known as π -conjugated polymers, CPs) are promising materials for the realization of high performance SCs. They have high conductivities in the charged state and fast charge-discharge properties. These properties allow development of SCs with decreased equivalent series resistance (ESR) and enhanced energy and power densities. CPs hold many other advantages and some of these advantages are good conductivity (in a doped state), superior storage capacity, large potential window, low cost and chemically tunable redox properties [12].

Pseudocapacitance of CPs depend on the reversible redox reactions. During oxidation reactions, electrolyte ions are moved to the backbone of polymer and then liberated to the electrolyte during reduction reactions. Reversible redox processes in the polymer take place throughout whole polymer not only on the polymer surfaces. These reactions are highly reversible and do not cause any phase changes during charge-discharge processes [9].

CPs may have different charges (positive or negative) depending on ion insertion as shown in Figure 11. Oxidized polymers which are positively charged are called as ‘p-doped’ and reduced polymers that are negatively charged are called as ‘n-doped’ [32].

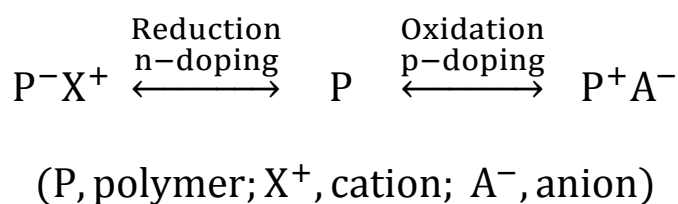


Figure 11. Doping process of CPs.

Many CPs have been extensively examined as active SC electrode materials. In energy storage applications, the most commonly used ones are polythiophene (PTh) [29], polypyrrole (PPy) [28], polyaniline (PANI) [30] and their derivatives [31], structures of which are provided in Figure 12. PPy and PANI are p-doped polymers and they are commonly used as cathodes. Polythiophene and its derivatives can be p- or n-type doped.

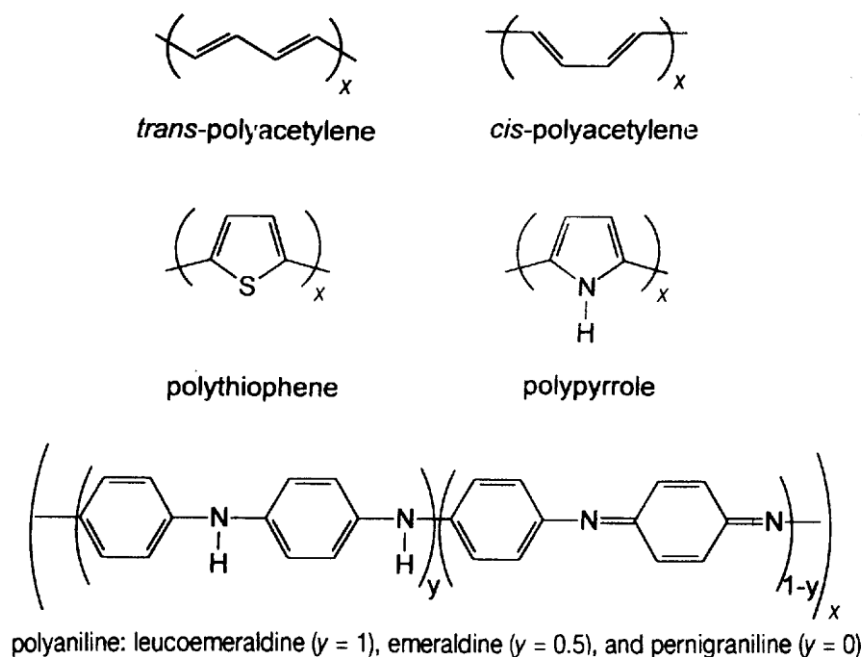


Figure 12. Structures of electrically conducting polymers [39].

To improve the electrochemical properties of CPs, they are formed nanocomposites with other conductive or capacitance materials such as carbon based materials [40-42], CNTs [43, 44] and metal oxides [45-47]. Nanocomposites of CPs with carbonaceous additives are especially important since both the specific surface area and the conductivity can be enhanced. The CNT based nanocomposites showed improved cycleability performance for the fabricated SC devices [44]. CNT/CP nanocomposites also have many other advantages such as decreased charge transfer resistance, improved wettability and electrolyte access, increased utilization of the CP and improved mechanical properties. In addition to this, in nanocomposite form CNTs also contribute to the double layer capacitance [43, 48].

1.4 Electrolytes

Electrolyte is a crucial part of the SC devices. Electrochemical properties of the SC devices rely on the electrochemically accessible pores of the electrodes and the compatibility of electrolyte ion size. Electrolyte's conductivity and the electrode-electrolyte compatibility is also crucial for enhancing the charge transport and capacitance. Chemical stability of the electrolyte solution in operating potential

window and temperature conditions determine the service life of the SC. The basic characteristics of the electrolyte solution are low flammability, low volatility, high decomposition resistance and low corrosion potential. Electrolyte solutions can be aqueous, organic, ionic liquids and polymer based solid electrolytes.

For an optimized SC system, electrolyte choice should be done according to ion size (electrolyte) and pore size (electrode) to decrease the resistance and self-discharge of the current.

1.4.1 Aqueous Electrolytes

Aqueous electrolytes are commonly preferred for their availability and low cost. Aqueous electrolytes can be utilized in ambient conditions and there is no need to use expensive inert atmosphere or glovebox environment. High conductivity, low hazard level and high ion mobility are the key benefits of aqueous electrolytes. There are many inorganic salts to be utilized in electrolytic solutions; however, chosen salt must be safe for the electrode active materials and should not damage the electrodes. Acidic electrolytes such as sulfuric acid (H_2SO_4), basic electrolytes such as potassium hydroxide (KOH) and neutral salts such as lithium sulfate (Li_2SO_4) are the most commonly used electrolyte solutions. Most aqueous electrolyte solutions have a potential window of 1 V and this value changes with respect to the pH of the solution. Therefore, it is crucial to choose a suitable operating potential window without electrolyte decomposition.

1.4.2 Organic Electrolytes

In SC market, most of the products use organic electrolytes due to their large potential window. Diethyl carbonate, tetrahydrofuran, propylene carbonate, acetonitrile, and γ -butyrolactone are the most commonly utilized organic solvents. These solvents are frequently used with the lithium salts such as lithium perchlorate (LiClO_4) or quaternary ammonium salts (tetraethylammonium tetrafluoroborate ($\text{N}(\text{Et})_4\text{BF}_4$)) or alkyl ammonium salts (triethyl(methyl) tetrafluoroborate ($\text{NMe}(\text{Et})_3\text{BF}_4$)). Organic electrolyte solutions usually have higher costs than aqueous electrolytes; however, they provide a larger potential window (typically 2.7 V) and

wider operating temperature window than the aqueous electrolyte solutions. Organic electrolytes provide higher energy density due to large potential windows and lower power density because of low ionic conductivity compared to the aqueous electrolytes.

1.4.3 Ionic Liquid Electrolytes

Ionic liquid (IL) electrolytes are very desirable due to their high ionic conductivity, large potential window, low vapor pressure and high thermal stability. The composition of the IL determines the potential window and the conductivity of the electrolyte increases with temperature. Therefore, ILs are not preferred for room temperature applications. However, at high temperatures, IL shows better performance than the aqueous and organic electrolytes due to its improved conductivity. Similar to organic electrolytes, the large potential window offered by ILs enhances energy density of the SC devices [12].

1.4.4 Gel or Solid State Polymer Electrolytes

Solid state polymer electrolytes are a combination of an acid, base or salt and a polymer matrix, which allows the ion mobility. Polyvinyl alcohol (PVA), poly(methylmethacrylate) (PMMA) and cellulose acetate (CA) are the most commonly used polymer matrixes for solid state electrolytes. Solid state electrolytes have lower conductivity than the aqueous and organic electrolytes; however, they supply better structural integrity than the liquid electrolytes. Gel electrolytes also eliminate the use of separators.

1.5 Electrochemical Testing

1.5.1 Electrochemical Cell

Electrochemical test cell configuration is very important to obtain the exact electrochemical performance of the electrode active materials. Test configuration significantly affects the obtained results. Therefore, cell design should be clearly described for proper evaluation and comparison.

1.5.1.1 Three-Electrode Configuration

Three electrode (or single electrode, half-cell) configuration contains a reference electrode, a working electrode, a counter electrode and an electrolyte solution. In three-electrode configuration, only working electrode include the electrode active material to be analyzed. Counter electrode (Platinum (Pt) foil or graphite rod) is used to compensate the charge polarization with respect to the working electrode. Therefore, counter electrode should have equal and/or larger surface area than the working electrode. A reference electrode is also used in the three electrode configuration and it measures the potential difference with respect to the working electrode. Normal hydrogen electrode (NHE), silver/silver chloride electrode (Ag/AgCl), reversible hydrogen electrode (RHE) and saturated calomel electrode (SCE) are the most commonly used standard reference electrodes.

The advantages of three-electrode configuration compared to two-electrode configuration can be listed as follows [9, 49, 50]. Firstly, reference electrode is used in three-electrode configuration and it monitors the applied potential. Secondly, three-electrode configuration gives more detailed results and have high sensitivity for the characterization of electrode active materials in working electrode. Lastly, it is possible and highly practical to test small size or tiny amounts of electrode active materials [50].

1.5.1.2 Two-Electrode Configuration

Two-electrode configuration (or full device) is most commonly used for testing full SC devices (including electrodes, electrolyte, separator, current collectors etc.) [49]. In this configuration, both electrodes (positive and negative) have the electrode active materials and the obtained electrochemical results are a combination of both electrodes. Two-electrode configuration is the most realistic scenario for an actual device. On the other hand, this configuration has difficulties to characterize asymmetric electrodes and nanocomposite electrodes. As shown in Figure 13, same electrodes have different electrochemical results and three-electrode configuration is more advantageous to analyze electrode active materials than the two-electrode configuration [49-51]. In two-electrode configuration, redox peaks of the

pseudocapacitive material was suppressed and it is almost impossible to diagnose redox activities.

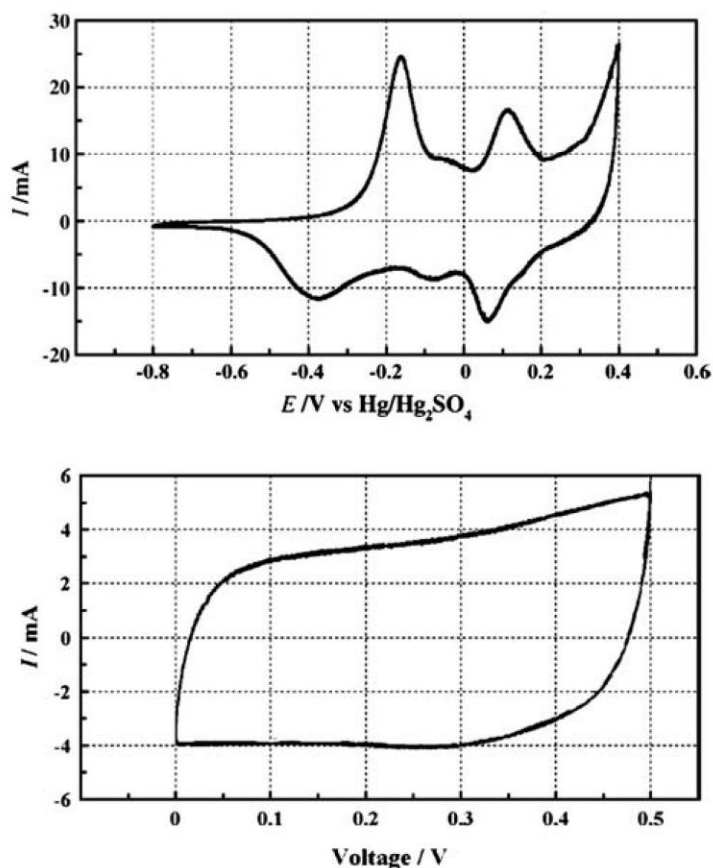


Figure 13. Cyclic voltammetry results of identical PANI/MWNT electrodes using three-electrode (top) and two-electrode (bottom) configuration [51].

1.5.2 Cyclic Voltammetry Measurements

Cyclic voltammetry (CV) is the most commonly used electrochemical technique and this potentiodynamic technique is utilized to collect qualitative and also quantitative data. CV measurements provide information about the electrochemical reaction kinetics, reversibility and mechanisms of reactions that take place on the electrode surface and in the electrolyte solution. CV measurements are made using a potential or voltage window and in this window, electrode potential is scanned and the current is recorded.

CV measurement provide in valuable information about the fabricated SC or its electrodes. For SCs, an ideal CV curve shape is rectangular and in some circumstances,

this rectangular shape deviates from ideality. Typical CV curve shapes for SCs are provided in Figure 14. For instance, SC with resistance have a parallelogram shape. For pseudocapacitive materials, redox peaks may appear in the CV curve [33].

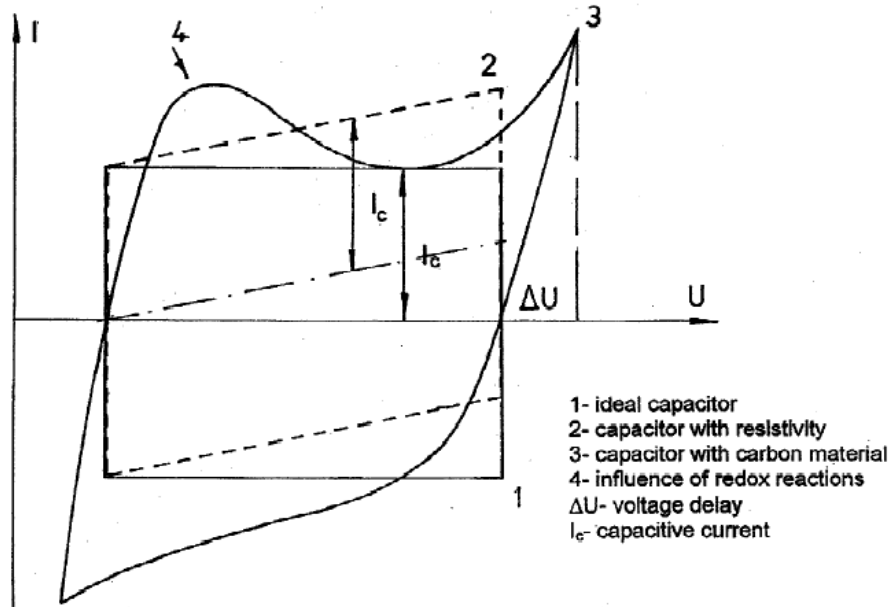


Figure 14. Typical CV curve shapes for supercapacitors [33].

Depending on the scan rate, electrochemical properties of the electrodes can be monitored and specific capacitance (C_{sp}) values can be calculated. For two-electrode configuration, the integration of the area within the CV curves provides the specific capacitance according to the formula:

$$C_{sp} = \frac{2}{m(V_2 - V_1)} \int_{t=0(V_1)}^{t(V_2)} i(V)dt$$

where i (A) is the measured current, m (g) is the mass of total active material in both electrodes, V_1 and V_2 are the initial and final voltage values within the voltage window.

For an ideal SC device, C_{sp} should be the same for all scan rates; however, in reality, C_{sp} value decreases due to slow reaction kinetics at high scan rates.

1.5.3 Galvanostatic Charge-Discharge (Chronopotentiometry) Measurements

Galvanostatic charge-discharge (GCD) or chronopotentiometry is the most reliable technique employed in SC studies. In this technique, constant current is applied in an entire potential or voltage window and obtained results were recorded with respect to time. This technique gives information about resistance, capacitance and cycle life of the SC devices.

C_{sp} value can be calculated using GCD curves by two different methods. For EDLC type materials, which have triangular GCD curve (or constant slope), C_{sp} is determined according to formula;

$$C_{sp} = \frac{I}{m \frac{\Delta V}{\Delta t}}$$

,where C_{sp} ($F g^{-1}$) is the specific capacitance, ΔV (V) is the potential window, m (g) is the total weight of electrode active materials, I (A) is the applied discharge current and the Δt (s) is the measured discharge time.

Pseudocapacitive materials and/or battery-type materials do not have a constant discharge slope. Thus, it is difficult to calculate C_{sp} for these material from the discharge slope. In this case, the integral of the area under the discharge curve give the discharge energy of the SC electrodes which allows the accurate calculation of C_{sp} values. GCD curves are used to calculate discharge energy (E), cell capacitance (C_{cell}) and C_{sp} of the fabricated devices according to the equations:

$$E = I \int_{t(V_{max})}^{t(V_{min})} V(t) dt \quad C_{cell} = \frac{2E}{V_{max}^2} \quad C_{sp} = 4C_{cell}$$

,where I (A) is the applied discharge current, V (V) is the voltage range after IR_{drop} , m (g) is the weight of the materials in both electrodes and t (s) is the discharge time. C_{cell} has two serially connected identical electrodes and contains the total mass of both electrodes. Therefore, calculated C_{sp} is 4 times higher than the C_{cell} value [50].

Energy (E_d) and power densities (P_d) of the fabricated SCs are computed using equations:

$$E_d = \frac{E}{m \cdot 3.6} \quad P_d = \frac{3600 \cdot E_d}{t}$$

where E is the discharge energy, t is the galvanostatic discharge time and m is the total weight in electrodes.

Energy and power densities of electrochemical storage devices are compared to other devices using Ragone plot (Figure 4). Therefore, fabricated supercapacitor devices with superior power and energy densities may be seen in upper right side of the Ragone plot.

1.5.4 Electrochemical Impedance Spectrometry (EIS)

Electrochemical impedance spectrometry (EIS) significantly differs from CV and GCD techniques, because it utilizes alternating current and voltage that are a function of frequency, while CV and GCD use direct current and voltage. Impedance (Z) can be explained as a function of oscillating frequency ($\omega = 2\pi f$):

$$Z(\omega) = Z_0 (\cos(\varphi) + j\sin(\varphi))$$

Given formula show that small phase angle ($0 < \varphi < -45^\circ$) are subjected to electrical resistivity and larger phase angle ($-45^\circ < \varphi < -90^\circ$) are subjected to capacitive properties of the SC devices. As shown in Figure 15, each SC device should have a physical model and it should be explained by an equivalent circuit model [9]. EIS is the best technique to explain intrinsic properties of SCs with all its components. Nyquist plot is used to demonstrate EIS results through comparing the real (Z') and imaginary ($-Z''$) components of the impedance (Figure 16). An equivalent circuit model used to fit EIS data is shown in Figure 16 [52]. The best circuit model is the simplest model, which fits the data and it may be easier to simplify model for the porous or composite electrodes. In the high frequency region, the intercept on the real axis (Z') shows the internal resistance (R_s) of the supercapacitor as a consequence of the electrolyte, electrode and current collector's resistance. A semicircle, observed at the high frequency region, originates from the contact and charge transfer resistances in the electrodes (R_{ct}).

There is a perpendicular line in the mid-frequency region of the Nyquist plot with a -45° angle. This is known as the Warburg resistance (W), which is due to the ionic diffusion in the interface. In some Nyquist plots, there is also a clear “knee” frequency, which is accounted for ionic impedance and bulk transport limits in the

supercapacitors. Knee frequency determines where the capacitive behavior dominates at the highest frequency. On the other hand, the vertical line with a sharp slope in low frequency region shows the capacitive behavior of the SC devices. Deviations from the sharp slope (90°) may be a result of the porous electrodes of the SCs.

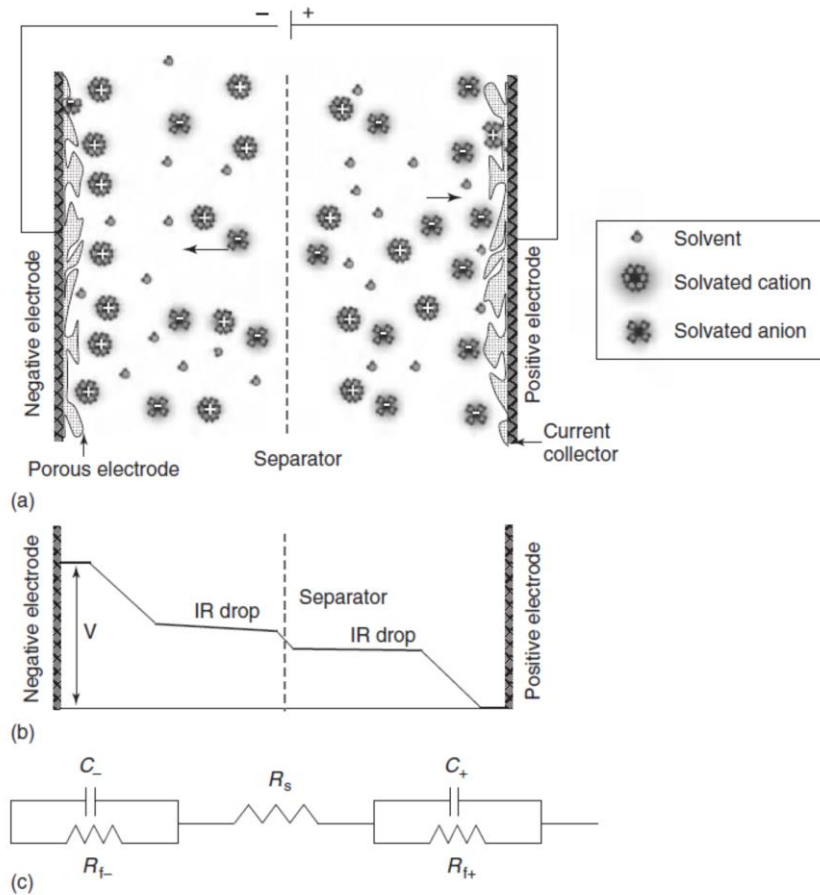


Figure 15. (a) Schematic of a typical supercapacitor with, (b) its potential profile at charged state and (c) its equivalent circuit model [9].

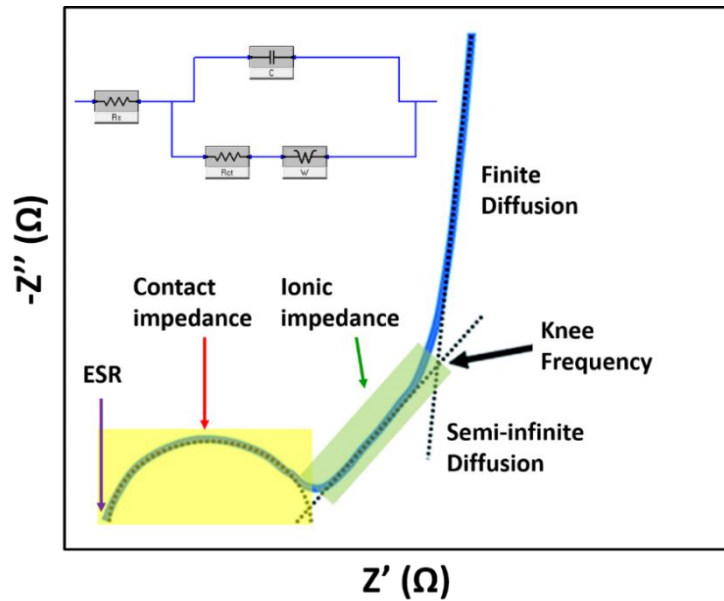


Figure 16. Typical Nyquist plot and its specific resistive and capacitive regions.

1.6 Carbon Nanotubes

Following the discovery of multi-walled carbon nanotubes (MWNT) by Iijima, carbon nanotubes (CNTs) became very important for both academic and industrial research because of their remarkable properties [53-55]. Most common production techniques of CNTs are laser-ablation, arc discharge, chemical vapor deposition (catalytic growth) and high-pressure carbon monoxide (CO) disproportionation (HiPCO) [56].

The electrical and thermal conductivity as well as mechanical properties of CNTs are exceptional. The Young's modulus and tensile strength of an individual Single walled carbon nanotubes (SWNT) can be up to 640 GPa and 37 GPa, respectively. SWNTs have an electrical conductivity of 10^6 S/m at room temperature, while that of aligned MWNTs can be 5000 S/m. Some small diameter SWNTs were found to exhibit superconductivity at low temperatures. Thermal conductivity of a SWNT is 6600 W/m.K at room temperature, whereas that of an individual MWNT is higher than 3000 W/m.K [54, 55].

The specific surface areas of SWNTs can be 1315 m^2/g and 400 m^2/g for tubes with a diameters of 1 and 7 nm, respectively [13]. CNTs have many different applications such as field emission displays, high-strength composites, hydrogen

storage media, energy storage and energy conversion devices, nanometer-sized semiconductor devices, rectifying diodes, radiation sources, interconnects, field-effect transistors, probes, sensors, single electron transistors [13].

In this thesis, SWNTs were preferred over MWNTs, this is due to better dispersibility and better thin film forming ability of SWNTs.

1.7 Carbon Nanotube Based Supercapacitors

CNTs are highly promising as SC electrode materials. High specific surface area and excellent conductivity of the CNTs is responsible for their encouraging electrochemical performance in SC devices.

C_{sp} values of CNT based SC electrodes range between 20 F g^{-1} and 300 F g^{-1} [9]. Niu et al. first reported a C_{sp} value of 113 F g^{-1} for MWNTs using sulfuric acid (H_2SO_4) solution as the electrolyte [57]. Ma et al. on the other hand reported relatively low C_{sp} values of $15\text{-}25 \text{ F g}^{-1}$ within H_2SO_4 solution [58]. SWNT bucky paper electrodes showed C_{sp} values of 40 F g^{-1} and $20\text{-}40 \text{ F g}^{-1}$ in 6 M potassium hydroxide (KOH) and sodium chloride (NaCl) solutions, respectively [59]. Shiraishi et al reported similar results for SWNTs in 1 M lithium perchlorate (LiClO_4)/propylene carbonate (PC) electrolyte [60]. On the other hand, a C_{sp} of 280 F g^{-1} for SWNT electrode with 0.1 M tetrabutylammonium hexafluorophosphate in acetonitrile electrolyte was reported by Liu et al. [61].

Functionable surfaces of the CNTs also allow the nanocomposite formation with metal oxides and CPs. As discussed earlier, the pseudocapacitance may increase, which the charge transfer resistance decreases in nanocomposite form.

1.8 Silver Nanowires

Among one-dimensional nanomaterials, silver nanowires (Ag NWs) draw extensive attention due to their high metallic conductivity and high aspect ratios. They were utilized in different devices such as photonic crystals [62], organic light emitting diodes (OLEDs) [63], photodetectors [64], catalysis [65], surface-enhanced Raman scattering (SERS) [66], biological nanosensors [67], organic solar cells [68] and energy storage devices [69-74].

There are several synthesis methods for Ag NWs and some of these methods include chemical synthesis [75], porous materials template [76], electrochemical technique [77], DNA template [78], hydrothermal method [79], ultraviolet irradiation photoreduction technique [80] and polyol process [81, 82]. Among all these methods, polyol method is the most promising one due to its easy processability, high yield, low cost and low amount of side products. Polyol method for the Ag NW synthesis was developed by Xia and co-workers [82]. In this method, poly(vinylpyrrolidone) (PVP), ethylene glycol (EG), and silver nitrate (AgNO_3) were used. Many studies followed this one in the literature with an intention to improve the polyol process of Ag NWs [81]. Synthesized Ag NWs may be deposited onto various substrates in the form of a thin film via spray, dip or spin coating techniques to form conductive Ag NW random network films.

Ag NW networks on glass or poly(ethyleneterephthalate) (PET) substrates show comparable sheet resistance and transparency values when compared to indium tin oxide (ITO) thin films. ITO is the most widely used and commercialized transparent conducting thin film because of its high conductivity and transparency in visible wavelengths. On the other hand, ITO has a brittle nature and this limits its use in flexible devices. In addition to this, limited resources of indium forces researchers to look for alternative transparent conducting films. Ag NWs that are synthesized through solution based polyol method can be used as alternative conductive electrode materials. Since Ag NWs have high aspect ratio, it is possible to obtain networks with low sheet resistance even at low nanowire densities. These random network films are also highly encouraging as supercapacitor electrodes due to high conductivity and good mechanical stability [69-74].

1.9 Silver Nanowire Based Supercapacitors

Nanomaterials with modified structure or design would improve the charge storage and decrease internal resistance of the SC devices. Ag NWs may be utilized in SCs as transparent conducting thin films on different substrates or conductive cores in core-shell structured nanocomposites. Both approaches have advantages with respect to the SC electrode specifications.

For efficient SC devices, both the charge collector and the electrode active material should be integrated. Active surfaces of Ag NWs allow the deposition of capacitive materials to get a core-shell or layered morphology. These nanostructures with Ag NWs advance charge transport and decrease the overall resistance, which seriously affect the electrochemical performance of the SC devices. Therefore, Ag NWs were utilized in SC devices in conjunction with graphene [72, 83], poly(3,4-ethylenedioxythiophene) polystyrene sulfonate (PEDOT:PSS) [69] and ITO [84] in a layered form. However, in these studies, Ag NWs were utilized with additional current collectors and active electrode materials were fabricated as a thin film onto charge collectors. Therefore, Ag NWs might have had a limited contribution to the charge transfer. On the other hand, in a core-shell architecture, nanocomposites with Ag NWs are highly encouraging for SC electrodes with a potential to decrease their internal resistance [73, 74].

DISSERTATION OBJECTIVES

According to recent studies, CNT and Ag NW based nanocomposites are highly promising for SC electrodes. On the other hand, there are no systematic studies to show electrochemical performance of these devices with smart functionalities such as bendability, transparency and color change. The aim of this dissertation is to investigate electrochemical properties of the nanocomposite SC devices using one-dimensional conductive nanomaterials.

The dissertation aims to fundamentally address the following important, unresolved scientific questions:

1. Is it possible to add smart functionalities to SC electrodes while retaining their electrochemical performance?
2. What is the influence of nanocomposite formation on the electrochemical performance of the SCs?
3. How one-dimensional conductive nanomaterials can be integrated to the SCs?

Seven specific chapters address these questions with the following objectives:

1. To investigate transparent and flexible CNT based SCs (Chapter 2),
2. To investigate the synergistic effect of ternary nanocomposite (SWNT/WO₃/PANI) formation on SC performance (Chapter 3),
3. To investigate the integration of nanocomposite electrode active materials on textile substrates and their electrochemical performances (Chapter 4),
4. To investigate electrochemical and spectroelectrochemical performance of CNT/CP based nanocomposite electrodes (Chapter 5),
5. To investigate the electrochemical performance of Ag NW/metal oxide based nanocomposite electrodes (Chapter 6 & 7),
6. To investigate electrochemical and spectroelectrochemical performance of Ag NW/CP based nanocomposite electrodes (Chapter 8).

CHAPTER 2

TRANSPARENT AND FLEXIBLE SUPERCAPACITORS WITH SINGLE WALLED CARBON NANOTUBE THIN FILM ELECTRODES

2.1 Introduction

SCs have received a lot of attention due to their high specific power and moderate energy densities. They have wide application areas spanning from electric vehicles to portable devices [12, 85, 86]. Significant efforts have been spent in the development of the basic parts of transparent and flexible devices, opening possibilities for new device concepts and form factors [87-91].

SC electrodes are highly attractive because of their good conductivity, chemical inertness and permeability [32, 33, 90, 91]. For practical device applications, these characteristics together with the fact that carbon typically forms a purely double layer make SWNT thin films unique. Other alternatives like pseudocapacitive materials, such as CPs and metal oxides (e.g. RuO_2 , MnO_2 and IrO_2) tend to suffer from reduced cyclability and power densities [32, 90, 91]. SWNT thin film electrodes, in fact, have already been successfully demonstrated in prototype devices, such as photodetectors [92], solar cells [93] and polymer light emitting diodes [94]. An alternative transparent electrode candidate, CPs, revealed high capacitance; but, showed rapid degradation, volumetric changes and limited cycle life [95]. In addition, CP electrodes are limited to work in a strict potential window. Possible over-charging and discharging during operation can easily damage the CPs [32]. Chemical routes, on the other hand, have difficulties in the synthesis of CPs [32, 43]. Many CPs have more than one oxidation step. Moreover, some polymers should be doped to increase their conductivities [88, 96]. Charged state and the doping nature of the CPs affect their electrochemical performance. Because of this, they are suited only for particular electrode and/or electrolyte systems. Therefore, it is difficult to use CPs as electrodes in a symmetric SC assembly [51].

Metal-oxide SCs have high specific capacity; but, they are not inherently conducting and necessitate the use of metallic or conductive fillers in a composite structure [97]. In addition, the optoelectronic properties and especially flexibility of thin film crystalline metal oxide (e.g. MnO_2 [98], RuO_2 [99], ITO [100]) SCs are far from that of the SWNT thin films [90, 101]. SWNT thin film electrodes can be made highly transparent and can be simply deposited onto poly(dimethylsiloxane) (PDMS) and PET substrates for the realization of flexible electrodes. The sheet resistance of SWNT films can simply be tuned with the nanotube density. Attained values are competitive to that of commercially used ITO thin films.

Electrolyte is another fundamental component of the SCs. Aqueous electrolytes have high ionic conductivity; but, they have distortion at near 1 V due to the electrolysis of water. Thus, they have narrower voltage window than organic electrolytes [102]. Besides, they can damage electrode active materials and metallic contacts in long term. In addition, liquid electrolytes have the risk of leakage, which could deteriorate electrochemical performance and is harmful. This adds the requirement of stricter packaging configurations. Solid electrolytes are available; but, their room temperature conductivity is lower than liquid electrolytes for high power applications. Organic gel electrolytes provide a good balance. They are physically more robust than liquid electrolytes whilst maintaining good ionic conductivity. In addition, organics also permit a large potential window up to 2.5 V [103]. The most commonly used gel electrolytes are composed of H_3PO_4 (or H_2SO_4) and polyvinyl alcohol (PVA).

In this work, we have fabricated transparent and flexible SWNT based supercapacitors using a gel electrolyte on PDMS substrates.

2.2 Experimental

2.2.1 Preparation of Samples

SWNTs were purchased from Carbon Solutions Inc. (SWNT P3, metal content 5-7 wt % from TGA in air and carbonaceous content more than 90 %). All other materials used in this work were of analytical grade and were purchased from Sigma-Aldrich and used without further purification.

PDMS preparation was done using Dow Corning's Sylgard 184 elastomer kit. Depending on the preparation parameters and thickness, one can tune the flexibility of PDMS. The curing agent and base mixed at a ratio of 1:10 in a petri dish. Following mixing, PDMS was stored at room temperature for one hour and then kept under vacuum for 12 hours. Elastomeric PDMS substrate was then cut into small pieces. Size and thickness of the PDMS substrates were 2 x 2 and 0.3 cm, respectively.

SWNT thin films were transferred onto, PDMS and PET substrates via vacuum filtration and consecutive stamping method [98]. As a substrate, PDMS is good in terms of its flexibility, chemical inertness and optically transparency. It also provides strong adhesion to various surfaces. It has already been used in microelectromechanical systems and microfluidic device fabrication, contact lens manufacturing, soft lithography and device encapsulation [104-110].

Following deposition, SWNT electrodes were treated with nitric acid (HNO_3 , 65 %) for 3 hours to improve their conductivity. The resulting circular thin films had an area of 2 cm^2 . Transmittance and sheet resistance of the prepared SWNT electrode was controlled with the filtration volume.

The gel electrolyte with a composition of tetrabutylammonium hexafluorophosphate (TBAPF_6): poly(methylmethacrylate) (PMMA): propylene carbonate (PC): acetonitrile (ACN) in a ratio of 3:7:20:70 by weight was used in SC devices. The gel electrolyte was produced by first dissolving TBAPF_6 and PMMA in ACN and slowly evaporating the ACN to reach a honey-viscous condition ($\sim 3 \text{ mS/cm}$) [103].

To fabricate SCs, conductive carbon paste was used as an external current collector. A commercial Celgard separator (Celgard 3401) was used as the separator. It was soaked in the gel electrolyte and sandwiched between two SWNT electrodes as shown in the schematic provided in Figure 17 (a). The SC device was then sealed with epoxy.

2.2.2 Characterizations

The structure and morphology of the fabricated SWNT thin films were characterized using SEM (FEI Nova Nano SEM 430, operated at 10 kV). Electrochemical performance of the SCs were investigated in a two-electrode setup using potentiostat/galvanostat Gamry 3000 setup 48 hours after fabrication. All measurements were conducted within 0 and 2 V voltage window provided through the use of an organic gel electrolyte. Optical transmittance measurements were conducted using Maya2000 Pro Spectrometer.

2.3 Results and Discussion

A schematic and photograph of the fabricated SCs are shown in the Figure 17 (a) and (b), respectively. The full device without external conductive carbon paste current collectors is highly transparent as can be seen in Figure 17 (b). The morphology of the SWNT electrodes uniformly deposited on the PDMS surface is shown in the SEM image provided in Figure 17 (c). 4 set of transparent and flexible devices with different SWNT densities were fabricated in this work. Sheet resistance of the thin films, their optical transmittance and corresponding SWNT weights are tabulated and provided in Table 2.

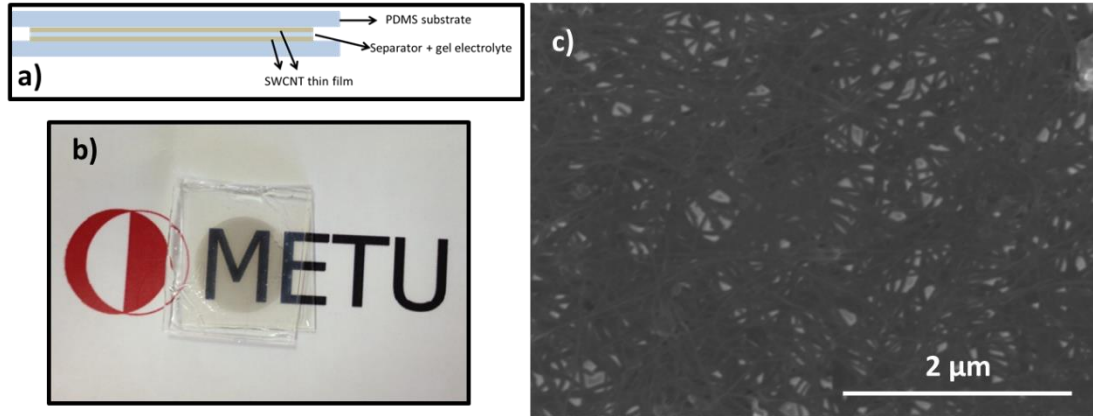


Figure 17. (a) A simple schematic and (b) photograph of the fabricated SCs without carbon paste current collectors. c) SEM image of a SWNT electrode with a sheet resistance of 75 ohm/sqr.

Table 2. Sheet resistance and % transmittance (at 550 nm) change with respect to SWNT weight for the fabricated supercapacitors.

SWNT mass (total)	Sheet Resistance (ohm/ sqr)	% Transmittance
0.02	260	82
0.04	210	75
0.06	155	63
0.08	75	56

Gel electrolyte with a composition of salt: PMMA: ACN: PC has high transmittance and ionic conductivity. Controlled viscosity of the gel electrolyte allowed stable electrochemical performance during bending. Instead of commonly used H_3PO_4/PVA , the use of $TBAPF_6/ PMMA/ PC/ ACN$ gel electrolyte with a wettable separator is an important point of our study and a major reason in obtaining high transparency on full devices. To our knowledge, it is the first time that this gel electrolyte composition is used in a SC application. It provides higher transparency and higher voltage window as compared to conventionally used H_3PO_4/PVA or H_2SO_4/PVA gel electrolytes.

Transmittance spectra for the fabricated SCs with different SWNT densities are provided in Figure 18. A transmittance of 82 % (at a wavelength of 550 nm) was obtained for the SCs with 0.02 mg SWNTs. Transmittance was found to decrease with SWNT density as shown in the figure, in agreement with the transparent SCs in literature [89, 90, 111].

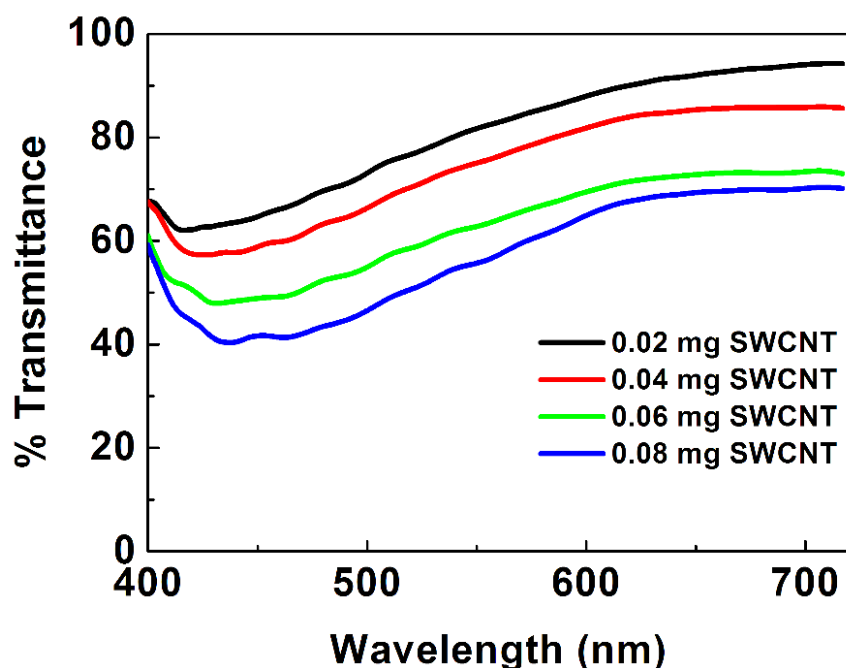


Figure 18. Optical transmittance characteristics of the full devices with respect to total SWNT weight in both electrodes.

CVs of the resulting transparent and flexible SCs are shown in Figure 19 (a). The CV measurements revealed almost rectangular shapes at $20 \text{ mV}\cdot\text{s}^{-1}$, as shown in the Figure 19 (a). Denser films with higher conductivities showed higher capacitance values as compared to films with lower densities. The CV measurements obtained at different rates are provided in the Figure 19 (b). The deviation from the ideal capacitor shape was attributed to the internal resistance of the devices. Devices were found to be unstable above 2 V, which was attributed to the presence of functional groups on the SWNTs reacting with the electrolyte beyond this voltage and instability of gel electrolyte components.

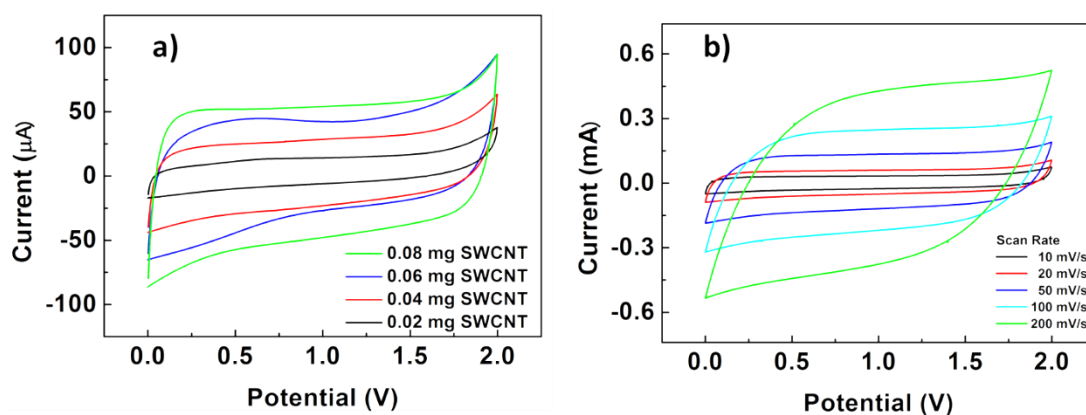


Figure 19. (a) CV curves of transparent and flexible SCs with different SWNT mass at $20 \text{ mV}\cdot\text{s}^{-1}$ scan rate. (b) CVs at different rates for a SWNT mass of 0.08 mg.

The functional and mechanical integrity of the fabricated SCs was also investigated by characterizing electrochemical properties while bending the device down to different radii of curvature. This is made possible by the flexible nature of both electrodes and electrolyte. In order to investigate the flexibility of SWNT thin films, resistance change in SWNT thin film on PET substrates was monitored, provided in Figure 20 (a), during bending cycles [112]. A commercial ITO thin film on PET substrate (Delta Technologies, 4-10 ohm/sqr.) was used as a reference. SWNT thin films provided higher flexibility than that of crystalline ITO films due to their web-like structure and mechanical stability of the individual SWNTs. This is evidenced in the stable resistance of the SWNT thin films upon bending, while the resistance of ITO thin film increases 7 times within 10 bending cycles. CVs of the fabricated SCs as a function of radius of curvature are shown in Figure 20 (b). Owing to easy ion transport and wide electrochemical window of gel electrolyte, bent SCs showed similar results to that of flat counterparts.

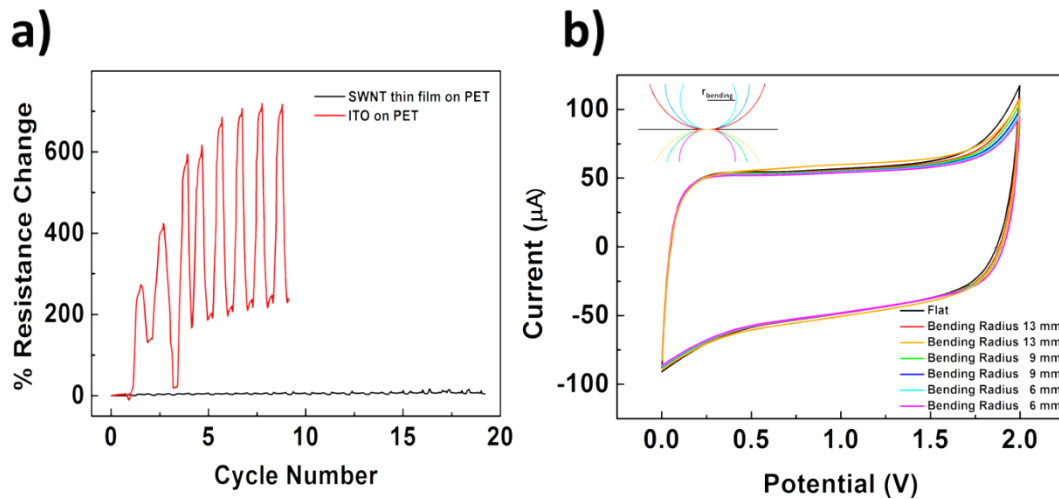


Figure 20. (a) Percent resistance change in ITO and SWNT thin films on ITO during bending cycles down to a radius of 6 mm [112]. (b) CVs for flexible SCs while bent to different radius of curvatures for the 0.08 mg of SWNT thin film at $20 \text{ mV}\cdot\text{s}^{-1}$ scan rate.

The GCD characteristics of the SCs with respect to SWNT loading measured at 1.25 A/g current density is provided in Figure 21 (a). A small IR_{drop} was observed in measurements. A significant increase in C_{sp} with increasing SWNT loading was expected due to enhanced charge storage [97]. The GCD characteristics measured at various current densities are provided in Figure 21 (b). Discharge profile of the fabricated SCs was changed with respect to applied current density.

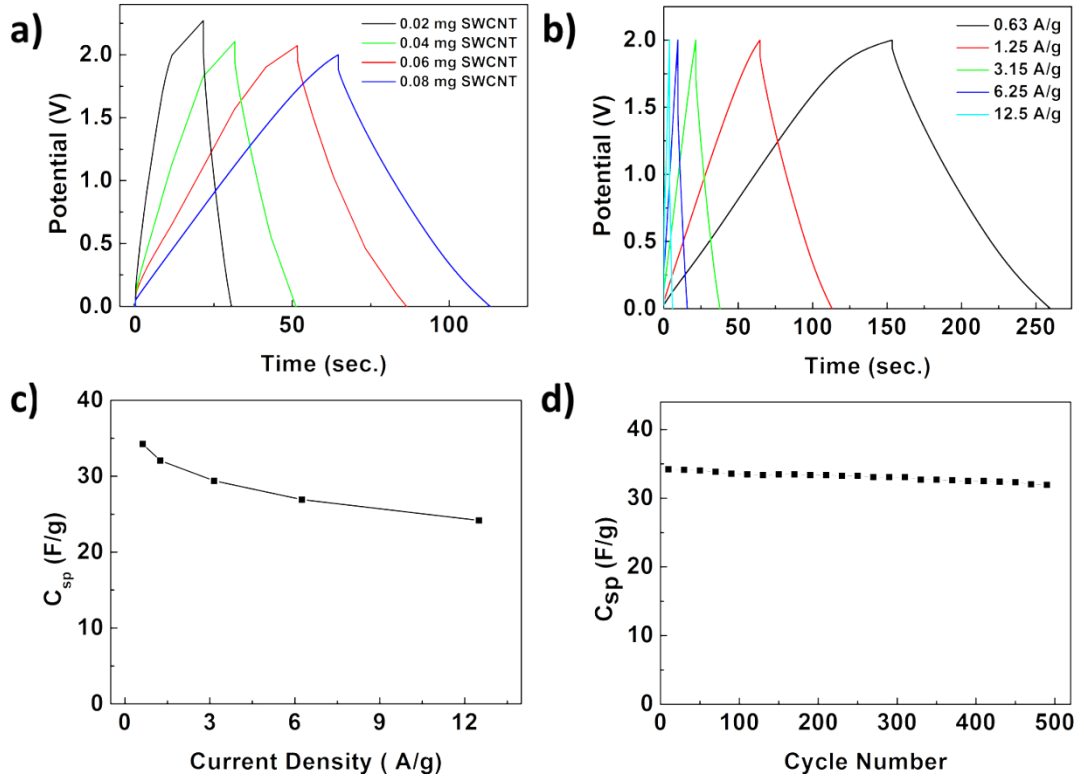


Figure 21. (a) GCD curves for SCs at 1.25 A/g and (b) at different current densities. (c) Dependence of C_{sp} on current densities. (d) Cycleability of fabricated SCs.

The cell capacitances (C_{cell}) were calculated from GCD curves (Figure 21 (a)-(b)) using the following equation:

$$C_{cell} = \frac{I}{\frac{dV}{dt}}$$

where I is the obtained current, m is the mass of SWNTs on both electrodes and dV/dt is the scan rate. The capacitance of the SC with a SWNT mass of 0.02 mg was calculated to be 25.2 F/g, whereas that for 0.08 mg SWNT mass was 31.9 F/g. These measurements were taken at $20 \text{ mV}\cdot\text{s}^{-1}$. The C_{sp} was calculated using the GCD curves of SCs provided in Fig. 21 (a)-(b) and the equation:

$$C_{sp} = \frac{I}{m \frac{dV}{dt}}$$

where t is the discharge time, I is the applied discharge current, m is the mass of SWNTs on both electrodes and V is the discharge voltage [91]. C_{sp} calculated at 0.63 A/g was 34.2 F/g for the SC device with a SWNT mass of 0.08 mg. C_{sp} is plotted as a function of the current densities in Figure 21 (c). A serious specific capacitance loss was found to occur with increasing current density. It is commonly observed that the capacitive performance of electrode active materials decrease with an increase in current density. This is due to the difficulties in penetration and diffusion of electrolyte ions into a poorly conductive layer and/or thick electrode films [113].

Capacity retention is another important factor in controlling the SC performance. In order to explore this, fabricated transparent and flexible SCs were charged and discharged over 500 cycles. No significant degradation in specific capacitance was obtained, as shown in Figure 21 (d). Quantitatively, 94 % of C_{sp} was retained over 500 cycles, resembling the decent capacity retention in the fabricated devices.

Our results showed that SWNT thin film electrodes work well in devices with non-aqueous gel electrolytes. No damage was visually observed on the SWNTs and carbon paste contact points due to contact with the electrolyte at the end of the measurements.

Energy and power densities of the fabricated SCs were calculated using the following equations:

$$E_{cell} = \frac{C_{cell}V^2}{2m} \quad P_{cell} = \frac{V^2}{4 * ESR * m}$$

where V is the applied potential, m is the total mass of SWNTs in both electrodes and the ESR is effective serial resistance calculated from Figure 17 (a) using equation:

$$ESR = \frac{IR_{drop}}{2I}$$

High ESR of the SCs was attributed to the absence of a separate charge collector, serial resistance of the SWNT thin films, resistance of the gel electrolyte and the contact resistance between the carbon paste contact with SWNTs. High flexibility and strong physical adhesion between SWNTs and PDMS substrate preserved the specific capacitance and power density without any deterioration upon bending. Owing to the

unique properties of SWNTs, good electrochemical performance was obtained from the fabricated supercapacitors. Minimizing the ESR would increase the C_{sp} and power density. Specific capacitance, power density and energy densities were found to be 34.2 F/g, 21.1 kW.kg⁻¹, 18.0 kWh.kg⁻¹, respectively. According to the Ragone plot, power density of the produced SCs with gel electrolytes was found to lie in low power range. Flexible SC devices need solid-state electrolytes to prevent electrolyte leakage. Therefore, it is difficult to compare our device performance with liquid electrolyte based devices. Therefore, we have compared our results with supercapacitors with non-liquid based electrolytes. Our results are found to be in reasonable agreement and sometimes competitive to the ones provided in literature [114, 115].

In this work, SWNT thin films were used both as the current collector and host for the double-layer. Therefore, an increase in specific capacitance would require higher SWNT mass, which necessitates sacrifice in transparency. Flexibility and transparency, simultaneously would not be possible if a separate current collector was used. It is possible to further improve the transparency of the fabricated devices through the reduction of SWNT bundles within the thin films. These absorb a significant proportion of the light and are responsible for a decrease in optical transmittance of the thin films. Power densities can be improved through the deposition of nano-sized oxide particles and/or polymers onto SWNTs.

2.4 Conclusions

In this study, we have demonstrated solid-state, highly flexible and transparent SCs with binder-free SWNT thin film electrodes. We have examined the effect of SWNT density, thus the SWNT mass, on the electrochemical properties of the SCs. SWNT density controlled the sheet resistance of the electrodes and transmittance of the overall devices. A typical EDLC behavior in a voltage window of 0 to 2 V was obtained. High conductance of the SWNT thin films eliminated the use of extra charge collectors. High bendability without significant deterioration in device properties was obtained. The measured specific capacitance, maximum energy and power density were 34.2 F/g, 18.0 kWh.kg⁻¹, 21.1 kW.kg⁻¹, respectively for 0.08 mg SWNT devices. The SCs had good stability and the variation in C_{sp} was found to be less than 6 % over 500

cycles. Moreover, the C_{sp} was found to change by less than 2 % through bending the devices down to a radius of 6 mm. Finally, a low cost and rapid route for the fabrication of SCs is presented. These SCs will be critical components of transparent and flexible devices.

CHAPTER 3

TERNARY NANOCOMPOSITE SWNT/WO₃/PANI THIN FILM ELECTRODES FOR SUPERCAPACITORS

3.1 Introduction

Among energy storage systems, SCs have received a lot of attention owing to their moderate specific energy and high specific power densities. They have wide application areas spanning from pulse power systems, electric vehicles to portable devices [12, 85, 86]. Depending on the charge storage mechanism, there are two major groups for supercapacitor electrode active materials. EDLC preserves charge electrostatically in double layers, whereas pseudocapacitors store charges on the surface of the electrode active materials as faradaic redox reactions. Carbon based materials are EDLC type, while metal oxides and CPs are pseudocapacitor type materials. EDLC have long-lasting life, while pseudocapacitors have high energy density. CNTs are highly appealing candidate materials for SC electrodes [90, 91, 116]. CNT thin films are a new class of materials where they are used in an ensemble form [98]. Thanks to their chemical inertness, functionability, permeability and high conductivity of SWNT thin films are good candidates for active SC electrode materials [32, 33, 90]. For practical device applications, these characteristics together with the fact that carbon typically forms a purely double layer make SWNT thin films unique.

In nanocomposite form, metal oxides and CPs could improve electrochemical and mechanical properties of the SCs [86]. RuO₂ is the most commonly used and highly pseudocapacitive material; but its high cost and poisoning nature are the major drawbacks limiting its widespread applications [32]. Therefore, researchers focused on the exploration of alternative pseudocapacitive metal oxides and especially cheap metal oxides such as MoO₂, MnO₂, Co₃O₄ and NiO have been investigated [12, 32, 85, 117]. Tungsten oxide (WO₃) is a n-type semiconducting oxide [118], which is readily used in electrochromic devices [119], gas sensors [120], and photocatalysis [121] while its electrochemical properties for SC devices have been relatively unexplored. Crystalline forms of WO₃ show non-prominent capacitance, while amorphous WO₃

shows high capacitance [122] due to the intercalation of small ions (H^+ and Li^+) [123]. WO_3 and a CP, PANI, are used separately [122, 124-126] and together [127-129] to examine their electrochemical potential, as electrode active materials, but the demonstration of ternary composite electrodes, combining WO_3 , PANI and SWNTs have remained elusive. Different methods are available for the synthesis of WO_3 ; but, synthesis of the WO_3 /PANI nanocomposite in one step can be simply realized by electrodeposition [127]. Cathodic electrodeposition of WO_3 takes place at low pH values; however those pH values are not suitable for many current collectors [130]. Moreover, PANI has different oxidation states and the most conductive state among them is the emeraldine salt, which is obtained at low pH values [131, 132]. Therefore, formation of WO_3 and PANI nanocomposites on SWNT thin films at one step electrodeposition through cyclic voltammetry is advantageous for fast and large scale fabrication of SC electrodes. SWNT thin film electrodes can be homogeneously covered by electrodeposited WO_3 and PANI to enhance electrochemical properties with respect to the individual components.

In this work, we have fabricated ternary nanocomposite SWNT/ WO_3 /PANI thin films based SC electrodes. Highly conductive SWNT electrodes resulted in the production of SCs with current collector free electrodes and enhanced the properties solely arised by the WO_3 and PANI components in a synergistic manner.

3.2 Experimental

3.2.1 Preparation of samples

SWNTs were purchased from Carbon Solutions Inc. (SWNT P3, metal content 5-7 wt % from TGA in air and carbonaceous content more than 90 %). All other materials used in this work were of analytical grade and were purchased from Sigma-Aldrich and used without further purification.

SWNT thin film electrodes were fabricated onto soda lime silicate glasses by vacuum filtration and consecutive stamping method [133]. To prepare SWNT thin films, firstly SWNTs were dispersed in 1 % sodium dodecyl benzene sulfonate (SDBS)

solution by tip-sonication. Then the SWNT solution (SWNT density: 2 mg/ml) was filtrated using mixed cellulose acetate (Merck MCE, pore size: 200 nm) filter membranes via vacuum filtration (flow rate $\sim 1 \text{ m}^3/\text{h}$). Following the settlement of SWNTs on filter membrane, filtration was repeated with deionized water to remove excess surfactant. Accumulation of SWNTs on the filter membrane controls the film homogeneity. The SWNT mass in the thin film (typically 0.08 mg) was determined by the volume of filtrated SWNT solution. SWNT film on the filter membrane transferred to soda-lime silicate glass substrate by compressively (under $200 \text{ g}/\text{cm}^2$) heating over a hot plate at 80°C . Following drying, filter membrane was removed by dissolving in acetone. Following deposition, SWNT electrodes were kept in nitric acid (HNO_3 , 65 %) for 3 hours to remove metal impurities and filter paper residues. Acid treatment also helps to improve SWNT thin film conductivity [101]. The resulting circular thin films had an area of 2 cm^2 . Conductive carbon paint was used to print external contact points.

WO_3/PANI nanocomposites were electrodeposited onto SWNT thin films by cyclic voltammetry at ambient conditions [127, 131]. A potential range between -0.6 and 0.9V at a scan rate of $50\text{mV}/\text{s}$ was used for 105 cycles and films were then rinsed with distilled water. The solution used for the deposition of composite films contained sodium tungstate dihydrate ($\text{Na}_2\text{WO}_4 \cdot 2\text{H}_2\text{O}$, 15 mM), sulfuric acid (H_2SO_4 , 0.25 M) and aniline monomer ($46 \mu\text{L}$). During electrodeposition, $\text{Na}_2\text{WO}_4 \cdot 2\text{H}_2\text{O}$ was added to the solution after the 5th cycle, whereas aniline was added after the 55th cycle.

3.2.2 Characterization

The morphology of the fabricated ternary nanocomposite films were analyzed by SEM (FEI Nova Nano SEM 430, operated at 10 kV). XPS measurements were conducted to determine chemical state of the constituent elements. A PHI 5000 VersaProbe spectrometer was used to record XPS spectra. High-resolution XPS scans of the W (4f) and O (1s) and C (1s) spectral regions were performed for the qualitative analyses. The C (1s) line at 284.5 eV were used for the charge correction. XPS signals were fitted with Gaussian curves. A Bruker IFS 66/S model spectrometer was used for Fourier transform infrared (FTIR) spectroscopy analyses. FTIR spectra of thin films

were collected in the ATR mode. A three-electrode setup was used for electrochemical measurements of the electrodes using Gamry Reference 3000 system. The counter and reference electrodes were platinum foil and Ag/AgCl, respectively. All electrochemical measurements were conducted in a 0.1M lithium perchlorate (LiClO_4) in propylene carbonate (PC) electrolyte solution. A microbalance was used to measure the mass of SWNT/ WO_3 /PANI and the weight of total active materials in SWNT/ WO_3 /PANI electrode was measured around 0.4 mg.

3.3 Results and Discussion

The electrodeposition of WO_3 and PANI composites on vacuum filtered SWNT film was achieved using CV between a potential window of -0.6 and 0.9 V at 50 mV/s scan rate. Evolution of ternary composite films is shown in Figure 22 (a) with respect to CV cycles. Peaks within the CV curves showed that the thickness of the WO_3 and PANI coating gradually increases on the SWNT film surface. Porous nature of the SWNT films facilitates deposition of WO_3 and PANI in a conformal manner.

CVs of the obtained films are shown in Figure 22 (b). The CV measurements revealed that the cathodic electrodeposition of WO_3 layer on SWNT thin films result in a broad peak at negative potential region, as shown in the Figure 22 (b). The SWNT/ WO_3 /PANI nanocomposite film showed complementary peaks corresponding to the redox pairs of WO_3 and PANI. Moreover, the peak positions corresponding to the redox process of WO_3 , in the CV curves of SWNT/ WO_3 /PANI were shifted to the higher potentials due to WO_3 and PANI related redox reactions.

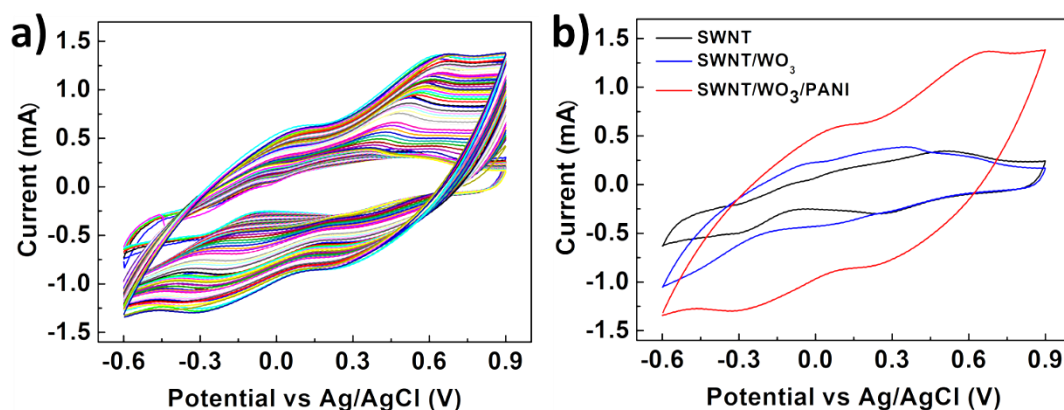


Figure 22. (a) Consecutive CVs for the electrodeposition of WO₃/PANI on SWNT films and (b) electrodeposited thin film electrodes at 50 mV/s scan rate.

Surface morphologies of the SWNT, SWNT/WO₃ and SWNT/WO₃/PANI thin films on the glass substrates were investigated through SEM analysis. SEM images of bare SWNT thin films, electrodeposited WO₃ layer on SWNT thin films and ternary nanocomposites (SWNT/WO₃/PANI) are provided in Figure 23 (a) - (d), respectively. Bare SWNTs (Figure 23 (a)) were coated with a thin WO₃ layer during electrodeposition as provided in the Figure 23 (a-b)). Thin metal oxide coating is necessary for the electrolyte ion intercalation to enhance surface reactions [134]. PANI not only fills the openings of SWNT/WO₃ composite but also covers the whole surface of composite films as evidenced in low and high resolution SEM images provided in Figure 23 (c) - (d), respectively. According to cross-sectional SEM images (not provided here), average thicknesses of the SWNT and SWNT/WO₃/PANI are 500 nm and 900 nm, respectively. Top hybrid WO₃/PANI layer within the ternary nanocomposite film improved the conductivity (as will be further discussed in EIS analysis) and also acted as a blanket to prevent the detachment of the WO₃ nanoparticles. No further annealing treatment was applied, thus the electrodeposited WO₃ layer is supposed to be in amorphous state.

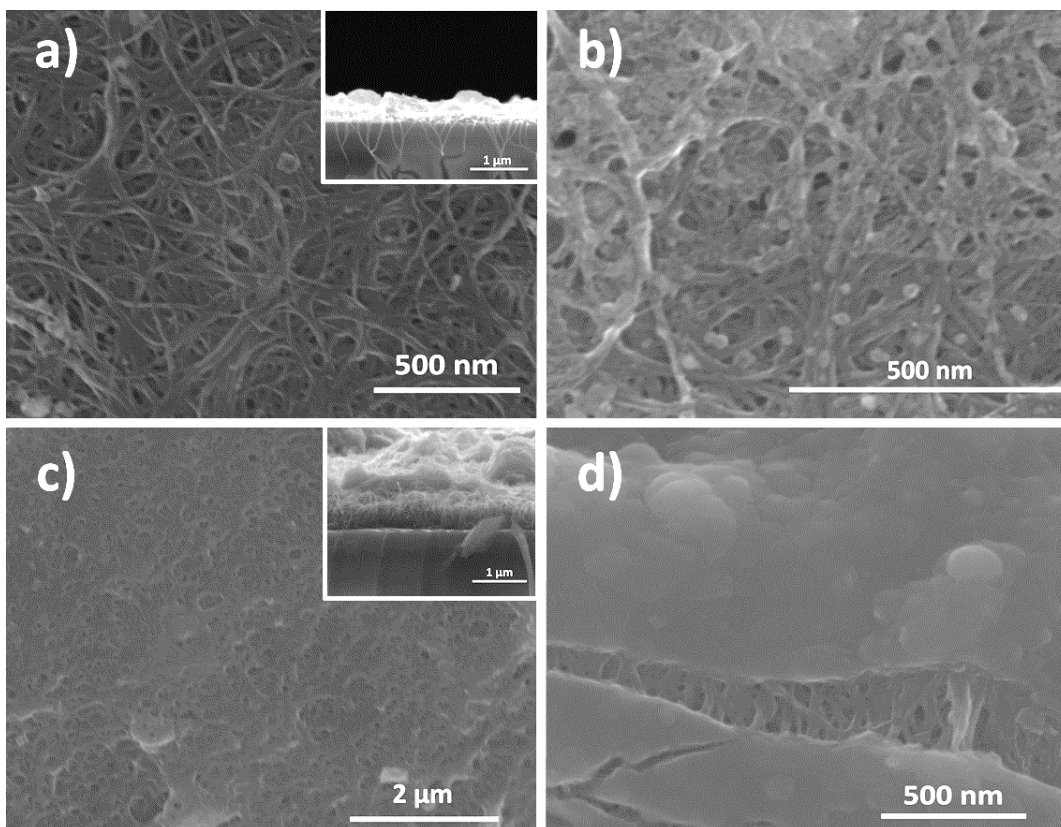


Figure 23. SEM images of (a) bare SWNT electrodes, (b) SWNT/WO₃ films and SWNT/WO₃/PANI film in low (c) and high (d) resolution.

Surface measurements by XPS were carried out for WO₃ in SWNT/WO₃ nanocomposite to verify the chemical composition and position correction was done with respect to C 1s peak. According to the Figure 24 (a), survey spectrum of the SWNT/ WO₃ nanocomposite have signals at 36.3-38.3, 284.5, and 532.1, which were attributed to the W 4f, C 1s and O 1s, respectively, indicating contributions from both SWNTs and WO₃. Spectra for bare SWNTs and ternary SWNT/WO₃/PANI nanocomposites are provided within the same figure for comparison. PANI brings out N peak, covers the surface of the ternary nanocomposite and suppresses W related peaks. Figure 24 (b) and (c) show the XPS core level spectra of W 4f_{7/2-5/2} and O1s, respectively, corresponding to WO₃ material, obtained after electrodeposition. As shown in Figure 24 (b), W 4f splits into two peaks as W 4f_{7/2} and W 4f_{5/2} that appeared respectively at 36.3 and 38.3 eV due to strong coupling. Deconvoluted XPS spectra of the W 4f revealed that it could only be attributed to W (VI) oxidation state [135, 136]. XPS O 1s core level spectrum (Figure 24 (c)) has a peak at 532.1 eV that was also assigned to WO₃. Table 3 summarizes BEs and FWHM values for the W 4f and O 1s

components. The XPS core level spectra of C 1s for the thin film electrodes are shown in Figure 24 (d)-(f). In Figure 24 (d), deconvolution of the C 1s spectrum of SWNT thin film results in three contributions, which are associated to sp^2 -hybridized graphitic carbon at 284.5 eV, C–OH phenolic surface groups at 285.6 eV, and a π – π^* transition peak due to the sp^2 -bound carbon at 288.9 eV. For SWNT/ WO_3 nanocomposite film, deconvoluted C 1s spectrum have similar contributions with the SWNT film, but the intensity of the spectrum is lower than that of SWNT film, as shown in Figure 24 (e). For SWNT/ WO_3 /PANI nanocomposite film C 1s spectrum show the asymmetric characteristics as shown in Figure 24 (f). C 1 s spectrum can be separated into four peaks centered at 284.5, 285.4, 286.0, and 288.0 eV.

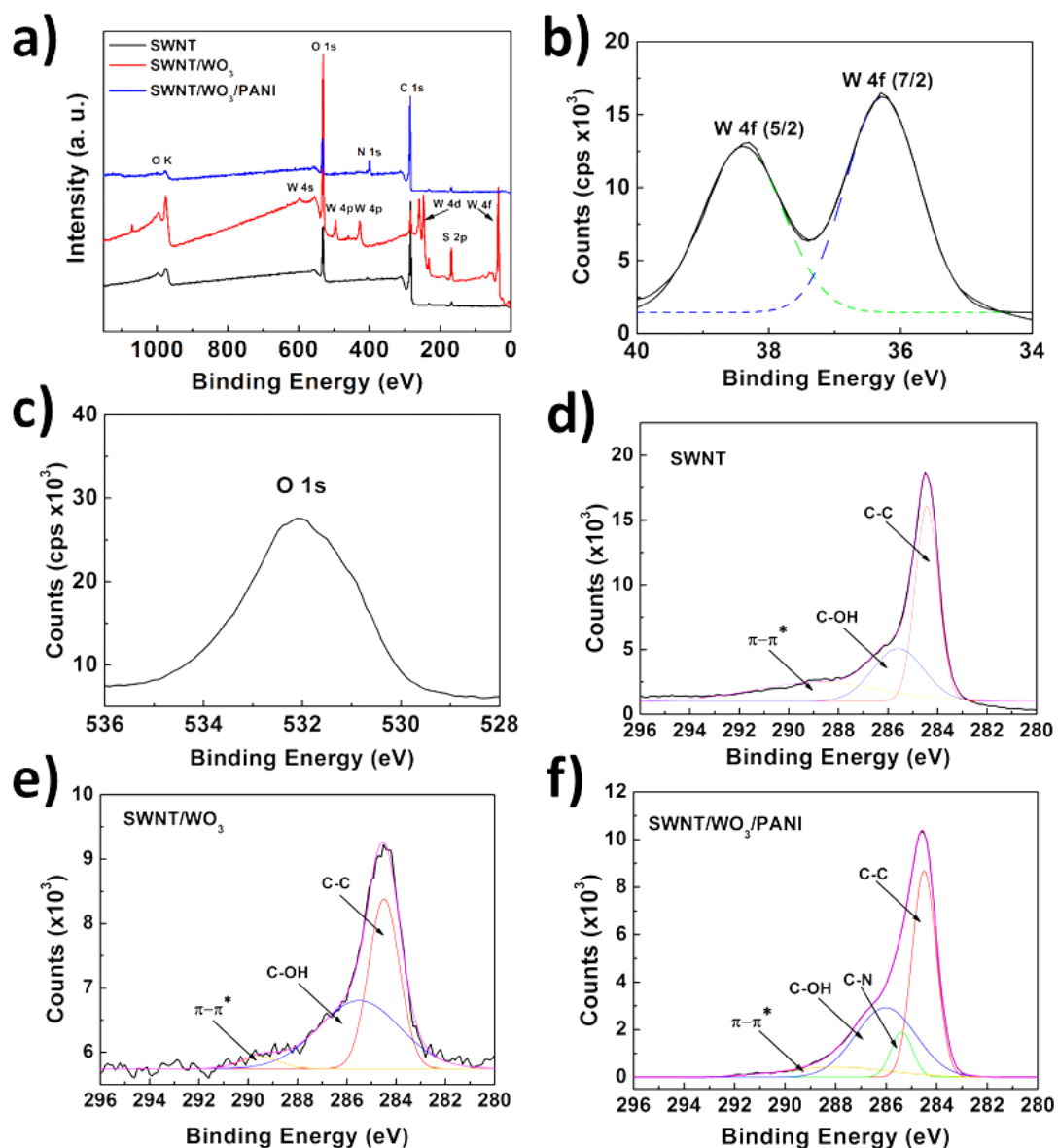


Figure 24. (a) XPS survey spectrum of the electrodes. XPS spectra of (b) W 4f, (c) O 1s and (d)-(f) C 1s.

Table 3. XPS core-level BEs and FWHMs of the XPS spectrum of the WO_3 .

Compound	BE of W 4f _{7/2-5/2} (eV)	FWHM of W 4f (eV)	BE of O 1s (eV)	FWHM of O 1s (eV)
WO_3	36.3-38.3	1.42-1.56	532.1	2.66

The chemical nature of the thin films was also investigated with FTIR. Figure 25 provides the FTIR spectra of SWNT/WO₃ and SWNT/WO₃/PANI thin films within the spectral range of 2000 - 400 cm⁻¹. The spectrum for SWNT thin films is provided for comparison. The bands in SWNT/WO₃ nanocomposite film spectrum located at 570 and 1020 (W-O stretching vibration), 735-862 (W-O-W stretching vibration), 1145 (C-H stretching vibration) and 1635 cm⁻¹ (δ (H₂O) in-plane bending vibration) are marked, when compared to pure SWNT spectrum. In the FTIR spectrum of SWNT/WO₃/PANI nanocomposite film, bands located at 614 and 1045 (W-O stretching vibration), 875 (W-O-W stretching vibration), 1225 (C=N stretching), 1485 (N-B-N benzenoid ring), 1305 (C-N stretching vibration), 1135 (C-H stretching vibration), 1570 (N=Q=N quinoid ring stretching vibration) and 1612 cm⁻¹ (δ (H₂O) in-plane bending vibration) are marked [137, 138], clearly showing the deposition of PANI. Associated peak shifts observed within SWNT/WO₃ and SWNT/WO₃/PANI nanocomposite films indicating the possible bond formation between the components.

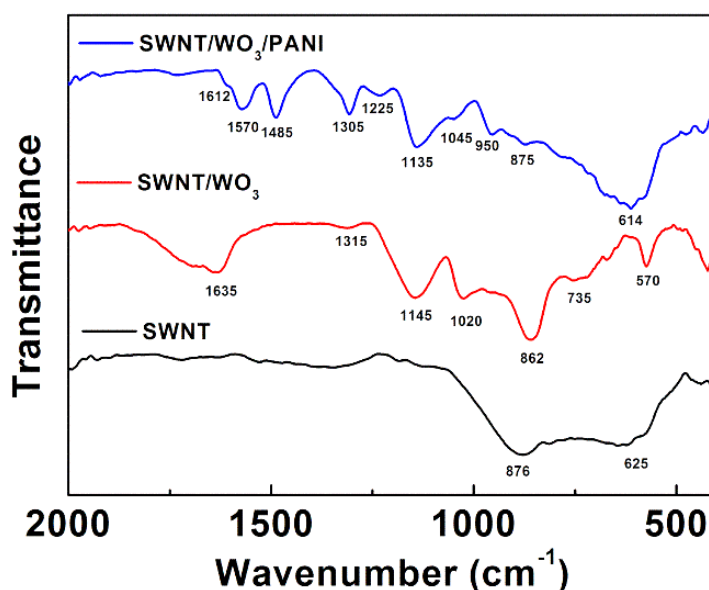


Figure 25. FTIR spectra of bare SWNT electrodes, SWNT/WO₃ and SWNT/WO₃/PANI nanocomposite electrodes.

CVs of the fabricated supercapacitor electrodes were recorded within a potential window of -1.5 and +1.5 V at 20 mV/s. Figure 26 compares the CV evolution of the prepared electrodes. High conductance of the SWNT thin films eliminated the use of extra charge collectors and they were also utilized as electrode active materials. Due to faradaic redox reactions, more charges were accumulated on the SWNT/WO₃

nanocomposite thin films as opposed to bare SWNT electrodes, evidenced by small and broad peaks at both oxidation and reduction regions of CV curves in Figure 26 [123]. This also signifies the governance of capacitance characteristics primarily by the pseudocapacitive properties [97]. WO_3 is a cathodic electroactive material and its pseudocapacitive activity takes place in the negative potential region when it is reduced by the electrolyte ions (Li^+ ions). On the other hand, PANI is an anodic electroactive material and its pseudocapacitive activity mostly takes place in positive potential region [137]. Broad CV curves and combination of redox peaks were due to the formation of a donor-acceptor pair between WO_3 and PANI. Composite form of SWNT/ WO_3 /PANI films tends to create synergistic and complementary effects while eliminating their individual drawbacks [123].

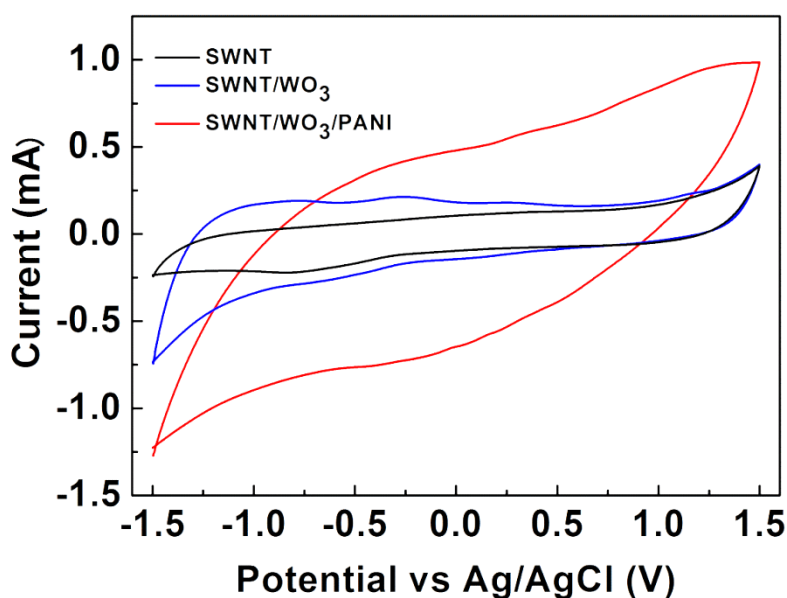


Figure 26. CV results of the fabricated thin film electrodes in 0.1 M LiClO_4 in PC at 20 mV/s.

CV measurements pointed that SWNT electrodes' electrochemical properties were significantly improved by the pseudocapacitive contribution of WO_3 and PANI because of the uniform distribution of thin layers of WO_3 and PANI on the surface of SWNTs. CV measurements of ternary nanocomposite SC electrodes at various scan rates are provided in Figure 27. These results show that nanocomposite electrodes

respond to increased scan rates although the resistance effects start to dominate after 100 mV/s scan rate.

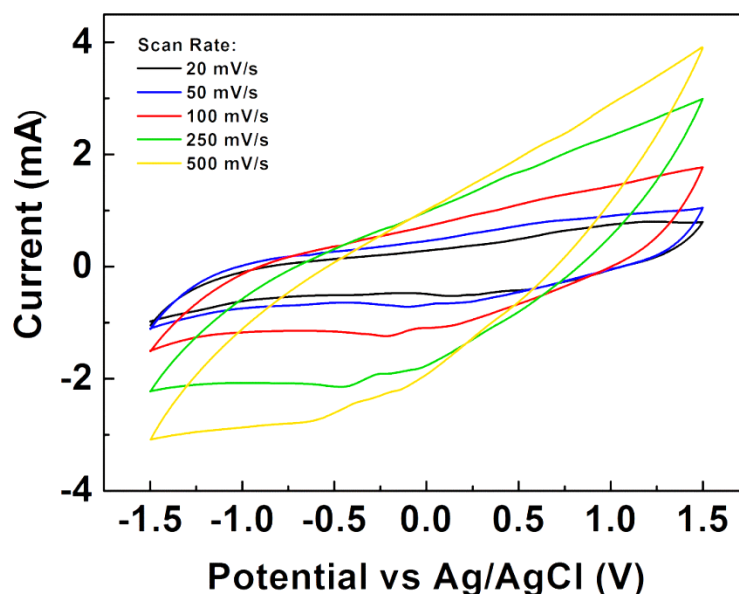


Figure 27. CV results of SWNT/WO₃/PANI nanocomposite electrodes at scan rates between 20 and 500 mV/s.

The obtained results indicate that the rate capability of nanocomposite films increase with the scan rate. The GCD characteristics of the electrodes were examined at 0.13 mA/cm² current density and results are given in Figure 28. Galvanostatic measurements were conducted from -1.5 V to +1.5 V [50]. A remarkable improvement in the charge storage capacity was observed due to the formation of a nanocomposite. The characteristic profile of SWNT films is shifted to pseudocapacitive due to the presence of WO₃ and PANI for SWNT/WO₃ and SWNT/WO₃/PANI nanocomposite films. Internal resistance drop (IR_{drop}) was observed in the measurements and it was due to the ESR (sum of electrolyte, electrode and contact resistance) [139].

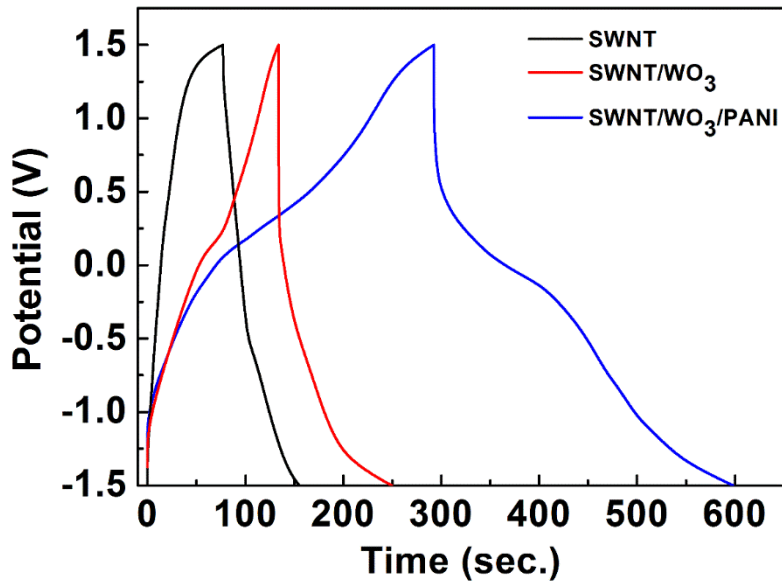


Figure 28. GCD curves of the fabricated electrodes at 0.13 mA/cm^2 current density.

The GCD characteristics measured at different densities are provided in Figure 29. GCD profiles of the fabricated SCs were discovered to rely on the applied current density. At different current densities, similar curve shapes have been attained.

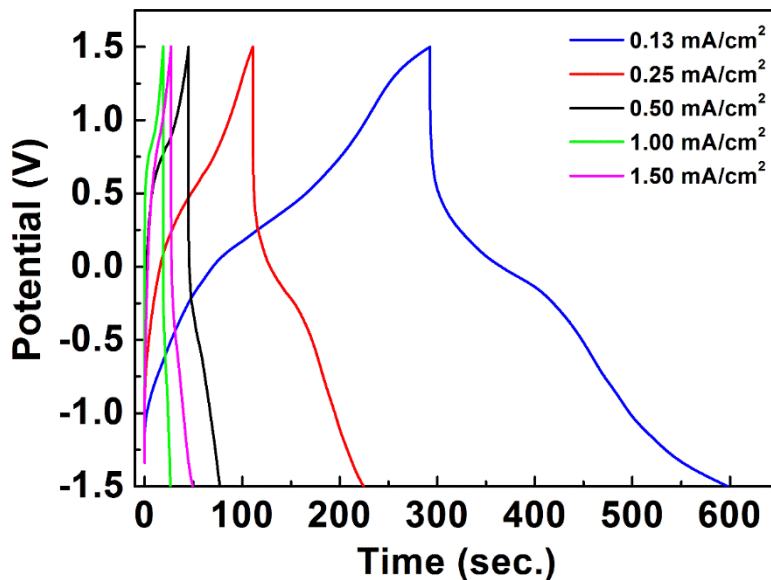


Figure 29. GCD curves of SWNT/WO₃/PANI nanocomposite electrode in 0.1 M LiClO₄ in PC at different current densities from 0.13 to 1.5 mA/cm².

The C_{sp} was found using the GCD curves of the supercapacitors provided in Figure 29 and the equation:

$$C_{sp} = \frac{I}{A \frac{dV}{dt}}$$

where t is the discharge time, I is the applied discharge current, A is the active area in cm^2 and V is the discharge voltage after IR_{drop} . The specific capacitance of the nanocomposite film was found as 28.5 mF/cm^2 at 0.13 mA/cm^2 current density. This value obtained for the nanocomposite film was comparable to that obtained by Nwanya et al (10 mF/cm^2) and Wei et al. (25 mF/cm^2) [123, 138] even if higher current density was applied in this work. For ternary nanocomposites, C_{sp} is plotted as a function of the galvanostatic discharge currents in Figure 30 (a). A C_{sp} loss was found to occur with increasing current density. It is commonly observed that the capacitive performance of the fabricated electrodes decreases with a current density increase. This is due to the difficulties in the diffusion of electrolyte ions into the conductive layer and/or thick electrode films because of the fast GCD cycles [113]. The dependence of the specific capacitance of the ternary nanocomposite films on current density is provided in Figure 30 (a). The C_{sp} was 28.5 mF/cm^2 and 14.5 mF/cm^2 at current densities of 0.13 and 1.5 mA/cm^2 , respectively. Capacitances calculated using galvanostatic discharge curves (Figure 25) were found to decrease by increasing withdrawn cell current. This is because, at higher current densities, the slower processes demonstrate a kinetic resistance and cannot participate in charge transfer onto or across the electrode/electrolyte interface [117].

The C_{sp} of the SWNTs was developed by the incorporation of WO_3 and PANI due to the homogeneous distribution of WO_3 nanoparticles between the SWNTs and blanket-like deposition and composite formation with PANI. Ternary nanocomposite films fabricated in this work showed higher capacitance values when compared to bare SWNT electrodes and binary WO_3/PANI nanocomposite electrodes.

Another important factor in determining the SC performance is capacity retention. In order to explore this, fabricated nanocomposite SC electrodes were charged and discharged for 2000 cycles, results of which are provided in Figure 30 (b). Quantitatively, 76 % of C_{sp} was retained after 2000 cycles, resembling decent capacity retention in the fabricated electrodes. Performance drop was attributed to the degradation of PANI as evidenced also by Wei et al [138]; however, capacity retention obtained herein this work is slightly better. Devices were fabricated and stored at

ambient conditions before the measurements. We believe that the capacity retention characteristics can be improved if the devices are fabricated under inert atmosphere and hermetically sealed.

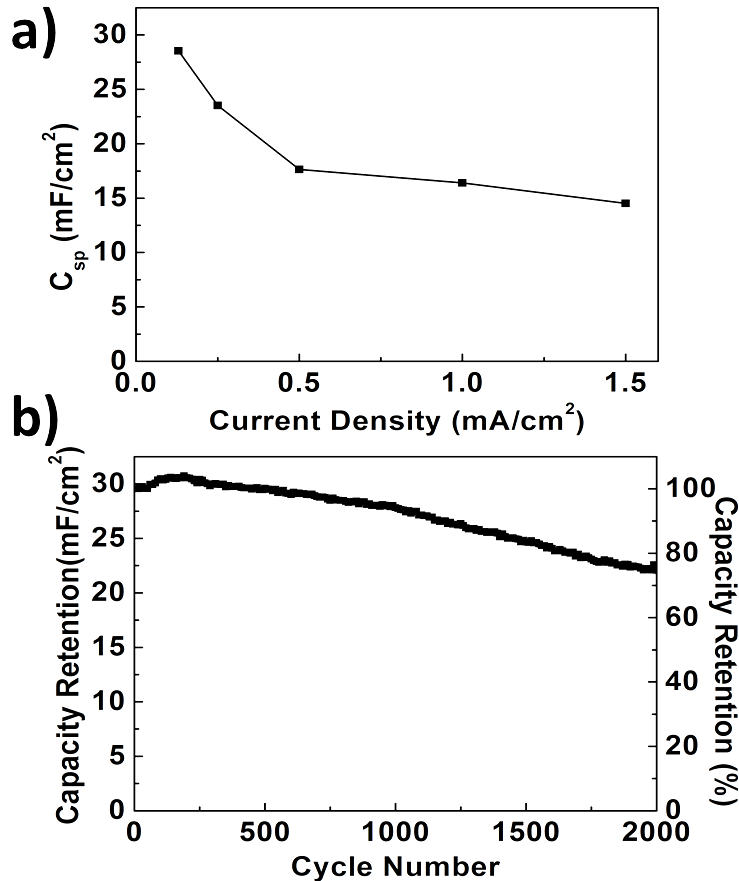


Figure 30. (a) Dependence of the specific capacitance of ternary SWNT/WO₃/PANI nanocomposite electrodes on current density. Lines are for visual aid. (b) Cycling performance of ternary SWNT/WO₃/PANI nanocomposite electrodes measured through GCD current at 0.13 mA/cm².

EIS was conducted to further elucidate the fabricated electrode's capacitive properties. Electrochemical impedance characteristics of the thin films were investigated at an applied AC potential of 0.01 V. Figure 31 provides the Nyquist plot measured within the range from 50 kHz to 50 mHz at 0 V vs Ag/AgCl. SC electrodes oscillate as a resistance at high frequencies and as a capacitance at low frequencies. In a theoretical Nyquist plot, there is a small semicircle in high frequency and a vertical line in low frequency region. Unfortunately, theoretical and experimental results are not always the same. The semicircle is attributed to the interactions at the electrode-

electrolyte interface, which is due to the charge-transfer resistance. Bare SWNT electrodes have the smallest semicircle, while those are too broad and unclear for the composite electrodes. The straight line arises in the low frequencies because of the pseudocapacitance and the steepest line is for SWNT electrodes, while the slope decreases for the composites. It is also shown in the figure that the resistance of ternary composites is smaller than the binary composite and bare SWNT electrodes. This could be attributed to the protonated nature of PANI, which decreases the uncompensated resistance. After 500 charge/discharge cycles, ternary nanocomposite was found to have an increased uncompensated resistance with enhanced pseudocapacitance as observed in the figure.

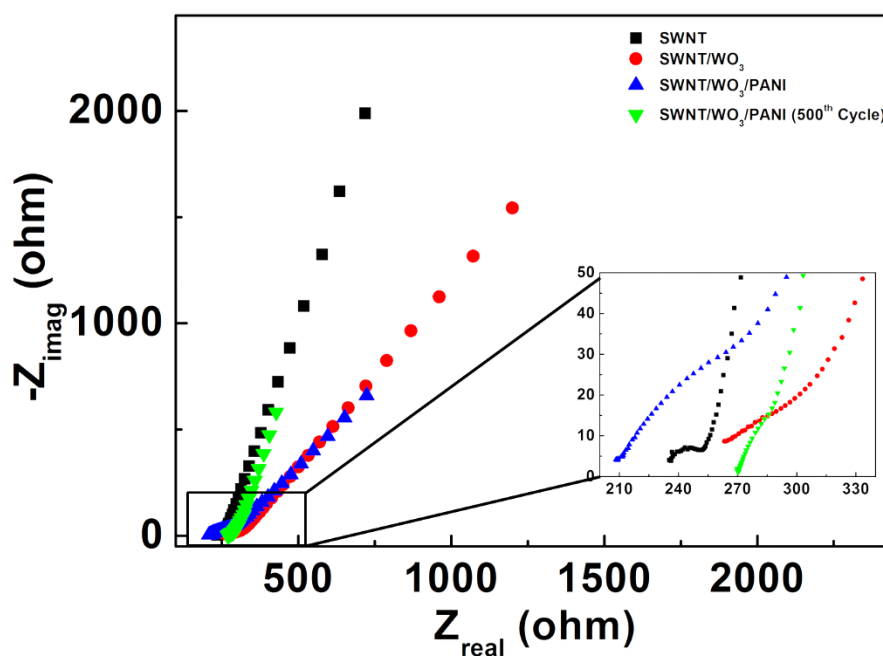


Figure 31. Impedance spectra of thin films measured within the range of 50 kHz to 50 mHz at a 0 V DCI. Inset shows the magnified high frequency region.

In this study, obtained results were reported in terms of areal capacitance due to the fact that the gravimetric measurements and following calculations of the electrode weight would have high systematic error because of the low mass of electrode. In addition, other parameters such as the heavy glass substrate, formation of metal oxide hydrates and humidity could also contribute to the error.

3.4 Conclusions

In this study, a low cost and simple route for the fabrication of SWNT based ternary nanocomposite electrodes were demonstrated and their synergistic and complementary effect on SC performance was investigated. Typical EDLC behavior of SWNT electrodes was improved with the pseudocapacitive properties of WO_3 and PANI. Fabricated ternary nanocomposite SC electrodes were found to have a specific capacity of 28.5 mF/cm^2 at 0.13 mA/cm^2 current density. Variation in the C_{sp} was found to be less than 24% after 2000 GCD cycles. Performance drop was attributed to the degradation of PANI at ambient conditions. Finally, ternary nanocomposite SWNT/ WO_3 /PANI films investigated herein are promising electrode active materials for electrochemical energy storage systems if an air-stable CP can be integrated into the structure.

CHAPTER 4

TEXTILE SUPERCAPACITORS BASED ON MNO_2 /SWNT/CONDUCTING POLYMER TERNARY COMPOSITES

4.1 Introduction

Textile based electronic systems (e-textile, smart textile or wearable electronics) may possibly be used in the future for high-tech workwear, portable energy systems, sportswear, health monitoring systems and military camouflages [140-142]. Functionalization of textiles with conducting and semiconducting materials imparts electronic properties and functionalized textiles could be used in conjunction with or even replace traditional textiles. Many portable electronic devices could be integrated with the functionalized textiles. Wearable electronics have unique functionalities such as stretchability, light weight and flexibility that are hard to be shown by classic electronics [143, 144].

In last decades, nanomaterials were applied to textiles to offer antibacterial, anti-odor, UV and heat protection properties. Textile based electronic devices, on the other hand, have many capabilities, such as body health monitoring, actuation, radio or microwave absorption, heating, electrostatic discharge protection, or wiring for electronic devices [140-142, 145-148]. All these integrated devices for wearable electronics need an energy source and textile based SCs are promising candidates for this purpose. Low-cost and highly efficient textile based SCs are already started to be integrated into prototype wearable electronics [145, 149].

Common textiles such as cotton, polyester, acrylonitrile are reusable, cheap, flexible, and hydrophilic [150]. Once flexibility and stretchability are concerned, textile-based substrates are advantageous when compared to plastic counterparts and paper [150, 151]. For instance, porous structure of textiles provides a novel support for the loading of the nanomaterials and facilitates rapid absorption of the electroactive material solution that can be applied through a simple dipping and drying method [152].

Textile based wearable energy storage systems can be improved to provide high electrochemical energy storage capacity with the utilization of promising materials. For instance, SWNTs strongly bind to the textile fabrics due to the van der Waals forces and impart properties such as foldability and stretchability [150, 153]. In addition to van der Waals forces, carboxyl group functionalized SWNTs adhere to the surface of the textile fibers with hydrogen bonds [143, 150]. Washing and other mechanical processes give almost no damage to these textiles. Dip coating is the most common, economic and effective method for the deposition of SWNTs onto textiles [143]. The production route is simple and scalable, similar to the ones in the textile factories [143]. Repeated dipping and drying cycles and adjustment of ink concentration allows control over the deposited SWNT mass and the conductivity.

SWNTs have large surface area, functionable surfaces and chemical stability; however, their electrochemical capacity is not as high as the metal oxides [55, 154]. Therefore, capacity of the textile-based SCs can also be improved upon coating with the pseudocapacitive materials that keep charges by a redox processes [155, 156]. Manganese oxide (MnO_2) as a pseudocapacitive material is cheap, naturally abundant, environmental friendly and shows high capacity [32, 157, 158]. Theoretical energy storage capacity of MnO_2 is very high; however, its poor conductivity, brittleness and dense morphology limits its practical applications [158, 159]. It is not possible for the electrolyte ions to diffuse into the thick MnO_2 layers; therefore, only surface atoms interact with the electrolyte ions [159-161]. Thus, thick MnO_2 layers result in a dead volume, high resistance and capacitance loss [158, 159]. To overcome this problem, MnO_2 should be applied as a thin layer onto the textile fibers and used in a composite form with a conducting additive [162, 163]. This signifies that the composite formation is the most suitable solution to overcome these drawbacks and to improve the electrochemical performance of MnO_2 . Deposition of MnO_2 onto SWNT layer for textile based electrodes result in a sharp decrease in capacitance and increase in resistance [143, 156, 159, 161, 164]. Another problem with bulk metal oxides is that the binder materials such as poly(tetrafluoroethylene) (PTFE) or carboxymethyl cellulose (CMC) should be added to improve the mechanical stability of the electrodes. However, presence of PTFE and CMC decreases the overall conductivity [157]. Therefore, a binder free conductive additive would lead to both disperse and improve the mechanical properties of MnO_2 . Enclosing MnO_2 layer with SWNT layer on textile

fibers overcome these problems and improve the energy storage capacity. SWNTs cover MnO₂ nanoparticles on the textile fibers, which also improves the mechanical properties of the electrodes.

CPs impart prominent properties if they are utilized in wearable electronics [147, 148, 153, 165, 166]. They have good conductivity and highly pseudocapacitive properties. However, their poor mechanical properties and short service life limits their application in SCs [166, 167]. Dip coating can also be used for the deposition of CPs such as PEDOT:PSS and PANI onto textile fibers. Numbers of dipping cycles determine the thickness of CP. Three-dimensional structures of the fibers allow CPs to access the whole surface of the porous textile [95, 167]. CPs provide excellent support to metal oxide/SWNT composites on textile fibers in addition to enhancing the electrochemical properties of the SCs. Enhanced charge storage properties of SCs with ternary composite electrodes using MnO₂/SWNT/CPs has already been reported [162, 163, 168-171]. In addition to their conductive nature, CPs and SWNTs also contribute to the energy storage process of the composites. These ternary composite films offer higher capacitance when compared to binary composites of MnO₂/SWNT [154, 156, 159, 160, 164], MnO₂/CP [172-174], and SWNT/CP [153, 175, 176]. Carboxyl group functionalized SWNTs show high electrical conductivity and they maintain their structural integrity within the composite [162, 168]. Pseudocapacitive contributions of MnO₂, PANI and PEDOT:PSS are strengthened by the mechanical and electrical properties of the SWNTs, which results in a complementary and synergistic effect.

In this work, we have fabricated textile-based high-performance, flexible and ternary nanocomposite SCs using MnO₂ nanoparticles, SWNTs, PEDOT:PSS or PANI as electrode active materials and a gel electrolyte. High conductivity of the CP and SWNTs eliminated the need for a separate charge collector within the fabricated SCs.

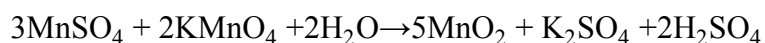
4.2 Experimental Details

4.2.1 Materials:

SWNTs were purchased from Carbon Solutions Inc. (SWNT P3, metal content 5-7 wt % from TGA in air and carbonaceous content more than 90 %). All the other materials used in this work were in analytical grade and used without further purification and obtained from Sigma-Aldrich.

4.2.2 Manganese (IV) oxide nanoparticles coated textile preparation:

MnO₂ nanoparticles were synthesized through the reaction of potassium permanganate (KMnO₄) with manganese sulfate (MnSO₄) in an aqueous medium according to the reaction below [158]:



Synthesized MnO₂ nanoparticles were twice centrifuged with deionized water. MnO₂ ink was then produced by dispersing 50 mg MnO₂ in 50 H₂O through tip sonication. Cotton textiles (size of 2 cm x 2 cm) were dip coated with MnO₂ ink and dried for 10 min at 80 °C. This process was repeated 3 times.

4.2.3 SWNT coated textile preparation:

SWNT ink was prepared as described in literature [143, 150]. Shortly, aqueous SWNT ink was prepared by dispersing SWNTs (1.6 mg/ml) in sodium dodecylbenzenesulfonate (SDBS, 5 mg/ml) using a tip sonicator. MnO₂ coated textiles were then dip coated with the prepared SWNT ink. Textile pieces quickly absorbed ink solution and get coated with the SWNT ink. SWNT coated textile pieces were then dried at 80 °C for 10 min. A conductive fabric was obtained through this simple process. This process was repeated 5 times.

4.2.4 Conducting polymer coated textile preparation:

Highly conductive grade PEDOT:PSS was diluted in a 1:9 ratio with isopropanol and textile pieces were dip coated with this solution of PEDOT:PSS (0.1 wt %). Following deposition, textile pieces were dried at 80 °C in a vacuum oven.

PANI was synthesized by chemical oxidation of aniline monomer in 1 M hydrochloric acid (HCl) using oxidizing agent ammonium peroxydisulfate ((NH₄)₂S₂O₈, APS) in 1 M HCl as described by Sainz et al. [176]. PANI was diluted in N-methylpyrrolidone (NMP) and the textile pieces were dip coated with PANI (0.1 wt %) similar to the PEDOT:PSS coating.

4.2.5 Preparation of gel electrolyte:

Gel electrolyte preparation was described in our previous work [133]. The gel electrolyte used in the SCs was composed of ACN (acetonitrile): PC (propylene carbonate): PMMA (poly(methylmethacrylate)): TBAPF₆ (tetrabutylammonium hexafluorophosphate) in a ratio of 70:20:7:3 by weight.

4.2.6 Fabrication of supercapacitors:

Schematics of the SC electrode fabrication steps are provided in Figure 32 (a). A Celgard separator (Celgard 2501) was utilized for the fabrication of fully operational SCs. Separator was wetted with the gel electrolyte and placed between two textile electrodes as shown in Figure 32 (b).

4.3 Characterization

Bare cotton fabric was cut into 2 cm x 2 cm pieces, washed with deionized water and dried. Prepared textile pieces were used as SC electrode substrates. SC electrodes were subjected to a mechanical adhesion test (standard tape test), which was followed

by a washing test (washing at 30° C for 30 minutes in deionized water), while the conductivity was monitored.

The morphology and structure of the textile based nanocomposite SC electrodes were characterized using SEM (FEI Nova Nano SEM 430, operated at 10 kV). A thin (10 nm) gold-palladium coating was utilized for SEM imaging for insulating samples. XRD measurements were carried out on a Rigaku D/Max-2000 pc diffractometer. A two-electrode setup was used to investigate the electrochemical performances of the SCs via Gamry Reference 3000 potentiostat/galvanostat system. Devices were measured after 48 hours of fabrication. All electrochemical measurements were carried out within a cell voltage window of 0 to +2.0 V provided through the use of an organic based gel electrolyte. The weights of total active materials in SCs were nearly 1 mg.

4.4 Results and Discussions

The ternary nanocomposite SC devices were assembled using dip coated textile based electrodes and photographs of the electrodes are provided in Figure 32 (c). Color change induced by the deposition of MnO₂ nanoparticles, SWNTs and CP layers on the cotton fabrics can be seen in the figure. The ink solution concentration and the number of dipping and drying cycles controlled the amount of active material. Ternary composite fabrics were used both as the electrodes and the current collectors. Natural flexibility and high liquid absorption capacity of the cotton textiles resulted in the improved mechanical properties of the electrode active materials.

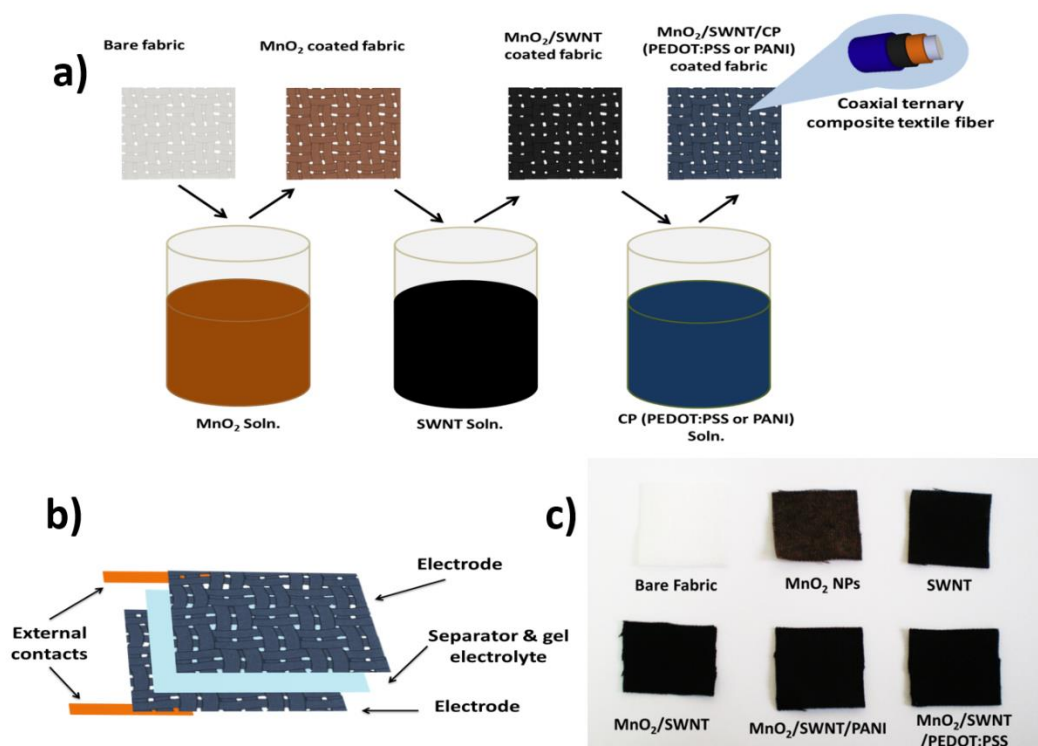


Figure 32. (a) Schematic of the electrode preparation steps, (b) fabricated SCs from ternary composite fabrics. (c) Photographs of the dip-coated textile based electrodes.

SWNT coated bare and MnO_2/SWNT coated textile pieces did not show SWNT dissolution in water and detachment with tape during washing and adhesion tests. The conductivity of SWNT coated samples showed almost no degradation following these tests. $\text{MnO}_2/\text{SWNT}/\text{PANI}$ ternary nanocomposite electrodes also survived washing and adhesion test. On the other hand, PEDOT:PSS is a water soluble CP and as expected, it was dissolved during the washing test. However, PEDOT:PSS coated textiles showed no degradation during tape test. These tests showed that active electrode materials were strongly adhered onto the textile fibers, which is very important for further applications.

SEM images of the textile fibers following each dip coating step is provided in Figure 33 (a)-(d). In Figure 33 (a), MnO_2 nanoparticle coated textile fibers are shown. The loading of MnO_2 layer was kept as low as possible in order to allow electrolyte ion permeation. Spherical MnO_2 nanoparticles are known to have high porosity, which results in their significant electrochemical properties [158]. Corresponding EDS

spectrum of the MnO₂ coated textile electrodes is provided in the inset of Figure 33 (a). Mn (from MnO₂) signals were evident within the spectrum. After 5 dipping and drying cycles with SWNT ink solution, a homogeneous surface coverage was achieved, as shown in Figure 33 (b). Resistance of the textile electrodes following SWNT coating was less than 50 Ω. It was possible to increase the conductivity via acid treatment [150, 165]; however, this process would damage the metal oxide layer on the textile fibers. CPs PANI and PEDOT:PSS were diluted with solvents (NMP for PANI and isopropanol for PEDOT:PSS) and used separately. Both polymers smoothly covered the MnO₂/SWNT coated textile fibers, as shown in Figure 33 (c) and (d), respectively. Thick CP layers on the MnO₂/SWNT layer would block the electrolyte ion diffusion towards the MnO₂ and SWNT layers leading to a loss in capacity. Therefore, CPs PEDOT:PSS and PANI were diluted before electrode preparation. The XRD patterns of MnO₂ nanoparticles prepared via wet chemistry are provided in Figure 33 (e). It contains sharp peaks at 2θ around 37.3° and 66.4°, which correspond to α-MnO₂ (JCPDS card No. 72-1982). The crystallinity of MnO₂ is poor because of the absence of a proper annealing process. The XRD pattern of MnO₂ corresponds to crystalline α-MnO₂, while broad peaks, which are not well defined, indicate the formation of amorphous α-MnO₂ [158].

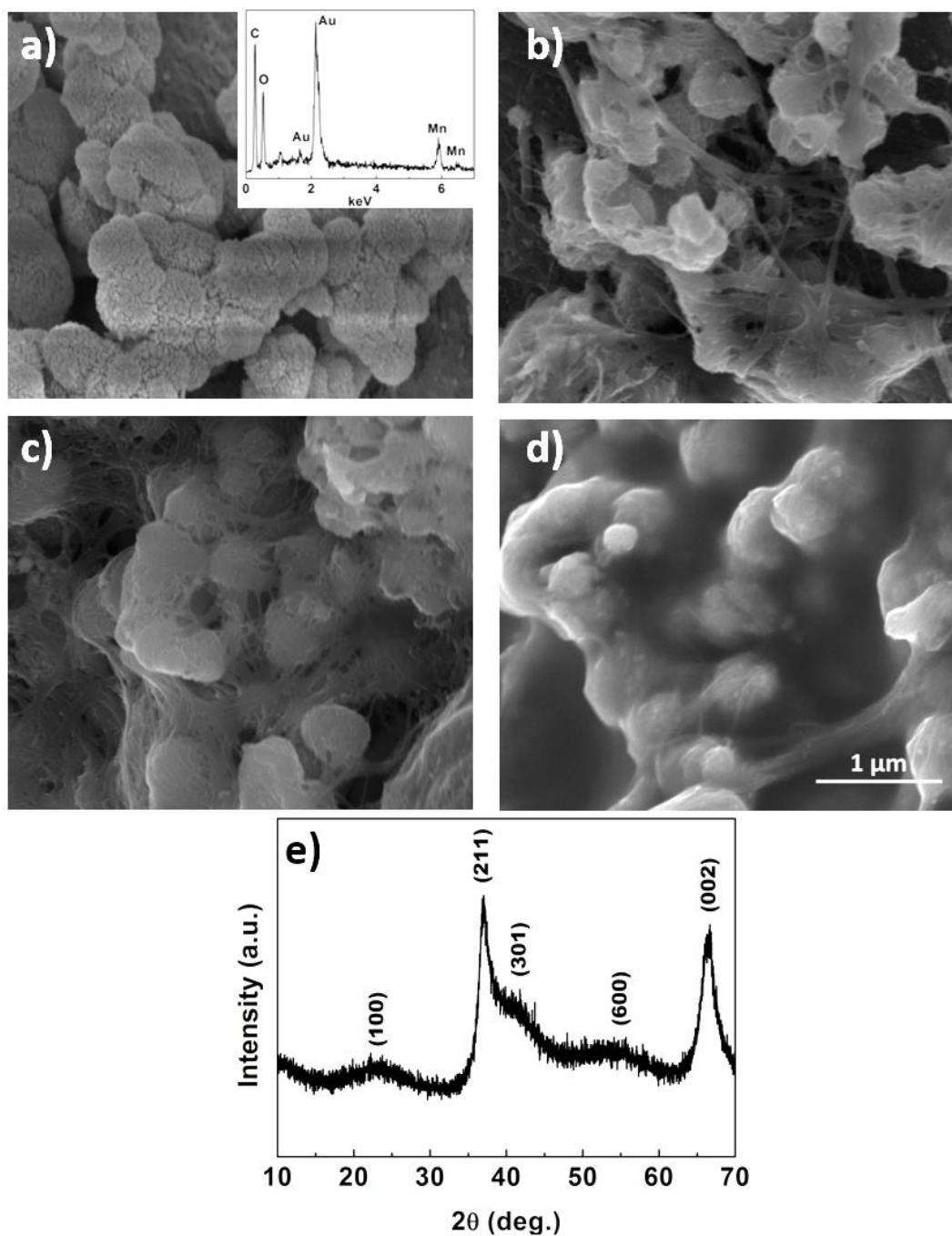


Figure 33. (a) SEM images of MnO₂, (b) MnO₂/SWNT, (c) MnO₂/SWNT/PANI, and (d) MnO₂/SWNT/PEDOT:PSS coated textile electrodes. All scales are the same. Inset shows the EDS spectrum of MnO₂ coated textile electrodes. (e) XRD pattern of the MnO₂.

Figure 34 shows surface resistance change with respect to number of dipping cycles of SWNT and CPs. The conductivity of the electrodes increased with the number of SWNT ink dipping and drying cycles. Following the deposition of SWNTs, CPs were applied to the textiles. The surface resistance of SWNT coated electrodes

was less than that of PEDOT:PSS coated electrodes. A little increase in the sheet resistance was observed upon PEDOT:PSS deposition onto the MnO₂/SWNT electrodes as shown in the figure. On the other hand, PANI deposited electrodes had slightly lower surface resistance than MnO₂/SWNT counterparts. Low surface resistance was important for the fabricated SCs since no separate current collector was used during measurements. Ternary composite active materials were used both as the host for the energy storage and the current collector.

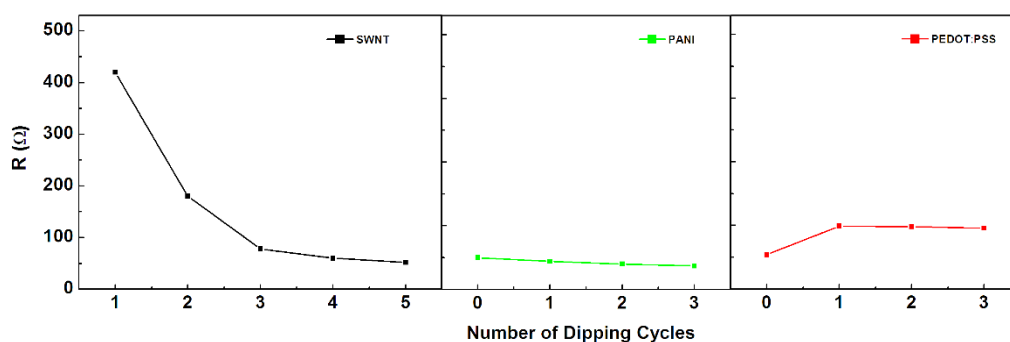


Figure 34. Surface resistance change with respect to number of dipping cycles into ink solutions of SWNT (black), PEDOT:PSS (red) and PANI (green) solutions. Lines are for visual aid.

Gel electrolyte was an ionic conductor with a honey-like viscosity. This viscosity of the electrolyte allowed stable electrochemical performance and electrolyte ions diffused through the all active material layers provided by the porous and three-dimensional structure of the cotton fabric. Instead of aqueous and PVA based gel electrolytes, the use of polymer based gel electrolyte with a wetted separator was the major point of this study and the main reason in obtaining good flexibility in fully-functioning devices. Absorption of the gel electrolyte by the fabric fibers provided more ion permeability as opposed to conventionally used low viscous PVA based gel electrolytes. It is worth mentioning that the external copper contact points were not damaged by the gel electrolyte. Another advantage of polymer based gel electrolyte was the large cell voltage window with respect to the aqueous electrolytes. The gel electrolyte was tested up to 2.0 V.

CVs of the fabricated textile-based ternary nanocomposite SCs are shown in Figure 35. As shown by CV measurements, the electrochemical performance of bare

SWNT SCs was significantly improved by the pseudocapacitive contribution of the uniformly distributed MnO₂ nanoparticles and CPs on the surface of the SWNTs. The electrochemical and mechanical stability of ternary nanocomposites were much better than pure MnO₂, CPs and their binary nanocomposites. Pseudocapacitive property of MnO₂ was realized by the high current collection efficiency of the SWNTs. In addition to this, SWNT layer prevents the pulverization of the MnO₂ layer when deposited on top, leading to mechanically robust electrodes. MnO₂/SWNT nanocomposite SC devices had both capacitive and resistive properties, while the addition of CP decreased the surface resistance and enhanced the electrochemical capacity of the nanocomposites as shown in the figure. Previous studies showed that MnO₂ deposition over SWNT layer on the textile-based electrodes results in an increase in capacitance; but, this may only be valid for a thin material layer due to the insulating nature of MnO₂ [154, 177]. SWNT coated textiles have purely electrochemical double layer capacitance (EDLC) behavior and functionalized surfaces of SWNT electrodes gained also pseudocapacitive properties. It is clear from Figure 35 that the charge storage capacity of the SCs increased following MnO₂ deposition. CP layer (PEDOT:PSS or PANI) on the MnO₂/SWNT deposited electrodes completed the ternary nanocomposite electrode structure. Pores of MnO₂/SWNT composites were filled with the CPs. Deposition of PANI onto MnO₂/SWNT electrodes enhanced the electrochemical capacity of the SCs more than the PEDOT:PSS counterpart.

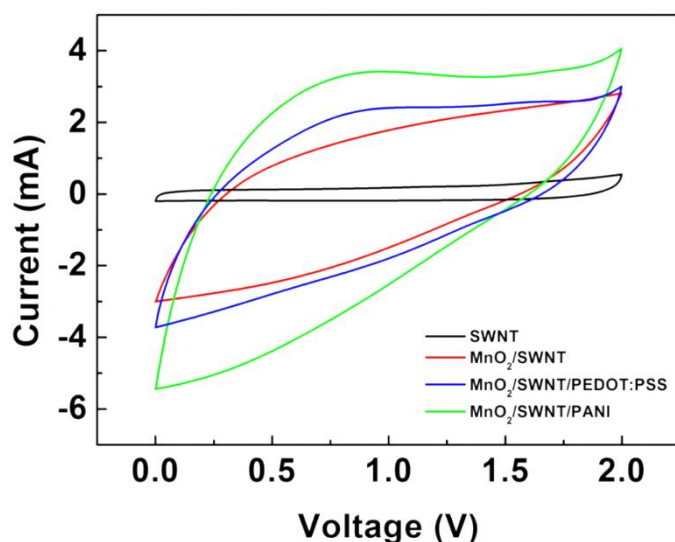


Figure 35. CVs of SWNT (black), MnO₂/SWNT (red), MnO₂/SWNT/PEDOT:PSS (blue) and MnO₂/SWNT/PANI (green) coated textile based SCs at 20 mV/s scan rate.

CV measurements of the ternary nanocomposite SCs with PEDOT:PSS and PANI at different rates are provided in Figure 36 (a) and (b), respectively. These results show the high rate capability of the nanocomposite SCs with increased scan rate. It is a common problem that the increase in the scan rates decreases the C_{sp} of the electrode active materials. This is due to the high scan rates resulting in the slow electrochemical response of the SC devices because of the reaction kinetics hindering the actual capacity of the devices. Internal resistance of the fabricated SCs resulted in the deviation from the ideal CV curve shape. PANI deposited ternary nanocomposite SC devices were found to have better charge storage characteristics compared to the PEDOT:PSS counterpart.

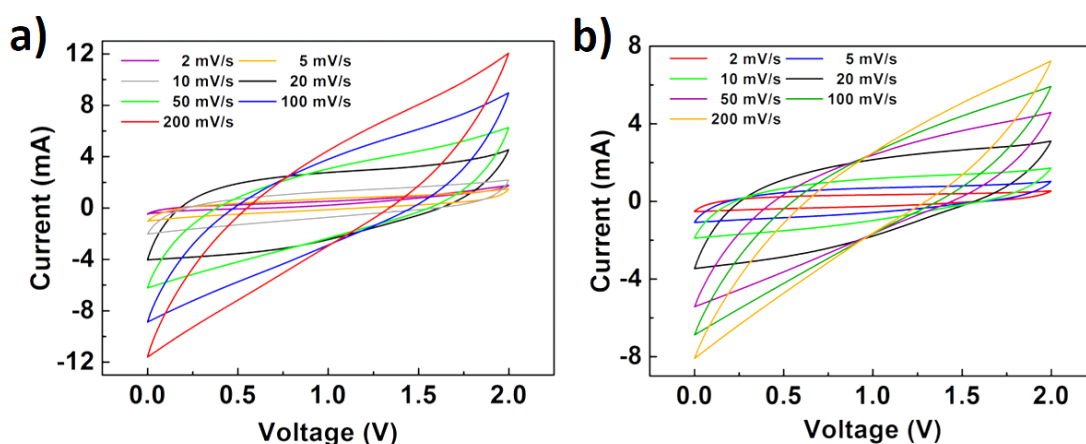


Figure 36. CVs of the fabricated (a) $\text{MnO}_2/\text{SWNT}/\text{PANI}$ and (b) $\text{MnO}_2/\text{SWNT}/\text{PEDOT:PSS}$ ternary nanocomposite electrodes at different rates.

The mechanical and functional integrity of the fabricated textile based ternary composite SCs were investigated through bending tests. CVs of the SCs measured during bending (with bending angles between 0° and 180°) are provided in Figure 37. Textile based SCs preserved their natural flexibility and were repeatedly bent with no significant variation in their electrochemical properties. Bending tests showed that the strong interface between electrode materials and gel electrolyte as well as the ionic transport within the gel electrolytes remained almost the same. This was attributed to the high flexibility of SWNTs and CPs. Small deviations during bending test are due to the movement of contact points and electrodes.

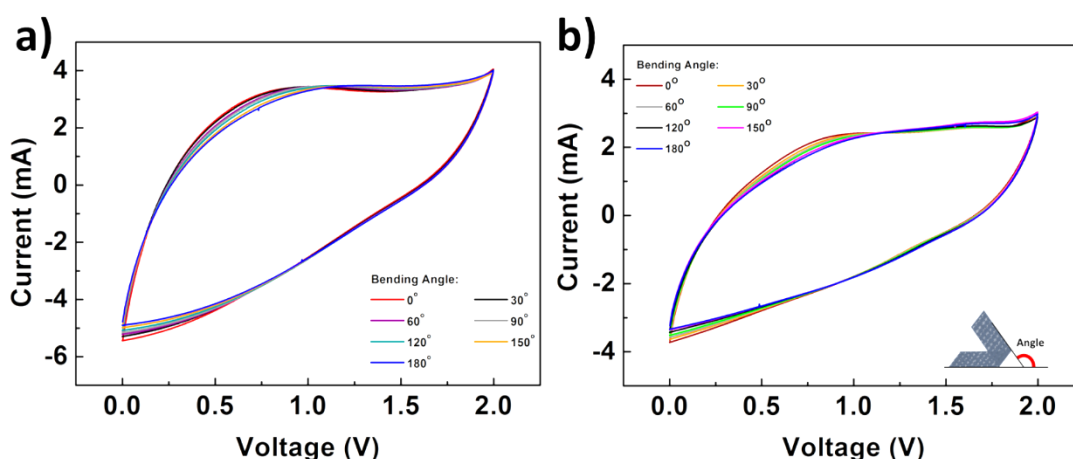


Figure 37. CV results of fabricated SCs with (a) $\text{MnO}_2/\text{SWNT}/\text{PANI}$ and (b) $\text{MnO}_2/\text{SWNT}/\text{PEDOT:PSS}$ ternary nanocomposite electrodes under different bending angles at 20 mV/s scan rate.

The GCD profiles of the devices were measured at 1 A/g and provided in Figure 38. Textile based SWNT SC devices had a discharge time of 20 seconds and it was improved as much as 10 times with the utilization of MnO₂. Integration of CPs into the SC devices increased the discharge times to 320 seconds and 340 seconds for MnO₂/SWNT/PANI and MnO₂/SWNT/PEDOT:PSS SCs, respectively. Bare SWNT device had a symmetric charge-discharge curve due to EDLC and low internal resistance. An important development in the charge storage capacity was seen with the formation of nanocomposites. The characteristic profile of the SWNT SCs was shifted to pseudocapacitive upon the addition of MnO₂ and CPs, as discussed earlier. The MnO₂/SWNT, MnO₂/SWNT/PEDOT:PSS and MnO₂/SWNT/PANI composite devices showed highly pseudocapacitive properties. Internal resistance drop (IR_{drop}) was observed in the measurements. It was attributed to the ESR that contains both electrolyte and electrode resistance, as well as the contact resistance among the electrodes, separator and the electrolyte [133].

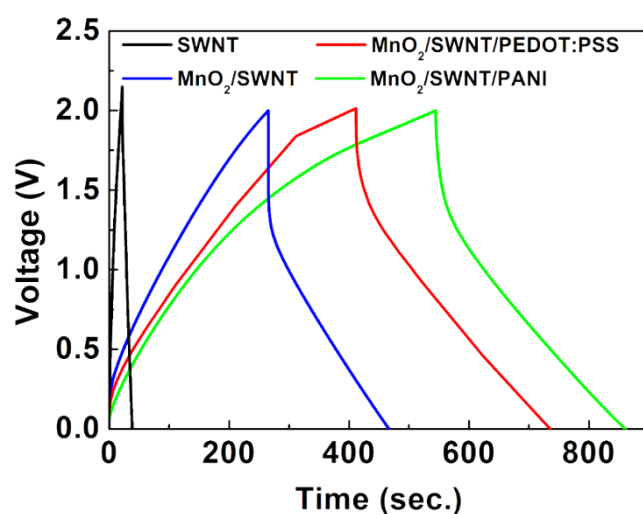


Figure 38. GCD profiles of the fabricated SCs at 1 A/g.

The GCD characteristics were measured at different current densities. Discharge profiles (provided in Figure 39) of the SCs depend on the applied current. Different current densities gave similar curve shapes. Dip coated electrode active materials resulted in the formation of thin layers on the surface of textile fibers. It is an advantage that textile fibers totally absorb the gel electrolyte and allow the electrolyte ions to reach all the active layers, which resulted in high charge accumulation.

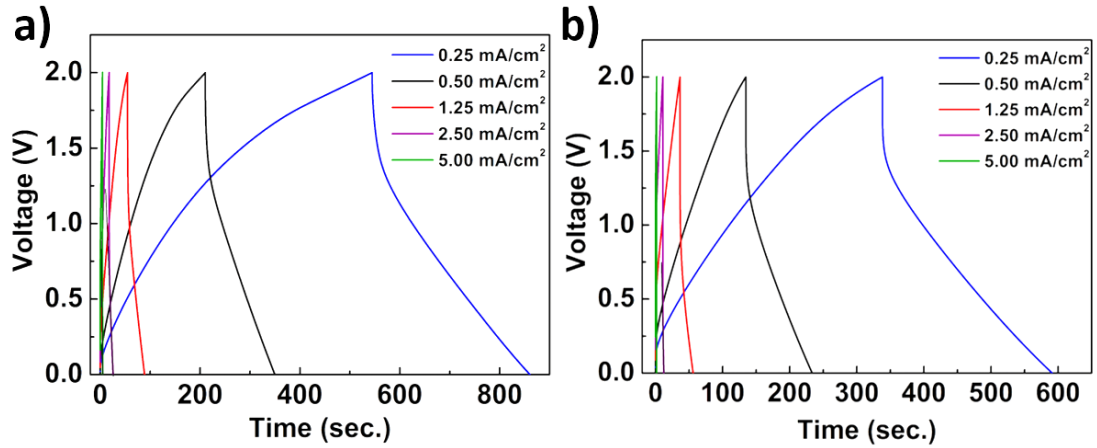


Figure 39. GCD curves of fabricated SCs with (a) MnO₂/SWNT/PANI and (b) MnO₂/SWNT/PEDOT:PSS ternary nanocomposite electrodes at current densities from 0.25 to 5 mA/cm².

GCD curves (shown in Figure 38-39) were used to find the C_{sp} of the fabricated supercapacitors using the equation:

$$C_{sp} = \frac{I}{m(dV/dt)}$$

where V is the discharge voltage after IR drop, I is the applied discharge current, t is the discharge time and m is the total mass of in both electrodes. Specific capacitances of the SC devices with respect to the current densities are plotted in Figure 40 (a). C_{sp} were calculated as 294 F/g and 246 F/g at 1 A/cm² for MnO₂/SWNT/PANI and MnO₂/SWNT/PEDOT:PSS devices, respectively. Specific capacitances at the same current density for bare SWNT and MnO₂/SWNT binary nanocomposite were 23.8 F/g and 209 F/g, respectively. It is clear that the ternary nanocomposite textile based SCs showed higher capacitance values as compared to bare SWNT and MnO₂/SWNT binary nanocomposite devices. The C_{sp} of the SWNT was improved by the incorporation of MnO₂ and CPs due to the homogeneous distribution of MnO₂ nanoparticles on the textile fibers and composite formation with CPs. A decrease in C_{sp} from 294 F/g to 84 F/g was obtained when the current density was increased from 1 A/g to 20 A/g for MnO₂/SWNT/PANI devices. A similar decrease from 246 F/g to 88 F/g was obtained under the same conditions for the MnO₂/SWNT/PEDOT:PSS counterparts. C_{sp} calculated using GCD curves (Figure 39) were found to decrease with increasing withdrawn cell current. This is due to the fact that at higher current densities

the slower processes show a resistance to measurement kinetics and also it hinders the charge transfer [117].

For the lifetime measurements, fabricated SCs were charged and discharged for 1000 cycles. As shown in Figure 40 (b), capacity retention for the MnO₂/SWNT/PANI and the MnO₂/SWNT/PEDOT:PSS ternary nanocomposite devices were 72 % and 74 %, respectively, after 1000 galvanostatic charge-discharge cycles. SWNT/MnO₂ binary composites and especially bare SWNT electrodes showed highly stable performance. Performance degradation of the ternary composites was attributed to the degradation of CPs at ambient conditions [132, 178]. Coulombic efficiencies of the fabricated SC devices are plotted in Figure 41. All SCs displayed stable device performance and their coulombic efficiencies after 1000 cycles were higher than 98 % of the initial values.

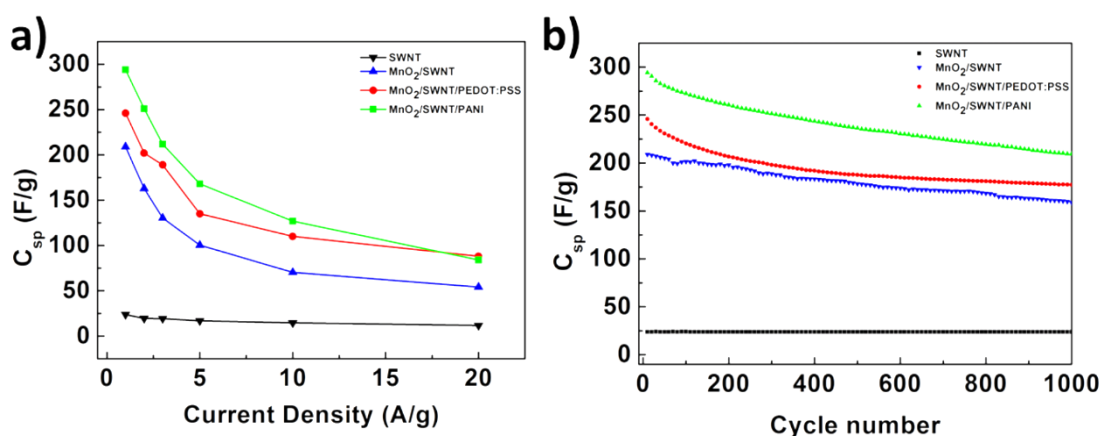


Figure 40. C_{sp} of the fabricated SC devices (a) with respect to current density (Lines are for visual aid) and (b) with respect to cycle number.

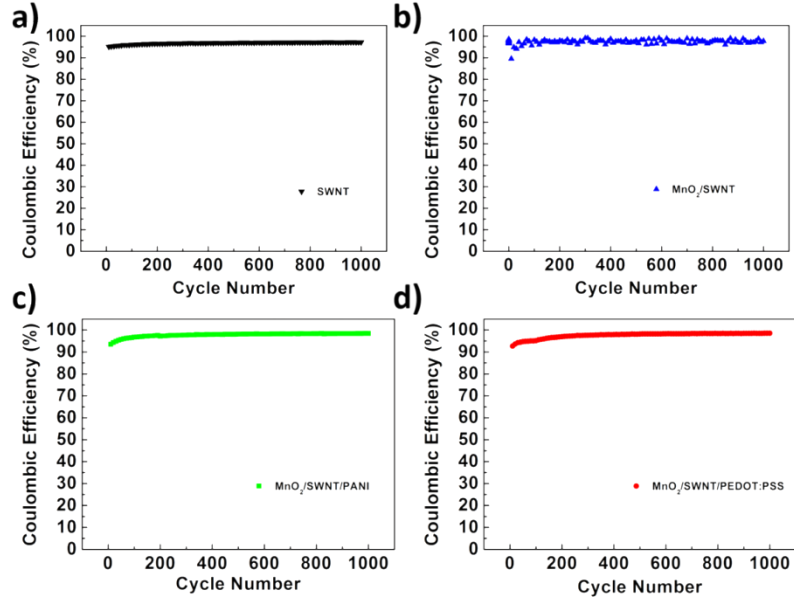


Figure 41. Coulombic efficiencies of (a) SWNT, (b) MnO₂/SWNT, (c) MnO₂/SWNT/PANI and (d) MnO₂/SWNT/PEDOT:PSS SC devices.

Following equations were used to calculate the power and energy densities of the ternary nanocomposite SCs:

$$P_{cell} = \frac{E_{cell}}{t} \quad , \quad E_{cell} = \frac{C_{cell} \cdot V^2}{2 \times m}$$

where m is the mass in both electrodes, V is the applied voltage and the t is galvanostatic discharge time. Power and energy densities and specific capacitance of the devices were calculated to be 746.5 W/kg, 66.4 Wh/kg, 294 F/g for MnO₂/SWNT/PANI and 60.2 Wh/kg, 640.5 W/kg, 246 F/g for MnO₂/SWNT/PEDOT:PSS, respectively. Obtained values were found to be at the moderate power range.

In practical sense, textile based SC devices should be washable, mechanically stable and flexible. In addition to these mechanical criteria, they should exhibit high electrochemical capacity [177]. Having met these mechanical constraints, we compared the electrochemical performance of our devices to those in literature within Table 4. It has to be noted that our devices operates on a larger potential window,

without aqueous electrolytes. In terms of capacitance and power densities, our devices give moderate results. For instance, capacitance values span from 1 to 500 mF/cm², for textile based SCs, while 73.5 and 64.5 mF/cm² were obtained for PANI and PEDOT: PSS containing nanocomposites, respectively, in this work.

Table 4. Textile based SCs from literature in conjunction with obtained results herein (Adapted and modified form ref. [17]).

Active Materials	Fabric	Electrolyte Type	Device Capacitance per area (mF/cm ²)	Refs.
Activated carbon	Cotton and polyester	1M Na ₂ SO ₄	240.00	[149]
SWNTs	Knitted cotton	1M LiPF ₆	480.00	[143]
SWNTs	Nonwoven cotton	Li ₂ SO ₄ /Na ₂ SO ₄	16.40	[150]
Graphene paint	Woven cotton	1M KOH	43.50	[179]
Graphene	Ni-coated nylon mesh	1M Na ₂ SO ₄	44.70	[180]
SWNTs + MnO ₂	Knitted cotton	2M Li ₂ SO ₄	276.00	[143]
Graphene/CNT/Fe ₃ O ₄ WO ₃ -x@Au@MnO ₂ core-shell Nanowires	Carbon fiber fabric	1M Na ₂ SO ₄	0.98	[181]
MnO ₂ /carbon	ZnO nanowires	0.1M Na ₂ SO ₄	57.00	[182]
MnO ₂ /carbon	ZnO nanowires	PVA-LiCl	26.00	[183]
MnO ₂ /SWNT/PANI	Cotton	TBAPF ₆ /PC/PMMA /ACN	73.50	This work
MnO ₂ /SWNT/PEDOT:PSS	Cotton	TBAPF ₆ /PC/PMMA /ACN	64.50	This work

4.5 Conclusions

In this study, highly flexible, solid-state textile-based SCs with binder-free ternary nanocomposite electrodes were fabricated. An economic and rapid route was demonstrated for the fabrication of flexible and high performance SCs. High conductivity of the SWNTs and the CP layers eliminated the necessity for extra charge collectors. We have examined the effect of components separately and together in ternary nanocomposite form on the electrochemical performances of the SCs. Surface resistance of the electrodes and of the overall devices were controlled by the densities of SWNTs and CP (PANI and PEDOT:PSS). The measured C_{sp} , power and energy density were 294 F/g, 746.5 W/kg, and 66.4 Wh/kg for MnO₂/SWNT/PANI and 246 F/g, 640.5 W/kg, and 60.2 Wh/kg for MnO₂/SWNT/PEDOT:PSS ternary composite devices, respectively. Fabricated SCs were highly stable and the variation in C_{sp} was less than 30% over 1000 GCD cycles. MnO₂/SWNT/PANI ternary nanocomposite SCs showed better electrochemical properties than the MnO₂/SWNT/PEDOT:PSS counterparts. Performance degradation was mainly attributed to degradation of CPs in ambient conditions. In addition, the change in C_{sp} was found to be less than 3 %, down to a bending angle of 180 degrees. Strong adhesion of the metal oxide nanoparticles, SWNTs and CPs to the textile fibers resulted in high bending performance without significant deterioration in device characteristics. We believe that these SCs will be critical components of wearable electronic devices and smart textiles.

CHAPTER 5

ALL-ORGANIC ELECTROCHROMIC SUPERCAPACITOR ELECTRODES

5.1 Introduction

There is an increasing demand for the portable electronics and hence SCs are good candidates to complement batteries in power compartment of those devices. SC devices provide high power and moderate energy densities [12, 85, 86]. Electrochromic materials may show the instant capacity via changing color. In contrast to commercial batteries, electrochromic SCs indicate their stored capacity without pressing on the contact points. Depending on the stored charge in the SC device, multiple color change may be observed in a reversible manner. In the literature, there are some examples of color changing supercapacitive energy storage systems. Metal oxides [184-187] and CPs [188-190] are the two common SC electrode materials that possess electrochromism. Among CPs, polyaniline (PANI) is the most frequently used one in SC devices and its electrochromic property was thoroughly investigated by many research groups [188-190]. However, color change in PANI is in a very narrow range, limited to light yellow, green and blue, which barely create color contrast [188]. PEDOT:PSS is another CP with reported electrochromism. It is utilized in SCs, primarily employed as the current collector with improved conductivity [190]. Tungsten oxide (WO_3) is the most commonly utilized electrochromic metal oxide and it experiences a color change from yellow to blue; but, its electrochemical energy storage capacity is low [185, 186]. Combination of WO_3 and PANI in a nanocomposite form was also used for electrochromic energy storage devices [128, 191]. Patterned hybrid WO_3 -PANI electrodes displayed optical contrast and were found to have lower capacitance values than WO_3 based supercapacitors. Ho et al. investigated the combined electrochromic properties of WO_3 nanoparticles and dye molecules in a thin film battery [192-194]. Vanadium pentoxide (V_2O_5) nanoparticles deposited on fluorine tin oxide (FTO) thin film coated glass substrates showed reversible color change from green to blue and performed as an electrochromic SC [184]. It is clear that new and novel materials with multi-chromaticity and promising electrochemical

properties are necessary for improving the electrochromic SCs. In terms of chromaticity polymers are more versatile compared to the metal oxides. Therefore, synthesis and application of new CPs by tailoring their electrochemical and optical properties is an essential point for electrochromic electrochemical capacitors. For electrochromic SCs, ease in processability and low cost are the two advantages that can be provided by the CPs.

High transparency and conductivity of SWNT thin films allows the integration of electrochemical and electrochromic properties of new polymers within a multifunctional device. CNT thin films are a new class of materials where they are used in an ensemble form [98] and are highly appealing candidate materials for SC electrodes [91, 133]. They can be utilized both as a charge collector and capacitive material, eliminating the use of extra charge collectors. They possess good chemical inertness and high porosity in addition to conductivity and transparency [32, 33, 90].

Here, we investigate production of versatile all-organic, SWNT/CP nanocomposite SC electrodes. Our SWNT/CP SC electrodes worked as an indicator displaying three different colors from purple-red to black and blue, which indicate the charge state of the SC electrodes.

5.2 Experimental Details

SWNTs were purchased from Carbon Solutions Inc. (SWNT P3, metal content 5-7 wt % from TGA in air and carbonaceous content more than 90 %). All other materials used in this work were of analytical grade and were purchased from Sigma-Aldrich and used without further purification.

5.2.1 SWNT thin film preparation:

SWNT film electrodes were deposited onto soda lime silicate glasses via filtration and consecutive stamping [133]. Filtration solution was prepared by dispersing SWNTs in 1 % sodium dodecyl benzene sulfonate (SDBS) in deionized water ((18.3 M Ω) by tip-sonication (at 90% power, 70 W, Bandelin Sonopuls HD 2070

ultrasonic homogenizer). Sonication was performed for 5 minutes. For vacuum filtration process, mixed cellulose acetate (MCE) (Merck, 200 nm pore size) membranes were used and the vacuum filtration flow rate was $\sim 1 \text{ m}^3/\text{h}$. After the accumulation of SWNTs on the filter membrane, excess surfactant was eliminated by washing. The film homogeneity was controlled by the accumulation of SWNTs on the filter membrane. The SWNT mass in the thin film (typically $0.01 \text{ mg}/\text{cm}^2$) was determined by the volume of filtration solution. SWNT film on MCE membrane was transferred onto soda-lime silicate glass substrates by applying pressure (about $0.2 \text{ kg}/\text{cm}^2$) and heat ($80 \text{ }^\circ\text{C}$ over a hot plate). After 2 hours, MCE filter membranes were dissolved in acetone. To remove filter paper residues, SWNT electrodes were treated with concentrated HNO_3 (65 %) for 3 hours. Acid treatment also helps to improve the SWNT thin film conductivity [101]. Sheet resistances of the SWNT thin films before and after acid treatment were 110 and 82 ohms/sq, respectively. The resulting circular thin films had an area of 2 cm^2 . Conductive carbon paint (Graphite conductive adhesive 112, Electron Microscopy Sciences) was painted with a brush to print external contact points of the electrodes. A transmittance of 79 % (at a wavelength of 550 nm) was obtained for the fabricated SWNT thin films. Density of the SWNT thin films was high enough to decrease series resistance; but, low enough to allow observation of color changes.

5.2.2 Conducting polymer synthesis:

The CP, poly(4-(dithieno[3,2-b:2',3'-d]thiophen-2-yl)-2-(2-octyldodecyl)-2H-benzo[d][1,2,3]triazole) was synthesized according to the procedure previously reported [195]. Bromination of benzothiadiazole and then reduction of brominated thiadiazole yielded 3,6-dibromobenzene-1 and 2-diamine. Cyclization was carried out and then alkyl chain, which was prepared by reaction of corresponding alcohol with PPh_3 and Br_2 , was introduced to yield 4,7-dibromo-2-(2-octyldodecyl)-2H-benzo[d][1,2,3]triazole. Polymerization via Stille coupling reaction was performed with 2,6-bis(tributylstannyl)dithieno[3,2-b:2',3'-d]thiophene and 4,7-dibromo-2-(2-octyldodecyl)-2H-benzo[d][1,2,3]triazole via bis(triphenylphosphine)palladium(II) dichloride catalyst. After 3 days of refluxing, bromobenzene and tributyl(thiophen-2-yl)stannane were used as the end capper. The polymer was collected with Soxhlet

extraction was performed with methanol, hexane and acetone in the given order. The scheme shown in Figure 42 illustrates the final step of the polymer synthesis. CP was dissolved in chloroform (0.5 mg/ml) and deposited onto SWNT thin films by spray coating. CP solution was deposited onto SWNT thin films using simple nitrogen fed air brush. A microbalance was used to measure the mass of CP and the weight of total active materials in the SWNT/CP nanocomposite electrode was measured as 0.04 mg.

5.2.3 Characterization

The morphology of the fabricated SC electrodes were characterized by SEM (FEI Nova Nano SEM 430, operated at 10 kV). Raman spectroscopy was performed on an inVia Renishaw microscope using 532 nm laser. FTIR spectroscopy analysis was conducted using a Bruker IFS 66/S model spectrometer to determine the chemical nature of the electrodes. FTIR spectra of the thin films were obtained in the ATR mode. Spectroelectrochemical studies of the polymers were carried on ITO coated glass substrates (Delta Technologies, 4-8 ohm) out by Varian Cary 5000 UV-Vis spectrophotometer. Electrochemical measurements of the SC electrodes were conducted in a three-electrode configuration using a Gamry Reference 3000 potentiostat/galvanostat.

5.3 Results and Discussion

Number average (M_n) and weight average (M_w) molecular weights of the synthesized polymer were 38 kDa and 412 kDa, respectively, according to the gel permeation chromatography.

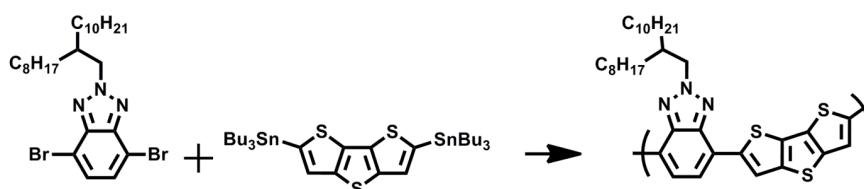


Figure 42. Synthetic pathway for poly(4-(dithieno[3,2-b:2',3'-d]thiophen-2-yl)-2-(2-octyldodecyl)-2H-benzo[d][1,2,3]triazole).

SEM images of bare SWNT thin films and spray coated CP layer on SWNT thin films are provided in Figure 43 (a) and (b), respectively. SWNTs (Figure 43 (a)) were percolated and spray coated polymer layer both fills the voids within the SWNT network and also covers the surface of the SWNT network as evidenced in SEM image provided in Figure 43 (b).

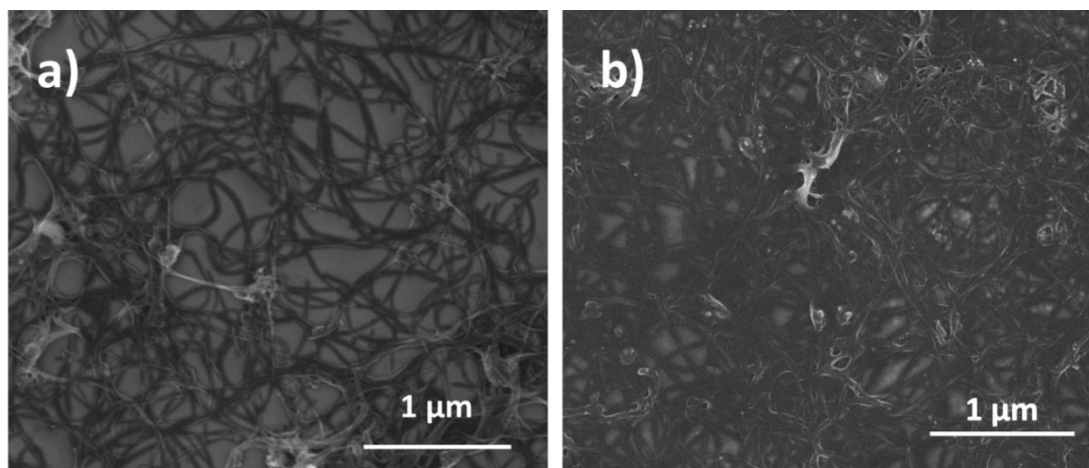


Figure 43. SEM images of (a) bare SWNT and (b) SWNT/CP nanocomposite electrodes.

Figure 44 (a) shows the FT-IR spectra of SWNT and SWNT/CP composite thin films within the spectral region $3500\text{--}400\text{ cm}^{-1}$. The bands in SWNT/CP nanocomposite film spectra located at 2917 and 2848 cm^{-1} are due to C-H stretching modes of saturated alkyl chains of the CP. The small peak at 1640 cm^{-1} is corresponding to C=N and C=C bonds in benzotriazole groups. The peak at 1260 cm^{-1} arises from the benzene ring in benzotriazole group of CP. The broad peaks at 882 and 745 cm^{-1} are due to aromatic rings in the SWNTs and they are dominant in both spectra [196, 197].

Further insight into the CP film structure can be gained by considering the changes in the Raman spectra. Figure 44 (b) shows the Raman spectra of SWNT and SWNT/CP nanocomposite thin films. The most pronounced effect is the suppression of the G-band (1575 and 1595 cm^{-1}) of SWNTs in the SWNT/CP nanocomposite film. The peaks for SWNT/CP appear at 1304 , 1435 and 1486 cm^{-1} for collective oscillation of the C=C bonds in dithienothiophene groups. The peaks at 1418 cm^{-1} and 1525 cm^{-1}

¹ are attributed to the benzotriazole group, due to the vibration of triazole unit and stretching of the benzotriazole ring [196, 198].

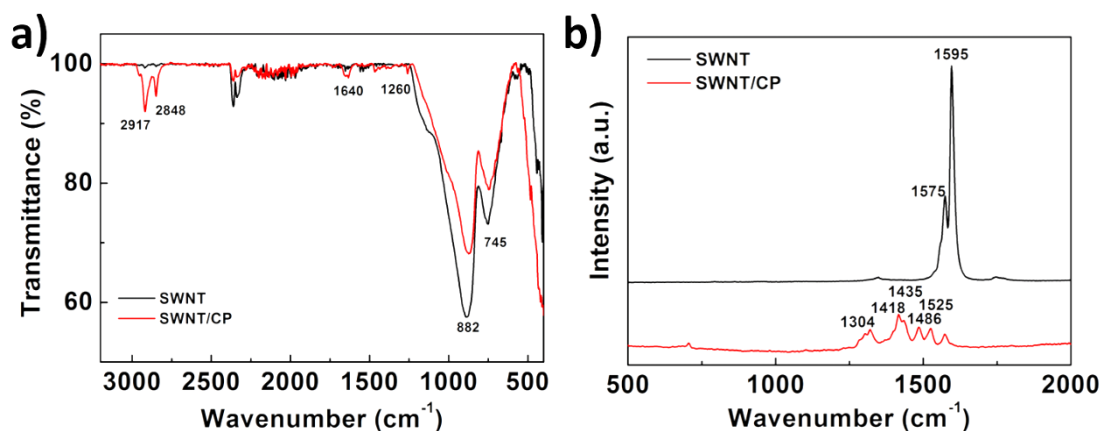


Figure 44. (a) FTIR and (b) Raman spectra of bare SWNT and SWNT/CP nanocomposite electrodes.

Spectroelectrochemical studies of the CP were examined to diagnose the changes in the UV-Vis during electrochemical measurements. The obtained UV-Vis-NIR spectra of the CP on ITO coated glass substrates are provided in Figure 45 (a) within a wavelength range of 380-1650 nm. The spectra were recorded with polarization within a potential range between -0.2 V and 1.3 V. It revealed an absorption peak at 530 nm due to π - π^* transition. The color of the CP was purple-red in its neutral state. During oxidation, the intensity of the peak at 530 nm was decreased and new bands appeared around 700 and 1260 nm due to the formation of charge carrier bands. Charge carrier band continued in the visible region and resulted in the observation of different colors at various potentials. CP had black color in its intermediate and blue color in its fully oxidized state. Among other CPs, the black color formation is not so common and it might have a particular importance for electrochromic applications. The UV-Vis-NIR spectra of the SWNT/CP nanocomposite electrodes have also been also recorded within the same wavelength range and provided in Figure 45 (b). The spectra show a somewhat similar behavior to that measured on ITO. Absorption peak at 530 nm was found to blue shift to 465 nm, which was attributed to the charge transfer between SWNTs and CP. Similarly, with the increase in applied potential, a decrease in absorption band was obtained. The

absorbance values were low due to the presence of underlying SWNT thin film. SWNT/CP nanocomposite electrodes also experienced multiple color changes from purple-red to black and blue with respect to the applied potential (Figure 45 (c)). SWNT/CP nanocomposite experiences a reversible and rapid color change due to ion insertion and extraction. Simultaneous color change, which can be directly observed by the naked eye, shows the state of the stored energy. Increasing polymer content in the nanocomposite film shows high color contrast though the optical transmittance was found to decrease. CP shows good electrochromic and electrochemical properties within the investigated potential range between -0.3 to 1.5 V. This wide potential window allows the observation of multichromatic properties with respect to the charged state, allowing simple visual monitoring.

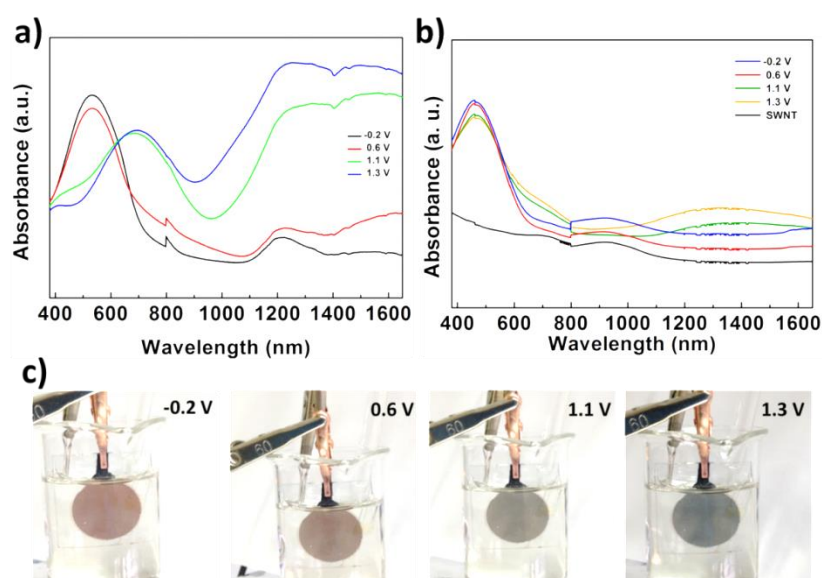


Figure 45. UV-Vis spectra of (a) CP on ITO thin film and (b) SWNT/CP nanocomposite film electrodes. (c) Photograph of the fabricated SWNT/CP electrodes at different charged states (purple-red: -0.2 V, black: 1.1 V and blue: 1.3 V).

CV results of the SC electrodes were recorded within a potential window of -0.3 V and +1.5 V at 20 mV/s. Figure 46 (a) compares the CV evolution of the prepared SWNT and SWNT/CP nanocomposite electrodes. SWNT thin films were utilized as double layer capacitive materials and their high conductivity eliminated the use of additional current collectors. A high degree of charge accumulation was observed on the SWNT/CP nanocomposite electrode when compared to the bare SWNT electrode.

This also indicated the domination of capacitance mainly by the pseudocapacitive property of the CP, which is homogeneously deposited onto the SWNTs. Faradaic redox reactions of the CP resulted in a broad CV curve and color changes were due to the electrolyte ion insertion into the CP layer. Nanocomposite form of SWNT/CP films tends to create synergistic and complementary effects while eliminating the drawbacks of individual components. CPs for instance, when used without SWNT thin films showed insufficient conductivity for current collection. CV measurement results of SWNT/CP nanocomposite electrodes at various rates are provided in Figure 46 (b). Supercapacitor electrodes were tested in various scan rates between from 5 mV/s to 1000 mV/s. High scan rates enlarged CV curves and broad cathodic peak shifted to negative potential region of CV curve. These results indicated high rate capability of the fabricated nanocomposite electrodes.

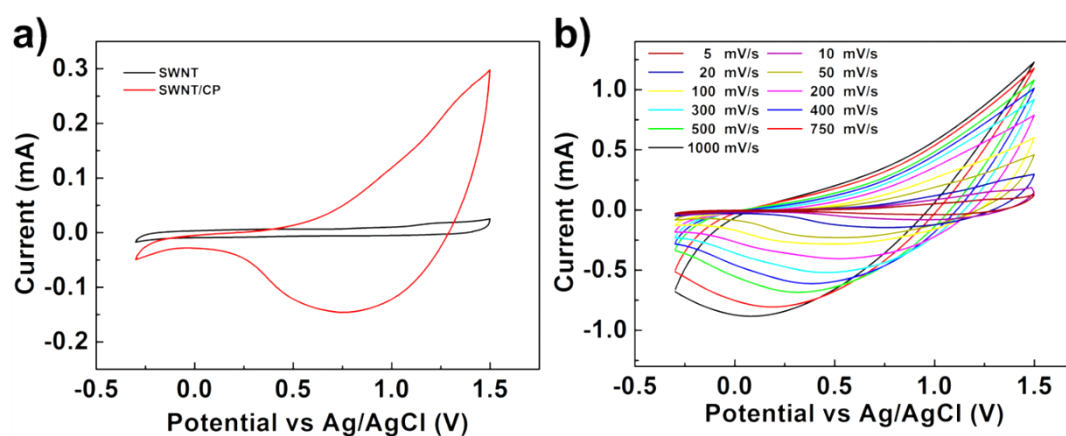


Figure 46. CV results of the SWNT and SWNT/CP nanocomposite electrodes in 0.1 M LiClO₄ in PC (a) at 20 mV/s and (b) at different scan rates.

The GCD measurements of the SWNT and SWNT/CP nanocomposite electrodes were conducted at 1.0 A/g and results are provided in Figure 47 (a). A remarkable enhancement in the charge storage capacity was observed for the nanocomposite electrodes. The characteristic triangular profile of the SWNT films are shifted to pseudocapacitive due to the presence of CP within the nanocomposite electrodes. A small IR_{drop} was observed in the measurements caused by ESR, which includes external contact points, electrolyte and electrode and interface resistance between them. The GCD characteristics measured at different current densities are provided in

Figure 47 (b). Discharge profiles of the fabricated SCs were found to depend on the current densities.

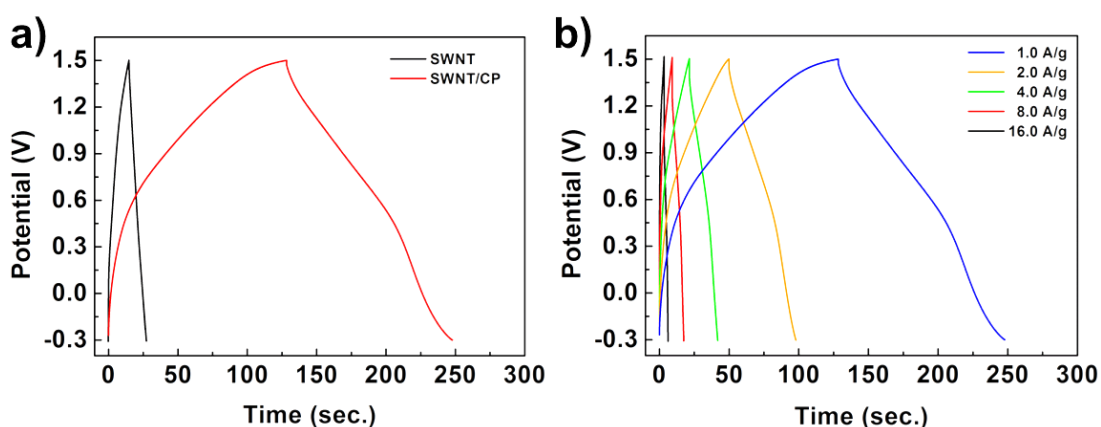


Figure 47. GCD curves of SWNT and SWNT/CP nanocomposite electrodes at 1.0 A/g and (b) at various current densities.

The C_{sp} was calculated using the GCD curves of the SC electrodes provided in Figure 47 in conjunction with the equation:

$$C_{sp} = \frac{I}{m(dV/dt)}$$

where t is the discharge time, V is the discharge voltage, I is the applied discharge current and m is the total mass of electrode active materials. The C_{sp} of the nanocomposite film was calculated as 112.4 F/g at 1.0 A/g. Nanocomposite films fabricated in this work showed higher capacitance values compared to bare SWNT electrodes (22.5 F/g). The C_{sp} of the SWNTs was remarkable enhanced by the CP deposition. For the nanocomposite electrodes, C_{sp} is plotted as a function of the current density in Figure 48 (a). The C_{sp} was 112.4 F/g and 59.8 F/g at various densities of 1.0 A/g and 16.0 A/g, respectively. Capacitances calculated using galvanostatic discharge curves (Figure 47 (b)) were found to decrease by increasing the cell current. This is because, at higher current densities, slow processes demonstrate a kinetic resistance and cannot participate in the charge transfer onto or across the electrode/electrolyte interface.

To determine the SC performance, capacity retention is another key factor. In order to explore this, fabricated SC electrodes were charged and discharged for 12500 cycles, results of which are provided in Figure 48 (b). Fabricated SC electrodes showed 82 % capacity retention after 12500 cycles. Coulombic efficiencies of the fabricated nanocomposite SC electrodes are plotted and shown in Figure 48 (b). Nanocomposite SC electrodes displayed enhanced performance and their coulombic efficiencies were almost unchanged after 12500 cycles.

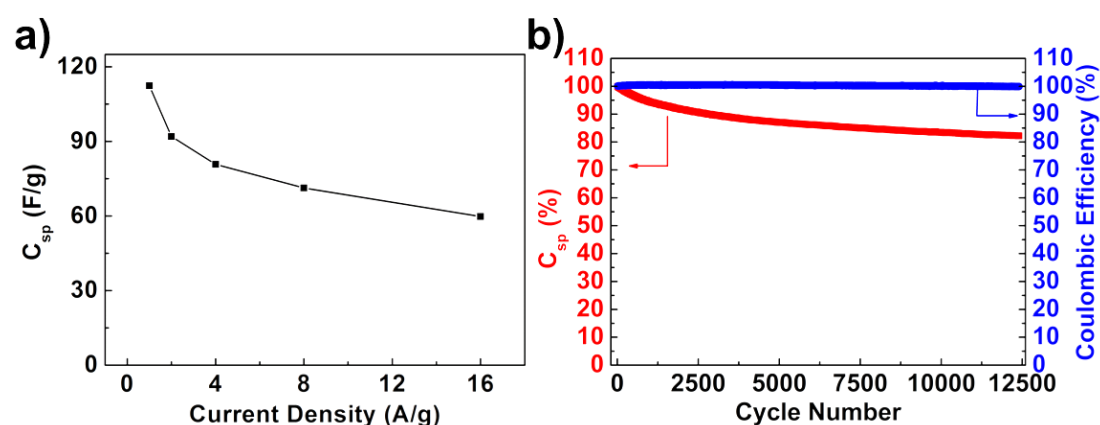


Figure 48. (a) Current density dependence of the specific capacitance of SWNT/CP nanocomposite electrodes. Lines are for visual aid. (b) Capacity retention and coulombic efficiency of SWNT/CP nanocomposite electrodes measured through a GCD at 1.0 A/g.

EIS was conducted to better understand the electrochemical properties of the fabricated SC electrodes. Electrochemical impedance characteristics of the SWNT and SWNT/CP electrodes were investigated at applied AC amplitude of 10 mV. Figure 49 (a) shows the Nyquist plots of the SWNT and SWNT/CP electrodes measured within the frequency range of 50 kHz and 50 mHz at 0 V vs Ag/AgCl. In the high frequency region, semicircle formation was not completed and data points were attributed to the electrode-electrolyte interactions at the interface. This occurred by the capacitance and the transfer resistance due to the charge polarization. The sharp slope in the low frequency part was due to the double layer capacitance and the sharpest line was obtained for SWNT electrodes. Nanocomposite supercapacitor electrodes were also tested upon the application of a few constant potentials for 60 seconds prior to EIS

measurements, results of which are provided in Figure 49 (b). Charge storage property of SWNT/CP nanocomposite film is dependent on the applied potentials and the slope of the low frequency region was raised up as the applied potential changed from -0.2 V to 1.3 V. This might be attributed to a characteristic of the CP that it demonstrates a potential-dependent pseudocapacitance. The external contact resistance resulted from conductive carbon paint and the electrolyte can be assigned to bulk serial resistance, which can be obtained from the Nyquist plots and it can be found from the real axis intercepts. It is difficult to determine charge transfer resistance from Nyquist plot due to lack of a clear semicircle. The slope of the curves at low frequency region was found to increase with respect to the applied potentials. Previously, the same phenomenon was also discussed in the CV evolution of the SWNT/CP nanocomposite electrodes (Figure 46 (a)). SWNT/CP nanocomposite electrodes have comparatively low charge storage at lower potentials and charge storage was found to improve with the increased potential. This trend confirmed the potential-dependent pseudocapacitance of electrochromic supercapacitor electrodes.

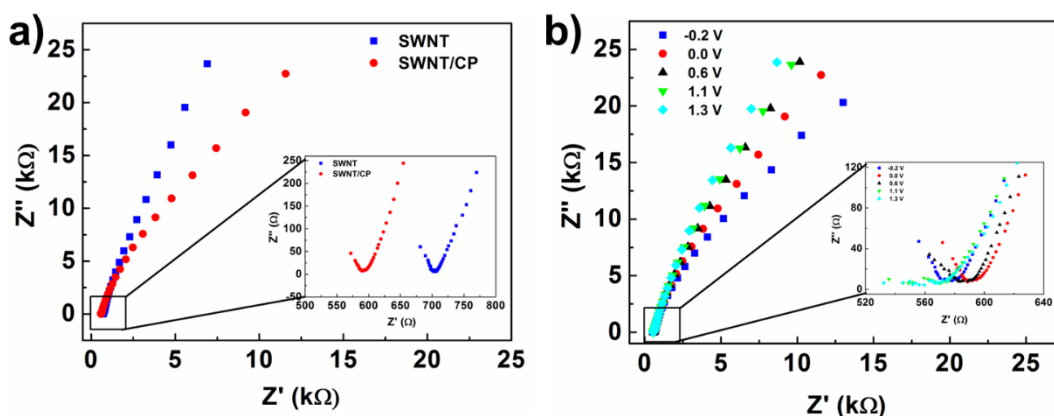


Figure 49. (a) Impedance spectra of the SWNT and SWNT/CP nanocomposite electrodes measured within the range of 50 kHz to 50 mHz at a 0 V DC potential. Inset shows the magnified high frequency region. (b) Impedance spectra of the SWNT/CP nanocomposite electrodes upon application of different DC potentials. Inset shows the magnified high frequency region.

All-organic SWNT/CP nanocomposite films investigated herein are encouraging electrode active materials for electrochromic SCs. Electrochromism allows an easy

practice to monitor the instant capacity of the fabricated SC electrodes and we believe that this work can easily be extended to other CP systems with different color combinations.

Color change is very attractive to human sense. The remained capacity within the device can be easily recognized by the human eye. Smart electronic devices that generate electricity, sense the environment and communicate with the user are getting more and more pronounced. Therefore, we have envisioned the use of electrochromic supercapacitors in portable, textile or body integrated, self-powered (solar, piezo etc.) devices (sensors, diagnostics etc.), where the detection is going to be made by humans.

5.4 Conclusions

In this study, fabrication and characterization of all-organic electrochromic nanocomposite supercapacitor electrodes with combination of SWNTs and CP was reported. The CP had multiple color changes depending on its oxidation state. Fabricated electrochromic supercapacitor electrodes were found to have a C_{sp} of 112.4 F/g at 1.0 A/g. In addition, obtained results simply showed the potential of SWNT/CP nanocomposites in SCs. Electrochromic SCs can effectively communicate with the user to alert how much charge and energy remained within the device; however, much more work on the fabrication of full devices should be conducted.

CHAPTER 6

COAXIAL SILVER NANOWIRE NETWORK CORE MOLYBDENUM OXIDE SHELL SUPERCAPACITOR ELECTRODES

6.1 Introduction

SCs have received extensive attention because of their high energy storage capability. However, they still need to be improved due to their limited energy density. The research on SCs mainly focuses on finding new electrode active materials. Efficient charge transfer between current collector and the electrode active material is an important point to increase charge storage of the SC devices. Resistance decrease is possible with the use of a good conductor and coaxial conductor-capacitive material design, which may result in high charge accumulation and enhanced charge transfer [199]. To attain maximum charge accumulation and to have high power and energy density, all active materials should be in close contact with the current collector; therefore, one-dimensional conductive nanomaterials such as nanotubes [133], nanowires [81], and nanorods [200] are appealing candidates for SC applications.

Nanomaterials with modified structure or design would improve charge storage and decrease internal resistance. Ag NW networks show good sheet resistance and transparency values when compared to indium tin oxide (ITO) thin films. They were started to be used as transparent conducting contacts in various optoelectronic devices [63][68]. These networks are also encouraging for SCs because of their mechanical stability and high conductivity [69]. For practical device applications, Ag NWs in network form typically form a good current collector. Since they have high aspect ratio, it is possible to obtain networks with low sheet resistance even at low nanowire densities. Therefore, Ag NWs were utilized in SC devices in conjunction with ITO [84] and PEDOT:PSS [69] in a layered form. For efficient supercapacitor devices, both the charge collector and the electrode material should be integrated. Coaxial hybrid form provides a solution and eliminates the use of additional conducting materials.

Pseudocapacitance and electrochemical double layer capacitance are the two main charge storage mechanisms for SC devices. Metal oxides and CPs are pseudocapacitor type materials and they store charges on the surface of the electrode through fast and reversible faradaic redox reactions. Various metal oxides have been widely studied ruthenium oxide (RuO_2) [201], manganese oxide (MnO_2) [202], nickel oxide (NiO) [203], cobalt oxide (Co_3O_4) [204] and molybdenum oxides (MoO_x , $x=2, 3, 2 < x < 3$) [205]. RuO_2 is the most commonly used and highly pseudocapacitive material; but, its high cost and serious environmental effects are the major limiting factors for its widespread applications [32]. Therefore, researchers have focused on the exploration of alternative pseudocapacitive transition metal oxides. As an alternative, MoO_2 stands out with its significant physical and chemical properties.

Molybdenum oxide have multiple valence states (MoO_x , $x=2, 3, 2 < x < 3$) and among these, most conductive one is MoO_2 [205, 206]. Some of its unique properties are low electrical resistivity, good chemical stability and high melting point and cycleability [205]. It has been reported that MoO_2 serves both as a pseudocapacitive material and a conducting support for the electrodes [207].

MoO_2 was synthesized by several methods for energy storage devices such as thermal decomposition [208], solvothermal [209], carbon templated [210], magnetron sputtering [211], electrodeposition and direct oxidation [212]. Different nanostructures of MoO_2 were reported in literature, including nanowires [213], nanorods [214], mesoporous [215] and tremella like shapes [216]. To date, there are several reports on the application of MoO_2 in nanocomposite form in conjunction with SWNTs [217], MWNTs [218], graphene [219] and ordered mesoporous carbon [210]. All these reports showed that the application of MoO_2 in a composite manner advance its electrochemical performance with respect to bare MoO_2 [210, 217, 219, 220].

Coaxial fiber shaped geometry has already been utilized in SC devices, where a single wire or fiber was used as the core [221-225]. Fiber shaped SCs should be long enough to enhance the capacity; however, increasing the length of the devices might increase the internal resistance. On the other hand, coaxial nanowire network electrodes would both decrease the internal resistance and enhance the capacity. To our knowledge, the use of metal nanowire network current collectors in coaxial geometry for SC electrodes remained elusive.

In this work, coaxial Ag NW/MoO₂ nanocomposite network electrodes were fabricated and characterized. High conductivity of the Ag NW electrodes allowed the conformal deposition of MoO₂ layer through electrodeposition and this core-shell structure eliminated the need for a separate current collector.

6.2 Experimental Details

6.2.1 Preparation of Electrodes

All materials used in this work were purchased from Sigma-Aldrich, were of analytical grade and used as received. Ag NWs were synthesized according to the polyol method [81].

MoO₂ shell layer was electrodeposited onto Ag NW networks potentiostatically. The solution used for the electrodeposition of MoO₂ contained sodium molybdate (Na₂MoO₄, 0.1 M). A cathodic potential of -1.2 V was applied (current-time diagram provided in Figure 50) typically for a few hundreds of seconds and films were then washed and dried.

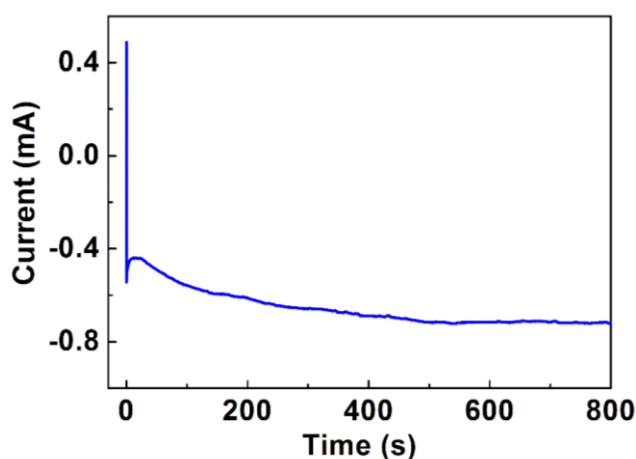


Figure 50. Current-time diagram for MoO₂ electrodeposition for 800 sec.

6.2.2 Characterization

SEM was performed to investigate the structure and morphology of the nanocomposite films. Compositional analysis was made through energy dispersive X-Ray spectroscopy (EDS). TEM was performed on a JEOL TEM 2100F microscope, operated at 200 kV. XRD measurements were carried out on a Rigaku D/Max-2000 pc diffractometer. Raman spectroscopy was performed on an inVia Renishaw microscope using a laser wavelength of 532 nm. A PHI 5000 VersaProbe spectrometer was used to collect XPS spectra. The C (1s) line at 284.5 eV was used for charge correction. Electrochemical performance tests of the SC electrodes were conducted in a three-electrode configuration using Gamry Reference 3000 potentiostat/galvanostat. Devices were fabricated, stored and characterized at ambient conditions. A microbalance (Sartorius Research R200D, Bradford, Germany) was used to measure the mass of deposited MoO₂ and the weight of material in the Ag NW/MoO₂ electrode was measured around 0.1 mg.

6.3 Results and Discussion

One-dimensional Ag NWs formed a conductive network and facilitated deposition of MoO₂ coating in a conformal manner during electrodeposition. During electrodeposition, the entire surface of Ag NWs get coated with the MoO₂ nanoparticles. Thickness of the MoO₂ coating gradually increased on the surfaces Ag NWs with time. Ag NWs stayed intact during electrodeposition monitored through in situ conductivity measurements.

Morphology of Ag NW/MoO₂ nanocomposites on the glass substrates were investigated through SEM and TEM analysis. SEM images of bare Ag NW network is provided in Figure 51 (a), while those electrodeposited MoO₂ layer on Ag NWs are provided in Figure 51 (b) and (c). MoO₂ layer covers the entire surface of Ag NW networks as evidenced in low and high-resolution images provided in Figure 51(b) and (c), respectively. It was also clearly seen in the TEM image that core Ag NWs were covered by the MoO₂ shell (Figure 51 (d)). The EDS result confirmed the presence of respective constituent elements in the electrodes, as shown in the Figure 51 (e). Ag from the NW core, Mo from the outer shell and Na from the substrate were evident in

the EDS spectra. Figure 51 (f) shows the change in the thickness of the MoO₂ (calculated from the diameter change within SEM images) with respect to the electrodeposition duration. Sharp increase in the MoO₂ thickness in the early stages of electrodeposition slowed down its pace as the process proceeds, as shown in the Figure 51 (f). Deposition times longer than 1600 sec were not investigated, since long electrodeposition processes resulted in the rupture of underlying Ag NWs, which was tentatively attributed to the shrinkage of excessive MoO₂ layer (Figure 52). For this reason, all electrochemical measurements were conducted for 800 sec electrodeposited sample.

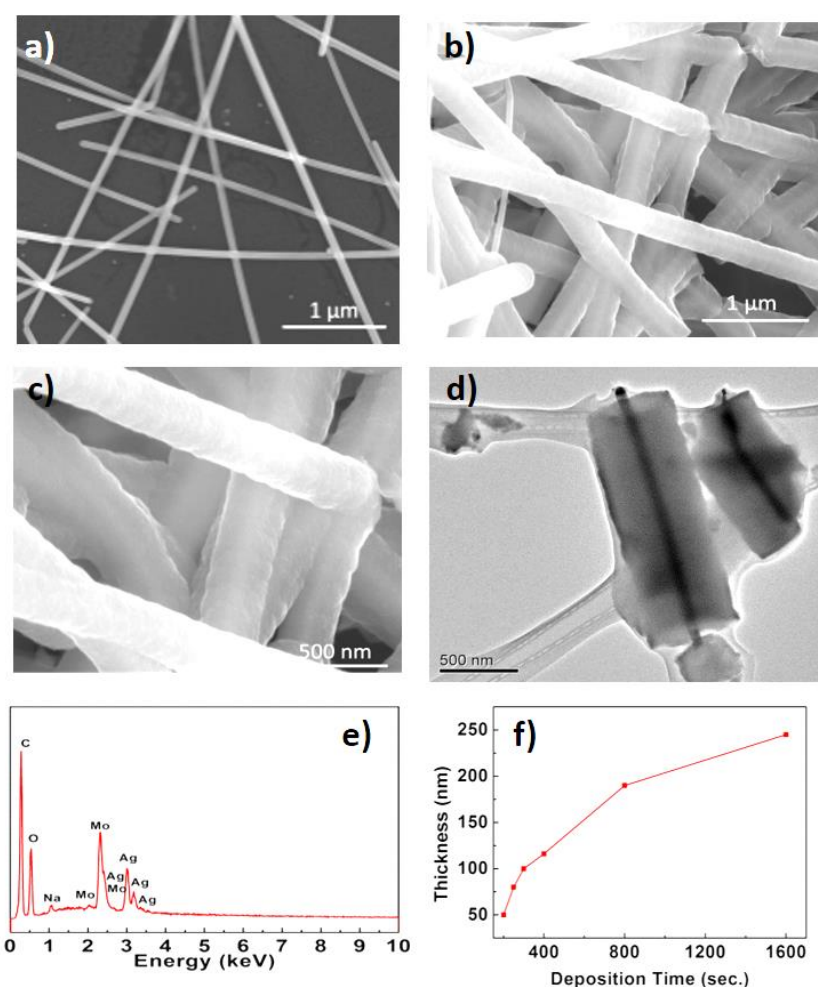


Figure 51. SEM images of (a) Ag NWs electrodes, Ag NW/MoO₂ nanocomposite electrodes in low and high (b, c) resolution. (d) TEM image of Ag NW/MoO₂ nanocomposite electrodes. (e) EDS spectrum of Ag NW/MoO₂ nanocomposite electrodes. (f) Time-dependent thickness change of MoO₂ layer during electrodeposition. Lines are for visual-aid.

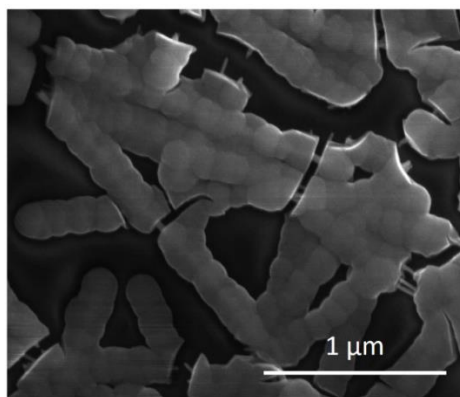


Figure 52. SEM image of the Ag NW/MoO₂ nanocomposite electrodes electrodeposited for 1600 sec.

XRD pattern of the Ag NW network on glass substrates is provided in Figure 53 (a). The XRD result shows clear diffraction peaks around 38.1° and 44.4° corresponding to Ag (JCPDS card 04-0783) (111) and (200) planes, respectively [81]. The XRD pattern of Ag NW/ MoO₂ nanocomposites is also provided within the same figure. Obtained diffraction peaks around 26.1°, 46.7° and 53.6° correspond to the (011), (121) and (022) lattice planes of the monoclinic MoO₂ (JCPDS 78-1070) [208, 226]. The small peak at 17.8° corresponding to Na_{0.9}Mo₆O₁₇ (JCPDS card 86-1683) could be due to the sodium ions of molybdenum salt used in the electrodeposition process. The crystallinity of MoO₂ was found to be high even in the absence of a proper annealing process.

The chemical nature of the deposited thin films was also investigated with Raman spectroscopy. Figure 53 (b) shows the Raman spectrum of Ag NW/MoO₂ nanocomposite within the spectral range of 200-1000 cm⁻¹. The spectrum for Ag NW network is provided for comparison. The bands in Ag NW/MoO₂ nanocomposite spectra located at 223, 339, 363 and 744 cm⁻¹ are marked for MoO₂. The Raman peak of molybdenum (VI) oxide (MoO₃) at 270 cm⁻¹ was detected and the peaks at 483, 800, 848 and 919 cm⁻¹ can be assigned to the MoO_x (2 < x < 3). Presence of O₂ in the medium can result in the easy oxidation of the Mo–Mo bonds to form MoO₃ layer on the surface of MoO₂ film [226, 227].

To further determine the chemical composition of the Ag NW/MoO₂ nanocomposite and the valence state of Mo in the nanocomposite, XPS measurements were carried out, results of which were provided in Figure 53 (c) and (d). According to the Figure 53 (c), survey spectrum of the Ag NW/MoO₂ nanocomposite have signals at 230.2-234.3, 284.5, 531.5 eV and 367.5-373.5 eV, which were attributed to the Mo 3d, C 1s, O 1s and Ag 3d, respectively. In Figure 53 (d), the deconvoluted high-resolution XPS Mo 3d core level spectrum displays four peaks; due to the +4 oxidation state of the Mo. In addition to Mo⁺⁴ peaks, at the higher energy, peaks at 234.3 and 231.6 eV were originated from Mo⁺⁵ 3d_{3/2} and Mo⁺⁵ 3d_{5/2} of MoO_x (x=2<x<3) [215, 218, 228].

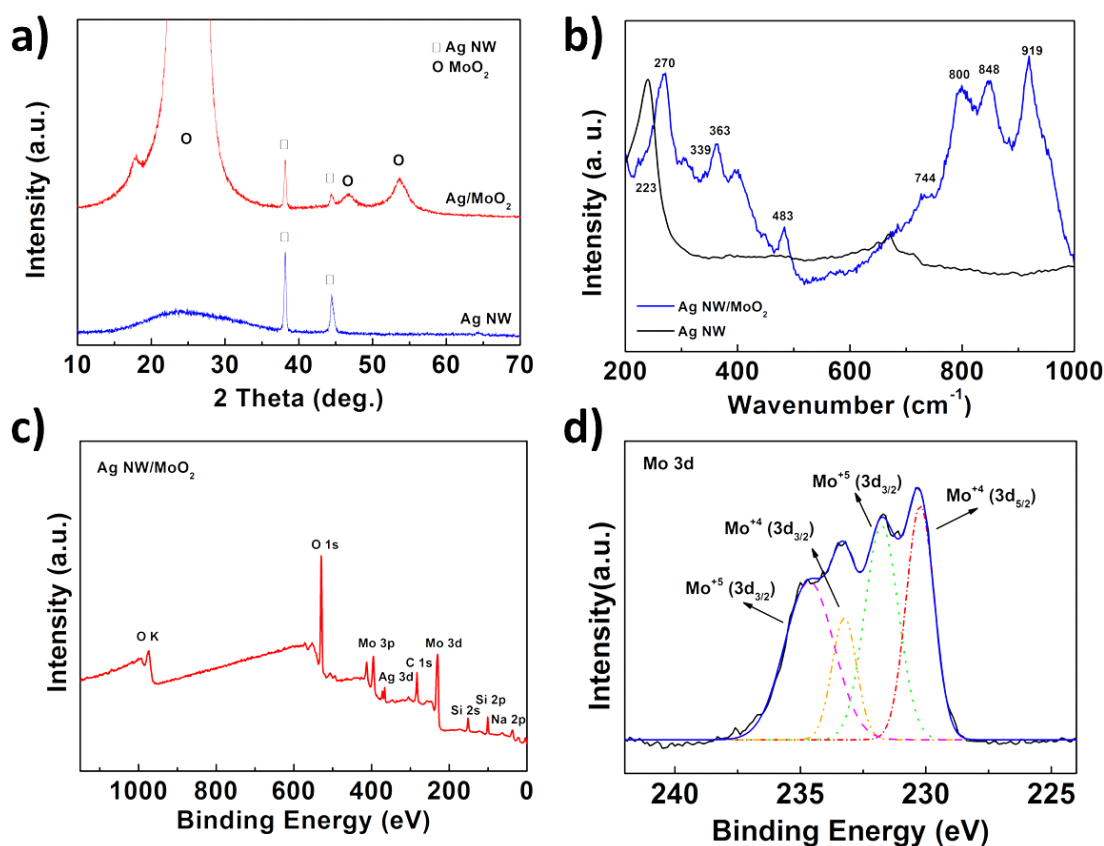


Figure 53. (a) XRD pattern and (b) Raman spectrum of bare Ag NWs and Ag NW/MoO₂ nanocomposite electrodes. (c) XPS survey spectrum of the Ag NW/MoO₂ nanocomposite and (d) deconvoluted core level spectra of Mo 3d of Ag NW/MoO₂ nanocomposite.

CVs were recorded within a potential window of -1.5 and 0 V to evaluate the charge storage properties of Ag NW/MoO₂ nanocomposite electrodes. Figure 54 shows the CV result of the bare Ag NW at 20 mV/s scan rate and Ag NW/MoO₂ nanocomposite electrodes at different scan rates. Ag NW network was utilized as a skeletal network for the deposition of MoO₂ layer and conformal coating facilitates the charge transfer from MoO₂ shell layer to the inner Ag NWs (within the core). Due to prevalent faradaic redox reactions, large amount of charges were accumulated within the Ag NW/MoO₂ nanocomposite electrode as opposed to bare Ag NW electrode, evidenced by large inner area within the CV curve. Increased scan rates enlarged CV curves and broad cathodic peak shifted to positive potentials of the potential region. These results indicated high rate capability of the fabricated nanocomposite electrodes. Ag NWs might have a naturally occurred thin oxide layer on the surface of nanowires and this oxide layer also has a very small pseudocapacitive property. This pseudocapacitive property is reversible and it is due to the redox reaction taking place between the Ag and silver (I) oxide (Ag₂O) [199]. This signifies the governance of capacitance characteristics primarily by the pseudocapacitive properties of MoO₂. MoO₂ is a cathodic electroactive material and its pseudocapacitive activity takes place in the negative potential region upon reduction by the electrolyte ions (Li⁺ ions) in this case [208]. Electrochemical characteristics of only 800 s deposited sample was reported here, although thinner samples were also elaborated. They are not used for comparison here, since the change in the thickness of the active layer makes it impossible to compare the electrodes performance.

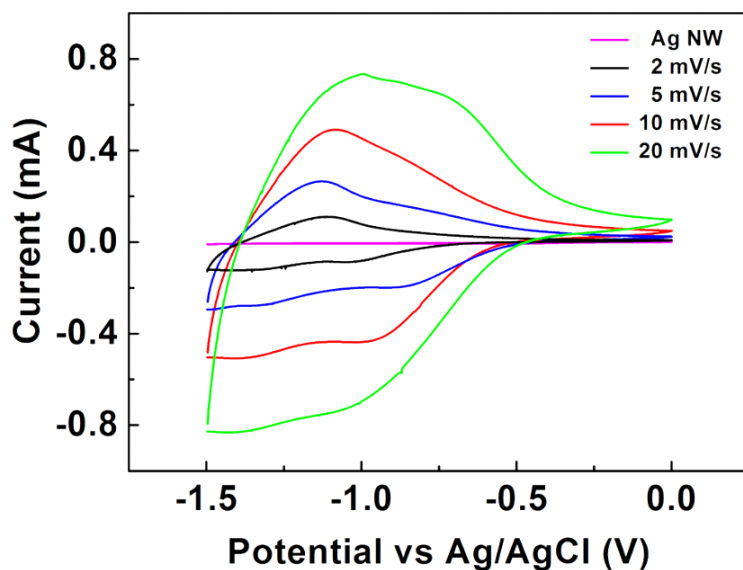


Figure 54. CV results of Ag NW (at 20 mV/s) and Ag NW/MoO₂ nanocomposite electrodes in 1 M LiClO₄ in PC at different scan rates.

The current profiles of the fabricated nanocomposite electrodes were measured at different densities and the results are provided in Figure 55 (a). Galvanostatic measurements have been conducted from -1.5 to 0 V. The GCD results of the nanocomposite electrodes showed a high inclination at positive potential region and low inclination at the negative potential region indicating highly pseudocapacitive property of the electrodes. Similar curve shapes have been obtained for different current densities.

EIS was conducted to elucidate properties of the bare Ag NWs and Ag NW/MoO₂ nanocomposite electrodes. Electrochemical impedance characteristics of the electrodes were investigated at an applied AC potential of 5 mV. Figure 55 (b) shows the Nyquist plots of the electrodes measured within 100 kHz to 0.01 Hz range. The EIS data of bare Ag NW electrode are provided for comparison. In the high frequency region of Ag NW/MoO₂ nanocomposite electrodes (Figure 55 (b)), semicircle formation was almost completed and data points were attributed to the interactions at interface of the electrode-electrolyte. On the other hand, semicircle formation was incomplete for the bare Ag NW electrode, while the moderate slope within the low frequency region was attributed to small pseudocapacitance.

GCD curves of the electrodes provided in Figure 55 (a) was used to calculate specific capacitance (C_{sp}). A C_{sp} of 500.7 F/g at 0.25 A/g was obtained. C_{sp} is plotted as a function of the GCD current densities in Figure 51 (c). C_{sp} was found to decrease to 378.5 F/g at 10.0 A/g. Capacitances calculated using GCD curves were found to decrease by increasing the withdrawn cell current. This is because, at higher current densities, the slower processes demonstrate a kinetic resistance and cannot participate in charge transfer onto or across the electrode/electrolyte interface.

In order to explore the capacity retention, fabricated nanocomposite SC electrodes were charged and discharged for 5000 cycles at 1 A/g, results of which are provided in Figure 55 (d). C_{sp} was retained after 5000 cycles, showing a reasonable capacity retention. Coulombic efficiencies of the fabricated nanocomposite SC electrodes were given in Figure 55 (d). Nanocomposite SC electrodes displayed enhanced performance and their columbic efficiencies were higher than 90 % of the initial values after 5000 cycles.

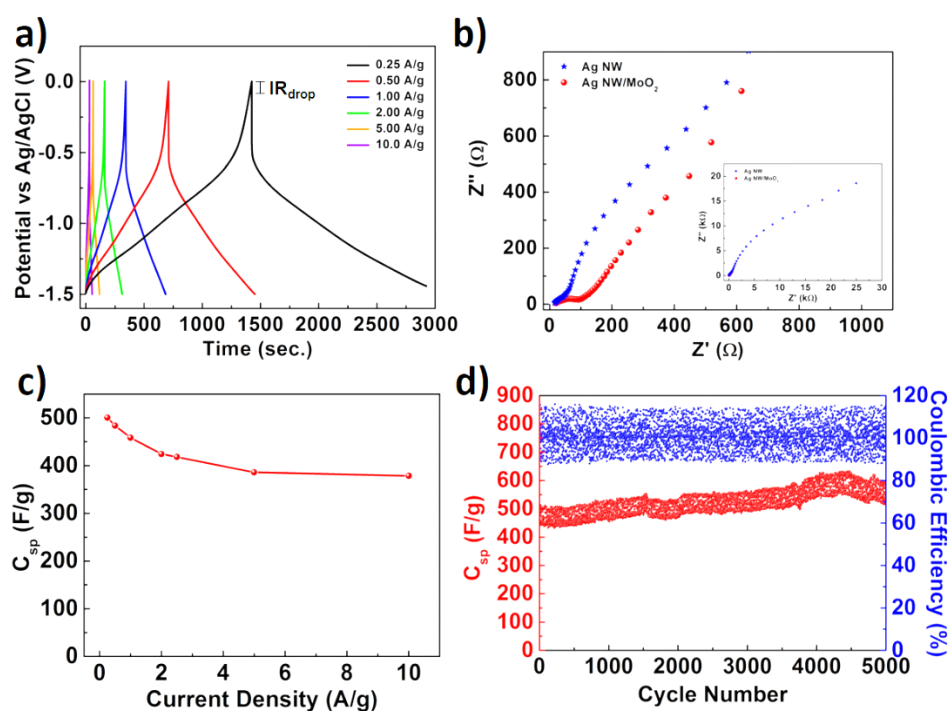


Figure 55. (a) GCD curves of Ag NW/MoO₂ nanocomposite electrode in 1 M LiClO₄ in PC at currents from 0.25 A/g to 10 A/g. (b) EIS spectra of thin films (Inset: Full spectra). (c) Dependence of the specific capacitance of Ag NW/MoO₂ nanocomposite electrodes on current density. (d) Cycling performance of Ag NW/MoO₂ nanocomposite electrodes.

Results obtained in this work was correlated and compared to those found in the literature regarding molybdenum oxide. Results are tabulated in Table 5. One of the highest C_{sp} values was found in this work for the molybdenum oxide containing non-carbonaceous electrodes as shown in the table.

Table 5. MoO₂ based SC electrode materials (adapted from [205]). (OMC: ordered mesoporous carbon; SWNT: single-walled carbon nanotube; EC: ethylene carbonate; rGO: reduced graphene oxide; DEC: diethyl carbonate; SCE: saturated calomel electrode).

Electrode Materials	Electrolyte	Voltage window (V)	Current density or Scan rate	C_{sp} (F/g)	Refs.
MoO ₂ nanorods	1.0 M H ₂ SO ₄	-0.3 to 0.4 (vs. Ag/AgCl)	1 mA/cm ²	140	[208]
OMC/MoO ₂	1.0 M H ₂ SO ₄	-0.2 to 0.6 (vs. SCE)	2 mV/s	395	[210]
Ordered mesoporous MoO ₂	1.0 LiOH	-1.2 to -0.5 (vs. SCE)	5 mV/s	146	[206]
MoO ₂ /SWNT	1.0 M Na ₂ SO ₄	0 to 1.0 (vs. SCE)	10 mV/s	597	[217]
rGO/MoO ₂	1.0 M LiPF ₆ in EC:DEC	0.005 to 3.0 (vs. Li/Li ⁺)	50mA/g	624	[219]
Ag NW/ MoO ₂	1.0 M LiClO ₄ in PC	-1.5 to 0.0 (vs. Ag/AgCl)	0.25 A/g	500.7	This work

6.4 Conclusions

In conclusion, coaxial Ag NW network core/MoO₂ shell nanocomposite electrodes investigated herein are good candidates electrode active materials for SCs. Conformal coating of MoO₂ allowed easy charge transport towards the Ag NW network to form efficient SC electrodes. All solution based approaches have been used to fabricate electrodes in this work. This allows economic and large-scale fabrication of the SCs, which can also be made flexible. In this work, the coaxial nature of the SCs were kept; but, the geometry was modified from individual wire to network of wires and obtained a C_{sp} of 500.7 F/g at 0.25 A/g current density. The use of NW networks eliminated the need for intensive lithographical processing, bringing this concept one more step closer to commercialization. This work can easily be extended to other metal oxide or CP systems.

CHAPTER 7

FLEXIBLE, SILVER NANOWIRE NETWORK NICKEL HYDROXIDE CORE-SHELL ELECTRODES FOR SUPERCAPACITORS

7.1 Introduction

SCs are accepted as one of the most essential devices for the 21st century. They have gathered extensive interest due to their moderate energy and high power densities among energy storage systems [12, 85]. There have many applications that utilize SCs spanning from portable electronics to electric motors [86]. However, their energy storage capacity and density still needs to be improved. Therefore, many research groups are focused on the developing active materials for SC electrodes. In addition to discovery of new electrode active materials, there are extensive efforts to facilitate the charge transfers between the electrode materials and the current collector. Binder or additive free electrodes allow efficient charge collection and minimize the dead electrode surface. Low resistance electrodes is a must and usually achieved by conductive additives. A coaxial conductor-capacitive material design, on the other hand, may give rise to both enhanced charge transfer and high charge accumulation [199]. In this configuration, current collectors and all active materials are tightly connected. For this reason, conductive nanomaterials with high aspect-ratio such as CNTs [133], NWs [81] and nanorods [200] might be ideal candidates for the realization of coaxial SCs. Carbonaceous materials have already been used but they still have some drawbacks such as expensive and time-consuming fabrication process [206, 229]. As an alternative, Ag NWs with high metallic conductivity are promising for energy storage systems [69-73]. Electrode active materials can be grown on Ag NWs, which might improve the charge transfer and allow fast redox reactions in a coaxial configuration.

Ag NW network electrodes have been already used in some optoelectronic devices, for instance polymeric light emitting diodes (LEDs) [63] and organic photovoltaic cells [68]. They display both high transmittance and low sheet resistance with respect to commercial ITO thin film electrodes. Thanks to their high aspect ratio,

Ag NW networks allow to fabricate transparent conducting electrodes with low sheet resistance at low NW concentrations. These network electrodes are also favorable for energy storage devices and they have important properties such as high conductivity, mechanical integrity (long cycle lifetime) and high accessible surface (power density) [69-73]. Ag NWs were used in SCs as an alternative to ITO [84], graphene [72, 83] and PEDOT:PSS [69] and CNTs. However, in all these prior arts on Ag NW SCs, active materials were deposited onto the electrodes in a layered form. However, as discussed earlier, Ag NWs in coaxial nanocomposite form offers a promising alternative for SC electrodes and also eliminate the need for additional conducting additives and binders.

In SCs, pseudocapacitance and electrochemical double layer capacitance are two main charge mechanism. While carbon based materials are listed in first group, metal oxides and CPs are listed in the second one. For pseudocapacitive materials, charge storage takes place at a few nanometers from the electrode surface via reversible faradaic redox processes. Among metal oxides, ruthenium oxide (RuO_2) [201], manganese oxide (MnO_2) [230], molybdenum oxides (MoO_2 ,) [73, 205], cobalt oxide (Co_3O_4) [204], and nickel oxide (NiO) [203, 231] have been investigated for their high capacity. RuO_2 and MnO_2 are purely pseudocapacitive materials and they are extensively studies in SCs. However, high cost of RuO_2 as well as environmental issues limit its widespread use [32]. On the other hand, MnO_2 have a dense morphology and it is difficult to achieve theoretical capacitance unless, a few nanometer thin film is used [232]. Therefore, recent research efforts have been concentrated on the finding new and novel pseudocapacitive materials. Among other metal oxides and hydroxides, $\text{Ni}(\text{OH})_2$ is one of the high-power-battery-type materials, which has a theoretical capacitance (2358 F g^{-1}) [233]. In fact, it is also reported that the experimental results go beyond the theoretical value (3152 F g^{-1}) [234]. Its reversible redox activity [235] and good stability in alkaline electrolytes make it a good candidate for high capacity energy storage devices [236]. $\alpha\text{-Ni}(\text{OH})_2$ and $\beta\text{-Ni}(\text{OH})_2$ are two polymorphs of $\text{Ni}(\text{OH})_2$ and $\beta\text{-Ni}(\text{OH})_2$ shows better stability than the $\alpha\text{-Ni}(\text{OH})_2$. Moreover, it is commonly utilized in high energy density devices due to its good thermal and chemical properties [237]. For thin film and nanostructured electrode materials, high surface areas result in the high charge storage capacity. Nevertheless, $\text{Ni}(\text{OH})_2$ usually forms flake-like nanostructures and these nanoflakes show high

charge storage capacity [230]. It is possible to synthesize Ni(OH)₂ via several methods such as chemical precipitation [238], thermal decomposition [239], hydrothermal [240], reverse micelle [241], solvothermal [242], sonochemical [243], electrodeposition [244] and electrophoretic deposition [245]. To date, there are several publications on the utilization of Ni(OH)₂ in nanocomposite form with MWNTs [236, 246, 247], graphene [248], reduced graphene oxide [245] and silicon carbide [249]. According to these publications, the application of Ni(OH)₂ in a composite manner enhance charge storage properties of Ni(OH)₂ with respect to its bare form.

Moreover, coaxial NW network electrodes prepared through electrodeposition of the shell on the conducting core could both increase the conductivity and advance the capacity. In addition to this, integration of metal NW networks and pseudocapacitive materials in core-shell structure for energy storage devices stayed elusive. In this study, one-dimensional coaxial Ag NW/Ni(OH)₂ nanocomposite network SC electrodes were fabricated and characterized. Highly conductive Ag NWs resulted in the conformal electrodeposition of Ni(OH)₂ layer and coaxial structure both excluded the external current collector and improved the charge transport.

7.2 Experimental Details

7.2.1 Electrode Fabrication

In this work, all materials were in analytical grade and purchased from Sigma-Aldrich. Following synthesis, for the purification the Ag NWs were dispersed within acetone (in a ratio 1:5) and centrifugation process was repeated two times (at 8000 rpm for 20 minutes). Centrifugation process was repeated with the ethanol and solid content was transferred to ethanol for spray-coating. Deposition of Ag NWs onto PET and glass was performed by spray-coating. For the instant removal of solvent during deposition, substrates were heated to 100 °C.

Ni(OH)₂ shell was potentiostatically deposited onto the Ag NW network electrodes [250]. A freshly prepared 0.1 M nickel acetate (Ni(CH₃COO)₂·4H₂O) solution was used for the conformal deposition of Ni(OH)₂. The working electrode was Ag NW network film (on glass/PET substrate). Electrodeposition process was

conducted at a potential of -0.9 V and typically it was applied for a few hundreds of seconds (200, 400, 600 and 800). Fabricated electrodes were washed with deionized water, dried with N₂ gas and stored under ambient conditions.

7.2.2 Characterization

SEM was used to investigate morphology of the fabricated nanocomposite films. Scanning/transmission electron microscopy (S/TEM) was performed on a JEOL FEG-TEM 2100F microscope, operated at 200 kV. Specimens for S/TEM analysis were diluted in ethanolic solution and thin foils were lifted from the substrates and they were transferred onto holey carbon-coated copper grids. Energy dispersive X-Ray spectroscopy (EDS) attached to S/TEM was conducted for the compositional analysis. Raman spectroscopy was carried out on a Renishaw inVia microscope (532 nm). XPS measurement was carried out for evaluation of the chemical state and chemical identification of the constituent elements. PHI 5000 VersaProbe spectrometer was used to collect XPS spectra. A high-resolution scan of the Ni (2p) spectral region was performed for the qualitative analysis. C (1s) line at 284.5 eV was used for reference and charge correction of the binding energies (BE). XRD measurements were performed on a Rigaku D/Max-2000 diffractometer at Bragg-Brentanno geometry at 40 kV. For electrochemical measurements, Gamry Reference 3000 potentiostat/galvanostat system were used in a three-electrode configuration and all potentials values were relative to the Ag/AgCl reference and platinum foil counter electrodes. A Sartorius Research R200D microbalance was used to measure the mass of deposited Ni(OH)₂. The mass of active material in the Ag NW/ Ni(OH)₂ electrode was measured around 0.1 mg for 800 s electrodeposited sample.

7.3 Results and Discussion

Ni(OH)₂ conformal layer was electrodeposited onto conductive network of Ag NWs. Ni(OH)₂ nanoflakes were gradually formed on the surfaces of Ag NWs during electrodeposition and at some stage started to form a continuous layer. Ni(OH)₂ layer thickness was monitored through the electrodeposition time. During electrodeposition,

Ag NW network stayed intact, which was monitored through in-situ conductivity measurements.

Structure and morphology of the Ag NW/Ni(OH)₂ nanocomposites were investigated by SEM and TEM analysis. In Figure 56 (a)-(c), bare Ag NW network and deposited Ni(OH)₂ layer on Ag NW network are shown in SEM images. The whole surface of Ag NW networks was covered by Ni(OH)₂ layer as demonstrated in low (Figure 56 (b)) and high-resolution (Figure 56 (c)) SEM images. Figure 56 (d) provides the thickness change of the Ag NW/Ni(OH)₂ nanocomposites (calculated using SEM images) during the electrodeposition process. The Ni(OH)₂ thickness changes with a constant rate during electrodeposition, as shown in the figure. In this study, the maximum deposition time was 1600 seconds and longer electrodeposition periods were not investigated. This is because, thicker Ni(OH)₂ layers were found to initiate cracks in the Ag NW networks.

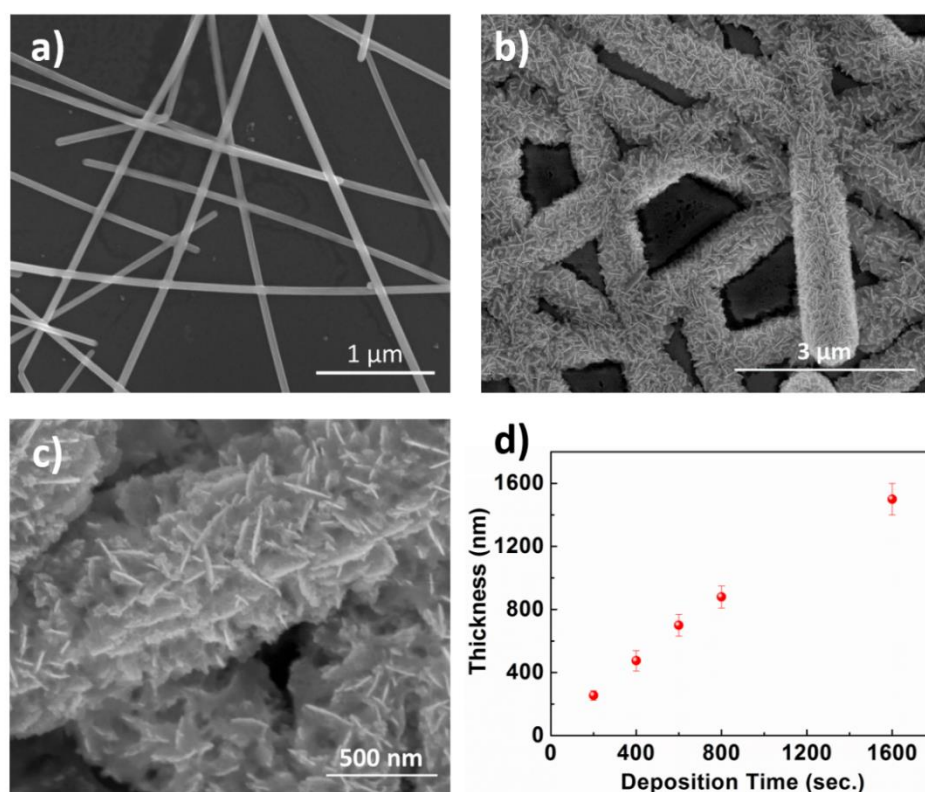


Figure 56. SEM images of (a) Ag NW and Ag NW/Ni(OH)₂ nanocomposite in (b) low and (c) high resolution. (d) Change in the thickness of Ag NW/Ni(OH)₂ nanocomposite with time during electrodeposition.

The crystallinity of the Ag NW/Ni(OH)₂ nanocomposites were analyzed by XRD analysis. XRD patterns of the Ag NW electrode and Ag NW/Ni(OH)₂ nanocomposites on glass substrates are provided in Figure 57 (a). Ag NWs have two diffraction peaks at 38.1 and 44.4°, which belong to (111) and (200) crystal planes of Ag (JCPDS card no. 04-0783), respectively [81]. Ag NW/Ni(OH)₂ nanocomposites have an XRD pattern, which contains peaks around 38.2, 52.1 and 64.4° corresponding to the β-Ni(OH)₂ planes of (011), (012) and (111) (JCPDS card no. 74-2075) with hexagonal structure [237, 242]. Some of the Bragg reflections of Ni(OH)₂ seems to be missing in the experimental data. This may indicate a pseudo-textured formation of Ni(OH)₂ along the Ag nanocrystals. As evidenced in the figure, Ag NW/Ni(OH)₂ nanocomposite only contains pure β-Ni(OH)₂ and Ag.

The chemical nature of the electrodeposited film was examined with Raman spectroscopy. Raman spectrum of the nanocomposite within a spectral range of 200-4000 cm⁻¹ was shown in Figure 57 (b). In the same figure, Ag NW spectrum is also given for comparison and observed bands were due to the residual PVP film layer on the Ag NWs. The Raman peaks for Ag NW/Ni(OH)₂ nanocomposite electrode observed at 535 and 3680 cm⁻¹ were attributed to A_{2u}(T) lattice of Ni(OH)₂ and the stretching of hydroxyl groups of Ni(OH)₂ layer, respectively [251-254].

XPS measurements were carried out for further characterization of Ni(OH)₂ layer and the oxidation of Ni within the nanocomposite. XPS results of Ag NW/Ni(OH)₂ nanocomposite were provided in Figure 57 (c) and (d). According to the Figure 57 (c), XPS survey spectrum of the nanocomposite has signals from C, O, Ni and Ag species, which comes from the components of Ag NW/Ni(OH)₂ nanocomposite electrode. The high resolution Ni 2p core level XPS spectrum (Figure 57 (d)) presents two major peaks at 854.0 and 871.6 eVs due to Ni 2p_{3/2} and Ni 2p_{1/2} species, respectively. The spin-energy separation of 17.6 eV agree well with the reported values for the Ni(OH)₂ phase [239, 249, 255, 256]. XPS Ni 2p core level spectrum also includes satellite peaks at 859.3 and 877.5 eV, which were due to Ni 2p_{3/2} and Ni 2p_{1/2}.

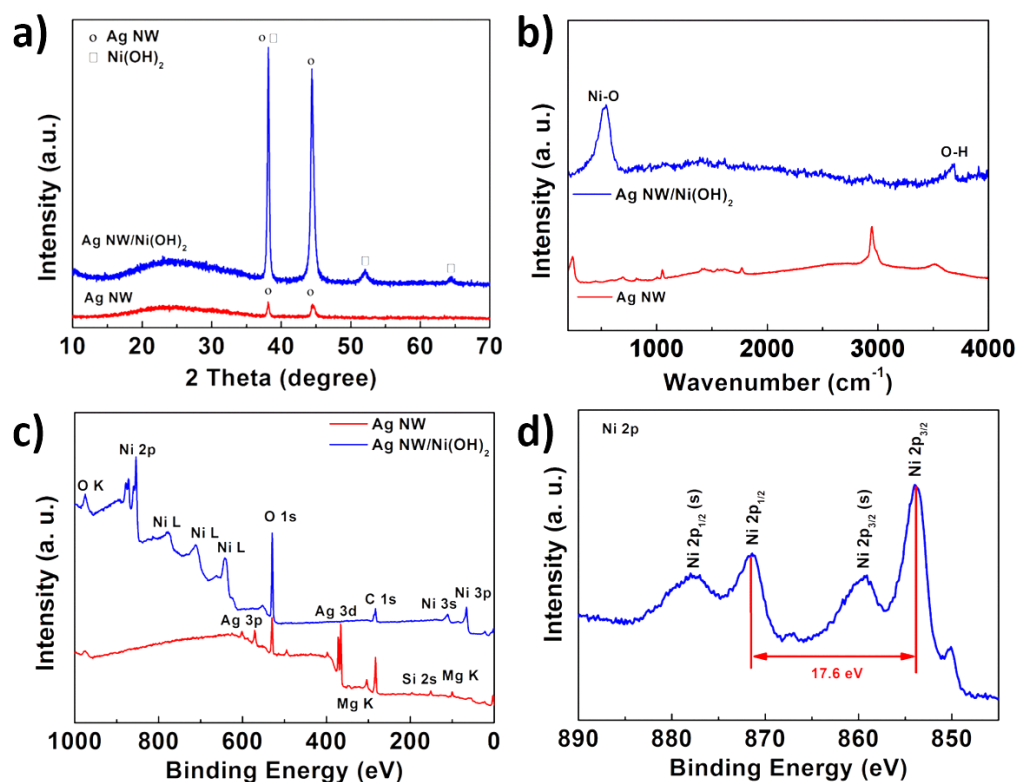


Figure 57 (a) XRD patterns, (b) Raman spectra and (c) XPS survey spectra of bare Ag NWs and Ag NW/ Ni(OH)₂ nanocomposite electrodes. (d) Deconvoluted XPS spectrum for Ni 2p of Ag NW/ Ni(OH)₂ nanocomposite.

Figures 58 (a) and (b) show the bright-field (BF) images of Ag NW/Ni(OH)₂ nanocomposites before and after 3000 GCD cycles, respectively. BF images clearly show that Ni(OH)₂ layer covers the entire surface of Ag NW core. The insets given as footers in the corresponding figures represent the high-angle annular dark field (HAADF), the Ni and Ag S/TEM EDS maps, respectively. The HAADF images confirm the structural and morphological stability after the charge-discharge cycles. The EDS maps justify the existence of Ni rich shell around the Ag core. The HRTEM images in Figure 58 (c) and (d) indicate that Ni(OH)₂ contains nanocrystals with less than 20 nm size in average. It is evident that the size and morphology remain unchanged after the charge-discharge cycles.

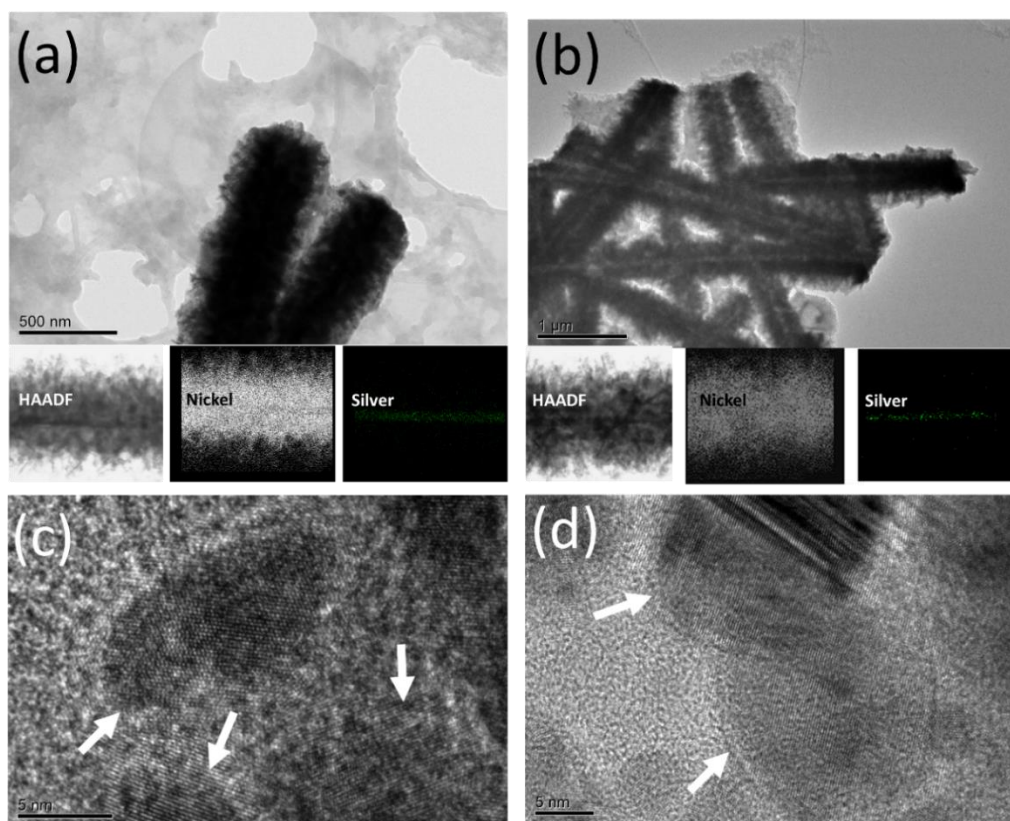


Figure 58. BF images of Ni(OH)₂ shell on Ag NW network core before (a) and after (b) 3000 GCD cycles. The insets represent HAADF, Ni and Ag mapping for conditions (a) and (b). (c) and (d) white arrows show representative nanocrystals in Ni(OH)₂ shell before and after cycling test.

The electrochemical performance of Ag NW/Ni(OH)₂ nanocomposite electrodes was examined by CV measurements within a potential window of 0 and 0.5 V (vs. Ag/AgCl) in 1 M KOH. This potential window was particularly chosen due to the strong and reversible redox reactions, which probably involved hydroxyl ions [255]. It also provides a safe operating window for Ag NWs. The reaction that takes place on the electrode surface is given below:

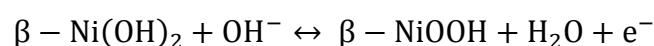


Figure 59 (a) provides the CV results of the nanocomposite supercapacitor electrodes with various deposition times at 20 mV s⁻¹ scan rate. Inner Ag NW core was employed as a conducting network for the deposition of Ni(OH)₂ layer and the coaxial structure facilitates the charge transfer between Ni(OH)₂ shell layer and the inner core.

Ag NWs have a chemically active surface and it is possible to form a thin surface oxide layer. This oxide layer onto Ag NWs has a reversible pseudocapacitive property and it might be resulted by the faradaic redox reaction between the Ag and silver (I) oxide (Ag_2O) are centered around 0.21 V and 0.07 V for anodic and cathodic peaks, respectively. However, pseudocapacitive property of native oxide of Ag NWs is less significant when considering the thickness of the electrodeposited $\text{Ni}(\text{OH})_2$ shell layer. This showed the reversible redox characteristics of $\text{Ni}(\text{OH})_2$ were primary pseudocapacitive source. Faradaic activity of $\text{Ni}(\text{OH})_2$ is clearly showed in Figure 59 (a) with respect to the deposition time. As a consequence of the dominant redox reactions, high amount of charges was collected onto nanocomposite electrodes. Oxidation and reduction peaks for the Ag NW/ $\text{Ni}(\text{OH})_2$ nanocomposite electrode are positioned at about 0.39 V and 0.24 V, respectively. It is clear from the Figure 59 (a) that the increased deposition time of $\text{Ni}(\text{OH})_2$ resulted in higher capacitance values.

The result of scan rate on the electrochemical behaviors of the nanocomposite SC electrodes was examined in the same potential window for 800 second electrodeposited sample. CV measurement results of Ag NW/ $\text{Ni}(\text{OH})_2$ nanocomposite electrodes at various rates are given in Figure 59 (b). Increased scan rates enlarged the CV curves and intense oxidation and reduction peaks shifted to opposite directions of the potential window, respectively. At high scan rates, the active layer had difficulties in enduring the fast redox processes, which might be responsible for the decrease in the capacitance. These results indicated rate-dependent charge storage capacity of the fabricated nanocomposite electrodes.

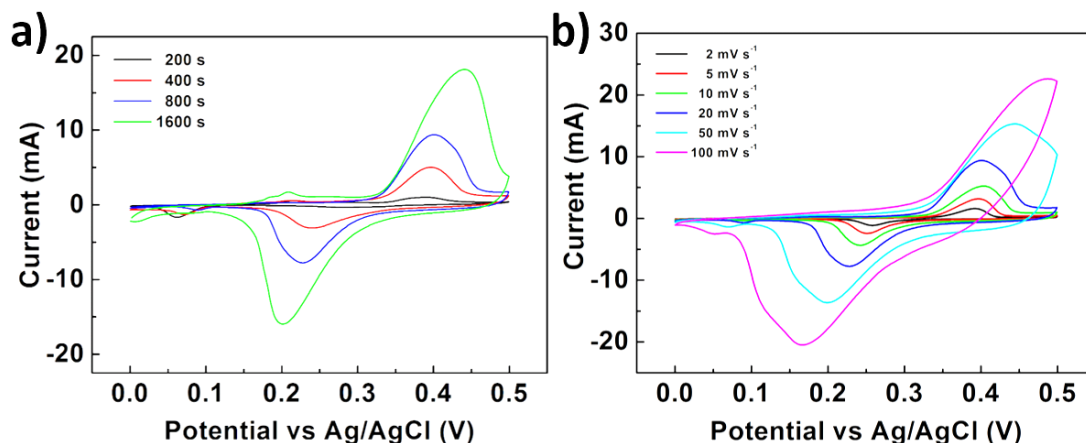


Figure 59. (a) CV results of the electrodeposited Ag NW/Ni(OH)₂ nanocomposite electrodes in 1 M KOH at 20 mV s⁻¹ scan rate. (b) CV results of 800 second deposited nanocomposite electrode at various scan rates.

The mechanical and functional integrity of the produced nanocomposite SC electrodes was also examined. Bending cycles were repeated for 1000 times and CV measurements were taken after each 200 times (Figure 60). The fabricated Ag NW/Ni(OH)₂ nanocomposite electrodes on PET substrates were realized to be highly flexible and might be continually bent without deterioration in energy storage performances. These measurements also indicated that the bending down to a radius of 2.5 mm do not have a serious effect on the mechanical integrity of the electrodes. This includes the adhesion of Ni(OH)₂ layer to the Ag NWs and adhesion of Ag NWs to the substrates.

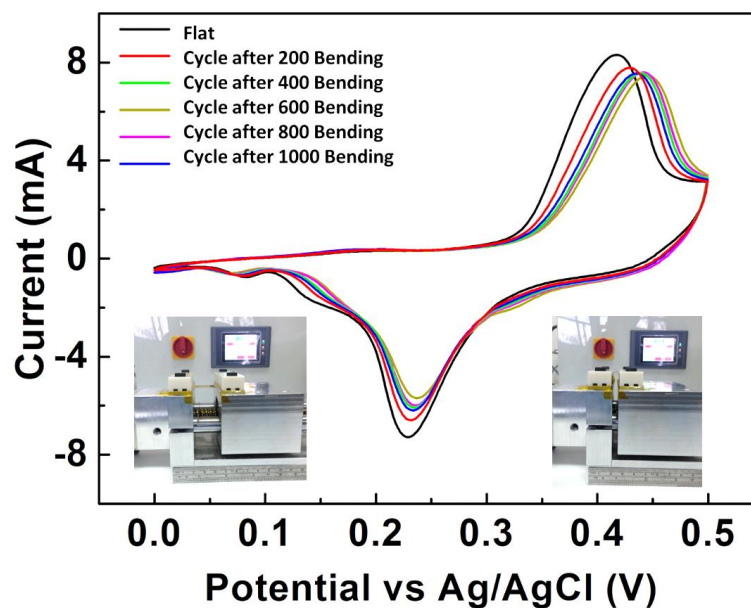


Figure 60. CV results of the Ag NW/Ni(OH)₂ nanocomposite electrodes following 200, 400, 600, 800 and 1000 bending cycles at 20 mV s⁻¹ scan rate. Inset show photos of home made bending setup.

Charge storage behaviors of the Ag NW/Ni(OH)₂ electrodes were also investigated by GCD measurements and GCD results of 800 second electrodeposited sample at various current densities are provided in Figure 61. Nonlinear galvanostatic charge–discharge profiles confirmed the pseudocapacitive property of the Ni(OH)₂. Similar discharge profiles have been observed at different current densities. Coaxial nanocomposite electrodes resulted in fast charge transfer and observed internal resistance drop (IR_{drop}) (5 Ω) was very low in the GCD curves.

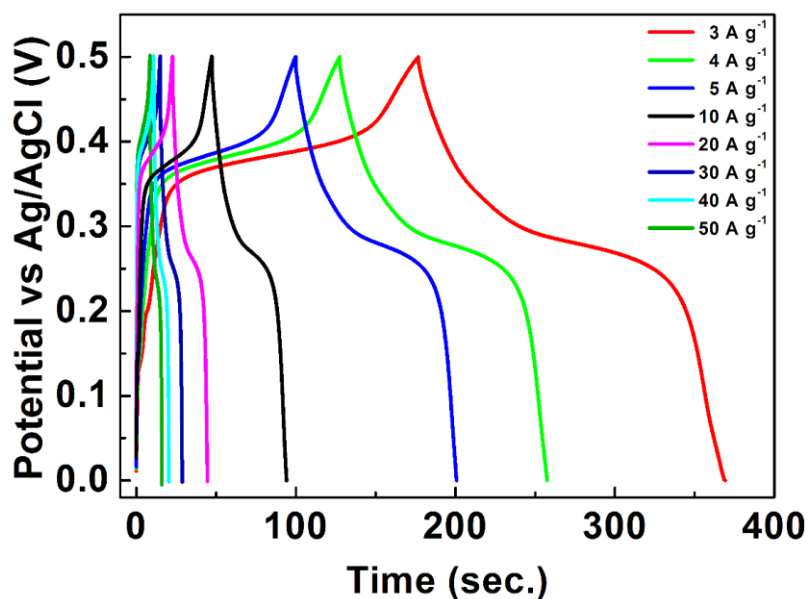


Figure 61. GCD curves of 800 second electrodeposited sample at different currents ranging from 3 A g⁻¹ to 50 A g⁻¹.

C_{sp} of the prepared nanocomposite electrodes were calculated using GCD curves provided in Figure 61. C_{sp} of the 800 second deposited sample is shown in Figure 62 (a) with respect to the applied current density. A C_{sp} of 1165.2 F g⁻¹ at 3.0 A g⁻¹ was obtained. C_{sp} was found to decrease to 863.0 F g⁻¹ at 50.0 A g⁻¹. It is a common phenomenon that slow electrochemical processes have difficulties to realize charge transfer through electrolyte/electrode interface and it might result in a dynamic resistance.

Capacity retention of the fabricated electrodes is also important parameter to evaluate their performance. Therefore, Ag NW/Ni(OH)₂ nanocomposite electrodes were tested for 3000 GCD cycles at 5 A g⁻¹. The obtained results of this measurement are given in Figure 62 (b). Fabricated SC electrodes showed good performance with a capacity retention almost 93 % after the 3000 charge-discharge cycles. High stability of the fabricated electrodes can be specifically attributed to the morphological stability of the nanocomposite core-shell structure. As evidenced by the TEM images (Figure 58), the morphology of the nanocomposite remains unchanged after 3000 charge-discharge cycles. In Figure 62 (b), coulombic efficiency of Ag NW/Ni(OH)₂ electrodes was also plotted as a function of the charge-discharge number. Nanocomposite

electrodes showed good performance and after 3000 cycles, columbic efficiencies were almost same with the initial values.

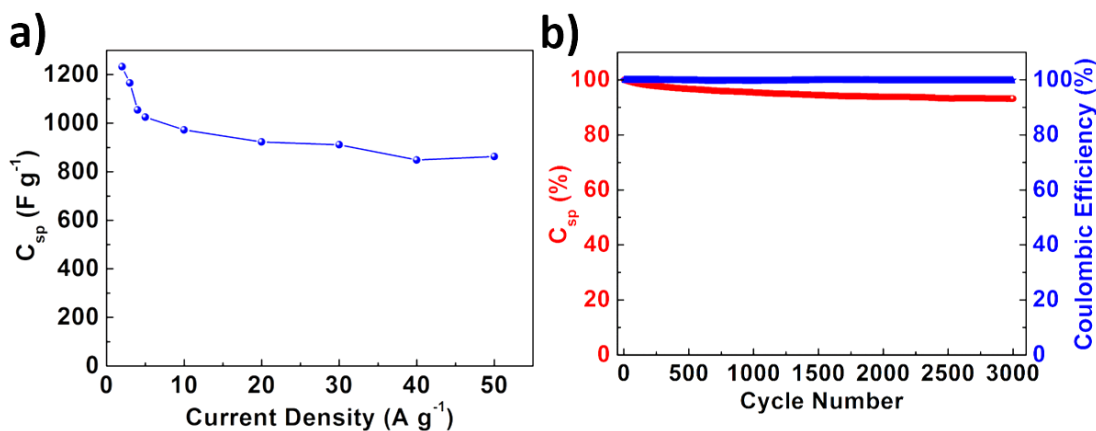


Figure 62. (a) C_{sp} of the fabricated electrodes as a function of GCD current density. Lines are for visual aid. (b) Capacity retention of Ag NW/ $Ni(OH)_2$ nanocomposite electrodes measured through a constant GCD at 5 $A g^{-1}$.

EIS was performed to clarify the electrochemical behaviors of the Ag NW/ $Ni(OH)_2$ nanocomposite electrodes. EIS behaviors of the fabricated electrodes were explored using a 5 mV AC perturbation. Nyquist plots of the fabricated electrodes measured within a limit of 50 kHz to 0.05 Hz is shown in Figure 63. Nyquist profile of fabricated electrodes were devoted to the interactions at the electrode surface. At high frequencies, electrochemical capacitors behave like a resistance, whereas they act a capacitance at low frequencies. It is clear that semicircle formation was not observed due to the high conductivity of the coaxial electrode architecture in high frequencies. The sharp inclination in the low frequencies was attributed to the pseudocapacitance of fabricated electrodes. EIS measurements of nanocomposite electrodes were also made under different DC potentials. The operated potentials of 0.44 V and 0.24 V correspond to fast redox reactions. Charge storage properties of the nanocomposite electrodes were found to depend on the applied potentials. Highest capacitive property was obtained for the sample under 0.44 V. This might be assigned to a characteristic of the $Ni(OH)_2$ that it demonstrates a potential-dependent pseudocapacitance. EIS measurement was also repeated for the sample after 3000 galvanostatic charge-discharge cycles. A slight decrease in the inclination of the low frequency region was observed but the pseudocapacitive property was found to remain almost constant.

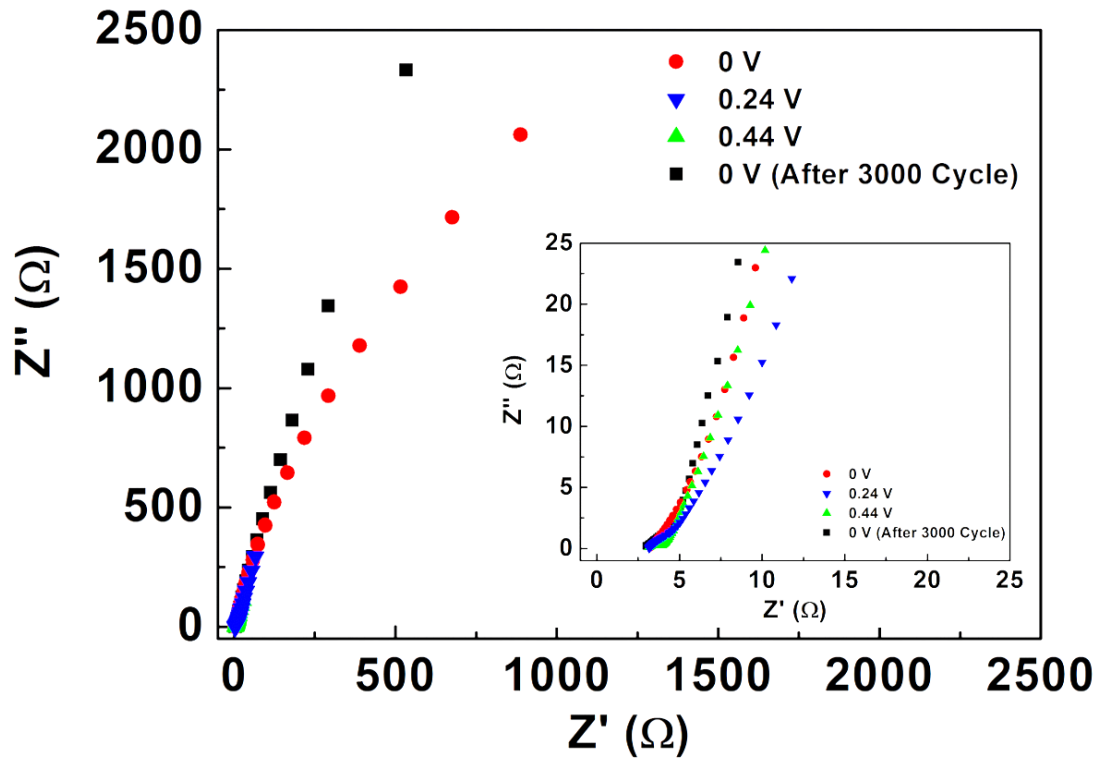


Figure 63. EIS spectra of 800 second deposited Ag NW/Ni(OH)₂ nanocomposite electrodes. Inset shows high frequency part of the EIS analyses.

Table 6 is prepared to compare the obtained results with the literature concerning Ni(OH)₂. It is clear that obtained results in this work are among the highest values for the Ni(OH)₂ containing SC electrodes.

Table 6. A comparison of various Ni(OH)₂ containing SC electrode materials performance.

Electrode Materials	Electrolyte	Potential window (V)	Current density or Scan rate	C_{sp} (F g⁻¹)	Refs.
α -Ni(OH) ₂	1.0 M KOH	0.55	5 mV s ⁻¹	805	[257]
β -Ni(OH) ₂	1.0 M KOH	0.55	2 mV s ⁻¹	395	[237]
β -Ni(OH) ₂	1.0 M KOH	0.55	2 A g ⁻¹	897	[258]
Ni(OH) ₂ /CNT	6.0 M KOH	0.50	5 mV s ⁻¹	1303	[259]
Ni(OH) ₂ /CNT	6.0 M KOH	0.50	10 mV s ⁻¹	432	[260]
α -Ni(OH) ₂ /graphene	6.0 M KOH	0.45	5 mV s ⁻¹	1215	[261]
β -Ni(OH) ₂ /graphene	1.0 M KOH	0.50	2.8 A g ⁻¹	1335	[262]
Ni(OH) ₂ /ZnO	1.0 M NaOH	0.55	15.7 A g ⁻¹	1310	[263]
Ni(OH) ₂ /CMK-3	2.0 M KOH	0.40	0.63 A g ⁻¹	2570	[264]
Ni(OH) ₂ /SiC NW	1.0 M KOH	0.70	2 A g ⁻¹	1724	[249]
Ag NW/ Ni(OH) ₂	1.0 M KOH	0.50	3 A g ⁻¹	1165.2	This work

7.4 Conclusions

In summary, flexible and coaxial core-shell Ag NW/Ni(OH)₂ nanocomposite electrodes were produced via solution based approaches and characterized. Conformal layer of Ni(OH)₂ allowed efficient charge transfer towards the inner Ag NW network. A C_{sp} of 1165.2 F g⁻¹ at 3 A g⁻¹ was obtained. It is possible that coaxial network structure may easily be applied to other CP or metal oxides to further exploit the advantage of this geometry.

CHAPTER 8

AN EFFICIENT ELECTROCHROMIC SUPERCAPACITOR SWITCHING BETWEEN GREEN AND TRANSPARENT

8.1 Introduction

SCs are considered one of the most important charge storage systems owing to their high power and excellent cycle life [85, 265-268]. The fast charge-discharge capabilities allow their application in consumer electronics, mobile and renewable energy systems [32, 269]. Integration of SCs to various other electronic systems possess the potential to have an impact in electronics industry if they gain smart functionalities, such as flexibility, color changing for charged-discharged states, environment friendliness and textile integrability. These multi-functional SC devices will be important for both industrial and commercial applications [270]. Electrochromic SCs that experience color change during ion intercalation/decalation or chemical oxidation/reduction processes indicate the amount of energy remained and the level at which the devices are charged or discharged [271]. This color change in the device can be both detected spectroscopically or by the naked eye, where the latter makes them suitable for functional devices with user interface.

Electrochromic materials started to be utilized in prototype color changing SCs. Integration of smart functionalities to SCs (i.e. environmental sensing, color change, user communication etc.) bring them a step closer to smart electronics. The remaining capacity within the SC devices that utilizes electrochromic materials can be easily recognized by the change of color and human eye is very sensitive to color changes. Moreover, electrochromic SCs may also prevent the overcharging (electrolyte decomposition, polymer degradation etc.), extending the life of the devices. Integration of electrochromism into the energy storage field, SCs in particular, will be a milestone for the smart energy storage systems.

Electrochromic SCs will be rationalized only if transparent current collectors are used for the electrodes. As transparent current collectors, ITO [189], fluorine-doped tin oxide (FTO) [187], CNT thin films [272] and Ag NW networks are the possible candidates for electrochromic SCs. ITO and FTO films have difficulties to be used in flexible SC electrodes, while CNT films have relatively lower transmittance values compared to ITO films and Ag NW networks. Among all these candidates, Ag NWs with high aspect ratio form a homogeneous network that is highly conductive and transparent with large openings. Ag NW networks can be deposited onto unconventional substrates such as PET, PDMS and textiles. The use of Ag NW networks in prototype optoelectronic devices as transparent conducting electrodes have already been demonstrated. The two most prominent devices include organic light emitting diodes [63] and photovoltaics [68]. In addition to these, Ag NW networks were demonstrated as current collectors in conjunction with ITO [84] and PEDOT:PSS [69] within a layered form for SCs. Ag NW networks as sole current collector was demonstrated by our research group in SC electrodes [73]. In addition to high transmittance and conductivity, Ag NW networks offer flexibility, which would allow their effortless integration to functional electronics.

In electrochromic SCs, most commonly utilized active materials are metal oxides and CPs. Tungsten oxides (WO_3 and $\text{W}_{18}\text{O}_{49}$) [128, 186, 187, 273], manganese oxide (MnO_2) [274], vanadium pentoxide (V_2O_5) [184] and nickel oxide (NiO) [275] are a few electrochromic and pseudocapacitive materials, which have already been demonstrated for SC electrodes. Among the metal oxides, WO_3 is the most prominently used one with a deep blue color in reduced form (-0.6 V vs Ag/AgCl), which is almost colorless in the bleached form. It is well documented that the electrochromic performance of WO_3 is quite irreversible due to ion trapping [271]. In addition to WO_3 , gyroid-nanostructured V_2O_5 electrodes were successfully utilized using block copolymer template method in electrochromic supercapacitors by Wei et al [184]. Templated V_2O_5 nanostructures showed very rapid color change compared to non-templated nanostructures in SC devices. Weak coloring efficiency and slow color switching are the two main drawbacks of these metal oxide based electrochromic devices. As an alternative, CPs are emerged as promising materials due to their fast processability, low-cost and rapid color shifts [271, 272]. Among CPs, polyaniline (PANI) is the most commonly used one with a color change from transparent to light

green (in reduced state) to blue color (in oxidized state) [189, 190, 276]. However, coloration efficiency and the color shifting of PANI is quite slow and when PANI switched between neutral and oxidized states (green to blue) the stability suffers significantly [276]. PANI shows good stability only when it switched between its fully neutral (transparent yellow) and neutral (or mildly oxidized) states (green) where the observed color change is dull. PEDOT [277] and polypyrrole [278] are the two other pseudocapacitive polymeric materials, which were also utilized in SC electrodes due to their processing ease, low cost and promising electrochemical properties, but with limited number of life cycles. A novel multi-chromatic CP that changes color from red to black and to blue was demonstrated. This was successfully utilized in SC electrodes with long cycle life [272]. PDOPEQ used in this study on the other hand, is the first ever example of a solution-processable green to transmissive polymer. The material showed superior electrochromic properties such as fast switching time and high optical contrast in addition to its significant long term switching stability. The material easily dissolves in common organic solvents and can be coated on large surfaces with easily via a variety of common coating techniques. For generation of high quality PANI and polypyrrole films on ITO on the other hand, it requires electrochemical polymerization methods.

In terms of hybrid electrodes, tungsten oxide ($W_{18}O_{49}$) was utilized in conjunction with PANI to create a synergistic effect [128]. In addition to metal oxide and CPs, some dye molecules were integrated into the energy storage devices to reveal their electrochromic properties during redox reactions of the dye molecules [192, 193]. However, color contrast between the reduced and oxidized states of dye molecules is low and thus lacks distinguishability in electrochromic energy storage devices. Therefore, discovery of novel materials with different color options, improved cyclic stability and electrochemical performance is necessary for the wide spread use of electrochromic supercapacitors.

In this study, electrochromic SC electrodes using highly conductive and transparent Ag NW networks with a novel pseudocapacitive conducting green polymer was fabricated. Electrochemical and electrochromic properties of the fabricated Ag NW/CP nanocomposite electrodes were investigated using an organic electrolyte solution.

8.2 Experimental Details

8.2.1 Preparation of Electrodes

All materials used in this work were of analytical grade, used as received and were purchased from Sigma-Aldrich. Purified Ag NWs were spray-coated onto 100 μm thick PET substrates. The CP used in this work was poly(2,3-bis(3,4-bis(decyloxy)phenyl)-5,8-bis(2,3-dihydrothieno[3,4-b][1,4]dioxin-5-yl)quinoxaline) (PDOPEQ), which was prepared as described elsewhere [279]. Upon synthesis, CP was dissolved in chloroform (0.5 mg/mL) under slow magnetic stirring on a hotplate (50 $^{\circ}\text{C}$) and deposited onto Ag NW networks through spray coating.

8.2.2 Characterization

The structural characterization of the fabricated nanocomposite films was made by SEM. Raman spectra was recorded by a Renishaw inVia Raman microscope (532 nm) and Raman samples were prepared on soda-lime silicate glass substrates. Spectroelectrochemical measurements of the fabricated electrodes were carried out via Varian Cary 5000 UV-Vis-NIR spectrophotometer. Gamry Reference 3000 potentiostat/galvanostat system was used in all electrochemical measurements in both three- and two-electrode configurations. A microbalance (Sartorius Research R200D, Bradford, Germany) was used to measure the mass of the deposited CP. The weight of total active material in the Ag NW/CP electrode was measured around 0.1 mg.

8.3 Results and Discussion

In this work, a chemically synthesized CP was used. The molecular structure of CP is provided in the Figure 1 (a). According to the gel permeation chromatography (GPC), number average (M_n) and weight average molecular weights (M_w) of the synthesized polymer were 31.8 kDa and 110 kDa, respectively [279]. High solubility of the CP in chloroform allowed its rapid and uniform deposition onto Ag NW network electrodes via spray coating method. The figure of merit $\sigma_{\text{Op}}(\lambda)/\sigma_{\text{DC}}$ ratio for the Ag

NWs networks used in this work was calculated as 400 at a percent transmittance and sheet resistance of 87% and $10 \Omega / \text{square}$, respectively. The nanowire density in the electrodes were $0.74 \text{ NW}/\mu\text{m}^2$.

Surface morphologies of the Ag NW and Ag NW/CP nanocomposite thin films on the PET substrates were investigated through SEM analysis, images of which are provided in Figures 64 (b) and (c), respectively. Spray-coated CP layer covered the whole surface of the Ag NW random network electrodes like a blanket and Ag NWs were visible beneath the CP layer (Figure 64 (c)). This method allowed uniform deposition of CP thin films over large length scales. The areal density of the CP film was measured as $0.05 \text{ mg}/\text{cm}^2$. Cross-sectional SEM image (Figure 65) showed that the nanocomposite film thickness was about 300 nm.

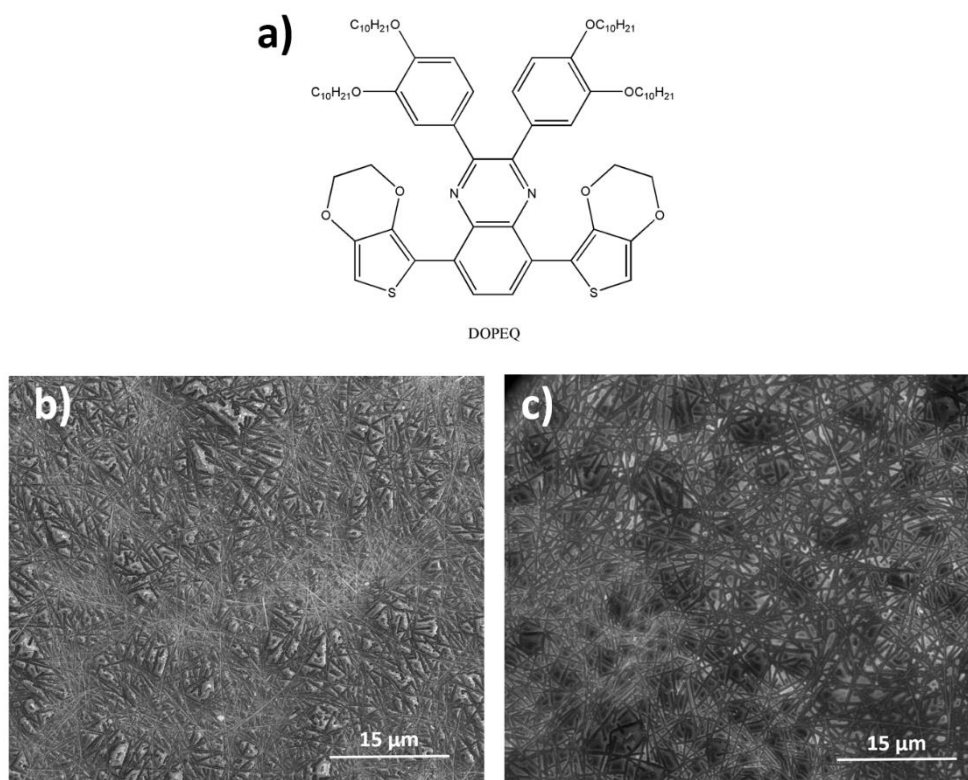


Figure 64. (a) The molecular structure of the CP used in this work. SEM images of (b) Ag NW networks and (c) Ag NW/CP nanocomposite film on PET substrates.

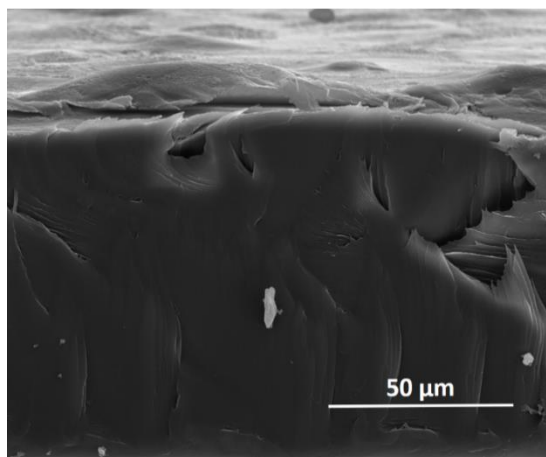


Figure 65. Cross-sectional SEM image of gold sputtered Ag NW/CP nanocomposite film on PET substrate.

Raman analysis was conducted to further characterize the fabricated nanocomposite electrodes. Raman spectra of the Ag NWs and Ag NW/CP nanocomposite films are shown in Figure 66 (a). Raman spectrum of bare Ag NW electrodes was recorded for comparison and observed peaks were due to the residual PVP layer on the Ag NWs. The molecular structure of CP is also shown in the inset of Figure 66 (a). In the Raman spectrum of the fabricated Ag NW/CP nanocomposite electrodes, Raman signals of Ag NWs were depressed, and the spectrum was dominated by the signals from CP. The Raman peak for Ag NW/CP nanocomposite at 442 cm^{-1} corresponds to collective oscillations of the C=C bonds in phenyl groups, whereas the peak at 656 cm^{-1} is assigned to the C-O vibrations in the entire polymer molecule. On the other hand, peaks at 1236 , 1308 , 1343 and 1495 cm^{-1} are attributed to the quinoxaline unit, due to the stretching of the C-N and C=N bonds. The observed peaks at 1371 and 1562 cm^{-1} are due to collective oscillations of C-H and C-C bonds in aromatic rings, respectively. In addition, the broad peak centered at 1440 cm^{-1} is attributed to long alkyl chains attached to the phenyl units.

UV-Vis absorption spectra of the fabricated electrodes within a wavelength range of 380-1100 nm at two different charged states are provided in Figure 66 (b). Fabricated nanocomposite electrodes had an intense green in its neutral state and the color is preserved at 0 V (reduced state). Two absorption peaks were evident within the spectra at 400 and 680 nm, which were originated from the CP and were blue-

shifted due to the charge transfer between the CP and Ag NWs [279]. Under an applied bias of 0.5 V (oxidized state), intensity of the absorption peaks was decreased and the peak was red-shifted towards the infrared region. Nanocomposite film electrodes were semi-transparent and the complete color change from green to transmissive state took place under higher potentials than 0.5 V. Within the operating window (0 - 0.5 V), fabricated nanocomposite electrodes showed reversible and rapid color change due to the redox reaction of the CP during ion insertion/extraction process. Our CP is not a multichromic one. Thus, photos of the fabricated electrochromic supercapacitor electrodes at two different potentials that clearly show the color change are provided in Figure 66 (b). The color change was evident even by naked-eye and might be used to display the charged state of the SCs. Transmittance spectra for the fabricated electrodes with different charged states are provided in Figure 66 (c). Transmittance values of 83 and 89 % (at a wavelength of 550 nm) were obtained for the Ag NW/CP electrodes at charged states of 0 and 0.5 V, respectively. In this study, unfortunately potentials above 0.5 V was not used in order to avoid the irreversible oxidation of Ag as shown in Figure 67.

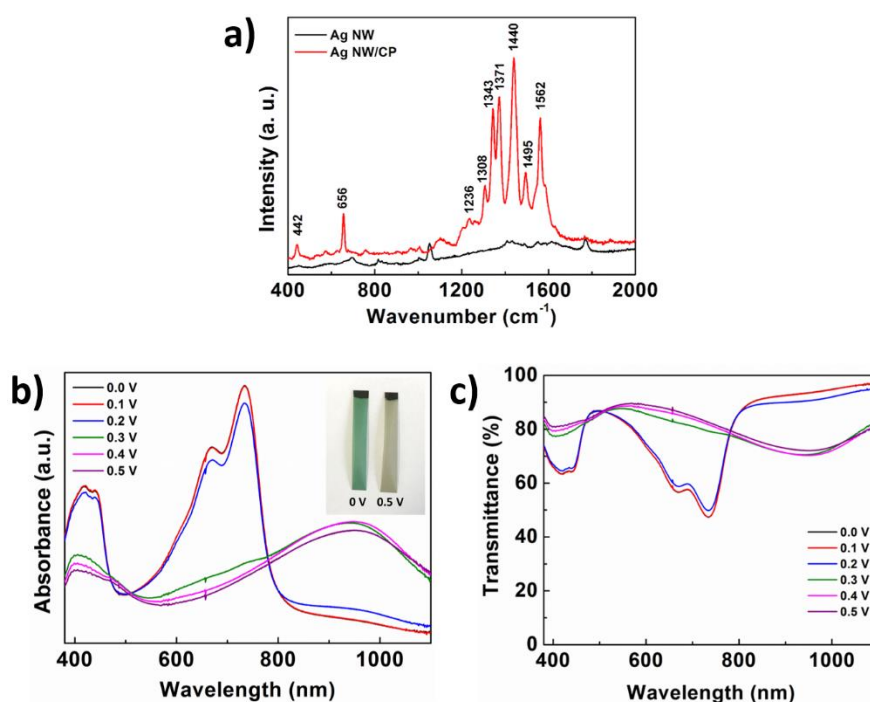


Figure 66. (a) Raman spectra of Ag NW and Ag NW/CP nanocomposite electrodes. (b) Absorbance and (c) transmittance spectra of the fabricated nanocomposite electrodes at different charged states. Inset shows a photo of the electrodes at different charged states.

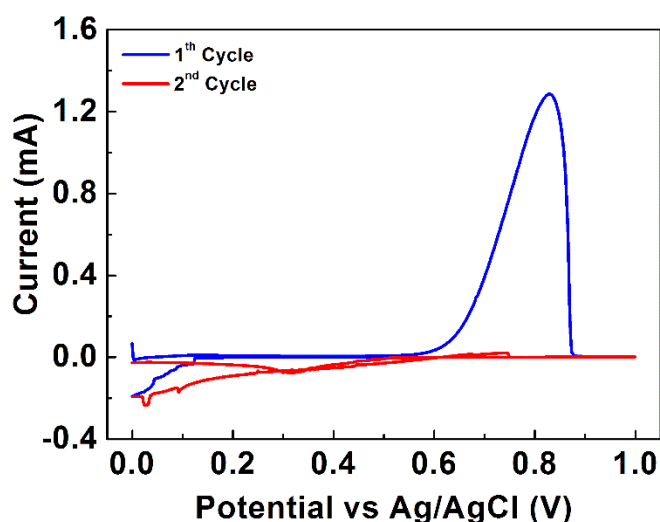


Figure 67. CV curves of bare Ag NW electrodes at a scan rate of 20 mV/s.

CV results of bare Ag NWs and Ag NW/CP nanocomposite electrodes are provided in Figure 68 (a). Ag NWs had a very small pseudocapacitance as a consequence of thin oxide layer formation on their surface. This pseudocapacitive property was quasi-reversible and the redox peaks were located in the low potential region of the CV curve. As seen in the figure, on the other hand, fabricated nanocomposite electrodes showed high charge accumulation because of the pseudocapacitive property of the CP. In the entire potential window, CV curves of the fabricated SC electrodes were very close to the ideal shape. The fabricated nanocomposite SC electrodes were also tested at various rates from 1 to 100 mV s^{-1} , results of which are provided in Figure 68 (b). Expansion in the typical rectangular shape is evident with increased scan rates.

Electrochemical performances of the fabricated electrodes were also examined using GCD measurements. As shown in the Figure 68 (c), electrodes were tested within a potential limit of 0 - 0.5 V at 0.10 A g^{-1} current density. Poor GCD performance of the Ag NWs were altered with the nanocomposite formation where a significant enhancement in the capacitance was obtained through the nanocomposite formation. GCD measurements of the fabricated nanocomposite electrodes were also conducted at various currents ranging from 0.10 to 10.0 A g^{-1} (Figure 68 (d)). In GCD measurements, nanocomposite electrodes showed highly pseudocapacitive properties attributed to their conductive nature resulting in the efficient charge transfer from CP

layer to the inner Ag NW network. As shown in the figure, internal resistance drop (IR_{drop}) was almost insignificant and the GCD curves were nearly symmetrical.

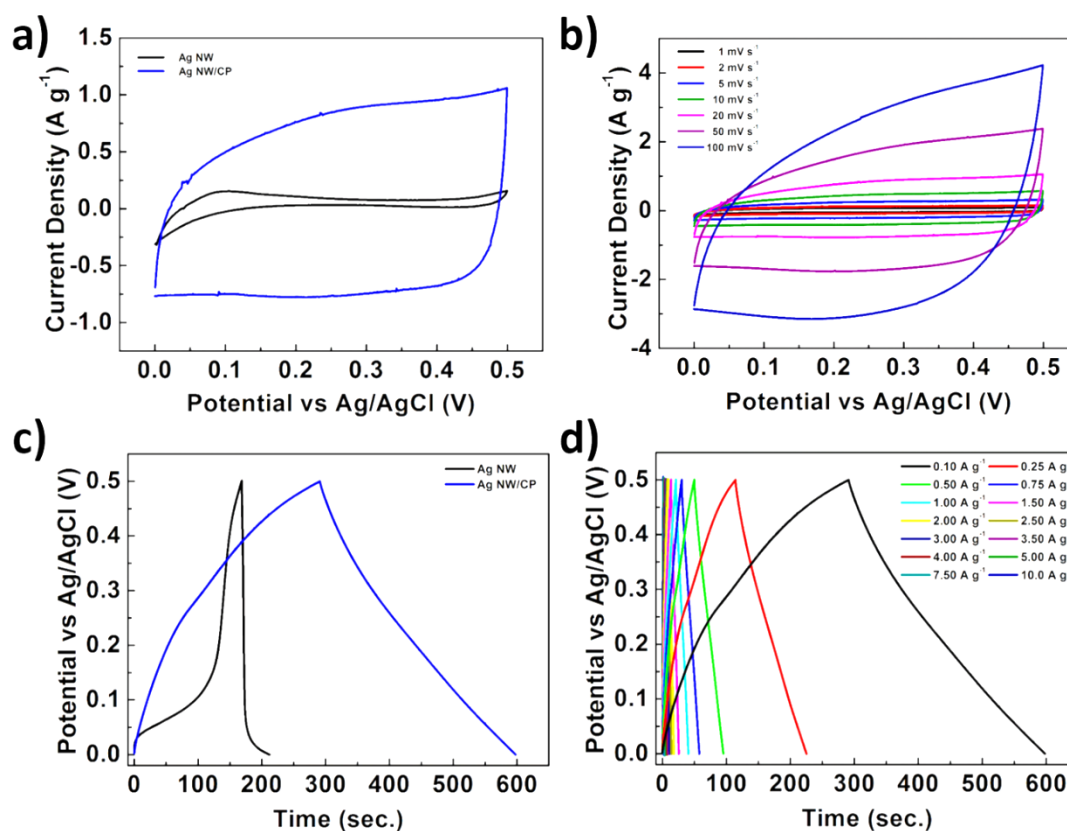


Figure 68. (a) CV results of the fabricated electrodes in 1 M LiClO₄ in PC, at 20 mV s⁻¹. (b) at different scan rates. (c) GCD curves of the fabricated electrodes at 0.1 A g⁻¹ current density and (d) at different current densities.

Nanocomposite SC electrodes were also fabricated on PET substrates, which was necessary to monitor the mechanical performance of the flexible electrodes. In order to measure CV performance upon flexing, they were bent (down to a radius of 1.5 mm) for 1000 times as demonstrated in the Figure 69. The photos of the flat and bent samples and home-built bending setup during bending test are provided in Figure 69 (b1)-(b3). CV characteristics of the bent samples after each 200 bending cycles were measured and provided in the Figure 69. True flexibility of the electrodes was attributed to the high aspect ratio Ag NWs and the homogeneous deposition of the polymer over layer. This resulted in the strong adhesion of Ag NWs to PET and CP to Ag NWs and eventually to PET substrates leading to high mechanical durability of the

electrodes. CV measurements proved that the electrochemical behavior of the bent electrodes were identical to that of the flat sample.

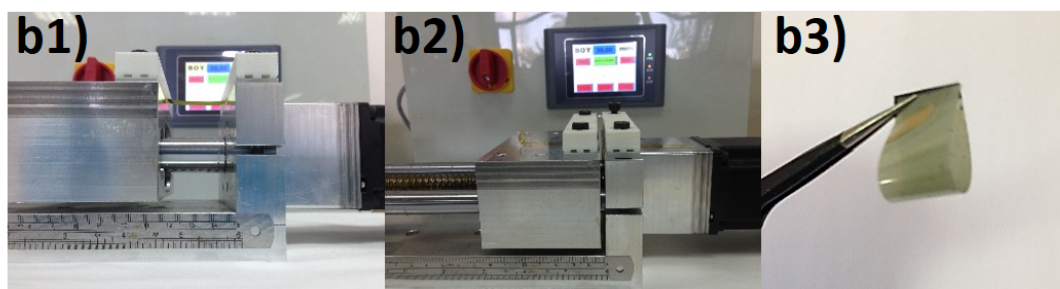
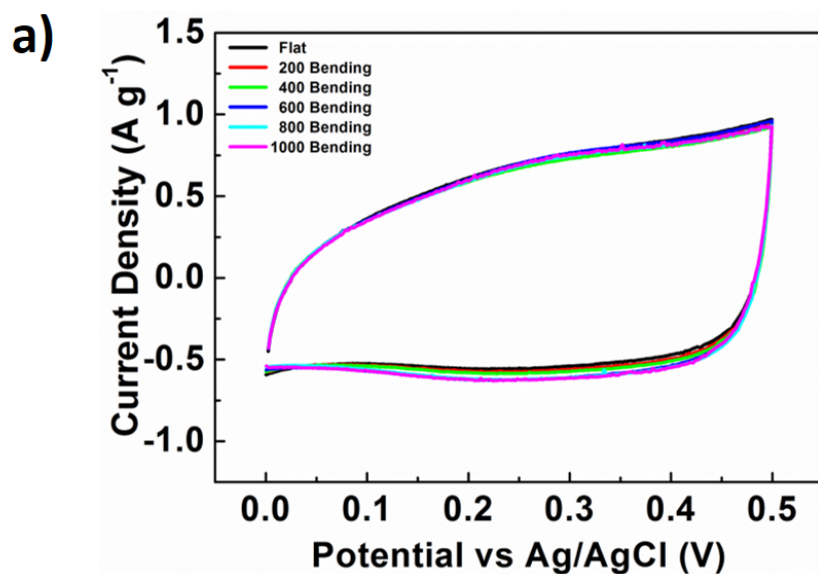


Figure 69. CV curves of the fabricated electrodes following each bending cycle at 20 mV s^{-1} . (b1)- (b2) shows the photos of bending setup with flat and bended samples and (b3) photo of the fabricated flexible nanocomposite electrode.

EIS was conducted for further investigation of the electrochemical properties of the fabricated nanocomposite electrodes. Both resistive and capacitive properties of the Ag NW/CP nanocomposite electrodes were measured within a limit of 100 kHz-10 mHz at a 5 mV AC perturbation. The Nyquist plot for the fabricated nanocomposite electrodes is provided in Figure 70. Fabricated electrodes showed low internal resistance evidenced by incomplete semicircle formation at high frequencies and a sharp slope in the low frequencies revealing the pseudocapacitive properties of the CP. Due to their porous nature, fabricated nanocomposite electrodes were evaluated as a constant phase element instead of a double layer capacitor. As evidenced by the GCD measurements, inner resistances of the fabricated electrodes were quite low and

uncompensated serial resistance was mainly due to the electrolyte resistance, contact point resistance and the electrode-electrolyte interface resistance. Impedance curve for the 20000 cycle tested sample was also shown within the same figure. Formation of a distinct semicircle for the resistance part and an increment in the slope for the low frequency capacitive region were observed as a result of the improved charge transfer. This might be succeeded by the activation of inactive pores in the nanocomposite during cycle life test.

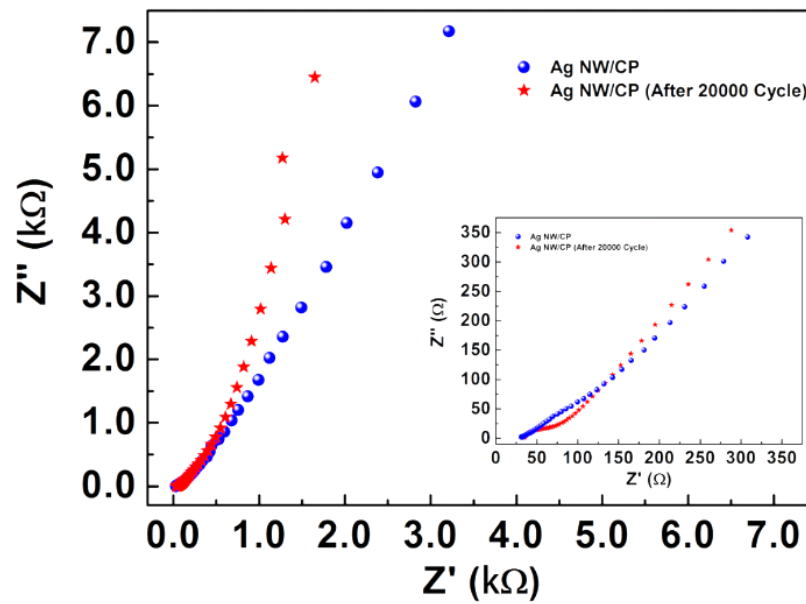


Figure 70. EIS spectra of the as-fabricated and 20000 times cycled nanocomposite electrodes. Inset shows the high-frequency region of the impedance spectra.

The C_{sp} of the fabricated electrodes were found using the GCD curves (Figure 68 (d)) according to the formula given below:

$$C_{sp} = \frac{I}{m \frac{\Delta V}{\Delta t}}$$

where m (g) is the total weight of active materials, I (A) is the discharge current, ΔV (V) is the potential window and the Δt (s) is the total discharge time. The calculated C_{sp} results were plotted as a function of the current density in Figure 71 (a). Fabricated nanocomposite electrodes showed a C_{sp} of 61.5 F g^{-1} at 0.1 A g^{-1} and this value decreased to 22.7 F g^{-1} at 10.0 A g^{-1} . Two orders of magnitude improvement in the current density resulted only a one-third decrease in the specific capacitance, since

slow electrochemical processes commonly results in a fall in the C_{sp} at high current densities. An areal capacitance of 3.1 mF cm^{-2} at a current density of $5 \mu\text{A cm}^{-2}$ was calculated for the nanocomposite supercapacitor electrodes. Nanocomposite electrodes showed dual electrochemical energy storage and electrochromic properties at the same time without any deterioration from the performance.

Long term cycleability and stability are the two other important factors for SCs. Fabricated nanocomposite electrodes were cycled for 20000 GCD at 1.0 A g^{-1} . Change in C_{sp} and coulombic efficiency for the fabricated electrodes as a function of the GCD cycles is provided in Figure 71 (b). A slight increase in the capacitance in early stages of the test gradually diminished and the capacitance was found as almost unchanged after 20000 galvanostatic charge-discharge cycles. This value is the highest number of cycles for a CP based SC. On the other hand, the coulombic efficiency of the fabricated electrodes were found to be essentially equal to 100 % after 20000 cycles, showing their electrochemical stability.

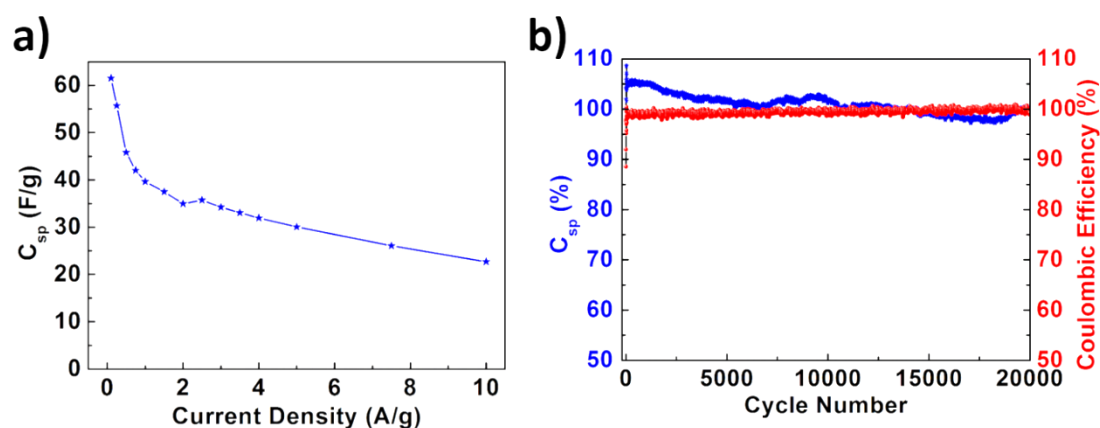


Figure 71. (a) C_{sp} change with respect to current density. (b) Cycling performance of the nanocomposite electrodes measured through GCD at 1 A g^{-1} .

Fabricated nanocomposite electrodes were also assembled into a full devices using a symmetric architecture. CV measurement of the symmetric SC device was conducted at 20 mV s^{-1} . CV results are provided in Figure 72 (a). Fabricated full SC devices showed decent CV characteristics and a small deviation from ideal CV shape due to the increased serial resistance. Imperfections in device architecture, such as organic electrolyte and separator usage, and resistance contribution of external contact

points could be the source of these deviations. GCD measurement of the SC was conducted at 0.1 A g^{-1} and the device showed a coulombic efficiency of more than 96 % as shown in Figure 72 (b). Both the full supercapacitor and half-cell devices had similar GCD profile, which indicate the promising electrochemical performance of the full SC device. Upon comparing the electrochemical results of the half-cell and the full device, it is evident that the full devices must be improved especially in terms of the charge transfer resistance.

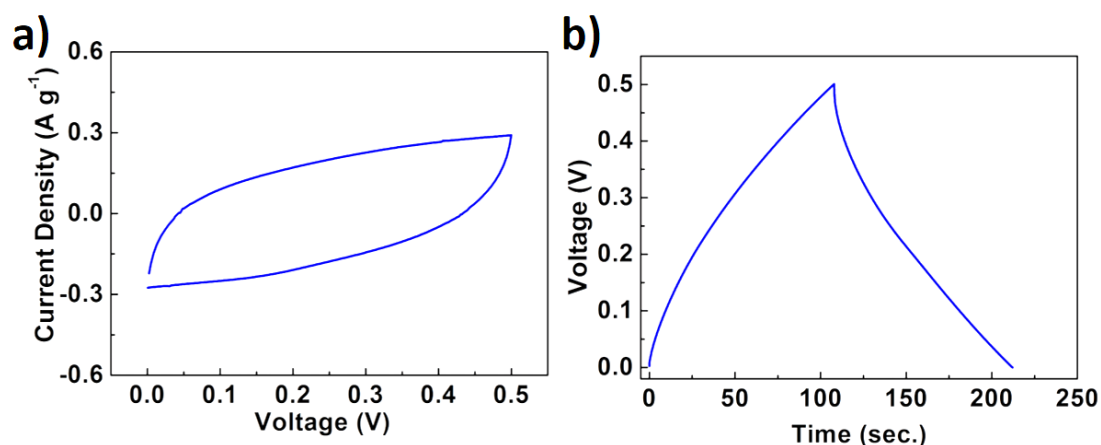


Figure 72. (a) CV curve of the Ag NW/CP nanocomposite SC device using a 1 M LiClO_4 in PC electrolyte solution at 20 mV s^{-1} . (b) GCD curve of the fabricated SC at a current density of 0.1 A g^{-1} .

In this work, a novel nanocomposite material, which showed dual electrochromic and electrochemical properties were reported. Fabricated nanocomposite electrode is an excellent alternative to electrochromic SCs due to its green to transparent color change and superior stability. Many of the CPs usually show poor cycle performance and a serious decrease in the capacity retention after a few thousands of GCD cycles. In our case, an almost unchanged capacity retention during 20000 GCD cycles was obtained. This capacity retention was higher than many CPs [189, 276]. Fabricated electrodes hold strong potential to be used in smart electronics, where it is possible to detect the charged state of the devices simply by the changes in the color.

8.4 Conclusions

In conclusion, nanocomposite Ag NW/CP SC electrodes were fabricated and their electrochromic and electrochemical properties were investigated. A C_{sp} of 61.5 F g^{-1} was obtained at 0.1 A g^{-1} and the capacitance was almost completely retained for 20000 GCD cycles. Fabricated electrodes showed rapid and reversible color change within the investigated potential window. Designed electrochromic SC electrodes makes it possible to visually determine the remaining energy and the charged state of these devices.

CHAPTER 9

CONCLUSIONS AND FUTURE RECOMMENDATIONS

This study contains a detailed analysis on the development of SC electrodes using one-dimensional conductive nanostructures and adding functionalities to fabricated SC electrodes. The obtained results allowed the following significant conclusions:

In Chapter 2, solid-state, highly flexible and transparent SCs with binder-free SWNT thin film electrodes were fabricated. The effect of SWNT density, thus the SWNT mass, on the charge storage behaviors of the supercapacitors were tested. SWNT density controlled the sheet resistance of the electrodes and transmittance of the overall devices. A typical EDLC behavior in a voltage window of 0 to 2 V was obtained. High conductance of the SWNT thin films eliminated the use of extra charge collectors. High bendability without significant deterioration in device properties was obtained. The specific capacitance was found to change by less than 2 % through bending the devices down to a radius of 6 mm. Finally, a low cost and rapid route for the fabrication of SCs is presented. These SCs will be critical components of transparent and flexible devices.

In Chapter 3, a simple and low cost route for the fabrication of SWNT/WO₃/PANI ternary nanocomposite electrodes was developed and their synergistic and complementary effect on SC performance were investigated. Typical EDLC behavior of SWNT electrodes was improved with the pseudocapacitive properties of WO₃ and PANI. Fabricated ternary nanocomposite SC electrodes were found to have a specific capacity of 28.5 mF/cm² at 0.13 mA/cm². Variation in the specific capacitance was found to be less than 24% after 2000 GCD cycles.

In Chapter 4, highly flexible, solid-state textile-based SCs with binder-free ternary nanocomposite electrodes were fabricated. An economic and rapid route was demonstrated for the fabrication of flexible and high performance SCs. High conductivity of the SWNTs and the CP layers eliminated the necessity for extra charge collectors. The effect of components, separately and together in ternary nanocomposite

form, on the electrochemical performances of the SCs were examined. Surface resistance of the electrodes and of the overall devices were controlled by the densities of SWNTs and CP (PANI and PEDOT:PSS). Fabricated SCs were highly stable and the variation in C_{sp} was less than 30% over 1000 GCD cycles. MnO_2 /SWNT/PANI ternary nanocomposite SCs showed better electrochemical properties than the MnO_2 /SWNT/PEDOT:PSS counterparts. Performance degradation was mainly attributed to degradation of CPs in ambient conditions. In addition, the change in specific capacitance was found to be less than 3 %, down to a bending angle of 180 degrees. Strong adhesion of the metal oxide nanoparticles, SWNTs and conducting polymers to the textile fibers resulted in high bending performance without significant deterioration in device characteristics. We believe that these SCs will be critical components of wearable electronic devices and smart textiles.

In Chapter 5, we analyze the production and characterization of all-organic electrochromic nanocomposite SC electrodes with combination of SWNTs and poly(4-(dithieno[3,2-b:2',3'-d]thiophen-2-yl)-2-(2-octyldodecyl)-2Hbenzo[d][1,2,3]triazole). The CP showed multiple color changes due to its charged states. Fabricated electrochromic SC electrodes were found to have a C_{sp} of 112.4 F/g at 1.0 A/g. Electrochromic SCs can effectively communicate with the user to alert how much charge and energy remained within the device; however, much more work on the fabrication and characterization of full devices need to be done.

In Chapter 6, coaxial Ag NW network core/ MoO_2 shell nanocomposite electrodes were investigated as promising electrode active materials for energy storage systems. Conformal coating of MoO_2 allowed easy charge transport towards the Ag NW network to form efficient SC electrodes. All solution based approaches have been used to fabricate electrodes and this allowed economic and large-scale fabrication of the SCs, which can also be made flexible. In this work, the coaxial nature of the SCs were kept; but, the geometry was changed from individual wire to network of wires. A C_{sp} of 500.7 F/g at a current density of 0.25 A/g was obtained. The use of NW networks eliminated the need for intensive lithographical processing, bringing this concept one more step closer to commercialization.

In Chapter 7, flexible and coaxial core-shell Ag NW/ $Ni(OH)_2$ nanocomposite electrodes were fabricated via solution based approaches and characterized.

Conformal layer of Ni(OH)₂ allowed efficient charge transfer towards the inner Ag NW network. A C_{sp} of 1165.2 F g⁻¹ at 3 A g⁻¹ was obtained. This coaxial network structure may easily be applied to other CP or metal oxides to further exploit the advantage of the investigated geometry.

In Chapter 8, nanocomposite Ag NW/ poly(2,3-bis(3,4-bis(decyloxy)phenyl)-5,8-bis(2,3-dihydrothieno[3,4-b][1,4]dioxin-5-yl)quinoxaline) SC electrodes were fabricated and their electrochemical and electrochromic properties were investigated. A C_{sp} of 61.5 F g⁻¹ was obtained at 0.1 A g⁻¹ and the capacitance was almost completely retained for 20000 GCD cycles. Fabricated electrodes showed rapid and reversible color change within the investigated potential range of 0-0.5 V. Designed electrochromic SC electrodes make it possible to visually determine the remaining energy and the charged state of these devices.

Although a number of important conclusions have been reached in this study, several phenomena reported here need further investigation. Some suggestions for future work are listed below:

1. The reported transparent and flexible SC devices showed good mechanical and electrochemical properties; however, their electrochemical properties may be tested in a real application.
2. Textile based wearable electronics draw huge attention and SCs are good candidates for their power sources. Therefore, textile based supercapacitor devices may be integrated in some portable electronics and tested their performance in a real application.
3. Ag NW based SC electrodes have efficient charge transfer and Ag NWs allow the deposition of many different capacitive materials. On the other hand, Ag NW based devices have restricted voltage window and more efforts should be done to enlarge the voltage window and to enhance the stability of the Ag NW.
4. Electrochromic or color changing SCs are admired as instant charge indicator and many research efforts are put on electrochromic energy storage devices. Therefore, novel electrode architectures should be constructed to show color change in symmetric devices.
5. In this thesis study, experiment oriented research was conducted and charge storage mechanism of some of the electrode active materials was still unclear.

Therefore, computational simulations should be used to clarify charge storage mechanisms of the electrodes and devices.

6. Although most of the nanocomposite materials in this study showed high stability and capacity retention, charge storage mechanism of the nanocomposite electrodes needs in-situ characterizations such as in-situ FTIR, Raman and/or XRD measurements that would lead to clarify these mechanisms.

REFERENCES

- [1] H. V. Helmholtz, *Ann. Phys.* 29 (1879).
- [2] H. E. Becker, U.S. Patent 2 800 616, 1957.
- [3] D. I. Boos, U.S. Patent 3 536 963, 1970.
- [4] B. E. Conway, Transition from supercapacitor to battery behavior in electrochemical energy-storage, *J Electrochem Soc* 138 (1991) 1539-1548.
- [5] S. Sarangapani, B. V. Tilak, C. P. Chen, Materials for electrochemical capacitors - theoretical and experimental constraints, *J Electrochem Soc* 143 (1996) 3791-3799.
- [6] T. C. Murphy, R. B. Wright, R. A. Sutula, US department of energy electrochemical capacitor development and testing activities, *Proceedings of the Symposium on Electrochemical Capacitors II* 96 (1997) 258-267.
- [7] B. E. Conway, *Electrochemical supercapacitors, scientific fundamental and technological applications*. 1999: Plenum Publishers.
- [8] Ultracapacitor Overview. [accessed: 14/11/2016]; Available from: <http://www.maxwell.com/products/ultracapacitors>.
- [9] F. Beguin, E. Frackowiak, *Supercapacitors materials, systems, and applications*. 2013: Wiley-VCH Verlag GmbH & Co.
- [10] Brake Energy Regeneration System. 2016 [accessed: 11/13/2016]; Available from: <http://www.mazda.com/en/innovation/technology/env/i-loop/>.
- [11] MAN Lion's City Hybrid. [accessed: 14/11/2016]; Sustainable in the future – the new MAN Lion's City Hybrid]. Available from: <http://www.bus.man.eu/naf/en/city-buses/man-lions-city-hybrid/overview-Overview.html>.
- [12] P. Simon, Y. Gogotsi, Materials for electrochemical capacitors, *Nat Mater* 7 (2008) 845-854.
- [13] S. Bose, T. Kuila, A. K. Mishra, R. Rajasekar, N. H. Kim, J. H. Lee, Carbon-based nanostructured materials and their composites as supercapacitor electrodes, *J Mater Chem* 22 (2012) 767-784.

- [14] R. Kotz, M. Carlen, Principles and applications of electrochemical capacitors, *Electrochim Acta* 45 (2000) 2483-2498.
- [15] Electric Double Layer Capacitors. 2014 19.05.2014 [cited 2014 20.05.2014]; Available from: http://en.wikipedia.org/wiki/Electric_double-layer_capacitor.
- [16] S. H. Chae, Y. H. Lee, Carbon nanotubes and graphene towards soft electronics, *Nano Convergence* 1 (2014).
- [17] K. Jost, G. Dion, Y. Gogotsi, Textile energy storage in perspective, *J Mater Chem A* 2 (2014) 10776-10787.
- [18] Y. J. Kang, B. Kim, H. Chung, W. Kim, Fabrication and characterization of flexible and high capacitance supercapacitors based on MnO₂/CNT/papers, *Synthetic Met* 160 (2010) 2510-2514.
- [19] S. G. Hwang, S. H. Ryu, S. R. Yun, J. M. Ko, K. M. Kim, K. S. Ryu, Behavior of NiO-MnO₂/MWCNT composites for use in a supercapacitor, *Mater Chem Phys* 130 (2011) 507-512.
- [20] L. S. Aravinda, K. K. Nagaraja, K. U. Bhat, B. R. Bhat, Magnetron sputtered MoO₃/carbon nanotube composite electrodes for electrochemical supercapacitor, *J Electroanal Chem* 699 (2013) 28-32.
- [21] Y. P. Zhang, X. W. Sun, L. K. Pan, H. B. Li, Z. Sun, C. Q. Sun, B. K. Tay, Carbon nanotube-zinc oxide electrode and gel polymer electrolyte for electrochemical supercapacitors, *J Alloy Compd* 480 (2009) L17-L19.
- [22] W. J. Wang, Q. L. Hao, W. Lei, X. F. Xia, X. Wang, Graphene/SnO₂/polypyrrole ternary nanocomposites as supercapacitor electrode materials, *RSC Advances* 2 (2012) 10268-10274.
- [23] X. Zhao, C. Johnston, P. S. Grant, A novel hybrid supercapacitor with a carbon nanotube cathode and an iron oxide/carbon nanotube composite anode, *J Mater Chem* 19 (2009) 8755-8760.
- [24] Z. Chen, V. Augustyn, J. Wen, Y. W. Zhang, M. Q. Shen, B. Dunn, Y. F. Lu, High-performance supercapacitors based on intertwined CNT/V₂O₅ nanowire nanocomposites, *Adv Mater* 23 (2011) 791-+.
- [25] Q. Wang, Z. H. Wen, J. H. Li, Carbon nanotubes/TiO₂ nanotubes hybrid supercapacitor, *J Nanosci Nanotechno* 7 (2007) 3328-3331.
- [26] X. B. Ren, H. Y. Lu, H. B. Lin, Y. N. Liu, Y. Xing, Preparation and characterization of the Ti/IrO₂/WO₃ as supercapacitor electrode materials, *Russ J Electrochem.* 46 (2010) 77-80.

- [27] Y. M. Chen, J. H. Cai, Y. S. Huang, K. Y. Lee, D. S. Tsai, Preparation and characterization of iridium dioxide-carbon nanotube nanocomposites for supercapacitors, *Nanotechnology* 22 (2011)
- [28] A. Clemente, S. Panero, E. Spila, B. Scrosati, Solid-state, polymer-based, redox capacitors, *Solid State Ionics* 85 (1996) 273-277.
- [29] A. Laforgue, P. Simon, C. Sarrazin, J. F. Fauvarque, Polythiophene-based supercapacitors, *J Power Sources* 80 (1999) 142-148.
- [30] K. S. Ryu, K. M. Kim, N. G. Park, Y. J. Park, S. H. Chang, Symmetric redox supercapacitor with conducting polyaniline electrodes, *J Power Sources* 103 (2002) 305-309.
- [31] C. Arbizzani, M. Mastragostino, F. Soavi, New trends in electrochemical supercapacitors, *J Power Sources* 100 (2001) 164-170.
- [32] G. P. Wang, L. Zhang, J. J. Zhang, A review of electrode materials for electrochemical supercapacitors, *Chem Soc Rev* 41 (2012) 797-828.
- [33] E. Frackowiak, F. Beguin, Carbon materials for the electrochemical storage of energy in capacitors, *Carbon* 39 (2001) 937-950.
- [34] M. Scarselli, P. Castrucci, M. De Crescenzi, Electronic and optoelectronic nano-devices based on carbon nanotubes, *J Phys-Condens Mat* 24 (2012)
- [35] H. Pan, C. K. Poh, Y. P. Feng, J. Y. Lin, Supercapacitor electrodes from tubes-in-tube carbon nanostructures, *Chem Mater* 19 (2007) 6120-6125.
- [36] Q. Y. Li, Z. S. Li, L. Lin, X. Y. Wang, Y. F. Wang, C. H. Zhang, H. Q. Wang, Facile synthesis of activated carbon/carbon nanotubes compound for supercapacitor application, *Chem Eng J* 156 (2010) 500-504.
- [37] B. E. Conway, V. Birss, J. Wojtowicz, The role and utilization of pseudocapacitance for energy storage by supercapacitors, *J Power Sources* 66 (1997) 1-14.
- [38] J. H. Park, J. M. Ko, O. O. Park, Carbon nanotube/RuO₂ nanocomposite electrodes for supercapacitors, *J Electrochem Soc* 150 (2003) A864-A867.
- [39] D. Gebler. Metallic State of Conducting Polymers. 2000 23.05.2000 [accessed: 23.05.2014]; Available from: <http://www.physics.ohio-state.edu/~ppl/metallic.html>.
- [40] W. C. Chen, T. C. Wen, Electrochemical and capacitive properties of polyaniline-implanted porous carbon electrode for supercapacitors, *J Power Sources* 117 (2003) 273-282.

- [41] Y. R. Lin, H. S. Teng, A novel method for carbon modification with minute polyaniline deposition to enhance the capacitance of porous carbon electrodes, *Carbon* 41 (2003) 2865-2871.
- [42] C. C. Hu, W. Y. Li, J. Y. Lin, The capacitive characteristics of supercapacitors consisting of activated carbon fabric-polyaniline composites in NaNO₃, *J Power Sources* 137 (2004) 152-157.
- [43] C. Peng, S. W. Zhang, D. Jewell, G. Z. Chen, Carbon nanotube and conducting polymer composites for supercapacitors, *Prog Nat Sci* 18 (2008) 777-788.
- [44] S. R. Sivakkumar, W. J. Kim, J. A. Choi, D. R. MacFarlane, M. Forsyth, D. W. Kim, Electrochemical performance of polyaniline nanofibres and polyaniline/multi-walled carbon nanotube composite as an electrode material for aqueous redox supercapacitors, *J Power Sources* 171 (2007) 1062-1068.
- [45] M. Mallouki, F. Tran-Van, C. Sarrazin, P. Simon, B. Daffos, A. De, C. Chevrot, J. Fauvarque, Polypyrrole-Fe₂O₃ nanohybrid materials for electrochemical storage, *J Solid State Electr* 11 (2007) 398-406.
- [46] R. Y. Song, J. H. Park, S. R. Sivakkumar, S. H. Kim, J. M. Ko, D. Y. Park, S. M. Jo, D. Y. Kim, Supercapacitive properties of polyaniline/Nafion/hydrous RuO₂ composite electrodes, *J Power Sources* 166 (2007) 297-301.
- [47] S. R. Sivakkumar, J. M. Ko, D. Y. Kim, B. C. Kim, G. G. Wallace, Performance evaluation of CNT/polypyrrole/MnO₂ composite electrodes for electrochemical capacitors, *Electrochim Acta* 52 (2007) 7377-7385.
- [48] G. J. Wilson, M. G. Looney, A. G. Pandolfo, Enhanced capacitance textile fibres for supercapacitors via an interfacial molecular templating process, *Synthetic Metals* 160 (2010) 655-663.
- [49] Aiping Yu, Victor Chabot, J. Zhang, *Electrochemical supercapacitors for energy storage and delivery: fundamentals and applications.*, 2013: CRC Press
- [50] M. D. Stoller, R. S. Ruoff, Best practice methods for determining an electrode material's performance for ultracapacitors, *Energ Environ Sci.* 3 (2010) 1294-1301.
- [51] K. V, E. Frackowiak, F. Beguin, Determination of the specific capacitance of conducting polymer/nanotubes composite electrodes using different cell configurations, *Electrochim Acta* 50 (2005) 2499-2506.

- [52] S. Maiti, A. Pramanik, S. Mahanty, Influence of imidazolium-based ionic liquid electrolytes on the performance of nano-structured MnO₂ hollow spheres as electrochemical supercapacitor, *RSC Adv* 5 (2015) 41617-41626.
- [53] S. Iijima, Helical microtubules of graphitic carbon, *Nature* 354 (1991) 56-58.
- [54] R. H. Baughman, A. A. Zakhidov, W. A. de Heer, Carbon nanotubes - the route toward applications, *Science* 297 (2002) 787-792.
- [55] V. N. Popov, Carbon nanotubes: properties and application, *Mat Sci Eng R* 43 (2004) 61-102.
- [56] M. Meyyappan, L. Delzeit, A. Cassell, D. Hash, Carbon nanotube growth by PECVD: a review, *Plasma Sources Sci T* 12 (2003) 205-216.
- [57] C. M. Niu, E. K. Sichel, R. Hoch, D. Moy, H. Tennent, High power electrochemical capacitors based on carbon nanotube electrodes, *Appl Phys Lett* 70 (1997) 1480-1482.
- [58] R. Z. Ma, J. Liang, B. Q. Wei, B. Zhang, C. L. Xu, D. H. Wu, Study of electrochemical capacitors utilizing carbon nanotube electrodes, *J Power Sources* 84 (1999) 126-129.
- [59] J. N. Barisci, G. G. Wallace, D. Chattopadhyay, F. Papadimitrakopoulos, R. H. Baughman, Electrochemical properties of single-wall carbon nanotube electrodes, *J Electrochem Soc* 150 (2003) E409-E415.
- [60] S. Shiraishi, H. Kurihara, K. Okabe, D. Hulicova, A. Oya, Electric double layer capacitance of highly pure single-walled carbon nanotubes (HiPco (TM) Buckytubes (TM)) in propylene carbonate electrolytes, *Electrochem Commun* 4 (2002) 593-598.
- [61] C. Y. Liu, A. J. Bard, F. Wudl, I. Weitz, J. R. Heath, Electrochemical characterization of films of single-walled carbon nanotubes and their possible application in supercapacitors, *Electrochem Solid St* 2 (1999) 577-578.
- [62] X. H. Hu, C. T. Chan, Photonic crystals with silver nanowires as a near-infrared superlens, *Appl Phys Lett* 85 (2004) 1520-1522.
- [63] S. Coskun, E. S. Ates, H. E. Unalan, Optimization of silver nanowire networks for polymer light emitting diode electrodes, *Nanotechnology* 24 (2013)
- [64] B. Aksoy, S. Coskun, S. Kucukyildiz, H. E. Unalan, Transparent, highly flexible, all nanowire network germanium photodetectors, *Nanotechnology* 23 (2012)

- [65] R. J. Chimentao, I. Kirm, F. Medina, X. Rodriguez, Y. Cesteros, P. Salagre, J. E. Sueiras, Different morphologies of silver nanoparticles as catalysts for the selective oxidation of styrene in the gas phase, *Chem Commun* (2004) 846-847.
- [66] J. T. Zhang, X. L. Li, X. M. Sun, Y. D. Li, Surface enhanced Raman scattering effects of silver colloids with different shapes, *J Phys Chem B* 109 (2005) 12544-12548.
- [67] P. Alivisatos, The use of nanocrystals in biological detection, *Nat Biotechnol* 22 (2004) 47-52.
- [68] D. S. Leem, A. Edwards, M. Faist, J. Nelson, D. D. C. Bradley, J. C. de Mello, Efficient organic solar cells with solution-processed silver nanowire electrodes, *Adv Mater* 23 (2011) 4371-+.
- [69] Z. A. Yu, C. Li, D. Abbitt, J. Thomas, Flexible, sandwich-like Ag-nanowire/PEDOT:PSS-nanopillar/MnO₂ high performance supercapacitors, *J Mater Chem A* 2 (2014) 10923-10929.
- [70] S. X. Wu, K. S. Hui, K. N. Hui, One-dimensional core-shell architecture composed of silver nanowire@hierarchical nickel-aluminum layered double hydroxide nanosheet as advanced electrode materials for pseudocapacitor, *J Phys Chem C* 119 (2015) 23358-23365.
- [71] J. Chen, H. Bi, S. R. Sun, Y. F. Tang, W. Zhao, T. Q. Lin, D. Y. Wan, F. Q. Huang, X. D. Zhou, X. M. Xie, M. H. Jiang, Highly conductive and flexible paper of 1d silver-nanowire-doped graphene, *ACS Appl Mater Inter* 5 (2013) 1408-1413.
- [72] J. Zhi, W. Zhao, X. Y. Liu, A. R. Chen, Z. Q. Liu, F. Q. Huang, Highly conductive ordered mesoporous carbon based electrodes decorated by 3D graphene and 1D silver nanowire for flexible supercapacitor, *Adv Funct Mater* 24 (2014) 2013-2019.
- [73] R. Yuksel, S. Coskun, H. E. Unalan, Coaxial silver nanowire network core molybdenum oxide shell supercapacitor electrodes, *Electrochim Acta* 193 (2016) 39-44.
- [74] R. Yuksel, S. Coskun, Y. E. Kalay, H. E. Unalan, Flexible, silver nanowire network nickel hydroxide core-shell electrodes for supercapacitors, *J Power Sources* 328 (2016) 167-173.

- [75] S. H. Kim, B. S. Choi, K. Kang, Y. S. Choi, S. I. Yang, Low temperature synthesis and growth mechanism of Ag nanowires, *J Alloy Compd* 433 (2007) 261-264.
- [76] S. Berchmans, R. G. Nirmal, G. Prabakaran, S. Madhu, V. Yegnaraman, Templated synthesis of silver nanowires based on the layer-by-layer assembly of silver with dithiodipropionic acid molecules as spacers, *J Colloid Interf Sci* 303 (2006) 604-610.
- [77] M. Mazur, Electrochemically prepared silver nanoflakes and nanowires, *Electrochem Commun* 6 (2004) 400-403.
- [78] E. Braun, Y. Eichen, U. Sivan, G. Ben-Yoseph, DNA-templated assembly and electrode attachment of a conducting silver wire, *Nature* 391 (1998) 775-778.
- [79] J. Xu, J. Hu, C. J. Peng, H. L. Liu, Y. Hu, A simple approach to the synthesis of silver nanowires by hydrothermal process in the presence of gemini surfactant, *J Colloid Interf Sci* 298 (2006) 689-693.
- [80] Y. Zhou, S. H. Yu, C. Y. Wang, X. G. Li, Y. R. Zhu, Z. Y. Chen, A novel ultraviolet irradiation photoreduction technique for the preparation of single-crystal Ag nanorods and Ag dendrites, *Adv Mater* 11 (1999) 850-+.
- [81] S. Coskun, B. Aksoy, H. E. Unalan, Polyol synthesis of silver nanowires: an extensive parametric study, *Cryst Growth Des* 11 (2011) 4963-4969.
- [82] S. E. Skrabalak, B. J. Wiley, M. Kim, E. V. Formo, Y. N. Xia, On the polyol synthesis of silver nanostructures: glycolaldehyde as a reducing agent, *Nano Lett* 8 (2008) 2077-2081.
- [83] W. W. Liu, C. X. Lu, X. L. Wang, R. Y. Tay, B. K. Tay, High-performance microsupercapacitors based on two-dimensional graphene/manganese dioxide/silver nanowire ternary hybrid film, *ACS Nano* 9 (2015) 1528-1542.
- [84] Y. J. Song, J. Chen, J. Y. Wu, T. Zhang, Applications of silver nanowires on transparent conducting film and electrode of electrochemical capacitor, *J Nanomater* (2014)
- [85] C. Liu, F. Li, L. P. Ma, H. M. Cheng, Advanced materials for energy storage, *Adv Mater* 22 (2010) E28.
- [86] X. Zhao, B. M. Sanchez, P. J. Dobson, P. S. Grant, The role of nanomaterials in redox-based supercapacitors for next generation energy storage devices, *Nanoscale* 3 (2011) 839-855.

- [87] M. Cole, P. Hiralal, K. Ying, C. Li, Y. Zhang, K. Teo, A. Ferrari, W. Milne, Dry-transfer of aligned multiwalled carbon nanotubes for flexible transparent thin films, *J Nanomater* (2012)
- [88] D. Wei, S. J. Wakeham, T. W. Ng, M. J. Thwaites, H. Brown, P. Beecher, Transparent, flexible and solid-state supercapacitors based on room temperature ionic liquid gel, *Electrochem Commun* 11 (2009) 2285-2287.
- [89] J. Ge, G. H. Cheng, L. W. Chen, Transparent and flexible electrodes and supercapacitors using polyaniline/single-walled carbon nanotube composite thin films, *Nanoscale* 3 (2011) 3084-3088.
- [90] P. C. Chen, G. Shen, S. Sukcharoenchoke, C. Zhou, Flexible and transparent supercapacitor based on In₂O₃ nanowire/carbon nanotube heterogeneous films, *Appl Phys Lett* 94 (2009)
- [91] P. Hiralal, H. L. Wang, H. E. Unalan, Y. L. Liu, M. Rouvala, D. Wei, P. Andrew, G. A. J. Amaratunga, Enhanced supercapacitors from hierarchical carbon nanotube and nanohorn architectures, *J Mater Chem* 21 (2011) 17810-17815.
- [92] E. S. Ates, S. Kucukyildiz, H. E. Unalan, Zinc oxide nanowire photodetectors with single-walled carbon nanotube thin-film electrodes, *ACS Appl Mater Inter* 4 (2012) 5142-5146.
- [93] A. D. Pasquier, H. E. Unalan, A. Kanwal, S. Miller, M. Chhowalla, Conducting and transparent single-wall carbon nanotube electrodes for polymer-fullerene solar cells, *Appl Phys Lett* 87 (2005)
- [94] J. Li, L. Hu, L. Wang, Y. Zhou, G. Gruner, T. J. Marks, Organic light-emitting diodes having carbon nanotube anodes, *Nano Lett* 6 (2006) 2472-2477.
- [95] G. A. Snook, P. Kao, A. S. Best, Conducting-polymer-based supercapacitor devices and electrodes, *J Power Sources* 196 (2011) 1-12.
- [96] E. Frackowiak, V. Khomenko, K. Jurewicz, K. Lota, F. Beguin, Supercapacitors based on conducting polymers/nanotubes composites, *J Power Sources* 153 (2006) 413-418.
- [97] I. Nam, S. Park, G. P. Kim, J. Park, J. Yi, Transparent and ultra-bendable all-solid-state supercapacitors without percolation problems, *Chem Sci* 4 (2013) 1663-1667.

- [98] H. E. Unalan, G. Fanchini, A. Kanwal, A. Du Pasquier, M. Chhowalla, Design criteria for transparent single-wall carbon nanotube thin-film transistors, *Nano Lett* 6 (2006) 677-682.
- [99] G. Gruner, Carbon nanotube films for transparent and plastic electronics, *J Mater Chem* 16 (2006) 3533-3539.
- [100] P. Hiralal, H. E. Unalan, G. A. J. Amaratunga, Nanowires for energy generation, *Nanotechnology* 23 (2012)
- [101] B. B. Parekh, G. Fanchini, G. Eda, M. Chhowalla, Improved conductivity of transparent single-wall carbon nanotube thin films via stable postdeposition functionalization, *Appl Phys Lett* 90 (2007)
- [102] J. Kang, J. Wen, S. H. Jayaram, A. Yu, X. Wang, Development of an equivalent circuit model for electrochemical double layer capacitors (EDLCs) with distinct electrolytes, *Electrochim Acta* 115 (2014) 587-598.
- [103] A. Cirpan, A. A. Argun, C. R. G. Grenier, B. D. Reeves, J. R. Reynolds, Electrochromic devices based on soluble and processable dioxythiophene polymers, *J Mater Chem* 13 (2003) 2422-2428.
- [104] Y. N. Xia, G. M. Whitesides, Soft lithography, *Angew Chem Int Edit* 37 (1998) 551-575.
- [105] N. Koo, M. Bender, U. Plachetka, A. Fuchs, T. Wahlbrink, J. Bolten, H. Kurz, Improved mold fabrication for the definition of high quality nanopatterns by soft UV-nanoimprint lithography using diluted PDMS material, *Microelectron Eng* 84 (2007) 904-908.
- [106] J. Friend, L. Yeo, Fabrication of microfluidic devices using polydimethylsiloxane, *Biomicrofluidics* 4 (2010)
- [107] P. C. Nicolson, J. Vogt, Soft contact lens polymers: an evolution, *Biomaterials* 22 (2001) 3273-3283.
- [108] C. J. Pino, F. R. Haselton, M. S. Chang, Seeding of corneal wounds by epithelial cell transfer from micropatterned PDMS contact lenses, *Cell Transplant* 14 (2005) 565-571.
- [109] J. C. Lotters, W. Olthuis, P. H. Veltink, P. Bergveld, The mechanical properties of the rubber elastic polymer polydimethylsiloxane for sensor applications, *J Micromech Microeng* 7 (1997) 145-147.

- [110] A. Mata, A. J. Fleischman, S. Roy, Characterization of polydimethylsiloxane (PDMS) properties for biomedical micro/nanosystems, *Biomed Microdevices* 7 (2005) 281-293.
- [111] B. Dan, G. C. Irvin, M. Pasquali, Continuous and scalable fabrication of transparent conducting carbon nanotube films, *ACS Nano* 3 (2009) 835-843.
- [112] P. Hiralal, 1-Dimensional nanomaterials for energy generation and storage, in Department of Engineering. 2011, Cambridge University: United Kingdom.
- [113] C. C. Hu, K. H. Chang, M. C. Lin, Y. T. Wu, Design and tailoring of the nanotubular arrayed architecture of hydrous RuO₂ for next generation supercapacitors, *Nano Lett* 6 (2006) 2690-2695.
- [114] H. J. Lin, L. Li, J. Ren, Z. B. Cai, L. B. Qiu, Z. B. Yang, H. S. Peng, Conducting polymer composite film incorporated with aligned carbon nanotubes for transparent, flexible and efficient supercapacitor, *Sci Rep-Uk* 3 (2013)
- [115] S. Hu, R. Rajamani, X. Yu, Flexible solid-state paper based carbon nanotube supercapacitor, *Appl Phys Lett* 100 (2012)
- [116] M. F. L. De Volder, S. H. Tawfick, R. H. Baughman, A. J. Hart, Carbon nanotubes: present and future commercial applications, *Science* 339 (2013) 535-539.
- [117] H. Farsi, F. Gobal, Z. Barzgari, A study of hydrated nanostructured tungsten trioxide as an electroactive material for pseudocapacitors, *Ionics* 19 (2013) 287-294.
- [118] O. Y. Khyzhun, Y. M. Solonin, Electronic structure of the monoclinic and hexagonal trioxides of tungsten and hexagonal hydrogen tungsten bronze H_{0.24}WO₃, *Powder Metall Met C+* 39 (2000) 287-294.
- [119] G. A. Niklasson, C. G. Granqvist, Electrochromics for smart windows: thin films of tungsten oxide and nickel oxide, and devices based on these, *J Mater Chem* 17 (2007) 127-156.
- [120] J. L. Solis, S. Saukko, L. Kish, C. G. Granqvist, V. Lantto, Semiconductor gas sensors based on nanostructured tungsten oxide, *Thin Solid Films* 391 (2001) 255-260.
- [121] K. Sayama, K. Mukasa, R. Abe, Y. Abe, H. Arakawa, Stoichiometric water splitting into H₂ and O₂ using a mixture of two different photocatalysts and an IO³⁻/I⁻ shuttle redox mediator under visible light irradiation, *Chem Commun* (2001) 2416-2417.

- [122] C. C. Huang, W. Xing, S. P. Zhuo, Capacitive performances of amorphous tungsten oxide prepared by microwave irradiation, *Scripta Mater* 61 (2009) 985-987.
- [123] A. C. Nwanya, C. J. Jafta, P. M. Ejikeme, P. E. Ugwuoke, M. V. Reddy, R. U. Osuji, K. I. Ozoemena, F. I. Ezema, Electrochromic and electrochemical capacitive properties of tungsten oxide and its polyaniline nanocomposite films obtained by chemical bath deposition method, *Electrochim Acta* 128 (2014) 218-225.
- [124] V. Gupta, N. Miura, High performance electrochemical supercapacitor from electrochemically synthesized nanostructured polyaniline, *Mater Lett* 60 (2006) 1466-1469.
- [125] J. Xu, T. T. Ding, J. Wang, J. Zhang, S. Wang, C. Q. Chen, Y. Y. Fang, Z. H. Wu, K. F. Huo, J. N. Dai, Tungsten oxide nanofibers self-assembled mesoscopic microspheres as high-performance electrodes for supercapacitor, *Electrochim Acta* 174 (2015) 728-734.
- [126] G. X. Xin, Y. H. Wang, X. X. Liu, J. H. Zhang, Y. F. Wang, J. J. Huang, J. B. Zang, Preparation of self-supporting graphene on flexible graphite sheet and electrodeposition of polyaniline for supercapacitor, *Electrochim Acta* 167 (2015) 254-261.
- [127] B. X. Zou, S. C. Gong, Y. Wang, X. X. Liu, Tungsten oxide and polyaniline composite fabricated by surfactant-templated electrodeposition and its use in supercapacitors, *J Nanomater* (2014)
- [128] Y. Y. Tian, S. Cong, W. M. Su, H. Y. Chen, Q. W. Li, F. X. Geng, Z. G. Zhao, Synergy of $W_{18}O_{49}$ and polyaniline for smart supercapacitor electrode integrated with energy level indicating functionality, *Nano Lett* 14 (2014) 2150-2156.
- [129] G. F. Cai, J. P. Tu, D. Zhou, J. H. Zhang, X. L. Wang, C. D. Gu, Dual electrochromic film based on WO_3 /polyaniline core/shell nanowire array, *Sol Energ Mat Sol C* 122 (2014) 51-58.
- [130] H. D. Zheng, J. Z. Ou, M. S. Strano, R. B. Kaner, A. Mitchell, K. Kalantar-Zadeh, Nanostructured tungsten oxide - properties, synthesis, and applications, *Adv Funct Mater* 21 (2011) 2175-2196.

- [131] B. X. Zou, Y. Liang, X. X. Liu, D. Diamond, K. T. Lau, Electrodeposition and pseudocapacitive properties of tungsten oxide/polyaniline composite, *J Power Sources* 196 (2011) 4842-4848.
- [132] G. Ciric-Marjanovic, Recent advances in polyaniline research: Polymerization mechanisms, structural aspects, properties and applications, *Synthetic Met* 177 (2013) 1-47.
- [133] R. Yuksel, Z. Sarioba, A. Cirpan, P. Hiralal, H. E. Unalan, Transparent and flexible supercapacitors with single walled carbon nanotube thin film electrodes, *ACS Appl Mater Inter* 6 (2014) 15434-15439.
- [134] B. O. Park, C. D. Lokhande, H. S. Park, K. D. Jung, O. S. Joo, Performance of supercapacitor with electrodeposited ruthenium oxide film electrodes - Effect of film thickness, *J Power Sources* 134 (2004) 148-152.
- [135] O. Y. Khyzhun, XPS, XES and XAS studies of the electronic structure of tungsten oxides, *J Alloy Compd* 305 (2000) 1-6.
- [136] J. C. Dupin, D. Gonbeau, P. Vinatier, A. Levasseur, Systematic XPS studies of metal oxides, hydroxides and peroxides, *Phys Chem Chem Phys* 2 (2000) 1319-1324.
- [137] B. X. Zou, X. X. Liu, D. Diamond, K. T. Lau, Electrochemical synthesis of WO₃/PANI composite for electrocatalytic reduction of iodate, *Electrochim Acta* 55 (2010) 3915-3920.
- [138] H. G. Wei, X. R. Yan, S. J. Wu, Z. P. Luo, S. Y. Wei, Z. H. Guo, Electropolymerized polyaniline stabilized tungsten oxide nanocomposite films: electrochromic behavior and electrochemical energy storage, *J Phys Chem C* 116 (2012) 25052-25064.
- [139] K. H. An, W. S. Kim, Y. S. Park, J. M. Moon, D. J. Bae, S. C. Lim, Y. S. Lee, Y. H. Lee, Electrochemical properties of high-power supercapacitors using single-walled carbon nanotube electrodes, *Adv Funct Mater* 11 (2001) 387-392.
- [140] K. Gniotek, I. Krucinska, The basic problems of textronics, *Fibres Text East Eur* 12 (2004) 13-16.
- [141] P. Lukowicz, T. Kirstein, G. Troster, Wearable systems for health care applications, *Method Inform Med* 43 (2004) 232-238.
- [142] S. Park, S. Jayaraman, Smart textiles: Wearable electronic systems, *MRS Bull* 28 (2003) 585-591.

- [143] L. B. Hu, M. Pasta, F. La Mantia, L. F. Cui, S. Jeong, H. D. Deshazer, J. W. Choi, S. M. Han, Y. Cui, Stretchable, porous, and conductive energy textiles, *Nano Lett* 10 (2010) 708-714.
- [144] Y. Feng, N. N. Feng, G. X. Du, Wearable carbon nanotube fibers for energy storage, *Int J Electrochem Sc* 7 (2012) 12432-12439.
- [145] A. P. S. Sawhney, B. Condon, K. V. Singh, S. S. Pang, G. Li, D. Hui, Modern applications of nanotechnology in textiles, *Text Res J* 78 (2008) 731-739.
- [146] M. Mao, J. Y. Hu, H. T. Liu, Graphene-based materials for flexible electrochemical energy storage, *Int J Energ Res* 39 (2015) 727-740.
- [147] R. V. Gregory, W. C. Kimbrell, H. H. Kuhn, Conductive textiles, *Synthetic Met* 28 (1989) C823-C835.
- [148] H. H. Kuhn, W. C. Kimbrell, J. E. Fowler, C. N. Barry, Properties and applications of conductive textiles, *Synthetic Met* 57 (1993) 3707-3712.
- [149] K. Jost, C. R. Perez, J. K. McDonough, V. Presser, M. Heon, G. Dion, Y. Gogotsi, Carbon coated textiles for flexible energy storage, *Energ Environ Sci* 4 (2011) 5060-5067.
- [150] M. Pasta, F. La Mantia, L. B. Hu, H. D. Deshazer, Y. Cui, Aqueous supercapacitors on conductive cotton, *Nano Res* 3 (2010) 452-458.
- [151] Y. Y. Liu, X. W. Wang, K. H. Qi, J. H. Xin, Functionalization of cotton with carbon nanotubes, *J Mater Chem* 18 (2008) 3454-3460.
- [152] L. B. Hu, Y. Cui, Energy and environmental nanotechnology in conductive paper and textiles, *Energ Environ Sci* 5 (2012) 6423-6435.
- [153] M. I. H. Panhuis, H. Wu, S. A. Ashraf, G. G. Wallace, Conducting textiles from single-walled carbon nanotubes, *Synthetic Met* 157 (2007) 358-362.
- [154] N. B. Huang, D. W. Kirk, S. J. Thorpe, C. H. Liang, L. S. Xu, W. Li, S. C. Zhang, M. Sun, Effect of carbon nanotube loadings on supercapacitor characteristics, *Int J Energ Res* 39 (2015) 336-343.
- [155] J. Yan, Z. J. Fan, T. Wei, J. Cheng, B. Shao, K. Wang, L. P. Song, M. L. Zhang, Carbon nanotube/MnO₂ composites synthesized by microwave-assisted method for supercapacitors with high power and energy densities, *Journal of Power Sources* 194 (2009) 1202-1207.
- [156] H. J. Zheng, F. Q. Tang, Y. Jia, L. Z. Wang, Y. C. Chen, M. Lim, L. Zhang, G. Q. Lu, Layer-by-layer assembly and electrochemical properties of sandwiched

- film of manganese oxide nanosheet and carbon nanotube, *Carbon* 47 (2009) 1534-1542.
- [157] W. F. Wei, X. W. Cui, W. X. Chen, D. G. Ivey, Manganese oxide-based materials as electrochemical supercapacitor electrodes, *Chem Soc Rev* 40 (2011) 1697-1721.
- [158] S. Devaraj, N. Munichandraiah, Effect of crystallographic structure of MnO₂ on its electrochemical capacitance properties, *J Phys Chem C* 112 (2008) 4406-4417.
- [159] H. Zhang, G. P. Cao, Z. Y. Wang, Y. S. Yang, Z. J. Shi, Z. N. Gu, Growth of manganese oxide nanoflowers on vertically-aligned carbon nanotube arrays for high-rate electrochemical capacitive energy storage, *Nano Lett* 8 (2008) 2664-2668.
- [160] J. H. Kim, K. H. Lee, L. J. Overzet, G. S. Lee, Synthesis and electrochemical properties of spin-capable carbon nanotube sheet/MnO_x composites for high-performance energy storage devices, *Nano Lett* 11 (2011) 2611-2617.
- [161] L. B. Hu, W. Chen, X. Xie, N. A. Liu, Y. Yang, H. Wu, Y. Yao, M. Pasta, H. N. Alshareef, Y. Cui, Symmetrical MnO₂-carbon nanotube-textile nanostructures for wearable pseudocapacitors with high mass loading, *ACS Nano* 5 (2011) 8904-8913.
- [162] Y. Hou, Y. W. Cheng, T. Hobson, J. Liu, Design and synthesis of hierarchical mno₂ nanospheres/carbon nanotubes/conducting polymer ternary composite for high performance electrochemical electrodes, *Nano Lett* 10 (2010) 2727-2733.
- [163] P. Lv, Y. Y. Feng, Y. Li, W. Feng, Carbon fabric-aligned carbon nanotube/MnO₂/conducting polymers ternary composite electrodes with high utilization and mass loading of MnO₂ for super-capacitors, *J Power Sources* 220 (2012) 160-168.
- [164] S. W. Lee, J. Kim, S. Chen, P. T. Hammond, Y. Shao-Horn, Carbon nanotube/manganese oxide ultrathin film electrodes for electrochemical capacitors, *ACS Nano* 4 (2010) 3889-3896.
- [165] D. Knittel, E. Schollmeyer, Electrically high-conductive textiles, *Synthetic Met* 159 (2009) 1433-1437.

- [166] P. Xue, X. M. Tao, Morphological and electromechanical studies of fibers coated with electrically conductive polymer, *J Appl Polym Sci* 98 (2005) 1844-1854.
- [167] F. Carpi, D. De Rossi, Electroactive polymer-based devices for e-textiles in biomedicine, *IEEE T Inf Technol B* 9 (2005) 295-318.
- [168] R. K. Sharma, L. Zhai, Multiwall carbon nanotube supported poly(3,4-ethylenedioxythiophene)/manganese oxide nano-composite electrode for super-capacitors, *Electrochim Acta* 54 (2009) 7148-7155.
- [169] Q. A. Li, J. H. Liu, J. H. Zou, A. Chunder, Y. Q. Chen, L. Zhai, Synthesis and electrochemical performance of multi-walled carbon nanotube/polyaniline/MnO₂ ternary coaxial nanostructures for supercapacitors, *J Power Sources* 196 (2011) 565-572.
- [170] C. H. Ng, H. N. Lim, Y. S. Lim, W. K. Chee, N. M. Huang, Fabrication of flexible polypyrrole/graphene oxide/manganese oxide supercapacitor, *Int J Energ Res* 39 (2015) 344-355.
- [171] W. K. Chee, H. N. Lim, N. M. Huang, Electrochemical properties of free-standing polypyrrole/graphene oxide/zinc oxide flexible supercapacitor, *Int J Energ Res* 39 (2015) 111-119.
- [172] R. Liu, S. B. Lee, MnO₂/Poly(3,4-ethylenedioxythiophene) coaxial nanowires by one-step coelectrodeposition for electrochemical energy storage, *J Am Chem Soc* 130 (2008) 2942-2943.
- [173] F. J. Liu, Electrodeposition of manganese dioxide in three-dimensional poly(3,4-ethylenedioxythiophene)-poly(styrene sulfonic acid)-polyaniline for supercapacitor, *Journal of Power Sources* 182 (2008) 383-388.
- [174] Q. Lu, Y. K. Zhou, Synthesis of mesoporous polythiophene/MnO₂ nanocomposite and its enhanced pseudocapacitive properties, *Journal of Power Sources* 196 (2011) 4088-4094.
- [175] J. N. Coleman, U. Khan, Y. K. Gun'ko, Mechanical reinforcement of polymers using carbon nanotubes, *Adv Mater* 18 (2006) 689-706.
- [176] R. Sainz, W. R. Small, N. A. Young, C. Valles, A. M. Benito, W. K. Maser, M. I. H. Panhuis, Synthesis and properties of optically active polyaniline carbon nanotube composites, *Macromolecules* 39 (2006) 7324-7332.
- [177] K. W. Nam, C. W. Lee, X. Q. Yang, B. W. Cho, W. S. Yoon, K. B. Kim, Electrodeposited manganese oxides on three-dimensional carbon nanotube

- substrate: Supercapacitive behaviour in aqueous and organic electrolytes, *J Power Sources* 188 (2009) 323-331.
- [178] R. Mazeikiene, A. Malinauskas, Kinetic study of the electrochemical degradation of polyaniline, *Synthetic Met* 123 (2001) 349-354.
- [179] W. W. Liu, X. B. Yan, J. W. Lang, C. Peng, Q. J. Xue, Flexible and conductive nanocomposite electrode based on graphene sheets and cotton cloth for supercapacitor, *J Mater Chem* 22 (2012) 17245-17253.
- [180] X. Li, X. B. Zang, Z. Li, X. M. Li, P. X. Li, P. Z. Sun, X. Lee, R. J. Zhang, Z. H. Huang, K. L. Wang, D. H. Wu, F. Y. Kang, H. W. Zhu, Large-area flexible core-shell graphene/porous carbon woven fabric films for fiber supercapacitor electrodes, *Adv Funct Mater* 23 (2013) 4862-4869.
- [181] H. H. Cheng, Z. L. Dong, C. G. Hu, Y. Zhao, Y. Hu, L. T. Qu, N. Chena, L. M. Dai, Textile electrodes woven by carbon nanotube-graphene hybrid fibers for flexible electrochemical capacitors, *Nanoscale* 5 (2013) 3428-3434.
- [182] X. H. Lu, T. Zhai, X. H. Zhang, Y. Q. Shen, L. Y. Yuan, B. Hu, L. Gong, J. Chen, Y. H. Gao, J. Zhou, Y. X. Tong, Z. L. Wang, $\text{WO}_{3-x}@\text{Au}@\text{MnO}_2$ core-shell nanowires on carbon fabric for high-performance flexible supercapacitors, *Adv Mater* 24 (2012) 938-+.
- [183] P. H. Yang, X. Xiao, Y. Z. Li, Y. Ding, P. F. Qiang, X. H. Tan, W. J. Mai, Z. Y. Lin, W. Z. Wu, T. Q. Li, H. Y. Jin, P. Y. Liu, J. Zhou, C. P. Wong, Z. L. Wang, Hydrogenated ZnO core-shell nanocables for flexible supercapacitors and self-powered systems, *ACS Nano* 7 (2013) 2617-2626.
- [184] D. Wei, M. R. J. Scherer, C. Bower, P. Andrew, T. Ryhanen, U. Steiner, A nanostructured electrochromic supercapacitor, *Nano Lett* 12 (2012) 1857-1862.
- [185] A. C. Dillon, A. H. Mahan, R. Deshpande, R. Parilla, K. M. Jones, S. H. Lee, Metal oxide nano-particles for improved electrochromic and lithium-ion battery technologies, *Thin Solid Films* 516 (2008) 794-797.
- [186] Z. Xie, X. J. Jin, G. Chen, J. Xu, D. Chen, G. Z. Shen, Integrated smart electrochromic windows for energy saving and storage applications, *Chemical Communications* 50 (2014) 608-610.
- [187] P. H. Yang, P. Sun, Z. S. Chai, L. H. Huang, X. Cai, S. Z. Tan, J. H. Song, W. J. Mai, Large-scale fabrication of pseudocapacitive glass windows that

- combine electrochromism and energy storage, *Angew Chem Int Edit* 53 (2014) 11935-11939.
- [188] X. L. Chen, H. J. Lin, J. Deng, Y. Zhang, X. M. Sun, P. N. Chen, X. Fang, Z. T. Zhang, G. Z. Guan, H. S. Peng, Electrochromic fiber-shaped supercapacitors, *Adv Mater* 26 (2014) 8126-8132.
- [189] H. G. Wei, J. H. Zhu, S. J. Wu, S. Y. Wei, Z. H. Guo, Electrochromic polyaniline/graphite oxide nanocomposites with endured electrochemical energy storage, *Polymer* 54 (2013) 1820-1831.
- [190] K. Wang, H. P. Wu, Y. N. Meng, Y. J. Zhang, Z. X. Wei, Integrated energy storage and electrochromic function in one flexible device: an energy storage smart window, *Energ Environ Sci* 5 (2012) 8384-8389.
- [191] K. H. Heckner, A. Kraft, Similarities between electrochromic windows and thin film batteries, *Solid State Ionics* 152 (2002) 899-905.
- [192] L. C. Chen, Y. H. Huang, K. S. Tseng, K. C. Ho, Novel electrochromic batteries: I. A PB-WO₃ cell with a theoretical voltage of 1.35V, *J New Mat Electr Sys* 5 (2002) 203-212.
- [193] L. C. Chen, K. S. Tseng, Y. H. Huang, K. C. Ho, Novel electrochromic batteries: II. An InHCF-WO₃ cell with a high visual contrast, *J New Mat Electr Sys* 5 (2002) 213-221.
- [194] T. S. Tung, L. C. Chen, K. C. Ho, An indium hexacyanoferrate-tungsten oxide electrochromic battery with a hybrid K⁺/H⁺-conducting polymer electrolyte, *Solid State Ionics* 165 (2003) 257-267.
- [195] S. C. Cevher, N. A. Unlu, A. C. Ozcelcaglayan, D. H. Apaydin, Y. A. Udum, L. Toppare, A. Cirpan, Fused structures in the polymer backbone to investigate the photovoltaic and electrochromic properties of donoracceptor-type conjugated polymers, *J Polym Sci Pol Chem* 51 (2013) 1933-1941.
- [196] J. Casado, V. Hernandez, O. K. Kim, J. M. Lehn, J. T. L. Navarrete, S. D. Ledesma, R. P. Ortiz, M. C. R. Delgado, Y. Vida, E. Perez-Inestrosa, Vibrational and quantum-chemical study of nonlinear optical chromophores containing dithienothiophene as the electron relay, *Chem-Eur J* 10 (2004) 3805-3816.
- [197] K. Dokken, L. E. Erickson, S. Castro, Fourier-transform infrared spectroscopy as a tool to monitor changes in plant structure in response to soil contaminants 1, (2002)

- [198] J. H. Kim, C. E. Song, N. Shin, H. Kang, S. Wood, I. N. Kang, B. J. Kim, B. Kim, J. S. Kim, W. S. Shin, D. H. Hwang, High-crystalline medium-band-gap polymers consisting of benzodithiophene and benzotriazole derivatives for organic photovoltaic cells, *ACS Appl Mater Inter* 5 (2013) 12820-12831.
- [199] Z. A. Hu, Y. X. Wang, Y. L. Xie, Y. Y. Yang, Z. Y. Zhang, H. Y. Wu, Ag nanowires and its application as electrode materials in electrochemical capacitor, *J Appl Electrochem* 40 (2010) 341-344.
- [200] S. Lee, M. S. Cho, J. D. Nam, Y. Lee, Fabrication of polypyrrole nanorod arrays for supercapacitor: effect of length of nanorods on capacitance, *J Nanosci Nanotechno* 8 (2008) 5036-5041.
- [201] N. Soin, S. S. Roy, S. K. Mitra, T. Thundat, J. A. McLaughlin, Nanocrystalline ruthenium oxide dispersed few layered graphene (FLG) nanoflakes as supercapacitor electrodes, *J Mater Chem* 22 (2012) 14944-14950.
- [202] H. Jiang, T. Zhao, J. Ma, C. Yan, C. Li, Ultrafine manganese dioxide nanowire network for high-performance supercapacitors, *Chemical Communications* 47 (2011) 1264-1266.
- [203] B. Wang, J. S. Chen, Z. Y. Wang, S. Madhavi, X. W. Lou, Green synthesis of nio nanobelts with exceptional pseudo-capacitive properties, *Adv Energy Mater* 2 (2012) 1188-1192.
- [204] R. Tummala, R. K. Guduru, P. S. Mohanty, Nanostructured Co_3O_4 electrodes for supercapacitor applications from plasma spray technique, *J Power Sources* 209 (2012) 44-51.
- [205] X. L. Hu, W. Zhang, X. X. Liu, Y. N. Mei, Y. Huang, Nanostructured Mo-based electrode materials for electrochemical energy storage, *Chem Soc Rev* 44 (2015) 2376-2404.
- [206] M. J. Zhi, C. C. Xiang, J. T. Li, M. Li, N. Q. Wu, Nanostructured carbon-metal oxide composite electrodes for supercapacitors: a review, *Nanoscale* 5 (2013) 72-88.
- [207] K. M. Hercule, Q. L. Wei, A. M. Khan, Y. L. Zhao, X. C. Tian, L. Q. Mai, Synergistic Effect of Hierarchical Nanostructured $\text{MoO}_2/\text{Co}(\text{OH})_2$ with largely enhanced pseudocapacitor cyclability, *Nano Lett* 13 (2013) 5685-5691.
- [208] J. Rajeswari, P. S. Kishore, B. Viswanathan, T. K. Varadarajan, One-dimensional MoO_2 nanorods for supercapacitor applications, *Electrochem Commun* 11 (2009) 572-575.

- [209] Y. Z. Lei, J. C. Hu, H. W. Liu, J. L. Li, Template-free synthesis of hollow core-shell MoO₂ microspheres with high lithium-ion storage capacity, *Mater Lett* 68 (2012) 82-85.
- [210] Y. Zhou, C. W. Lee, S. K. Kim, S. Yoon, Ordered mesoporous carbon/MoO₂ nanocomposites as stable supercapacitor electrodes, *ECS Electrochem Lett* 1 (2012) A17-A20.
- [211] C. Liu, Z. C. Li, Z. J. Zhang, Molybdenum oxide film with stable pseudocapacitive property for aqueous micro-scale electrochemical capacitor, *Electrochim Acta* 134 (2014) 84-91.
- [212] Y. G. Liang, Z. H. Yi, X. F. Lei, X. L. Ma, S. J. Yang, J. T. Sun, L. J. Yuan, Y. H. Zhou, A novel route to prepare nano-sized MoO₂ powders in various dimensions, *J Alloy Compd* 421 (2006) 133-135.
- [213] Q. S. Gao, L. C. Yang, X. C. Lu, J. J. Mao, Y. H. Zhang, Y. P. Wu, Y. Tang, Synthesis, characterization and lithium-storage performance of MoO₂/carbon hybrid nanowires, *J Mater Chem* 20 (2010) 2807-2812.
- [214] B. K. Guo, X. P. Fang, B. Li, Y. F. Shi, C. Y. Ouyang, Y. S. Hu, Z. X. Wang, G. D. Stucky, L. Q. Chen, Synthesis and lithium storage mechanism of ultrafine MoO₂ nanorods, *Chem Mater* 24 (2012) 457-463.
- [215] Y. F. Shi, B. K. Guo, S. A. Corr, Q. H. Shi, Y. S. Hu, K. R. Heier, L. Q. Chen, R. Seshadri, G. D. Stucky, Ordered mesoporous metallic MoO₂ materials with highly reversible lithium storage capacity, *Nano Lett* 9 (2009) 4215-4220.
- [216] L. C. Yang, Q. S. Gao, Y. H. Zhang, Y. Tang, Y. P. Wu, Tremella-like molybdenum dioxide consisting of nanosheets as an anode material for lithium ion battery, *Electrochem Commun* 10 (2008) 118-122.
- [217] F. L. Gao, L. J. Zhang, S. M. Huang, Fabrication horizontal aligned MoO₂/single-walled carbon nanotube nanowires for electrochemical supercapacitor, *Mater Lett* 64 (2010) 537-540.
- [218] A. Bhaskar, M. Deepa, T. N. Rao, MoO₂/multiwalled carbon nanotubes (MWCNT) hybrid for Use as a Li-ion battery anode, *ACS Appl Mater Inter* 5 (2013) 2555-2566.
- [219] P. X. Han, W. Ma, S. P. Pang, Q. S. Kong, J. H. Yao, C. F. Bi, G. L. Cui, Graphene decorated with molybdenum dioxide nanoparticles for use in high energy lithium ion capacitors with an organic electrolyte, *J Mater Chem A* 1 (2013) 5949-5954.

- [220] Y. D. Zhang, B. P. Lin, Y. Sun, P. Han, J. C. Wang, X. J. Ding, X. Q. Zhang, H. Yang, MoO₂@Cu@C composites prepared by using polyoxometalates@metal-organic frameworks as template for all-solid-state flexible supercapacitor, *Electrochim Acta* 188 (2016) 490-498.
- [221] Z. Liu, Y. J. Zhan, G. Shi, S. Moldovan, M. Gharbi, L. Song, L. L. Ma, W. Gao, J. Q. Huang, R. Vajtai, F. Banhart, P. Sharma, J. Lou, P. M. Ajayan, Anomalous high capacitance in a coaxial single nanowire capacitor, *Nat Commun* 3 (2012)
- [222] L. Kou, T. Q. Huang, B. N. Zheng, Y. Han, X. L. Zhao, K. Gopalsamy, H. Y. Sun, C. Gao, Coaxial wet-spun yarn supercapacitors for high-energy density and safe wearable electronics, *Nat Commun* 5 (2014)
- [223] V. T. Le, H. Kim, A. Ghosh, J. Kim, J. Chang, Q. A. Vu, D. T. Pham, J. H. Lee, S. W. Kim, Y. H. Lee, Coaxial fiber supercapacitor using all-carbon material electrodes, *ACS Nano* 7 (2013) 5940-5947.
- [224] D. Harrison, F. L. Qiu, J. Fyson, Y. M. Xu, P. Evans, D. Southee, A coaxial single fibre supercapacitor for energy storage, *Phys Chem Chem Phys* 15 (2013) 12215-12219.
- [225] Z. A. Yu, J. Thomas, Energy storing electrical cables: integrating energy storage and electrical conduction, *Adv Mater* 26 (2014) 4279-4285.
- [226] L. Kumari, Y. R. Ma, C. C. Tsai, Y. W. Lin, S. Y. Wu, K. W. Cheng, Y. Liou, X-ray diffraction and Raman scattering studies on large-area array and nanobranched structure of 1D MoO₂ nanorods, *Nanotechnology* 18 (2007)
- [227] M. Dieterle, G. Mestl, Raman spectroscopy of molybdenum oxides - Part II. resonance Raman spectroscopic characterization of the molybdenum oxides Mo₄O₁₁ and MoO₂, *Phys Chem Chem Phys* 4 (2002) 822-826.
- [228] X. Y. Zhao, M. H. Cao, B. Liu, Y. Tian, C. W. Hu, Interconnected core-shell MoO₂ microcapsules with nanorod-assembled shells as high-performance lithium-ion battery anodes, *J Mater Chem* 22 (2012) 13334-13340.
- [229] J. W. Zhao, J. Chen, S. M. Xu, M. F. Shao, Q. Zhang, F. Wei, J. Ma, M. Wei, D. G. Evans, X. Duan, Hierarchical NiMn layered double hydroxide/carbon nanotubes architecture with superb energy density for flexible supercapacitors, *Adv Funct Mater* 24 (2014) 2938-2946.

- [230] H. Jiang, T. Zhao, C. Z. Li, J. Ma, Hierarchical self-assembly of ultrathin nickel hydroxide nanoflakes for high-performance supercapacitors, *J Mater Chem* 21 (2011) 3818-3823.
- [231] S. Vijayakumar, S. Nagamuthu, G. Muralidharan, Supercapacitor studies on nio nanoflakes synthesized through a microwave route, *ACS Appl Mater Inter* 5 (2013) 2188-2196.
- [232] S. C. Pang, M. A. Anderson, T. W. Chapman, Novel electrode materials for thin-film ultracapacitors: comparison of electrochemical properties of sol-gel-derived and electrodeposited manganese dioxide, *J Electrochem Soc* 147 (2000) 444-450.
- [233] Z. Y. Lu, Z. Chang, W. Zhu, X. M. Sun, Beta-phased Ni(OH)₂ nanowall film with reversible capacitance higher than theoretical Faradic capacitance, *Chem Commun* 47 (2011) 9651-9653.
- [234] G. W. Yang, C. L. Xu, H. L. Li, Electrodeposited nickel hydroxide on nickel foam with ultrahigh capacitance, *Chem Commun* (2008) 6537-6539.
- [235] S. B. Yang, X. L. Wu, C. L. Chen, H. L. Dong, W. P. Hu, X. K. Wang, Spherical alpha-Ni(OH)₂ nanoarchitecture grown on graphene as advanced electrochemical pseudocapacitor materials, *Chem Commun* 48 (2012) 2773-2775.
- [236] H. Yi, H. W. Wang, Y. T. Jing, T. Q. Peng, Y. R. Wang, J. Guo, Q. L. He, Z. H. Guo, X. F. Wang, Advanced asymmetric supercapacitors based on CNT@Ni(OH)₂ core-shell composites and 3D graphene networks, *J Mater Chem A* 3 (2015) 19545-19555.
- [237] M. Aghazadeh, A. N. Golikand, M. Ghaemi, Synthesis, characterization, and electrochemical properties of ultrafine beta-Ni(OH)₂ nanoparticles, *Int J Hydrogen Energ* 36 (2011) 8674-8679.
- [238] M. B. J. G. Freitas, Nickel hydroxide powder for NiOOH/Ni(OH)₂ electrodes of the alkaline batteries, *Journal of Power Sources* 93 (2001) 163-173.
- [239] X. Chen, X. H. Chen, F. Q. Zhang, Z. Yang, S. M. Huang, One-pot hydrothermal synthesis of reduced graphene oxide/carbon nanotube/alpha-Ni(OH)₂ composites for high performance electrochemical supercapacitor, *J Power Sources* 243 (2013) 555-561.

- [240] W. P. Sun, X. H. Rui, M. Ulaganathan, S. Madhavi, Q. Y. Yan, Few-layered Ni(OH)₂ nanosheets for high-performance supercapacitors, *J Power Sources* 295 (2015) 323-328.
- [241] M. H. Cao, X. Y. He, J. Chen, C. W. Hu, Self-assembled nickel hydroxide three-dimensional nanostructures: A nanomaterial for alkaline rechargeable batteries, *Cryst Growth Des* 7 (2007) 170-174.
- [242] A. Al-Hajry, A. Umar, M. Vaseem, M. S. Al-Assiri, F. El-Tantawy, M. Bououdina, S. Al-Heniti, Y. B. Hahn, Low-temperature growth and properties of flower-shaped beta-Ni(OH)₂ and NiO structures composed of thin nanosheets networks, *Superlattice Microst* 44 (2008) 216-222.
- [243] M. Vidotti, C. van Greco, E. A. Ponzio, S. I. C. de Torresi, Sonochemically synthesized Ni(OH)₂ and Co(OH)₂ nanoparticles and their application in electrochromic electrodes, *Electrochem Commun* 8 (2006) 554-560.
- [244] S. L. Chou, F. Y. Cheng, J. Chen, Electrochemical deposition of Ni(OH)₂ and Fe-doped Ni(OH)₂ tubes, *Eur J Inorg Chem* (2005) 4035-4039.
- [245] H. T. Zhang, X. Zhang, D. C. Zhang, X. Z. Sun, H. Lin, C. H. Wang, Y. W. Ma, One-Step Electrophoretic deposition of reduced graphene oxide and Ni(OH)₂ composite films for controlled syntheses supercapacitor electrodes, *J Phys Chem B* 117 (2013) 1616-1627.
- [246] D. P. Dubal, G. S. Gund, C. D. Lokhande, R. Holze, Decoration of spongelike Ni(OH)₂ nanoparticles onto MWCNTs using an easily manipulated chemical protocol for supercapacitors, *ACS Appl Mater Inter* 5 (2013) 2446-2454.
- [247] R. R. Salunkhe, J. J. Lin, V. Malgras, S. X. Dou, J. H. Kim, Y. Yamauchi, Large-scale synthesis of coaxial carbon nanotube/Ni(OH)₂ composites for asymmetric supercapacitor application, *Nano Energy* 11 (2015) 211-218.
- [248] H. J. Yan, J. W. Bai, B. Wang, L. Yu, L. Zhao, J. Wang, Q. Liu, J. Y. Liu, Z. S. Li, Electrochemical reduction approach-based 3D graphene/Ni(OH)₂ electrode for high-performance supercapacitors, *Electrochim Acta* 154 (2015) 9-16.
- [249] L. Gu, Y. W. Wang, R. Lu, W. Wang, X. S. Peng, J. Sha, Silicon carbide nanowires@Ni(OH)₂ core-shell structures on carbon fabric for supercapacitor electrodes with excellent rate capability, *J Power Sources* 273 (2015) 479-485.
- [250] G. R. Fu, Z. A. Hu, L. J. Xie, X. Q. Jin, Y. L. Xie, Y. X. Wang, Z. Y. Zhang, Y. Y. Yang, H. Y. Wu, Electrodeposition of nickel hydroxide films on nickel

- foil and its electrochemical performances for supercapacitor, *Int J Electrochem Sc* 4 (2009) 1052-1062.
- [251] M. C. Bernard, R. Cortes, M. Keddad, H. Takenouti, P. Bernard, S. Senyari, Structural defects and electrochemical reactivity of beta-Ni(OH)₂, *J Power Sources* 63 (1996) 247-254.
- [252] S. Sarkar, M. Pradhan, A. K. Sinha, M. Basu, Y. Negishi, T. Pal, An aminolytic approach toward hierarchical beta-Ni(OH)₂ nanoporous architectures: a bimodal forum for photocatalytic and surface-enhanced raman scattering activity, *Inorg Chem* 49 (2010) 8813-8827.
- [253] C. Murli, S. M. Sharma, S. K. Kulshreshtha, S. K. Sikka, High-pressure behavior of beta-Ni(OH)₂ - A Raman scattering study, *Physica B* 307 (2001) 111-116.
- [254] J. Yan, W. Sun, T. Wei, Q. Zhang, Z. J. Fan, F. Wei, Fabrication and electrochemical performances of hierarchical porous Ni(OH)₂ nanoflakes anchored on graphene sheets, *J Mater Chem* 22 (2012) 11494-11502.
- [255] J. Yan, Z. J. Fan, W. Sun, G. Q. Ning, T. Wei, Q. Zhang, R. F. Zhang, L. J. Zhi, F. Wei, Advanced asymmetric supercapacitors based on Ni(OH)₂/graphene and porous graphene electrodes with high energy density, *Adv Funct Mater* 22 (2012) 2632-2641.
- [256] V. Srinivasan, J. W. Weidner, Studies on the capacitance of nickel oxide films: Effect of heating temperature and electrolyte concentration, *J Electrochem Soc* 147 (2000) 880-885.
- [257] J. W. Lee, J. M. Ko, J. D. Kim, Hierarchical Microspheres based on alpha-Ni(OH)₂ nanosheets intercalated with different anions: synthesis, anion exchange, and effect of intercalated anions on electrochemical capacitance, *J Phys Chem C* 115 (2011) 19445-19454.
- [258] Y. F. Yuan, X. H. Xia, J. B. Wu, J. L. Yang, Y. B. Chen, S. Y. Guo, Nickel foam-supported porous Ni(OH)₂/NiOOH composite film as advanced pseudocapacitor material, *Electrochim Acta* 56 (2011) 2627-2632.
- [259] S. Chen, J. W. Zhu, H. Zhou, X. Wang, One-step synthesis of low defect density carbon nanotube-doped Ni(OH)₂ nanosheets with improved electrochemical performances, *RSC Adv* 1 (2011) 484-489.
- [260] C. G. Liu, Y. S. Lee, Y. J. Kim, I. C. Song, J. H. Kim, Electrochemical characteristics of hydrothermally deposited nickel hydroxide on multi-walled

- carbon nanotube for supercapacitor electrode, *Synthetic Met* 159 (2009) 2009-2012.
- [261] J. W. Lee, T. Ahn, D. Soundararajan, J. M. Ko, J. D. Kim, Non-aqueous approach to the preparation of reduced graphene oxide/ α -Ni(OH)₂ hybrid composites and their high capacitance behavior, *Chem Commun* 47 (2011) 6305-6307.
- [262] H. L. Wang, H. S. Casalongue, Y. Y. Liang, H. J. Dai, Ni(OH)₂ nanoplates grown on graphene as advanced electrochemical pseudocapacitor materials, *J Am Chem Soc* 132 (2010) 7472-7477.
- [263] J. P. Liu, C. W. Cheng, W. W. Zhou, H. X. Li, H. J. Fan, Ultrathin nickel hydroxidenitrate nanoflakes branched on nanowire arrays for high-rate pseudocapacitive energy storage, *Chem Commun* 47 (2011) 3436-3438.
- [264] J. Zhang, L. B. Kong, J. J. Cai, H. Li, Y. C. Luo, L. Kang, Hierarchically porous nickel hydroxide/mesoporous carbon composite materials for electrochemical capacitors, *Micropor Mesopor Mat* 132 (2010) 154-162.
- [265] X. F. Wang, K. Jiang, G. Z. Shen, Flexible fiber energy storage and integrated devices: recent progress and perspectives, *Materials Today* 18 (2015) 265-272.
- [266] S. W. Pan, Z. T. Zhang, W. Weng, H. J. Lin, Z. B. Yang, H. S. Peng, Miniature wire-shaped solar cells, electrochemical capacitors and lithium-ion batteries, *Materials Today* 17 (2014) 276-284.
- [267] P. Simon, Y. Gogotsi, B. Dunn, Where do batteries end and supercapacitors begin?, *Science* 343 (2014) 1210-1211.
- [268] A. Vlad, N. Singh, C. Galande, P. M. Ajayan, Design considerations for unconventional electrochemical energy storage architectures, *Adv Energy Mater* 5 (2015)
- [269] Y. Gogotsi, P. Simon, True performance metrics in electrochemical energy storage, *Science* 335 (2012) 167-167.
- [270] S. W. Pan, J. Ren, X. Fang, H. S. Peng, Integration: an effective strategy to develop multifunctional energy storage devices, *Adv Energy Mater* 6 (2016)
- [271] P. Yang, P. Sun, W. Mai, Electrochromic energy storage devices, *Materials Today*
- [272] R. Yuksel, S. C. Cevher, A. Cirpan, L. Toppare, H. E. Unalan, All-organic electrochromic supercapacitor electrodes, *J Electrochem Soc* 162 (2015) A2805-A2810.

- [273] J. Zhang, J. P. Tu, X. H. Xia, X. L. Wang, C. D. Gu, Hydrothermally synthesized WO₃ nanowire arrays with highly improved electrochromic performance, *J Mater Chem* 21 (2011) 5492-5498.
- [274] M. Chigane, M. Ishikawa, Manganese oxide thin film preparation by potentiostatic electrolyses and electrochromism, *J Electrochem Soc* 147 (2000) 2246-2251.
- [275] G. F. Cai, X. Wang, M. Q. Cui, P. Darmawan, J. X. Wang, A. L. S. Eh, P. S. Lee, Electrochromo-supercapacitor based on direct growth of NiO nanoparticles, *Nano Energy* 12 (2015) 258-267.
- [276] X. Chen, H. Lin, J. Deng, Y. Zhang, X. Sun, P. Chen, X. Fang, Z. Zhang, G. Guan, H. Peng, Electrochromic fiber-shaped supercapacitors, *Adv Mater* 26 (2014) 8126-32.
- [277] A. M. Osterholm, D. E. Shen, A. L. Dyer, J. R. Reynolds, Optimization of PEDOT films in ionic liquid supercapacitors: demonstration as a power source for polymer electrochromic devices, *ACS Appl Mater Inter* 5 (2013) 13432-13440.
- [278] P. Camurlu, Polypyrrole derivatives for electrochromic applications, *RSC Adv* 4 (2014) 55832-55845.
- [279] G. E. Gunbas, A. Durmus, L. Toppare, A unique processable green polymer with a transmissive oxidized state for realization of potential RGB-based electrochromic device applications, *Adv Funct Mater* 18 (2008) 2026-2030.

APPENDIX A: PERMISSION LICENSES

AMERICAN CHEMICAL SOCIETY LICENSE

Title: Transparent and Flexible Supercapacitors with Single Walled Carbon Nanotube Thin Film Electrodes

Author: Recep Yuksel, Zeynep Sarioba, Ali Cirpan, et al

Publication: Applied Materials & Interfaces

Publisher: American Chemical Society

Date: Sep 1, 2014

Copyright © 2014, American Chemical Society

PERMISSION/LICENSE IS GRANTED FOR YOUR ORDER AT NO CHARGE

This type of permission/license, instead of the standard Terms & Conditions, is sent to you because no fee is being charged for your order. Please note the following:

- Permission is granted for your request in both print and electronic formats, and translations.
- If figures and/or tables were requested, they may be adapted or used in part.
- Please print this page for your records and send a copy of it to your publisher/graduate school.
- Appropriate credit for the requested material should be given as follows: "Reprinted (adapted) with permission from (COMPLETE REFERENCE CITATION). Copyright (YEAR) American Chemical Society." Insert appropriate information in place of the capitalized words.

One-time permission is granted only for the use specified in your request. No additional uses are granted (such as derivative works or other editions). For any other uses, please submit a new request.

THE ELECTROCHEMICAL SOCIETY LICENSE

Request for Permission to Reproduce or Re-Publish ECS Material

Please fax this form to: The Electrochemical Society (ECS), Attn: Permissions Requests, 1.609.730.0629.
You may also e-mail your request to: copyright@electrochem.org. Include all the information as required on this form. Please allow 3-7 days for your request to be processed.

I am preparing a (choose one): paper chapter book thesis

entitled: Nanomaterials for Supercapacitors

to be published by: Recep Yuksel

in an upcoming publication entitled: _____

I request permission to use the following material in the publication noted above, and request nonexclusive rights for all subsequent editions and in all foreign language translations for distribution throughout the world.

Description of material to be used—Indicate what material you wish to use (figures, tables, text, etc.) and give the full bibliographic reference for the source publication. You may attach a separate list, organized by ECS title.

I want to use my article "All-Organic Electrochromic Supercapacitor Electrodes" (Journal of The Electrochemical Society, 162 (14) A2805-A2810 (2015)) in my thesis as full article.

Signature: _____ Date: Nov 16, 2016

Name: Recep Yuksel

Address: Middle East Technical University, Metallurgical & Materials Eng. Dept., Ankara, Turkey

Telephone: +90 555 327 42 20 Fax: _____

E-mail: reyuksel@gmail.com

Permission is granted to include the above-referenced paper in your thesis, provided that you obtain permission of the other individual authors. In the thesis, please acknowledge the authors and the citation given above, and include the words: "Reproduced by permission of ECS — The Electrochemical Society."

NOV 16 2016

Date



Annie Goedkoop, Director of Publications Production

ELSEVIER LICENSE
TERMS AND CONDITIONS

Nov 16, 2016

This Agreement between Recep Yuksel ("You") and Elsevier ("Elsevier") consists of your license details and the terms and conditions provided by Elsevier and Copyright Clearance Center.

License Number: 3990641081322

License date: Nov 16, 2016

Licensed Content Publisher: Elsevier

Licensed Content Publication: Electrochimica Acta

Licensed Content Title: Coaxial silver nanowire network core molybdenum oxide shell supercapacitor electrodes

Licensed Content Author: Recep Yuksel,Sahin Coskun,Husnu Emrah Unalan

Licensed Content Date: 1 March 2016

Licensed Content Volume Number: 193

Licensed Content Issue Number: n/a

Licensed Content Pages: 6

Start Page: 39

End Page: 44

Type of Use: reuse in a thesis/dissertation

Intended publisher of new work: other

Portion: full article

Format: both print and electronic

Are you the author of this Elsevier article?: Yes

Will you be translating?: No

Order reference number:

Title of your thesis/dissertation: Nanomaterials for Supercapacitors

Expected completion date: Jan 2017

Estimated size (number of pages): 200

Elsevier VAT number: GB 494 6272 12

Requestor Location: Recep Yuksel

Middle East Technical University

Ankara, 06800

Turkey

Attn: Recep Yuksel

Total: 0.00 USD

**ELSEVIER LICENSE
TERMS AND CONDITIONS**

Nov 16, 2016

This Agreement between Recep Yuksel ("You") and Elsevier ("Elsevier") consists of your license details and the terms and conditions provided by Elsevier and Copyright Clearance Center.

License Number: 3990650003508

License date: Nov 16, 2016

Licensed Content Publisher: Elsevier

Licensed Content Publication: Journal of Power Sources

Licensed Content Title: Flexible, silver nanowire network nickel hydroxide core-shell electrodes for supercapacitors

Licensed Content Author: Recep Yuksel,Sahin Coskun,Yunus Eren Kalay,Husnu Emrah Unalan

Licensed Content Date: 1 October 2016

Licensed Content Volume Number: 328

Licensed Content Issue Number: n/a

Licensed Content Pages: 7

Start Page: 167

End Page: 173

Type of Use: reuse in a thesis/dissertation

Intended publisher of new work: other

Portion: full article

Format: both print and electronic

Are you the author of this Elsevier article?: Yes

Will you be translating?: No

Order reference number:

Title of your thesis/dissertation: Nanomaterials for Supercapacitors

Expected completion date: Jan 2017

Estimated size (number of pages): 200

Elsevier VAT number: GB 494 6272 12

Requestor Location: Recep Yuksel

Middle East Technical University

Ankara, 06800

Turkey

Attn: Recep Yuksel

Total: 0.00 USD

ELSEVIER LICENSE
TERMS AND CONDITIONS

Nov 16, 2016

This Agreement between Recep Yuksel ("You") and Elsevier ("Elsevier") consists of your license details and the terms and conditions provided by Elsevier and Copyright Clearance Center.

License Number: 3990630706189

License date: Nov 16, 2016

Licensed Content Publisher: Elsevier

Licensed Content Publication: Journal of Alloys and Compounds

Licensed Content Title: Ternary nanocomposite SWNT/WO₃/PANI thin film electrodes for supercapacitors

Licensed Content Author: Recep Yuksel,Caner Durucan,Husnu Emrah Unalan

Licensed Content Date: 15 February 2016

Licensed Content Volume Number: 658

Licensed Content Issue Number: n/a

Licensed Content Pages: 7

Start Page: 183

End Page: 189

Type of Use: reuse in a thesis/dissertation

Intended publisher of new work: other

Portion: full article

Format: both print and electronic

Are you the author of this Elsevier article?: Yes

Will you be translating?: No

Order reference number:

Title of your thesis/dissertation: Nanomaterials for Supercapacitors

Expected completion date: Jan 2017

Estimated size (number of pages): 200

Elsevier VAT number: GB 494 6272 12

Requestor Location: Recep Yuksel

Middle East Technical University

Ankara, 06800

Turkey

Attn: Recep Yuksel

Total: 0.00 USD

Terms and Conditions

INTRODUCTION

1. The publisher for this copyrighted material is Elsevier. By clicking "accept" in connection with completing this licensing transaction, you agree that the following terms and conditions apply to this transaction (along with the Billing and Payment terms and conditions established by Copyright Clearance Center, Inc. ("CCC"), at the time that you opened your Rightslink account and that are available at any time at <http://myaccount.copyright.com>).

GENERAL TERMS

2. Elsevier hereby grants you permission to reproduce the aforementioned material subject to the terms and conditions indicated.

3. Acknowledgement: If any part of the material to be used (for example, figures) has appeared in our publication with credit or acknowledgement to another source, permission must also be sought from that source. If such permission is not obtained then that material may not be included in your publication/copies. Suitable acknowledgement to the source must be made, either as a footnote or in a reference list at the end of your publication, as follows:

"Reprinted from Publication title, Vol /edition number, Author(s), Title of article / title of chapter, Pages No., Copyright (Year), with permission from Elsevier [OR APPLICABLE SOCIETY COPYRIGHT OWNER]." Also Lancet special credit - "Reprinted from The Lancet, Vol. number, Author(s), Title of article, Pages No., Copyright (Year), with permission from Elsevier."

4. Reproduction of this material is confined to the purpose and/or media for which permission is hereby given.

5. Altering/Modifying Material: Not Permitted. However figures and illustrations may be altered/adapted minimally to serve your work. Any other abbreviations, additions, deletions and/or any other alterations shall be made only with prior written authorization of Elsevier Ltd. (Please contact Elsevier at permissions@elsevier.com)

6. If the permission fee for the requested use of our material is waived in this instance, please be advised that your future requests for Elsevier materials may attract a fee.

7. Reservation of Rights: Publisher reserves all rights not specifically granted in the combination of (i) the license details provided by you and accepted in the course of this licensing transaction, (ii) these terms and conditions and (iii) CCC's Billing and Payment terms and conditions.

8. License Contingent Upon Payment: While you may exercise the rights licensed immediately upon issuance of the license at the end of the licensing process for the transaction, provided that you have disclosed complete and accurate details of your proposed use, no license is finally effective unless and until full payment is received from you (either by publisher or by CCC) as provided in CCC's Billing and Payment terms and conditions. If full payment is not received on a timely basis, then any license preliminarily granted shall be deemed automatically revoked and shall be void as if never granted. Further, in the event that you breach any of these terms and conditions or any of CCC's Billing and Payment terms and conditions, the license is automatically revoked and shall be void as if never granted. Use of materials as described in a revoked license, as well as any use of the materials beyond the scope of an unrevoked license, may constitute copyright infringement and publisher reserves the right to take any and all action to protect its copyright in the materials.

9. Warranties: Publisher makes no representations or warranties with respect to the licensed material.

10. Indemnity: You hereby indemnify and agree to hold harmless publisher and CCC, and their respective officers, directors, employees and agents, from and against any

and all claims arising out of your use of the licensed material other than as specifically authorized pursuant to this license.

11. **No Transfer of License:** This license is personal to you and may not be sublicensed, assigned, or transferred by you to any other person without publisher's written permission.

12. **No Amendment Except in Writing:** This license may not be amended except in a writing signed by both parties (or, in the case of publisher, by CCC on publisher's behalf).

13. **Objection to Contrary Terms:** Publisher hereby objects to any terms contained in any purchase order, acknowledgment, check endorsement or other writing prepared by you, which terms are inconsistent with these terms and conditions or CCC's Billing and Payment terms and conditions. These terms and conditions, together with CCC's Billing and Payment terms and conditions (which are incorporated herein), comprise the entire agreement between you and publisher (and CCC) concerning this licensing transaction. In the event of any conflict between your obligations established by these terms and conditions and those established by CCC's Billing and Payment terms and conditions, these terms and conditions shall control.

14. **Revocation:** Elsevier or Copyright Clearance Center may deny the permissions described in this License at their sole discretion, for any reason or no reason, with a full refund payable to you. Notice of such denial will be made using the contact information provided by you. Failure to receive such notice will not alter or invalidate the denial. In no event will Elsevier or Copyright Clearance Center be responsible or liable for any costs, expenses or damage incurred by you as a result of a denial of your permission request, other than a refund of the amount(s) paid by you to Elsevier and/or Copyright Clearance Center for denied permissions.

LIMITED LICENSE

The following terms and conditions apply only to specific license types:

15. **Translation:** This permission is granted for non-exclusive world **English** rights only unless your license was granted for translation rights. If you licensed translation rights you may only translate this content into the languages you requested. A professional translator must perform all translations and reproduce the content word for word preserving the integrity of the article.

16. **Posting licensed content on any Website:** The following terms and conditions apply as follows: Licensing material from an Elsevier journal: All content posted to

the web site must maintain the copyright information line on the bottom of each image; A hyper-text must be included to the Homepage of the journal from which you are licensing at <http://www.sciencedirect.com/science/journal/xxxxx> or the Elsevier homepage for books at <http://www.elsevier.com>; Central Storage: This license does not include permission for a scanned version of the material to be stored in a central repository such as that provided by Heron/XanEdu.

Licensing material from an Elsevier book: A hyper-text link must be included to the Elsevier homepage at <http://www.elsevier.com> . All content posted to the web site must maintain the copyright information line on the bottom of each image.

Posting licensed content on Electronic reserve: In addition to the above the following clauses are applicable: The web site must be password-protected and made available only to bona fide students registered on a relevant course. This permission is granted for 1 year only. You may obtain a new license for future website posting.

17. For journal authors: the following clauses are applicable in addition to the above:

Preprints:

A preprint is an author's own write-up of research results and analysis, it has not been peer-reviewed, nor has it had any other value added to it by a publisher (such as formatting, copyright, technical enhancement etc.).

Authors can share their preprints anywhere at any time. Preprints should not be added to or enhanced in any way in order to appear more like, or to substitute for, the final versions of articles however authors can update their preprints on arXiv or RePEc with their Accepted Author Manuscript (see below).

If accepted for publication, we encourage authors to link from the preprint to their formal publication via its DOI. Millions of researchers have access to the formal publications on ScienceDirect, and so links will help users to find, access, cite and use the best available version. Please note that Cell Press, The Lancet and some society-owned have different preprint policies. Information on these policies is available on the journal homepage.

Accepted Author Manuscripts: An accepted author manuscript is the manuscript of an article that has been accepted for publication and which typically includes author-incorporated changes suggested during submission, peer review and editor-author communications.

Authors can share their accepted author manuscript:

- immediately
 - via their non-commercial person homepage or blog
 - by updating a preprint in arXiv or RePEc with the accepted manuscript
 - via their research institute or institutional repository for internal institutional uses or as part of an invitation-only research collaboration work-group
 - directly by providing copies to their students or to research collaborators for their personal use
 - for private scholarly sharing as part of an invitation-only work group on commercial sites with which Elsevier has an agreement
- after the embargo period
 - via non-commercial hosting platforms such as their institutional repository
 - via commercial sites with which Elsevier has an agreement

In all cases accepted manuscripts should:

- link to the formal publication via its DOI
- bear a CC-BY-NC-ND license - this is easy to do
- if aggregated with other manuscripts, for example in a repository or other site, be shared in alignment with our hosting policy not be added to or enhanced in any way to appear more like, or to substitute for, the published journal article.

Published journal article (JPA): A published journal article (PJA) is the definitive final record of published research that appears or will appear in the journal and embodies all value-adding publishing activities including peer review co-ordination, copy-editing, formatting, (if relevant) pagination and online enrichment.

Policies for sharing publishing journal articles differ for subscription and gold open access articles:

Subscription Articles: If you are an author, please share a link to your article rather than the full-text. Millions of researchers have access to the formal publications on ScienceDirect, and so links will help your users to find, access, cite, and use the best available version.

Theses and dissertations which contain embedded PJAs as part of the formal submission can be posted publicly by the awarding institution with DOI links back to the formal publications on ScienceDirect.

If you are affiliated with a library that subscribes to ScienceDirect you have additional private sharing rights for others' research accessed under that agreement. This includes use for classroom teaching and internal training at the institution (including use in course packs and courseware programs), and inclusion of the article for grant funding purposes.

Gold Open Access Articles: May be shared according to the author-selected end-user license and should contain a [CrossMark logo](#), the end user license, and a DOI link to the formal publication on ScienceDirect.

Please refer to Elsevier's [posting policy](#) for further information.

18. **For book authors** the following clauses are applicable in addition to the above: Authors are permitted to place a brief summary of their work online only. You are not allowed to download and post the published electronic version of your chapter, nor may you scan the printed edition to create an electronic version. **Posting to a repository:** Authors are permitted to post a summary of their chapter only in their institution's repository.

19. **Thesis/Dissertation:** If your license is for use in a thesis/dissertation your thesis may be submitted to your institution in either print or electronic form. Should your thesis be published commercially, please reapply for permission. These requirements include permission for the Library and Archives of Canada to supply single copies, on demand, of the complete thesis and include permission for Proquest/UMI to supply single copies, on demand, of the complete thesis. Should your thesis be published commercially, please reapply for permission. Theses and dissertations which contain embedded PJAs as part of the formal submission can be posted publicly by the awarding institution with DOI links back to the formal publications on ScienceDirect.

Elsevier Open Access Terms and Conditions

You can publish open access with Elsevier in hundreds of open access journals or in nearly 2000 established subscription journals that support open access publishing. Permitted third party re-use of these open access articles is defined by the author's choice of Creative Commons user license. See our [open access license policy](#) for more information.

Terms & Conditions applicable to all Open Access articles published with Elsevier:

Any reuse of the article must not represent the author as endorsing the adaptation of the article nor should the article be modified in such a way as to damage the author's honour or reputation. If any changes have been made, such changes must be clearly indicated.

The author(s) must be appropriately credited and we ask that you include the end user license and a DOI link to the formal publication on ScienceDirect.

If any part of the material to be used (for example, figures) has appeared in our publication with credit or acknowledgement to another source it is the responsibility of the user to ensure their reuse complies with the terms and conditions determined by the rights holder.

Additional Terms & Conditions applicable to each Creative Commons user license:

CC BY: The CC-BY license allows users to copy, to create extracts, abstracts and new works from the Article, to alter and revise the Article and to make commercial use of the Article (including reuse and/or resale of the Article by commercial entities), provided the user gives appropriate credit (with a link to the formal publication through the relevant DOI), provides a link to the license, indicates if changes were made and the licensor is not represented as endorsing the use made of the work. The full details of the license are available at <http://creativecommons.org/licenses/by/4.0>.

CC BY NC SA: The CC BY-NC-SA license allows users to copy, to create extracts, abstracts and new works from the Article, to alter and revise the Article, provided this is not done for commercial purposes, and that the user gives appropriate credit (with a link to the formal publication through the relevant DOI), provides a link to the license, indicates if changes were made and the licensor is not represented as endorsing the use made of the work. Further, any new works must be made available on the same conditions. The full details of the license are available at <http://creativecommons.org/licenses/by-nc-sa/4.0>.

CC BY NC ND: The CC BY-NC-ND license allows users to copy and distribute the Article, provided this is not done for commercial purposes and further does not permit distribution of the Article if it is changed or edited in any way, and provided the user gives appropriate credit (with a link to the formal publication through the relevant DOI), provides a link to the license, and that the licensor is not represented as endorsing the use made of the work. The full details of the license are available at <http://creativecommons.org/licenses/by-nc-nd/4.0>. Any commercial reuse of Open Access articles published with a CC BY NC SA or CC BY NC ND license requires permission from Elsevier and will be subject to a fee.

Commercial reuse includes:

- Associating advertising with the full text of the Article
- Charging fees for document delivery or access
- Article aggregation

- Systematic distribution via e-mail lists or share buttons

Posting or linking by commercial companies for use by customers of those companies.

20. Other Conditions:

v1.8

Questions? customercare@copyright.com or +1-855-239-3415 (toll free in the US)
or +1-978-646-2777.

**JOHN WILEY AND SONS LICENSE
TERMS AND CONDITIONS**

Nov 16, 2016

This Agreement between Recep Yuksel ("You") and John Wiley and Sons ("John Wiley and Sons") consists of your license details and the terms and conditions provided by John Wiley and Sons and Copyright Clearance Center.

License Number: 3990650352000

License date: Nov 16, 2016

Licensed Content Publisher: John Wiley and Sons

Licensed Content Publication: International Journal of Energy Research

Licensed Content Title: Textile supercapacitors-based on
MnO₂/SWNT/conducting polymer ternary composites

Licensed Content Author: Recep Yuksel, Husnu Emrah Unalan

Licensed Content Date: Oct 22, 2015

Licensed Content Pages: 11

Type of use: Dissertation/Thesis

Requestor type: Author of this Wiley article

Format: Print and electronic

Portion: Full article

Will you be translating?: No

Title of your thesis / dissertation: Nanomaterials for Supercapacitors

Expected completion date: Jan 2017

Expected size (number of pages): 200

Requestor Location: Recep Yuksel

Middle East Technical University

Ankara, 06800

Turkey

Attn: Recep Yuksel

Publisher Tax ID: EU826007151

Billing Type: Invoice

Billing Address: Recep Yuksel

Middle East Technical University

Ankara, Turkey 06800

Attn: Recep Yuksel

Total: 0.00 USD

Terms and Conditions

TERMS AND CONDITIONS

This copyrighted material is owned by or exclusively licensed to John Wiley & Sons, Inc. or one of its group companies (each a "Wiley Company") or handled on behalf of a society with which a Wiley Company has exclusive publishing rights in relation to a particular work (collectively "WILEY"). By clicking "accept" in connection with completing this licensing transaction, you agree that the following terms and conditions apply to this transaction (along with the billing and payment terms and conditions established by the Copyright Clearance Center Inc., ("CCC's Billing and Payment terms and conditions"), at the time that you opened your RightsLink account (these are available at any time at <http://myaccount.copyright.com>).

Terms and Conditions

- The materials you have requested permission to reproduce or reuse (the "Wiley Materials") are protected by copyright.

You are hereby granted a personal, non-exclusive, non-sub licensable (on a stand-alone basis), non-transferable, worldwide, limited license to reproduce the Wiley Materials for the purpose specified in the licensing process. This license, **and any CONTENT (PDF or image file) purchased as part of your order**, is for a one-time

use only and limited to any maximum distribution number specified in the license. The first instance of republication or reuse granted by this license must be completed within two years of the date of the grant of this license (although copies prepared before the end date may be distributed thereafter). The Wiley Materials shall not be used in any other manner or for any other purpose

- , beyond what is granted in the license. Permission is granted subject to an appropriate acknowledgement given to the author, title of the material/book/journal and the publisher. You shall also duplicate the copyright notice that appears in the Wiley publication in your use of the Wiley Material. Permission is also granted on the understanding that nowhere in the text is a previously published source acknowledged for all or part of this Wiley Material. Any third party content is expressly excluded from this permission.
- With respect to the Wiley Materials, all rights are reserved. Except as expressly granted by the terms of the license, no part of the Wiley Materials may be copied, modified, adapted (except for minor reformatting required by the new Publication), translated, reproduced, transferred or distributed, in any form or by any means, and no derivative works may be made based on the Wiley Materials without the prior permission of the respective copyright owner. **For STM Signatory Publishers clearing permission under the terms of the [STM Permissions Guidelines](#) only, the terms of the license are extended to include subsequent editions and for editions in other languages, provided such editions are for the work as a whole in situ and does not involve the separate exploitation of the permitted figures or extracts,** You may not alter, remove or suppress in any manner any copyright, trademark or other notices displayed by the Wiley Materials. You may not license, rent, sell, loan, lease, pledge, offer as security, transfer or assign the Wiley Materials on a stand-alone basis, or any of the rights granted to you hereunder to any other person.
- The Wiley Materials and all of the intellectual property rights therein shall at all times remain the exclusive property of John Wiley & Sons Inc, the Wiley Companies, or their respective licensors, and your interest therein is only that of having possession of and the right to reproduce the Wiley Materials pursuant to Section 2 herein during the continuance of this Agreement. You agree that you own no right, title or interest in or to the Wiley Materials or any of the intellectual property rights therein. You shall have no rights hereunder other than the license as provided for above in Section 2. No right, license or interest to any trademark, trade name, service mark or other branding ("Marks") of WILEY or its licensors is granted hereunder, and you agree that you shall not assert any such right, license or interest with respect thereto
- NEITHER WILEY NOR ITS LICENSORS MAKES ANY WARRANTY OR REPRESENTATION OF ANY KIND TO YOU OR ANY THIRD PARTY, EXPRESS, IMPLIED OR STATUTORY, WITH RESPECT TO THE

MATERIALS OR THE ACCURACY OF ANY INFORMATION CONTAINED IN THE MATERIALS, INCLUDING, WITHOUT LIMITATION, ANY IMPLIED WARRANTY OF MERCHANTABILITY, ACCURACY, SATISFACTORY QUALITY, FITNESS FOR A PARTICULAR PURPOSE, USABILITY, INTEGRATION OR NON-INFRINGEMENT AND ALL SUCH WARRANTIES ARE HEREBY EXCLUDED BY WILEY AND ITS LICENSORS AND WAIVED BY YOU.

- WILEY shall have the right to terminate this Agreement immediately upon breach of this Agreement by you.
- You shall indemnify, defend and hold harmless WILEY, its Licensors and their respective directors, officers, agents and employees, from and against any actual or threatened claims, demands, causes of action or proceedings arising from any breach of this Agreement by you.
- IN NO EVENT SHALL WILEY OR ITS LICENSORS BE LIABLE TO YOU OR ANY OTHER PARTY OR ANY OTHER PERSON OR ENTITY FOR ANY SPECIAL, CONSEQUENTIAL, INCIDENTAL, INDIRECT, EXEMPLARY OR PUNITIVE DAMAGES, HOWEVER CAUSED, ARISING OUT OF OR IN CONNECTION WITH THE DOWNLOADING, PROVISIONING, VIEWING OR USE OF THE MATERIALS REGARDLESS OF THE FORM OF ACTION, WHETHER FOR BREACH OF CONTRACT, BREACH OF WARRANTY, TORT, NEGLIGENCE, INFRINGEMENT OR OTHERWISE (INCLUDING, WITHOUT LIMITATION, DAMAGES BASED ON LOSS OF PROFITS, DATA, FILES, USE, BUSINESS OPPORTUNITY OR CLAIMS OF THIRD PARTIES), AND WHETHER OR NOT THE PARTY HAS BEEN ADVISED OF THE POSSIBILITY OF SUCH DAMAGES. THIS LIMITATION SHALL APPLY NOTWITHSTANDING ANY FAILURE OF ESSENTIAL PURPOSE OF ANY LIMITED REMEDY PROVIDED HEREIN.
- Should any provision of this Agreement be held by a court of competent jurisdiction to be illegal, invalid, or unenforceable, that provision shall be deemed amended to achieve as nearly as possible the same economic effect as the original provision, and the legality, validity and enforceability of the remaining provisions of this Agreement shall not be affected or impaired thereby.
- The failure of either party to enforce any term or condition of this Agreement shall not constitute a waiver of either party's right to enforce each and every term and condition of this Agreement. No breach under this agreement shall be deemed waived or excused by either party unless such waiver or consent is in writing signed by the party granting such waiver or consent. The waiver by or consent of a party to a breach of any provision of this Agreement shall not operate or be construed as a waiver of or consent to any other or subsequent breach by such other party.

- This Agreement may not be assigned (including by operation of law or otherwise) by you without WILEY's prior written consent.
- Any fee required for this permission shall be non-refundable after thirty (30) days from receipt by the CCC.
- These terms and conditions together with CCC's Billing and Payment terms and conditions (which are incorporated herein) form the entire agreement between you and WILEY concerning this licensing transaction and (in the absence of fraud) supersedes all prior agreements and representations of the parties, oral or written. This Agreement may not be amended except in writing signed by both parties. This Agreement shall be binding upon and inure to the benefit of the parties' successors, legal representatives, and authorized assigns.
- In the event of any conflict between your obligations established by these terms and conditions and those established by CCC's Billing and Payment terms and conditions, these terms and conditions shall prevail.
- WILEY expressly reserves all rights not specifically granted in the combination of (i) the license details provided by you and accepted in the course of this licensing transaction, (ii) these terms and conditions and (iii) CCC's Billing and Payment terms and conditions.
- This Agreement will be void if the Type of Use, Format, Circulation, or Requestor Type was misrepresented during the licensing process.
- This Agreement shall be governed by and construed in accordance with the laws of the State of New York, USA, without regards to such state's conflict of law rules. Any legal action, suit or proceeding arising out of or relating to these Terms and Conditions or the breach thereof shall be instituted in a court of competent jurisdiction in New York County in the State of New York in the United States of America and each party hereby consents and submits to the personal jurisdiction of such court, waives any objection to venue in such court and consents to service of process by registered or certified mail, return receipt requested, at the last known address of such party.

WILEY OPEN ACCESS TERMS AND CONDITIONS

Wiley Publishes Open Access Articles in fully Open Access Journals and in Subscription journals offering Online Open. Although most of the fully Open Access journals publish open access articles under the terms of the Creative Commons Attribution (CC BY) License only, the subscription journals and a few of the Open Access Journals offer a choice of Creative Commons Licenses. The license type is clearly identified on the article.

The Creative Commons Attribution License

The [Creative Commons Attribution License \(CC-BY\)](#) allows users to copy, distribute and transmit an article, adapt the article and make commercial use of the article. The CC-BY license permits commercial and non-

Creative Commons Attribution Non-Commercial License

The [Creative Commons Attribution Non-Commercial \(CC-BY-NC\)License](#) permits use, distribution and reproduction in any medium, provided the original work is properly cited and is not used for commercial purposes.(see below)

Creative Commons Attribution-Non-Commercial-NoDerivs License

The [Creative Commons Attribution Non-Commercial-NoDerivs License](#) (CC-BY-NC-ND) permits use, distribution and reproduction in any medium, provided the original work is properly cited, is not used for commercial purposes and no modifications or adaptations are made. (see below)

Use by commercial "for-profit" organizations

Use of Wiley Open Access articles for commercial, promotional, or marketing purposes requires further explicit permission from Wiley and will be subject to a fee.

Further details can be found on Wiley Online

Library <http://olabout.wiley.com/WileyCDA/Section/id-410895.html>

Other Terms and Conditions:

v1.10 Last updated September 2015

Questions? customercare@copyright.com or +1-855-239-3415 (toll free in the US) or +1-978-646-2777.

CURRICULUM VITAE

RECEP YUKSEL

Department of Micro and Nanotechnology,
Science and Society Center,
Middle East Technical University (METU)
06800, Ankara, TURKEY.
e-mail: reyuksel@gmail.com
mobile: +90 (555) 327 4220

FORMAL EDUCATION

- **Doctor of Philosophy (Candidate)**, Department of Micro & Nanotechnology (October 2011- Present) Middle East Technical University (METU); Ankara TURKEY
Dissertation: “Development of Supercapacitors with One Dimensional Nanomaterials”
- **Master of Science**, Department of Chemistry (October 2011) Middle East Technical University (METU); Ankara TURKEY
Dissertation: “Sensitive & Quantitative Determination of Cysteine by Surface Enhanced Raman Spectrometry Based On Their Induced Aggregates of Gold & Silver Nanostructures”
- **Bachelor of Science**, Department of Chemistry Education; (June 2008) Middle East Technical University (METU); Ankara TURKEY

ACADEMIC RESEARCH EXPERIENCE

- Research Assistant (September 2010 - ongoing)
Science and Society Center, Middle East Technical University(METU); Ankara TURKEY

PUBLICATIONS

1. **R. Yuksel**, E. Ataoglu, J. Turan, E. Alpugan, S. Ozdemir, L. Toppare, A. Cirpan, H. E. Unalan, G. Gunbas, A New, Processable Blue to Transmissive Polymer with Superior Properties and its Use in High Performance

- Electrochromic Supercapacitors, accepted to Journal of Polymer Science, Part A: Polymer Chemistry (2016).
2. **R. Yuksel**, S. Coskun, G. Gunbas, A. Cirpan, L. Toppare, H. E. Unalan, An efficient electrochromic supercapacitor with a color change from green to transparent, accepted to J. Electrochem. Soc. (2016).
 3. **R. Yuksel**, S. Coskun, Y. E. Kalay, H. E. Unalan, Flexible, silver nanowire network nickel hydroxide core-shell electrodes for supercapacitors, J. Power Sources 328 (2016) 167-173.
 4. C. Gokoglan, S. Soylemez, M. Kesik. I. Dogru, O. Turel, **R. Yuksel**, H. E. Unalan, L. Toppare, A novel approach for the fabrication of a flexible glucose biosensor: the combination of vertically aligned CNTs and a conjugated polymer, Food Chemistry 220 (2016) 299-305.
 5. D. Dursun, S. Ozkul, **R. Yuksel**, H. E. Unalan, Enhancing Capacitive Deionization Technology as an Effective Method for Water Treatment Using Commercially Available Graphene, accepted for Water Science and Technology (2016).
 6. M. B. Durukan, **R. Yuksel**, H. E. Unalan, Cobalt oxide nanoflakes on single walled carbon nanotube thin films for supercapacitor electrodes, accepted for Electrochimica Acta (2016).
 7. **R. Yuksel**, S. Coskun, H. E. Unalan, Coaxial silver nanowire network core molybdenum oxide shell electrodes for supercapacitors, Electrochimica Acta 193 (2016) 39.
 8. **R. Yuksel**, C. Durucan, H. E. Unalan, Ternary nanocomposite SWNT/WO₃/PANI thin film electrodes for supercapacitors, J. Alloy Compd. 658 (2016) 183-189.
 9. **R. Yuksel**, S. C. Cevher, A. Cirpan, L. Toppare, H. E. Unalan, All-organic electrochromic supercapacitor electrodes, J. Electrochem. Soc. 162 (2015) A2805-A2810.
 10. **R. Yuksel**, H. E. Unalan, Textile Supercapacitors Based on MnO₂/SWNT/Conducting Polymer Ternary Composites, Int. J. Energy Res. 39 (2015) 2042-2052.
 11. **R. Yuksel**, Z. Sarioba, A. Cirpan, P. Hiralal, H. E. Unalan, Transparent and flexible supercapacitors with single walled carbon nanotube thin film electrodes, ACS Appl. Mater. Interfaces 6 (2014) 15434.

PRESENTATIONS

1. Vertically Aligned Carbon Nanotube-Polyaniline Nanocomposite Electrodes for Supercapacitors, A. Aydinli, R. Yuksel, H. E. Unalan, MRS Fall' 2016 USA.
2. Silver Nanowire-Nickel Hydroxide Nanocomposites for Pseudocapacitors, R. Yuksel, S. Coskun, H. E. Unalan, IMMC' 2016 Istanbul, Turkey.
3. Low Dimensional Multilayered Nanostructures for Plasmonic Applications, Ezgi Abacioglu, R. Yuksel, B. B. Turgut, F. B. Atar, H. E. Unalan, A. Bek, Photonics' 2016 Ankara, Turkey.
4. Surface Enhanced Raman Scattering Activity of 0 and 1 Dimensional Silver Nanostructures, Ozge Demirtas, R. Yuksel, H. E. Unalan, A. Bek, Photonics' 2016 Ankara, Turkey.
5. Silver Nanowire- Molybdenum Oxide Nanocomposites for Supercapacitors, R. Yuksel, S. Coskun, H. E. Unalan, MRS Fall' 2015 USA.
6. Carbon Nanotube - Conducting Polymer Electrodes for Electrochromic Supercapacitors, R. Yuksel, A. Cirpan, H. E. Unalan, MRS Fall' 2015 USA.
7. Carbon Nanotube- Cobalt Oxide Nanocomposites for High Performance Supercapacitors, M. B. Durukan, R. Yuksel, H. E. Unalan, MRS Fall' 2015 USA.
8. Coaxial Capacitors with ALD Deposited Alumina on Silver Nanowires, R. Yuksel, S. Coskun, S. Sagkal, H. Eren, H. E. Unalan, N. Biyikli, ALD' 2015 USA.
9. Textile Based Ternary Nanocomposite Supercapacitors, R. Yuksel, Z. Sarioba, H.E. Unalan, TMS Meeting' 2015 USA.
10. Carbon Nanotube- Cobalt Oxide Nanocomposites for High Performance Supercapacitors, M. B. Durukan, R. Yuksel, H. E. Unalan, MESC-IS 2015, Ankara, Turkey.
11. Carbon Nanotube - Conducting Polymer Electrodes for Electrochromic Supercapacitors, R. Yuksel, A. Cirpan, H. E. Unalan, MESC-IS 2015, Ankara, Turkey.
12. Flexible Textile Based Ternary Nanocomposite Supercapacitors, R. Yuksel, Z. Sarioba, H.E. Unalan, MRS Fall' 2014 USA.

13. Transparent and Flexible Vacuum Filtered Single Walled Carbon Nanotube Thin Film Supercapacitors, R. Yuksel, Z. Sarioba, H.E. Unalan, MRS Fall' 2014 USA.
14. Carbon Nanotube - Tungsten Oxide - Polyaniline Ternary Nanocomposite Electrodes for Supercapacitors, R. Yuksel, H.E. Unalan, MRS Fall' 2014 USA.
15. Transparent and Flexible SWNT Thin Film Supercapacitors, R. Yuksel, H. E. Unalan, Turkish – German Conference On Energy Technologies 2014, Ankara, Turkey.
16. Single Walled Carbon Nanotube Thin Film Electrodes for Transparent and Flexible Supercapacitors, R. Yuksel, Z. Sarioba, A. Cirpan, P. Hiralal, H. E. Unalan, IMRC' 2014 Mexico.
17. Textile Based Supercapacitors Using SWNTs/Manganese Oxide/PEDOT:PSS, R. Yuksel, Z. Sarioba, H. E. Unalan, 10th Nanoscience and Nanotechnology Conference (NanoTR 10)' 2014, Istanbul, Turkey.
18. Transparent and Flexible Supercapacitor Electrodes Using SWNT Thin Films, R. Yuksel, Z. Sarioba, H. E. Unalan, 10th Nanoscience and Nanotechnology Conference (NanoTR 10)' 2014, Istanbul, Turkey.
19. Silicon Nanowire-Single Walled Carbon Nanotube Hybrid Electrodes for Supercapacitors with Gel Electrolyte, R. Yuksel, E. Mulazimoglu, Z. Sarioba, H.E. Unalan, MRS Fall' 2013 USA.